

Characterising the Cellular and Molecular Landscape of the Murine Diabetic Heart

Charles D. Cohen

B.Sc. (Hons)

Submitted in total fulfilment of the requirements of the degree of Doctor of Philosophy

College of Science, Health & Engineering

School of Life Sciences

Department of Physiology, Anatomy and Microbiology

La Trobe University

November 2021

ORCID ID: 0000-0002-4700-6368

The work within this dissertation is dedicated in memoriam of Linda Ann O'Callaghan

A loving mother, taken too soon.

1958-2000.

Abstract

Diabetes mellitus is a metabolic disease primarily characterised by hyperglycaemia and is associated with a significantly elevated risk of heart failure. Diabetes is associated with left-ventricular dysfunction, cardiac fibrosis, cardiomyocyte dysfunction, ROS generation and inflammation. While significant advancements have been made in this field, the cellular and molecular protagonists that underpin the development of heart failure in diabetes remain unclear. In recent years, the cardiac cellular composition has been reappraised in homeostasis and disease, which has been facilitated by the utility of single-cell technologies. These analyses however, are yet to be applied to the context of diabetic heart failure.

To address this gap in knowledge, cardiac and systemic flow cytometry was performed using two disparate mouse models of type-2 diabetes (T2D). Moreover, cardiac single-cell transcriptomics and histology was conducted in a separate cohort of T2D mice. Cardiac function was also assessed by *in vivo* echocardiography, to determine the degree of cardiac functional impairment in each murine model of T2D. Indeed, both models of T2D exhibit marked differences in their cardiac cellular composition compared to their non-diabetic controls, accompanied by detectable cardiac dysfunction. Notably, I observed resident mesenchymal cell expansion and fibroblast hyperplasia in both models of T2D. In addition, I observed increased numbers in cardiac monocytes, reflecting the concomitant systemic monocytosis. Single-cell transcriptomic analysis revealed a concerted diabetes-induced cell-specific response for adverse pathological cardiac remodelling. These include activation of unprecedented gene expression programs, as well as those corresponding to established pathways associated with the phenotype of the diabetic heart.

The work in this dissertation offers a comprehensive framework for understanding the specific cellular and molecular changes accompanying diabetes-induced cardiac pathology. Targeting the pathways that drive these changes may offer novel therapeutic avenues to address the cardiac complications associated with diabetes.

Declarations and Statement of Authorship

Except where reference is made in the text of the thesis, this thesis contains no material published elsewhere or extracted in whole or in part from a thesis accepted for the award of any other degree or diploma. No other person's work has been used without due acknowledgment in the main text of the thesis. This thesis has not been submitted for the award of any degree or diploma in any other tertiary institution.

Charles D. Cohen: 15th November, 2021

Acknowledgements

First and foremost, I extend my sincere gratitude and thanks to my supervisors, Dr. Alexander Pinto, Prof. Rebecca Ritchie, Dr. Miles De Blasio and Prof. Grant Drummond. I am extremely grateful to have such supportive and patient mentors, who have guided me through this challenging journey. I am honoured to work alongside these leading experts in cardiovascular research, and feel privileged to contribute to such important work in this rapidly emerging field.

Second, I would like to thank my family for supporting me through this rollercoaster of a journey. In particular, I would first like to thank my beloved mother, who sadly passed from sudden cardiac arrest in May 2000. The work presented hence here forth is dedicated to her, in the hope that I have made her proud and can further contribute to cardiovascular research in her honour. Second, I would like to thank my father A/Prof. Neale Cohen, who has supported me not only through this tough journey, but also for his ongoing support throughout my life. I would also like to thank my siblings Miranda and Tess Cohen, as well as Alon and Deon Jacks for their continuing support. Moreover, I extend my heartfelt thanks to Leora Jacks, who has acted as a mother figure during this journey. I am incredibly fortunate to have such a fantastic support network around me.

Third, I thank my fellow colleagues who have had to put up with me for the last few years. From the Heart Failure Pharmacology laboratory, I would particularly like to thank Dr. Darnel Prakoso, Dr. Mitchel Tate, Jesse Walsh, Andrew Willis, Anida Velagic, David Nash and Minh Deo. I thank them for making each day enjoyable and memorable and for their continuing support. From the Cardiac Cellular Systems laboratory, I would like to thank Gabriella Farrugia, Malathi Dona, Ian Hsu, Crisdion Krstevski and Taylah Gaynor. I thank them for creating such a nurturing, fun environment for me to expand my knowledge and grasp the challenging concepts of emerging research techniques. Principally however, I thank each and every colleague for the laughs (and cries) shared throughout this journey. I am extremely lucky to be surrounded by such a supportive ‘work family’.

Finally, I would like to thank the funding bodies that have supported me financially for the duration of my candidature. I thank La Trobe University and the Baker Heart and Diabetes Institute for providing me with both fee remission and for facilitating scholarship support from the Australian Government Research Training Program. I give additional thanks to the Baker Institute for offering an additional ‘Bright Sparks’ top-up scholarship and for providing an additional travel fellowship. Moreover, I thank the relevant funding bodies that have contributed to my work, namely the National Health and Medical Research Council (NHMRC) of Australia and Diabetes Australia. I would also like to extend my gratitude to Monash Institute of Pharmaceutical Sciences, who have not only welcomed me into their Institute as an adjunct, but also shared their facilities and expertise.

Abbreviations

ACTA2.....	Alpha-smooth muscle actin
AGE.....	Advanced glycation end-products
Ang II.....	Angiotensin II
ANGPTL4.....	Angiopoietin-like 4
ANP.....	Atrial Natriuretic Peptide
AWd.....	Anterior wall dimension
BNP.....	Brain Natriuretic Peptide
β -MHC.....	β -myosin heavy chain
CAD.....	Coronary artery disease
CCR2.....	C-C motif chemokine receptor 2
CHF.....	Congestive heart failure
CSF-1.....	Colony stimulating factor-1
CVD.....	Cardiovascular disease
DM.....	Diabetes mellitus
DT.....	Deceleration time
EC.....	Endothelial cell
ECM.....	Extracellular matrix
EDTA.....	Ethylenediaminetetraacetic acid
FACS.....	Fluorescence-activated cell sorting
FS.....	Fractional shortening
FVB/NJ.....	Friend Virus B NIH
GO.....	Gene ontology
HbA1c.....	Glycated haemoglobin
HF.....	Heart Failure
HFD.....	High-Fat Diet
HFpEF.....	Heart Failure with preserved Ejection Fraction
HR.....	Heart rate
IFN.....	Interferon
IL-1 β	Interleukin-1 beta
IL-6.....	Interleukin-6
IPGTT.....	Intraperitoneal glucose tolerance test

IPITT.....	Intraperitoneal insulin tolerance test
IVC.....	Intra-Ventricular Septum
IVRT.....	Isovolumic relaxation time
LEC.....	Lymphatic endothelial cell
LV.....	Left Ventricle
LVEDD.....	LV end-diastolic dimension
LVESD.....	LV end-systolic dimension
MCP-1.....	Monocyte chemoattractant protein-1
MHCII.....	Major histocompatibility complex II
MI.....	Myocardial Infarction
MMP.....	Matrix-metalloproteinases
NADPH.....	Nicotinamide adenine dinucleotide phosphate
NETs.....	Neutrophil extracellular traps
PDGF.....	Platelet-derived growth factor
PWd.....	Posterior wall dimension
RMC.....	Resident mesenchymal cell
ROS.....	Reactive oxygen species
RV.....	Right Ventricle
scRNAseq.....	Single-cell RNA sequencing
SMC.....	Smooth muscle cell
SPADE.....	Spanning-tree progression analysis for density-normalized events
STZ.....	Streptozotocin
T1D.....	Type-1 diabetes
T2D.....	Type-2 diabetes
TGF- β	Transforming growth factor-beta
TIMP.....	Tissue inhibitory metalloproteinases
TNF α	Tumour necrosis factor alpha
tSNE.....	t-distributed stochastic neighbour embedding
VEC.....	Vascular endothelial cell

Table of Contents

Chapter 1	10
Introduction	10
1.1 Background	10
1.2 Classical characteristics of diabetes-induced HF	11
1.2.1 Diastolic dysfunction	11
1.2.2 Cardiomyocyte hypertrophy	12
1.2.3 Cardiomyocyte apoptosis	12
1.2.4 Cardiac fibrosis	13
1.2.5 ROS generation and oxidative stress	13
1.3 The emerging role of leukocytes in diabetes and CV disease	16
1.3.1 Leukocytes	16
1.3.2 Granulocytes	16
1.3.3 Monocytes and macrophages	18
1.3.4 Lymphocytes	19
1.3.5 The specific role of leukocytes in diabetes-induced HF remains unknown	20
1.4 Reappraising the cardiac cellular composition	21
1.4.1 Single-cell RNA sequencing	21
1.4.2 Single-cell RNA sequencing of the healthy murine myocardium	23
1.4.3 Single-cell RNA sequencing of the diseased murine myocardium	23
1.4.4 Transcriptomic profiling in the diabetic heart – current knowledge	24
1.5 Summary	25
1.6 Aims and Hypothesis	25
Chapter 2	28
General methodology	28
2.1 Experimental animals	28
2.2 Animal models of diabetes	28
2.2.1 STZ-HFD model of type-2 diabetes	28
2.2.2 $Lep^{db-J}/db/db$ model of type-2 diabetes	28
2.3 Experimental design	29
2.3.1 Aim 1: To determine the differences in the cardiac non-myocyte cellular landscape in the STZ-HFD mouse model of T2D-induced heart failure	29
2.3.2 Aim 2: To assess the progressive cardiac cellular differences in the db/db mouse model of T2D – a time-course study.	29
2.3.3 Aim 3: To interrogate the single-cell cardiac transcriptome using single-cell RNA sequencing in the $dbdb$ mouse model of T2D-induced heart failure.	30
2.3.4 Aim 4: To assess the differences in circulating leukocytes from human blood in patients with diabetes: a preliminary clinical trial	30
2.4 Animal monitoring	31

2.5 Blood glucose monitoring and HbA _{1c} measurement.....	32
2.6 Animal euthanasia and tissue collection	32
2.7 Cardiac flow cytometry.....	33
2.8 Flow cytometry of whole blood, spleen and bone marrow	33
2.9 Cardiac single-cell RNA sequencing	35
2.10 <i>In silico</i> analysis of single-cell RNA-sequencing data	37
2.10.1 Differential gene expression analysis.....	37
2.10.2 Gene ontology analysis	37
2.10.3 Ligand-receptor intercellular communication analysis	37
2.10.4 Incorporation of bulk RNA-sequencing data	38
2.11 Immunofluorescence staining and confocal microscopy	38
2.12 Cardiac Oil-red O staining	39
2.13 Body composition analysis	39
2.14 Intraperitoneal glucose (IPGTT) and insulin (IPITT) tolerance testing.....	39
2.14.1 IPGTT	39
2.14.2 IPITT	39
2.15 Echocardiography for cardiac LV function <i>in vivo</i>	40
2.15.1 Doppler echocardiography for diastolic function.....	40
2.15.2 M-Mode echocardiography for systolic function.....	40
2.16 Statistical analyses	42
Chapter 3	44
3.1 Integrative commentary	44
3.2 Declarations for Thesis chapter 3.....	44
3.3 Diastolic Dysfunction in a Pre-Clinical Model of Diabetes is Associated with Changes in the Cardiac Non-myocyte Cellular Composition.....	45
3.3.1 Statement of contributions	45
3.4 Publication	46
3.5 Supplementary material	58
Chapter 4	67
Exploring the progressive differences in cardiac cellular composition in the <i>db/db</i> model of type-2 diabetes	67
4.1 Introduction.....	67
4.2 Methodology	68
4.3 Results.....	70
4.3.1 The systemic characteristics of <i>db/db</i> mice recapitulate features of clinical T2D.....	70
4.3.2 Cardiac dysfunction is evident in <i>db/db</i> mice <i>in vivo</i>	70
4.3.2.1 Pulsed-wave mitral Doppler echocardiography.....	70
4.3.2.2 M-mode echocardiography.....	70

4.3.3 Profiling the circulating leukocytes in <i>db/h</i> and <i>db/db</i> mice.....	75
4.3.4 The cardiac cellular composition of 10-week old <i>db/h</i> and <i>db/db</i> mice	77
4.3.5 The cardiac cellular composition of 17-week old <i>db/h</i> and <i>db/db</i> mice	77
4.3.6 The cardiac cellular composition of 24-week old <i>db/h</i> and <i>db/db</i> mice	80
4.4 Discussion	82
4.4.1 Systemic characteristics in male <i>db/db</i> mice recapitulate clinical features of T2D	82
4.4.2 Cardiac dysfunction is most evident in 17-week old <i>db/db</i> mice	83
4.4.3 The differences in cardiac cellularity in <i>db/h</i> and <i>db/db</i> mice are age-dependent	84
4.4.4 Study Limitations.....	87
4.4.5 Future considerations studying mouse models of diabetic heart disease	88
4.4.6 Additional strategies to address the mechanisms dictating altered cardiac cellularity	89
4.5 Conclusions.....	90
Chapter 5	91
Single-cell transcriptomic analysis of the T2D mouse heart.....	91
5.1 Introduction.....	91
5.2 Research Design and Methods.....	92
5.3 Results.....	92
5.3.1 Single-cell transcriptomic profiling reveals extensive heterogeneity of non-myocytes ...	92
5.3.2 Cardiac differential gene expression indicates cell-specific and broad transcriptomic patterns	93
5.3.3 Cardiac non-myocytes increase ligand and receptor expression in a cell-specific manner	95
5.3.4 <i>Identifying key genes that regulate cardiac lipid accumulation</i>	99
5.3.5 Revealing the expanding fibroblast subsets in the T2D (<i>db/db</i>) heart	101
5.3.6 Expanding fibroblasts do not exhibit transcriptomic signatures related to fibrosis	101
5.3.7 Identification and comparison of cardiac macrophage subtypes in <i>db/h</i> and <i>db/db</i> mice	104
5.3.8 Macrophage subtype 3 exhibits a reduced capability to perform reverse cholesterol transport	104
5.3.9 Identifying common molecular pathways in the diabetic heart	107
5.4 Discussion	109
5.4.1 Fibroblast expansion is apparent in murine T2D without evidence of ECM remodelling	109
5.5.2 Lipotoxicity in <i>db/db</i> mice is a contributing feature driving impaired cardiac function	110
5.4.4 A subtype of cardiac macrophages are unable to perform reverse cholesterol efflux in the <i>db/db</i> heart	112
5.4.5 Angiogenesis and dysregulated leukocyte trafficking are characteristics of the <i>db/db</i> heart	113
5.4.6 Gene expression programs are distinct between murine models of T1D and T2D.....	115
5.4.7 Limitations	116
5.4.8 Future prospects	116

5.5 Conclusion	117
Chapter 6	118
Profiling circulating leukocytes in diabetic patients: a pilot study	118
6.2 Introduction.....	118
6.3 Methodology	119
6.3.1 Experimental design.....	119
6.3.2 Participant enrolment and statistical power	119
6.4 Results.....	120
6.4.1 <i>Participant characteristics</i>	120
6.4.2 Circulating myeloid cells	120
6.4.3 Circulating lymphoid cells	121
6.5 Discussion	124
6.5.1 Preliminary insights into the circulating leukocyte profile of diabetic patients.....	124
6.5.2 Experimental limitations and considerations for future studies	125
6.6 Conclusions.....	127
Chapter 7	128
General Discussion	128
7.1 Overview	128
7.2 Degrees of cardiac dysfunction in T2D-induced HF	128
7.3 Cardiac non-myocyte cellular alterations that characterise the diabetic heart	129
7.3.1 Fibroblast expansion in STZ-HFD and 17-week old <i>db/db</i> mice	129
7.3.2 Cardiac vascular alterations	131
7.3.3 The contribution of the immune system.....	135
7.4 Future directions	136
7.5 Conclusions.....	137
Chapter 8	139
References.....	139
Appendix.....	173
9.1 Review: New perspectives of the cardiac cellular landscape: mapping cellular mediators of cardiac fibrosis using single-cell transcriptomics	173

Chapter 1

Introduction

1.1 Background

Diabetes mellitus is a chronic metabolic disease that is primarily characterised by hyperglycaemia. It is classified into two main ‘types’: type-1 diabetes (T1D) or type-2 diabetes (T2D) mellitus. T1D represents approximately 5-10% of the global prevalence and arises from the auto-immune destruction of pancreatic β -islet cells, with age of onset typically occurring in adolescence [1–3]. T2D is associated with a range of concomitant metabolic abnormalities including insulin resistance, dyslipidaemia, hypertension and obesity [1,3–5]. Recent estimates of global diabetes prevalence suggest that over 450 million individuals currently live with diabetes, with evidence suggesting a large additional burden of undiagnosed cases [5]. In 2017, the worldwide financial cost of diabetes-related therapy was projected to exceed \$850 billion USD [6], approximately 11% of the world’s total health expenditure [6]. Moreover, T2D (~90% of cases) is accountable for approximately 5.2% of total global deaths each year [7], in 2015 contributing to 1.6 million deaths alone [9].

Cardiovascular (CV) disease is the most prevalent disease worldwide, with an estimated 423 million cases and accounting for over 17 million deaths in 2015 [10]. Ischaemic heart disease and stroke account for the majority of CV disease deaths (~9 million and ~3 million people, respectively). Heart failure (HF) is another important class of CV disease, characterised by aberrant cardiac function [11,12]. The current prevalence of HF is estimated to exceed 37 million individuals worldwide; however it is difficult to assess the mortality and incidence of HF, as this is often secondary to numerous aetiologies and diagnosed by various health professionals [12]. Total health expenditure across the European Union from CV disease treatment is estimated to cost €210 billion (equivalent to approximately USD\$245 billion) per annum, which has doubled since 2010 [13].

Diabetes results in a significantly elevated risk of CV death and hospitalisation for HF [14]. The socioeconomic consequences of diabetes are substantial and account for the majority of this burden. With recent technological innovations, optimal management is on the horizon for T1D, in the form of closed-loop insulin delivery systems [15–17]. On the contrary, management of T2D remains sub-optimal due to its complex, multifactorial nature and limited treatment options, hence the urgency for a solution [18]. Clinical HF in diabetes is often accompanied by preserved ejection fraction with left ventricle (LV) diastolic dysfunction, which is associated with augmented cardiac fibrosis, cardiomyocyte hypertrophy and apoptosis, aberrant leukocyte function and oxidative stress in rodent models of T2D [19–22]. However, the cellular and molecular mechanisms facilitating these features remain unclear, underscoring the need for more detailed interrogation of the diabetic heart. Indeed, novel cellular and molecular targets beyond hyperglycaemia and oxidative stress are required to pinpoint the precise pathophysiology for therapeutic manipulation. In this chapter, I will discuss the traditional concepts in diabetes and cardiovascular research, the emerging importance

of leukocytes in the development of CV disease and diabetes, as well as the current gaps in knowledge that this dissertation aims to address.

1.2 Classical characteristics of diabetes-induced HF

1.2.1 Diastolic dysfunction

Diastolic dysfunction is a hallmark physiological characteristic of diabetes-related HF, often manifesting before systolic dysfunction [23,24]. Diastolic dysfunction is usually asymptomatic, leaving many diabetic patients unaware of their existing condition until their diagnosis [25]. Diastolic dysfunction is associated with LV wall stiffening, resulting in impaired LV relaxation and filling capacity during diastole [26]. This hindered ventricular relaxation can lead to a reduction in myocardial ejection fraction and impaired myocardial perfusion [27,28]. Using Doppler echocardiography, impaired diastole is typically detected by a reduction in mitral blood flow during the early (E-wave) phase of diastole, thus more blood fills the LV in the late (A-wave) phase to compensate. Such functional assessments of diastolic dysfunction are typically diagnosed by reduced ratios of annular transmitral blood flow (E:A) and valve (e':a') velocity [29,30]. Other echocardiographic measurements of diastolic dysfunction include prolonged isovolumic relaxation time (IVRT) and increased deceleration time (DT), although these measurements are dependent on myocardial load and thus should be interpreted with caution [25,26,30–32]. Hence, utility of load-independent parameters derived from echocardiography are often used to overcome this limitation, such as the E/e' ratio, which considers the ratio of passive LV filling relative to myocardial relaxation [33]. In addition, other load-insensitive, haemodynamic measurements are routinely used to more accurately determine diastolic function. For example, *in vivo* pressure volume (P-V) loop analysis allows for real-time measurement of LV pressure and ventricular volume, independent of load [34]. This analysis provides more robust measurements of diastolic dysfunction, deriving important haemodynamic information including the end-diastolic pressure volume relationship (EDVPR) and Tau [35,36]. However, this alternative approach to assess cardiac function requires invasive catheterization and is thus a terminal procedure, providing difficulties when assessing temporal aspects of cardiac dysfunction. Cardiac magnetic resonance imaging (cMRI), is currently the gold standard, non-invasive method for obtaining higher resolution cardiac functional data, providing information regarding the heart's structure, blood flow, and cardiac metabolism [37,38]. A seminal report using cMRI suggested that T2D patients with subclinical LV diastolic dysfunction exhibit altered cardiac energy metabolism and reduced coronary perfusion [39]. More recent reports validate this in patients with HF with preserved ejection fraction (HFpEF), emphasising impaired microvascular perfusion [40,41] and excessive intramyocardial adipose tissue deposition [42] as key characteristics of HFpEF. Non-invasive imaging capabilities are becoming increasingly effective for detecting functional cardiac abnormalities, [43] however it is important to consider the morphological and molecular characteristics that contribute to cardiac dysfunction.

1.2.2 Cardiomyocyte hypertrophy

Cardiomyocyte hypertrophy is believed to occur as a compensatory response to the circulating stressors characterising diabetes and is a key contributor to diastolic dysfunction [19,44–46]. T1D mouse models induced by the pancreatic β -cell toxin streptozotocin (STZ) typically exhibit cardiomyocyte hypertrophy (see Table 1.1 for phenotypic comparisons of relevant mouse models) [47–50]. Moreover, mice receiving high-fat diet (HFD) display increases in myocyte size, accompanied by aberrant contractile function relative to chow fed animals [51,52]. In addition, mice administered STZ and HFD concomitantly, also display similar degrees of cardiomyocyte hypertrophy (Table 1.1) [53]. Common markers of diabetes-induced cardiomyocyte hypertrophy include elevated mRNA expression of atrial natriuretic peptide (ANP), β -myosin heavy chain (β -MHC) and insulin-like growth factor-1 (IGF-1) [45,47,49,54]. However, there remain conflicting reports in the literature, considering spontaneously induced T1D (Akita $\text{Ins}^{2\text{WT}/\text{C96Y}}$) [55] and T2D ($\text{Lepr}^{\text{db-}}/\text{db/db}$) [56] mouse models do not tend to display increases in cardiomyocyte size, despite impairments in cardiac function detected by echocardiography (Table 1.1) [56,57]. Non-invasive clinical studies using various imaging modalities also suggest increased LV mass [58–60], which is believed to be, at least in part, associated with myocyte hypertrophy. Furthermore, basic histological examination of human cardiac biopsies reveal increases in cardiomyocyte size and basal laminar thickness in patients diagnosed with diabetic cardiomyopathy [61]. While cardiomyocyte hypertrophy and increased LV mass are positively correlated [62], this is one of the many characteristics that contribute to the diabetic heart phenotype. Whether cardiomyocyte hypertrophy is essential for the development of diabetes-induced HF is yet to be definitively elucidated, but remains an important consideration in the pathology of diabetic heart disease.

1.2.3 Cardiomyocyte apoptosis

Cardiomyocyte apoptosis has long been established in the diabetic heart, from both human biopsies [63,64] and in various rodent models of diabetes (Table 1.1) [19,44,65]. Cardiomyocyte size is considered to be inversely proportional to cardiomyocyte number in models of diabetes-induced HF [66]. Early studies suggested that hyperglycaemia alone can induce cardiomyocyte apoptosis by inducing mitochondrial cytochrome C release and concomitantly increasing flux of the pro-apoptotic Bax-caspase 3 cascade [67,68]. *In vitro* activation of this same pro-apoptotic pathway in human pancreatic β -islet cells administered high glucose has also been documented [69]. Furthermore, reactive oxygen species (ROS) production in cardiomyocytes also contributes to apoptosis via the same cascade [70], as well as directly facilitating cardiomyocyte autophagy and necroptosis [71]. Although the mechanism of ROS facilitating myocyte apoptosis remains unclear, a number of pharmacological agents targeting NADPH-oxidase subunits (further discussed in section 1.2.5) mitigate cardiomyocyte apoptosis in T1D [21,72] and T2D mouse models [73], highlighting the importance of ROS generation in diabetic heart disease.

1.2.4 Cardiac fibrosis

Another important structural characteristic of diabetes-induced HF is cardiac fibrosis. The cardiac extracellular matrix (ECM) consists predominantly of collagen, elastin, fibronectin and laminin, and provides structural support for all cells [74–76]. These components that constitute the ECM are regulated mainly by ECM degrading enzymes such as matrix-metalloproteinases (MMPs), which themselves are inhibited by tissue inhibitory metalloproteinases (TIMPs) [77,78]. Cardiac fibrosis in diabetes is evident both as interstitial and perivascular [66,79] and relies predominantly on deposition of collagen types I and III [77,78,80–83]. Indeed, in human cardiac biopsies, patients with diabetes exhibit a marked increase in both left and right ventricular cardiac fibrosis [84,85]. In rodent models of T1D and T2D, reduced MMPs and elevated TIMPs have been shown to increase collagen deposition, resulting in LV stiffness and diastolic dysfunction (Table 1.1) [86]. Hyperglycaemia has been reported to directly contribute to collagen deposition in rats with T1D, which is closely associated with the levels of glycated haemoglobin (% HbA1c, Table 1.1) [86]. *In vitro* cultured fibroblasts isolated from T2D (*db/db*) mouse hearts exhibit decreased activation of protein-kinase B (otherwise known as Akt) and subsequently increased nuclear factor kappa B (NFκB) transcription, which suggests a role for inflammation T2D-induced cardiac fibrosis [87]. Advanced glycated end-products (AGEs) are also implicated in remodelling in the diabetic heart [88–90]. AGEs are a group of heterogeneous compounds, such as proteins or lipids that become glycated in the context of hyperglycaemia [88,91]. Rats with STZ-induced T1D exhibit increases in AGEs, which are associated with greater collagen cross-linking and deposition in cardiac tissue, associated with impaired diastolic function [80,92]. T1D patients also typically display elevated circulating AGEs [92,93], although this is not described in clinical T2D. Despite acknowledging the importance of cardiac fibrosis in diabetic heart disease, there still remains a significant gap in our knowledge regarding induction and progression of fibrosis in the diabetic heart (as detailed in our recent review included in the Appendix Section [76]).

1.2.5 ROS generation and oxidative stress

The development and progression of diabetes-induced HF is also associated with oxidative stress and generation of ROS [94]. Endogenous oxidant species such as superoxide, hydrogen peroxide, hydroxyl radicals and peroxynitrite are the major components contributing to the imbalance in myocardial ROS, all of which are typically elevated in diabetes-induced HF [95–97]. Exogenous hydroxyl radicals administered *ex vivo* to isolated mouse hearts reduces LV contractility by modulating sarcoplasmic reticulum calcium handling [98]. Moreover, superoxide and peroxynitrite have also been associated with pathological cardiomyocyte hypertrophy [95]. NADPH oxidase (NOX) is a transmembrane protein on intracellular organelles that is a primary source of ROS in cardiomyocytes [99] and is believed to catalyse the production of superoxide in diabetes [21,100,101]. Specific genetic depletion of the Rac1 protein in cardiomyocytes has been reported to attenuate myocardial fibrosis and cardiomyocyte hypertrophy in murine T1D-induced cardiomyopathy via NOX-signalling [102]. Subunits of NOX including p22^{phox} and p47^{phox} are also

elevated in experimental models of T1D and T2D [71,94]. Furthermore, supplementation of the antioxidant coenzyme Q10 in mice with STZ-induced T1D [54] and *db/db* T2D mice [19] reduces the diabetes-induced increase in p22^{phox} and p47^{phox} expression, and is associated with attenuated diastolic dysfunction and reduced apoptosis. Despite showing efficacy in pre-clinical trials [96,97,103–106], and safety in clinical trials [107], it remains to be determined if coenzyme Q10 achieves protection against diabetes-induced HF, or indeed, any form of CV disease in the clinic. This is the case with most ROS-reducing agents; effective antioxidants are yet to be stringently investigated in well-designed clinical trials in patients with diabetes and HF. Importantly, ROS generation is also closely associated with inflammation and dysregulated immune cell activity, but is less described in the context of diabetes-induced HF.

Table 1.1: Phenotypic summary of most commonly used mouse models for studying diabetes

<i>Mouse models of diabetes</i>	<i>Type of diabetes</i>	<i>BGL</i>	<i>Body weight</i>	<i>Cardiac function</i>	<i>Myocyte size</i>	<i>Myocyte apoptosis</i>	<i>Cardiac fibrosis</i>	<i>Oxidative stress</i>	<i>References</i>
STZ	T1D	↑	↓	↓	↑	↑	↑	↑	[45,47-50]
STZ-HFD	T2D	↑	↔	↓	↔	↔	↔	↑	[5,53]
Ins^{2WT/C96Y} Akita	T1D	↑	↔	↓	↔	↑	↑	↔	[55,237]
<i>Lep^{db-}</i> (<i>db/db</i>)	T2D	↑	↑	↓	↔	↑	↔	↑	[19,55,87]
<i>Lep^{ob-}</i> (<i>ob/ob</i>)	T2D	↑	↑	↓	↔	↑	↔	↑	[198-200]
HFD	T2D	↑	↑	↓	ND	↑	↑	↑	[51,52]

T1D = type-1 diabetes, T2D = type-2 diabetes, BGL = blood glucose levels, HFD = high-fat diet. ND, not yet determined; ↑, increased; ↓, decreased; ↔, unchanged.

Established characteristics of the diabetic heart

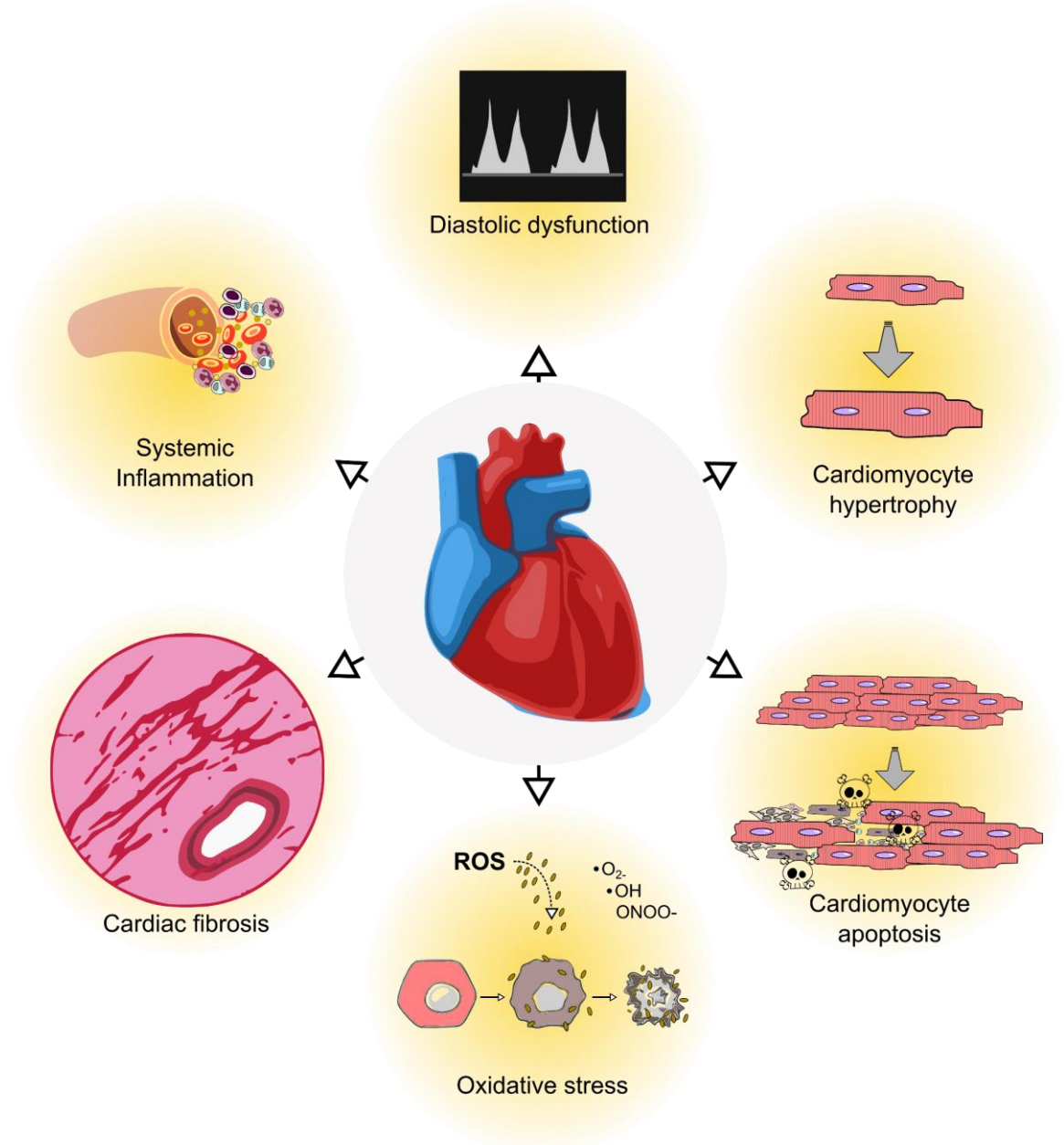


Figure 1.1: Classical characteristics contributing to diabetes-induced heart failure

Illustrates the aforementioned characteristics that contribute to pathological remodelling of the diabetic heart. These highlight the multifactorial mechanisms that contribute to cardiac pathology in diabetes: with myocyte hypertrophy and apoptosis, ROS generation and oxidative stress, cardiac fibrosis, and systemic inflammation (further discussed in Section 1.3).

1.3 The emerging role of leukocytes in diabetes and CV disease

1.3.1 Leukocytes

Whilst the role of inflammation in the pathogenesis of diabetes and HF has been broadly described [108,109] less attention has been applied to the role of specific immune cells in this context. Leukocytes are essential cellular mediators of immune responses, providing the host with protection from invading pathogens. These are generally derived from bone marrow-derived stem-cell haematopoiesis [110], however a range of tissue-specific (resident) leukocytes are also present in low numbers in most tissues, originating from embryogenesis [111,112]. T1D and T2D are associated with elevated circulating leukocyte levels in both animal models [113,114] and in the clinic [115–119]. Furthermore, pro-inflammatory cytokines (primarily released from leukocytes) such as interleukin (IL)-1 β , IL-6 and TNF α are chronically elevated in T2D [118,120–122]. An increased circulating leukocyte count is also an independent risk factor for CV disease [123–126]. Systemic leukocytes secrete various factors in clinical CV disease such as TGF- β , IL-1 β , IL-6, CSF-1 and IFN [127–129]. Furthermore, leukocytes have been comprehensively studied in the setting of atherosclerosis; typically migrating to fatty streaks within plaque obstructed vessels where they contribute to advancement of atherosclerotic lesion development [130–135]. It is likely that leukocytes are involved in the development and progression of diabetes and CV disease, however the extent to which they exert their effects remain unclear. In this section, I discuss the current knowledge regarding the role of leukocytes in both CV disease and diabetes in order to obtain a detailed picture regarding their known role in disease.

1.3.2 Granulocytes

Granulocytes are leukocyte subtypes including neutrophils and mast cells, with characteristic ‘granules’, containing catalytic enzymes that are released upon infection and allergic reaction. Neutrophils, a mature sub-type of the myeloid-granulocyte lineage, generally regulate the acute-phase response of the innate immune system to stress and are implicated in diabetes and CV disease [136]. Hyperglycaemia is associated with neutrophil dysfunction in diabetes [118,120–122]. Hyperglycaemia-driven neutrophil activation has been shown to impair wound healing in both T1D and T2D mice [121], by undergoing a process known as deposition of ‘neutrophil extracellular traps’ (NETosis) [137]. It is postulated that neutrophil dysfunction in diabetes contributes to microvascular complications and leads to increased rates of limb amputation [138]. An important mechanistic study in murine T1D, suggests that neutrophils release the S100A8/9 heterodimer as a response to hyperglycaemic stress [113]. The release of S100A8/9 from neutrophils increases circulating pro-inflammatory Ly6C^{hi} monocytes through activation of AGE receptors (RAGE) on liver K pffer cells, which in turn stimulates haematopoiesis within the bone marrow, resulting in monocytosis [113]. Neutrophilia is also commonly reported in the setting of atherosclerosis. Hypercholesterolaemic ApoE^{-/-} knockout (KO) mice susceptible to atherosclerosis in the absence of diabetes demonstrated increased neutrophil degranulation and migration to vascular plaques [132]. In the same study, the degree of atherosclerosis was reduced by repetitive intraperitoneal

(i.p.) injections of the neutrophil-depleting antibody ‘1A8’ (which binds neutrophil-specific surface protein Ly6G), highlighting their role in the pathogenesis of experimental atherosclerosis. Neutrophils also play a critical role in myocardial infarction (MI) [139]. Post-infarct, neutrophils are among the first immune cells to initiate adverse myocardial remodelling in ischemia-reperfusion (I/R)-induced MI [140]. Although some trials suggest neutrophils facilitate pathological cardiac remodelling [141,142], there are conflicting reports regarding their function. Indeed, neutrophils can also exhibit reparative properties in response to MI injury by communicating with macrophages, which subsequently polarise toward a ‘pro-resolving’ phenotype [143]. While there is a clear appreciation for a role of neutrophils in acute HF such as MI, the role of neutrophils in chronic HF development remains ambiguous. Furthermore, the role of neutrophils in clinical diabetes remains unclear despite these cells being implicated in animal models of diabetes.

Mast cells are a structurally similar granulocyte-myeloid progenitor to neutrophils, however these cells tend to reside exclusively within tissues [144,145]. Interestingly, mast cells are typically associated with the allergic response, and are also implicated in HF [146,147]. The presence of cardiac mast cells was first discovered in the 1950s [131], however studies in the early 1990’s serendipitously implicated their role in the heart, suggesting that healthy patients can suffer from MI after wasp stings [148,149]. Although cardiac mast cells are present in low numbers in the heart, they are particularly vulnerable to circulating mediators, such as chemokines, cytokines, and pro-inflammatory monocytes [150,151]. Mast cells in CV disease are stimulated by several circulating immune factors including IgE and IgG antibodies, as well as the many circulating cytokines (mentioned in Section 1.3.1) [152]. The mast cell secretome has been implicated in the development of cardiac fibrosis and collagen deposition in pressure-overload mouse models, through chronic release of TNF α , IL-1 β , TGF- β , chymase and tryptase [152]. Mast cells also secrete renin, contributing to Ang II-induced hypertension and consequent cardiovascular abnormalities [153,154]. These mediators are also reported to communicate with fibroblasts to initiate their differentiation and activation [152]. Activated mast cells induce rat and human endothelial cell (EC) apoptosis *in vitro* by releasing chymase and TNF α to inactivate pro-survival focal adhesion kinase (FAK) signalling [155]. In a similar fashion, mast cell chymase release also induces apoptosis of vascular smooth muscle cells *in vitro*, via disruption of NF- κ B signalling, FAK-inactivation, and inhibition of Akt phosphorylation [156]. *In vivo* studies suggest a more complex involvement of mast cells in cardiac pathology. Early rodent studies demonstrate that cardiac hypoxia can trigger mast cell degranulation and concomitant leukocyte emigration in mesenteric arteries [157]. Furthermore, mast cells have the capacity to increase cardiac platelet-derived growth factor alpha (PDGF-A) gene and protein expression in pressure-overload HF, increasing cardiac fibrosis and contributing to atrial fibrillation [150]. Endothelial cell-derived C-type natriuretic peptide (CNP) limits perivascular mast cell degranulation after I/R injury [158], highlighting the importance of EC-mast cell communication. The role of mast cells in CV disease is still controversial, and their role in the development of diabetes-induced HF is understudied. Comprehensive *in vitro* studies do

suggest their role in CV disease, however further investigations in animal models are required. Furthermore, detection methods for identifying mast cells *in vivo* are currently limited, making it difficult to assess their physiological involvement in CV disease.

1.3.3 Monocytes and macrophages

Monocytes are a key patrolling hematopoietic cell population regulating cellular homeostasis, with diabetes leading to monocytosis and dysregulated function [159,160]. Monocytes typically egress from blood vessels into tissues, where they differentiate, and secrete factors specific to their local environment [161]. There is mounting evidence that monocytosis occurs in both diabetic animal models [113–115,119] and in diabetic patients [162,163]. Monocytes from patients with T1D [162] and T2D [163] augment secretion of pro-inflammatory T-cell specific cytokines, increasing T_H17 and T_H1 lymphocytes [163] to areas of local injury, highlighting the communication between both adaptive and innate arms of the immune system.

Resident cardiac macrophages also play a pivotal role in regulating circulating leukocyte extravasation, attracting effector cells such as monocytes, neutrophils and lymphocytes [164]. Increased macrophage abundance in the pancreatic islets has been linked to T2D in both rodents [165] and humans [166]. More recently, using both multiphoton and electron microscopy, Zinselmeyer *et al.* reported that mouse pancreatic macrophages phagocytose functional insulin-containing vesicles released from pancreatic β -islets, while the islets themselves remain functional [167]. These macrophages subsequently present immunogenic insulin peptides on their major histocompatibility complex 2 (MHCII) antigens, for other patrolling leukocytes to detect. This could, at least in part, explain pancreatic dysfunction in diabetes, however the driving factors regulating insulin endocytosis into neighbouring macrophages remain understudied. While this study may suggest a possible mechanism for global insulin resistance, no study to date has reported this phenomenon in other organs.

Macrophages in the kidneys of T2D patients are increased in number [168], which has traditionally been associated with renal failure [169,170]. Macrophage abundance is also prominent in adipose tissue, most accumulating in visceral deposits in humans [171]. Current theories pertaining to adipose tissue suggest that resident macrophages induce monocyte and granulocyte infiltration to adipose and neighbouring tissues by secreting monocyte and granulocyte growth stimulating factors (M and G-CSF respectively) as well as the predominant monocyte chemoattractant ‘C-C motif ligand 2’ (CCL2/MCP-1) [172]. This may partially explain the low-grade systemic inflammation that is evident in diabetes [173], particularly in obese patients with T2D [171].

Resident cardiac macrophages are also abundant in the healthy murine myocardium accounting for approximately 10% of cardiac cell abundance [174]. Although resident cardiac macrophages are considered to be quiescent at steady state, they become heavily involved in immune cell recruitment and cardiac repair in CV disease [175]. Fate-mapping of murine macrophages post MI suggests that

circulating monocytes are recruited to the infarct, by releasing a number of pro-inflammatory, chemotactic mediators [176]. Several studies however, suggest paradoxical roles of cardiac macrophages in cardiac pathogenesis [177–180] and cardiac repair [181,182], which is similarly reported in other tissues such as the adipose [114,171,172]. Resident macrophages have also been associated with regulation of cardiac electrical conductance via communication with gap-junctions in the atrioventricular node [183], which is consistent with earlier literature in humans, rabbits and rats [180,184–186]. Moreover, monocyte-derived macrophages can also contribute to collagen deposition by secreting cytokines including, but not limited to, $\text{TNF}\alpha$, $\text{IL-1}\beta$, $\text{TGF-}\beta$ and IL-6 , which in turn either directly or indirectly activate fibroblasts to promote ECM deposition [187].

Macrophages and monocytes can also accumulate in atherosclerotic plaques in the lead up to coronary artery disease (CAD) by adhering to the vascular wall and exacerbating the vascular plaque [188]. Single-cell RNA sequencing (scRNAseq; discussed further in Section 1.4.1) of atherosclerotic plaques from mice on a Western diet recently revealed numerous disparate clusters of macrophages residing in atherosclerotic lesions, highlighting their heterogeneity in this pathology [189]. Work from our laboratories using the same technique also suggests similar heterogeneity of macrophages in the heart during Ang II-induced hypertension (Jelenic M*, Dona M.I* *et al*, *unpublished*). Although macrophages can be perceived an attractive therapeutic target, these cells are not monolithic and form a complex cellular network relative to their environment. Because of their plasticity and our lack of knowledge surrounding macrophage phenotypes and function, it may be difficult to develop therapeutics that target pro-inflammatory macrophages without simultaneously targeting anti-inflammatory macrophages. What remains clear is the consistency in which monocytes and macrophages contribute to immunometabolic dysfunction in a tissue specific manner, which exemplifies the importance of understanding macrophage function in disease.

1.3.4 Lymphocytes

Lymphocytes include Natural Killer (NK) cells as well as T and B-cells, which also originate in the bone marrow. Immature lymphocytes that travel to the thymus mature into T-lymphocytes, whilst the remaining cells differentiate into B-lymphocytes in the spleen [190]. Lymphocytes are systemically altered in human T1D and T2D [119], and have been widely studied particularly in T1D due to their implication in autoimmune diseases [191]. An anti-inflammatory T-lymphocyte, T-regulatory cells (Tregs) exhibit defective anti-inflammatory function in T1D [192,193], which is recognised as a primary contribution to the demise of the pancreas and to other autoimmune abnormalities [194–197]. B-cells in obese mouse models (Leptin ligand deficient ‘*ob/ob*’ [198–200] and HFD-induced obese mice) facilitate cellular cross-talk with macrophages and T-cells, resulting in markedly elevated pathogenic IgG antibodies [201]. Reversal of this was also achieved in the same study by administration of anti-CD20, a B-cell depleting antibody [201]. Furthermore, these authors report that elevated B-cell cytokine release is proportional to glucose intolerance in

the *ob/ob* mouse, suggesting glucose handling is impaired by chronic B-cell activation. NK cells are also implicated in obesity and possibly diabetes. NK cells are innate lymphocytes that carry out cytotoxic actions against pathogens without previous antigen exposure [202]. In human childhood obesity, increased lipid flux and consequent intracellular lipid accumulation in NK cells alters their intracellular programming and reduces their effector function [202,203]. Although little evidence exists in regards to diabetes, aberrant C-type lectin-like NKG2D signalling in murine T1D [204,205] and in T1D-adolescents [206] has been reported, suggesting that hyperglycaemia may also contribute to defective NK function [207,208]. Although this is yet to be characterised in T2D, NK dysfunction is highly probable considering the range of comorbidities of T2D.

In CV disease, low systemic lymphocyte count in humans is used as a prognostic marker for acute CV disease [209]. This was corroborated by a large-scale clinical trial ('EVEREST' trial) indicating an inverse correlation with lymphocyte count and all-cause mortality, CV mortality and hospitalisation for HF in admitted patients with HFpEF [210]. However, there are conflicting reports pertaining to clinical lymphocytopenia, depending on the disease context. Patients with chronic or congestive HF (CHF) increase production of T-lymphocytes, particularly the CD4⁺ T lymphocytes (T-helper 1; [Th1]) and Th17 phenotypes rather than anti-inflammatory T-regulatory cells (Tregs) [211,212]. In the murine ischemic heart post-MI, Tregs become dysfunctional, exhibiting deficient immunosuppression, anti-angiogenic properties and elevated pro-inflammatory cytokine secretion [213]. Similarly, Ang II-induced hypertension increases T-cell accumulation in the aorta accompanied by elevated CCL2 expression, which is also attributed to monocyte migration [212]. In the context of the diabetic heart, little is known about the specific role of lymphocytes. Patients with concomitant CAD and T2D co-morbidities exhibit an elevated Th1 cytokine profile and reduced Th2 profile in peripheral blood [214]. Genetic knockdown of Rag1—resulting in loss of mature lymphocytes—in STZ-induced murine diabetic cardiomyopathy [215] attenuates cardiac fibrosis and improves cardiac function, implicating lymphocytes in the pathogenesis of diabetes-induced cardiac remodelling [216]. Although broadly targeting lymphocytes in heart disease is an unlikely therapeutic avenue, more specific analyses of their subtypes may provide valuable insights into their specific role in cardiac pathology.

1.3.5 The specific role of leukocytes in diabetes-induced HF remains unknown

As discussed, much is known about the immune system in the setting of CV disease and diabetic complications, however the specific role of leukocytes in the progression and development of HF in diabetes remains understudied. There have been attempts at demonstrating individual roles of immune cells such as macrophages [217] and mast cells [47] and other immune cells [109] in diabetes-induced HF, as well as clinical association studies suggesting their involvement [122,139,210,218]. However, it is becoming clear that understanding the role of the immune system in the diabetic heart requires more comprehensive analysis in the context of the entire cardiac cell

ecosystem, to gain a comprehensive picture of the primary cellular and molecular protagonists leading to HF in diabetes.

1.4 Reappraising the cardiac cellular composition

In the last five years, there has been a paradigm shift regarding our knowledge of the cardiac cellular composition, which has been catalysed by innovations in tissue flow cytometry and the inception of single-cell transcriptomics (scRNAseq). The mammalian heart consists of a complex, heterogeneous network of cells, which until recently have not been systematically validated [174]. Cardiomyocytes contribute to the majority of heart mass [219] and hence cardiac cell abundance was historically considered to primarily constitute myocytes. Advances in tissue cytometry have allowed for quantification of non-myocyte cell abundance in the heart, highlighting distinct cardiac cellular diversity (Figure 1.2). The non-myocyte fraction of the heart is composed of endothelial cells (ECs; ~64%), resident mesenchymal cells (RMCs; ~27%) and leukocytes (~9%), far outweighing cardiomyocyte abundance [174]. In this study however, the disparate cardiac chambers (LV, right ventricle [RV] and intraventricular septum [IVC]) of the murine hearts were not assessed, but rather pooled together. In addition, the atria were not considered providing an important gap in knowledge yet to be answered. This is important given the bulk cardiac transcriptomic landscape differs significantly between the anatomical regions of the heart [220], which is likely accompanied by cellular composition changes. Nevertheless, enigmatic cell types such as pericytes, lymphatic ECs (LECs), endocardial cells and NK cells are among the many cell types now detectable in the heart using these modalities (Figure 1.2), highlighting their efficacy in detecting even rare cell populations. Moreover, recent high-resolution proteomic approaches are providing additional information regarding cellular alterations and translation of the cardiac transcriptome, given that transcriptomic changes may not always reflect proteomic perturbations [221]. These improvements in our knowledge of cardiac cellular abundance has facilitated identification of novel cardiac cells, providing a framework for more comprehensive surveying of the heart, using techniques such as scRNAseq.

1.4.1 Single-cell RNA sequencing

More recently, a significant leap in our understanding of the heart has been supported by technologies such as scRNAseq [222], enabling transcriptional profiling of individual cardiac cells in unprecedented detail. Historically, the majority of transcriptional analyses of tissue systems, including the heart, have been conducted under the assumption that these are a homogenous collection of cells, resulting in less sensitive and possibly skewed data. Single-cell transcriptomics is a recently established technology enabling high-resolution RNA sequencing of individual cellular transcriptomes within a given tissue or cell preparation, providing mechanistic insights into the cellular dynamics of a given tissue [223–225]. Information about tissue heterogeneity is critical for applying techniques such as scRNAseq, to avoid oversampling of highly abundant cells, such as cardiac endothelial cells. Successful implementation of techniques such as flow cytometry and

scRNAseq provide important advancements toward understanding the molecular processes in health and disease.

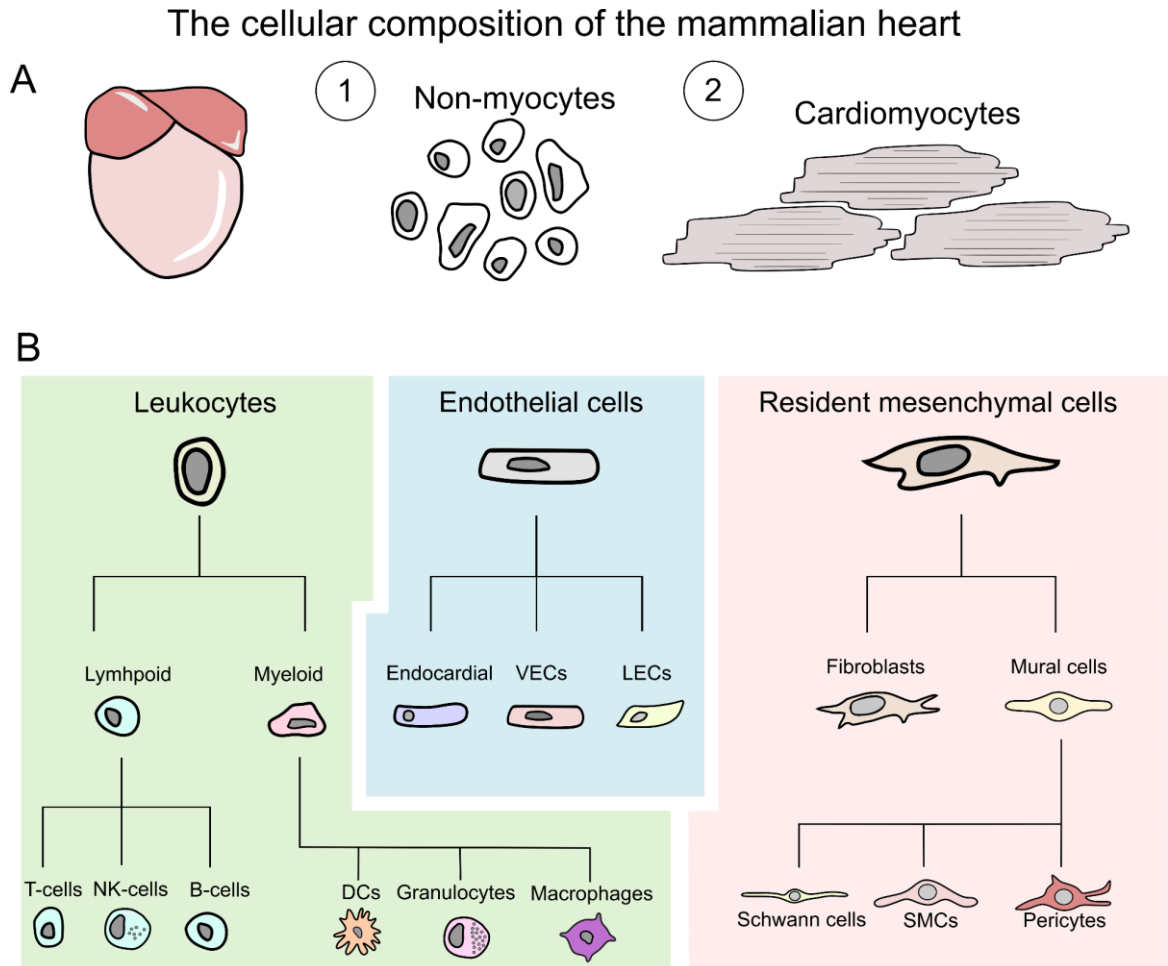


Figure 1.2: The cellular composition of the murine heart

(A) The murine heart (left) and its two major cellular components; (1) the non-myocyte fraction and (2) the cardiomyocyte fraction. **(B)** Illustrates the non-myocyte cellular fraction only, showing the disparate array of cell classes that exist within the murine myocardium. Abbreviations: DCs = dendritic cells, VECs = vascular endothelial cells, LECs = lymphatic endothelial cells, SMCs = smooth muscle cells.

1.4.2 Single-cell RNA sequencing of the healthy murine myocardium

Skelly and colleagues [225] reported the one of the first single-cell transcriptomic analyses of cardiac non-myocytes in healthy adult mouse hearts. Using the droplet-based, 10X Chromium platform, scRNAseq of cardiac non-myocytes revealed a complex ensemble of cells and communication networks in homeostasis [225]. Advancements in bioinformatic pipelines have also allowed for inference of autocrine and paracrine inter-cellular communications *in silico*, highlighting the importance of non-myocytes in maintaining cardiac homeostasis [226]. It was also noted that fibroblasts were most highly enriched for transcripts corresponding to vessel trophic factors, such as *Vegf* and *Igf1* [225]. Fibroblasts also actively secrete cytokines such as *Csf1* and *Il34*, which bind to CSF-1 receptors, regulating resident macrophage homeostasis [225] further implying they play a role in maintaining the local cellular milieu. Other cells such as pericytes also actively secrete a range of ligands including *Il34*, nerve growth factor (*Ngf*) and neurotrophin 3 (*Ntf3*), which support macrophage and neuron homeostasis [225,227,228]. Cell-specific sexual dimorphisms between male and female hearts were also distinctly evident, which is unsurprising considering male and female cardiac pathology differs in the clinic [229]. The granularity of such data has resulted in increasing interest about the cardiac cellulome in the setting of disease, considering the importance of non-myocyte cells in cardiac homeostasis. Moreover, scRNAseq and other next generation sequencing techniques, such as transposase-mediated analysis of open chromatin regions (ATAC-Seq) [230] and high resolution proteomics [221] will provide additional mechanistic insight into the cellular dynamics in disease.

1.4.3 Single-cell RNA sequencing of the diseased murine myocardium

Among the first studies to utilise scRNAseq in cardiac pathology was reported in the context of MI, whereby cardiac cells were collected exclusively from the infarct area (or equivalent for sham mice), including cardiomyocytes [231]. This study focused heavily on fibroblasts, suggesting that cytoskeleton-associated protein-4 (CKAP4) is a primary regulator in fibroblast activation in MI relative to sham controls. This was further validated histologically in mouse and human heart sections, whereby CKAP4 co-localises with common fibroblast markers such as platelet-derived growth factor receptor (PDGFR) and alpha smooth muscle actin (ACTA2) [231]. Furthermore, cardiomyocytes separate into 4 distinct clusters according to their genetic signature, suggesting variability in myocyte phenotype and function. Of note, this study showed that a cardiomyocyte subtype in close proximity to the epicardium highly expresses Myozenin-2 (*Myoz2*), which is known to inhibit calcineurin-induced myocyte hypertrophy [232]. Although its biological relevance is ambiguous, it suggests that cardiomyocytes may also display heterogeneity and that some subtypes may be more susceptible to various stressors than others. A similar study also focused on non-myocyte heterogeneity in the setting of MI, however isolated the entire non-myocyte fraction of the murine heart, rather than the infarct area alone [233]. Cardiac macrophages in this study displayed distinct differences in their genetic signature and abundance, skewing toward a ‘pro-inflammatory’ phenotype (*Ccr2^{hi}F4/80^{hi}Ly6c2^{hi}H2-Ad^{hi}*) 3-days post MI [233]. Furthermore, these

macrophages displayed heterogeneity in the form of 8 transcriptionally-distinct subtypes, which has not previously described. Seven-days post MI, the cardiac macrophage clusters are characterised primarily by ‘M2-like’ phenotype (*Ccr2^{hi}F4/80^{hi}H2-Aa^{hi}Ly6c2^{lo}*) as well as a distinct shift in fibroblast phenotype, to a ‘myofibroblast-like’ phenotype [233]. Furthermore, two novel fibroblast populations were identified; ‘Wnt-Fibroblasts’ (*Pdgfra^{hi}Col1a1^{hi}Wif1^{hi}*) and Transitory-Fibroblasts (*Pdgfra^{hi}Col1a1^{hi}Cfh^{hi}*) [233], which have also been recently identified by our lab in Ang II-induced cardiac dysfunction [234]. Sub-clustering and *in silico* trajectory analysis of all fibroblasts also revealed that the majority of fibroblasts possess a distinctly different gene signature 3 days post-MI (transitory-like phenotype), the majority of which (~99%) are completely differentiated into myofibroblast-like fibroblasts (*Plac8^{hi}Cthrc1^{hi}Fn1^{hi}*) on day 7 post-MI [233]. Interestingly, *Wif1* encodes multiple ligands in fibroblasts and has been reported to drive cardiac fibrosis [235] while concomitantly contributing to macrophage plasticity, angiogenesis and cardiac repair [236]. The contradictory nature of these fibroblasts suggests that targeting this particular pathway may prove difficult and potentially disrupt important signalling networks for cardiac homeostasis. Indeed, scRNAseq analysis of the acutely insulted myocardium has provided important, novel information regarding the cellular dynamics of MI and cardiac wound healing. However, given that diabetes is a chronic and progressive cardiac stressor, detailed analyses are still warranted in the setting of chronic HF.

The aforementioned gap in knowledge was recently addressed in a murine model of chronic hypertensive HF, whereby chronic Ang II infusion yielded a number of novel and established gene expression programs in the heart [234]. Of note, two transcriptionally distinct novel fibroblast populations significantly upregulated in Ang II treated hearts, namely ‘Fibroblast-*Cilp*’ and ‘Fibroblast-*Thbs4*’. In line with the aforementioned study [233], ‘Wnt-Fibroblasts’ (alternatively denoted as *Wif1*⁺ fibroblasts in this study) were identified, however, were unaltered between experimental groups. Interestingly, both Fibroblast-*Cilp* and Fibroblast-*Thbs4* exclusively emerge after Ang II treatment, and do not actively express *Acta2* – a ubiquitous myofibroblast and smooth muscle cell marker. This was further confirmed histologically, whereby *Acta2*⁺ fibrosis and *Thbs4*⁺ fibroblasts are distributed at different loci. This suggests that in chronic hypertensive HF, cardiac fibrosis is not driven by myofibroblasts, but rather by new matrifibroblast-like cells, highly expressing genes *Cilp* and *Thbs4*. It is also worth noting that (with the exclusion of *Cilp* and *Thbs4* fibroblasts) cell-specific gene expression in this study is highly sexually dimorphic, suggesting that sex should be considered a confounder when developing therapeutics. The findings from this study contribute further knowledge regarding the molecular changes in the cardiac cellulome after chronic AngII insult.

1.4.4 Transcriptomic profiling in the diabetic heart – current knowledge

To date, there are no studies that assess the cardiac transcriptome at the single-cell level, in the context of T2D. Microarray bulk transcriptomic profiling of T1D (Akita^{Ins2^{WT}/C96Y}) male mouse

hearts has shown significant increases in genes including fibroblast growth factor-12 (*Fgf12*), natriuretic peptide type-A (*Nppa*), thrombospondin type-1 (*Thbs1*) and angiopoietin-like-4 (*Angptl4*) [237]. *Fgf12* and *Thbs1* are genes encoding for proteins known to induce cardiac fibrosis via various pathways [238,239], which is also evident histologically in this study [237]. Elevated *Nppa* and other associated cardiac pro-hypertrophic genes were also histologically validated by increases in cardiomyocyte size. *Angptl4* is well documented in diabetes and obesity, regulating glucose homeostasis [240,241], lipid metabolism [241,242] and insulin sensitivity [240,243] throughout the body, however its role in the heart is still unclear. A recent transcriptomic study using a similar methodology in *db/db* mice identified a number of up-regulated mitochondrial genes such as *Ucp3*, *Atpb* and *Pdk4* which are associated with altered cardiac lipid metabolism [244]. Interestingly, *Angptl4* is also among the top genes significantly up-regulated in the *db/db* heart [244], consistent with the Akita mouse heart [237]. These findings provide exciting insights into the bulk transcriptomic changes in the diabetic heart. However, there remains an unmet need for more high-resolution and cell-specific information in the diabetic heart. Utility of single-cell technologies in this context will aim to fill this knowledge gap, in order to mechanistically understand the transcriptomic catalysts driving diabetic heart disease.

1.5 Summary

Diabetes confers an increased risk of cardiovascular death and hospitalisation for HF. While classical characteristics of cardiac failure in diabetes are established, the precise cellular and molecular pathophysiology remains unresolved, resulting in difficulty treating this epidemic and its complications. The immune system's involvement in cardiovascular disease and diabetes is becoming increasingly recognised, however the specific role of the immune system in initiation and progression of diabetes-induced HF, remains unclear. Furthermore, considering that the cardiac cellular and molecular composition has been characterised in homeostasis [174,225] and models of CV disease [231,233,234,245], this has yet to be applied to the context of diabetes-induced cardiac dysfunction. While there are some examples of bulk transcriptomic profiling of the heart in the setting of diabetes [237,246], there is still an urgent demand for more detailed, cell-specific analyses. As such, there remains a clear knowledge gap regarding the molecular and cellular dynamics in diabetes-induced HF, which can be filled using single-cell technologies such as flow cytometry and scRNAseq. This new era in cardiac research represents an exciting step forward, which will allow for more comprehensive assessments of cellular and molecular abnormalities in CV disease and hopefully aid in development of more targeted therapies.

1.6 Aims and Hypothesis

The overarching aims of this thesis were to (1) determine the differences in cardiac cellularity in two mouse models of T2D, (2) to determine the cardiac single-cell transcriptome in the *db/db* mouse model of T2D, and (3) to immunophenotype human blood from healthy and diabetic patients, to better understand the understudied biochemical processes that may underlie diabetes-induced cardiac dysfunction. For Chapter 3, I selected the STZ-HFD mouse model of diabetic

cardiomyopathy for initial analysis of the cardiac cellular landscape due to its recent characterisation and availability [53]. Pertaining to Chapter 4, due to the variability in cardiac phenotype in the literature, I conducted a time-course experiment using *db/db* mice, in order to determine the appropriate age in which this model exhibits cardiac dysfunction, to proceed with single-cell transcriptomic analysis. In this thesis, I postulated that T2D would alter the cardiac cellular and molecular landscape associated with cardiac functional impairment. In addition, I propose that leukocytes will play a key role in cardiac remodelling in this context. Each specific aim is briefly outlined below, in chapter format.

Chapter 2

General methodology relevant to all of the data in this dissertation.

Chapter 3

Aim 1: To determine the differences in the cardiac non-myocyte cellular landscape in a mouse model of T2D-induced HF. Here, I have performed cardiac and systemic flow cytometry as well as immunohistochemistry to decipher the key non-myocyte cells that are altered in a murine model of T2D-induced HF [53].

Chapter 4

Aim 2: To determine the progressive alterations in cardiac cellularity in a time-course study, using the *db/db* mouse model of T2D. Separate cohorts of *db/db* mice and their heterozygote control counterparts (*db/h*) were monitored and subsequently euthanised at 10, 17 and 24-weeks of age. Analogous to Chapter 2, I have performed cardiac and systemic flow cytometry at each of these time points in separate cohorts, to determine the cellular shifts as a consequence of genetically induced murine T2D.

Chapter 5

Aim 3: To interrogate the cardiac single-cell transcriptome (using scRNAseq) of the *db/db* mouse heart. Mice were euthanised at 17-weeks of age in this Aim. Here, I have identified a number of transcriptional alterations that provide novel insights into the cell-specific molecular processes contributing to T2D-induced cardiac dysfunction.

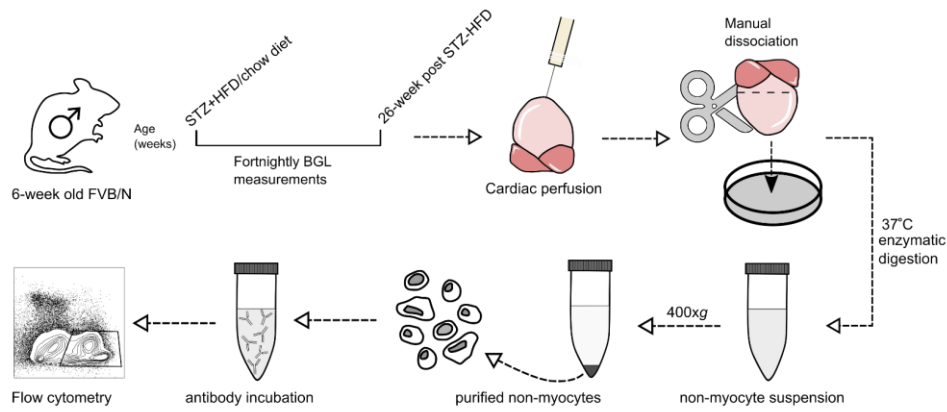
Chapter 6

Aim 4: To determine the cellular changes in human blood in patients with or without diabetes via a preliminary clinical trial held at the Baker Heart and Diabetes Institute Diabetes Clinic. Considering that diabetes typically elicits monocytosis and neutrophilia, I conducted a small clinical trial and performed whole-blood flow cytometry capable of detecting circulating leukocyte proportions in patients with T1D and T2D, as well as incorporation of appropriate ND controls. While I have attempted to obtain adequate statistical power, recruitment for this study was halted due to the COVID-19 pandemic. Hence, the data from this study is preliminary, due to unprecedented low *n* values.

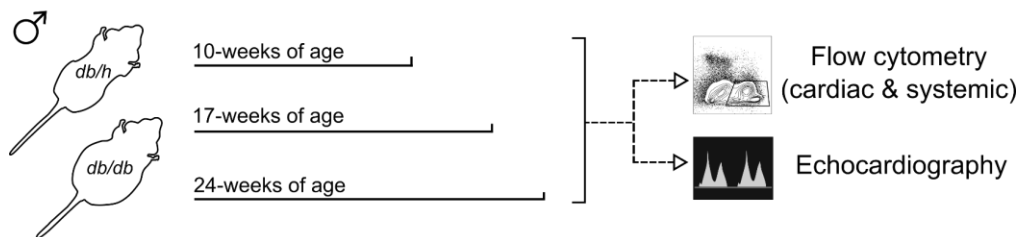
Chapter 7

General discussion: Here, I discuss the significance and broader picture of the findings from all the studies within this thesis, and highlight the future directions for research in diabetes-induced heart disease.

Aim 1 - optimising and completing cardiac flow cytometry in STZ-HFD diabetic mice

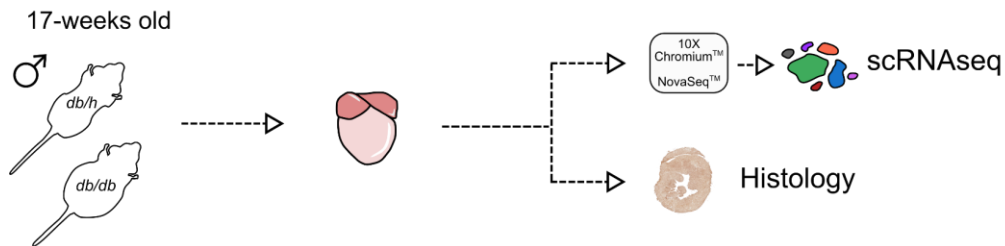


Aim 2 - Cardiac flow cytometry in *db/db* mice at three time-points

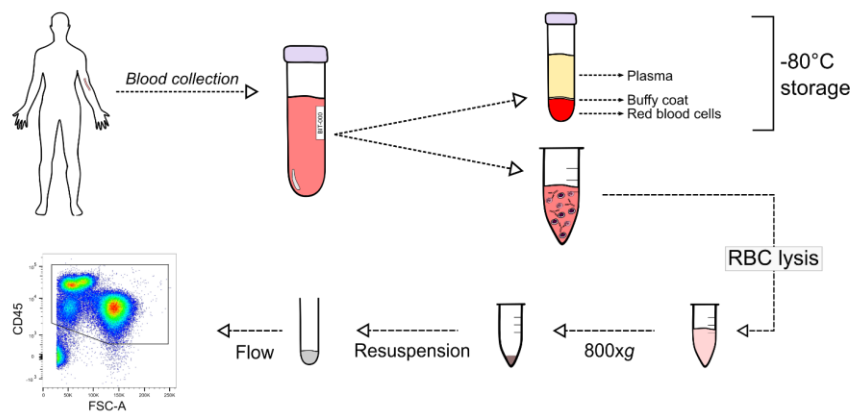


Aim 3 - Single-cell RNA sequencing in *db/db* mice at 17-weeks of age

scRNAseq component



Aim 4 - Immunophenotyping human blood in diabetes: a preliminary clinical trial



Outcome

Framework for understanding the cellular and molecular dynamics in diabetic heart disease

Figure 1.3: Illustrates the general experimental design of each Aim and also summarises major results findings from each Aim. Abbreviations: scRNAseq = single-cell RNA sequencing, RBC = red blood cell, STZ = streptozotocin, HFD = high-fat diet, T1D = type-1 diabetes, T2D = type-2 diabetes.

Chapter 2

General methodology

2.1 Experimental animals

All animal-related experiments were approved by the Alfred Research Alliance (ARA) Animal Ethics Committee (Ethics approval numbers: E/1681/2016/B, E/1880/2019/B) and were performed in accordance with the National Health and Medical Research Council of Australia (NHMRC). Mice had access to food and water *ad libitum* and were housed at 22°C on a 12 hour light/dark cycle.

2.2 Animal models of diabetes

2.2.1 STZ-HFD model of type-2 diabetes

Friend Virus B NIH (FVB/N/J) mice were sourced from the ARA Animal Services (provided in three separate cohorts). Male 6-week-old FVB/N/J mice were randomly allocated into the non-diabetic (ND, $n = 7$) citrate vehicle control group fed standard chow diet (12% energy intake from lipids), or diabetes mellitus (diabetes, $n = 19$) which was induced by the combination of low-dose streptozotocin (STZ; cat# AG-CN2-0046, AdipoGen Life Sciences, NSW, Australia) and fed a high-fat-diet (HFD; SF04-001, Specialty Feeds, WA, Australia, 43% energy intake from lipids). STZ was administered by three consecutive daily intraperitoneal (i.p.) injections (55mg/kg body weight in 0.1mol/L citric acid vehicle, pH 4.5 [cat# 251275, Sigma-Aldrich, USA]). Mice administered STZ were subsequently fed a HFD *ad libitum* for 26-weeks, as previously described [53]. While on this occasion this STZ-HFD mice exhibited hyperglycaemia, monocytosis and impaired glucose tolerance; I did not observe elevated fat mass (in grams or % body weight) or insulin resistance, relative to our previous characterisation of this model [53]. As such, our publication using this model (Chapter 3), I refer to this mouse model more broadly as ‘diabetes mellitus’ (DM).

2.2.2 $Lep^{db-J/db/db}$ model of type-2 diabetes

Male Lep^{db-J} mice (db/db) mice [247] ([B6.BKS(D)-Lepr^{db/J}], stock #000697) were obtained from The Jackson Laboratory (Bar Harbor ME, USA) in three separate cohorts (10, 17 and 24-weeks of age at endpoint). Homozygous db/db mice (spontaneous autosomal recessive global knockout for the leptin receptor) are observably obese at approximately 3-4 weeks of age, with concomitant hyperglycaemia and hyperinsulinaemia. In addition, db/db mice are also polyphagic, polydipsic, and polyuric. In order to confirm the severity of T2D at each time-point, I conducted a range of physiological tests, further elucidated in Section 2.3.1. For flow cytometry experiments, $n = 8$ /genotype unless otherwise stated. For scRNAseq experiments, $n = 4$ for db/db and db/h heterozygote counterparts, unless otherwise stated. Mice had free access to food and water *ad libitum* and were housed at 22°C on a 12-hour light/dark cycle.

2.3 Experimental design

2.3.1 Aim 1: To determine the differences in the cardiac non-myocyte cellular landscape in the STZ-HFD mouse model of T2D-induced heart failure.

Animal care and induction of diabetes is discussed in Section 2.2.1. Blood glucose levels were measured fortnightly via saphenous vein bleeds using a glucometer (Accu-Chek® Performa II, Roche Diagnostics, NSW, Australia). Intraperitoneal glucose and insulin tolerance tests were conducted at endpoint (26-weeks of diabetes, in this model) to assess glucose clearance and insulin resistance *in vivo*, as previously described [53]. Whole-body composition analysis was performed at endpoint using an Echo-MRI™ 4-in-1 700 Analyser (EchoMRI, Houston, TX, USA) to assess percentage fat mass and total lean mass. Percentage glycated haemoglobin (% HbA_{1c}) was also measured at endpoint to assess long-term blood glucose levels (Cobas b 101 POC system, Roche Diagnostics, NSW, Australia). Echocardiography was conducted in mice under anaesthesia (Ketamine/Xylazine/Atropine [KXA], 80/8/0.96mg/kg, i.p.) at 26-weeks post diabetes (32-weeks of age), to assess the extent of cardiac dysfunction. Analysis was conducted at the Baker Heart and Diabetes Institute and quality control was completed by technicians at the Preclinical Cardiology Microsurgery & Imaging Platform (PCMIP). Mice were euthanised by administration of Ketamine/Xylazine (85/8.5mg/kg, i.p.), followed by subsequent exsanguination. As previously described [248], the thoracic cavity was exposed and right atrium was cut to allow for cardiac perfusion through the left-ventricular apex, after which the heart was excised and ventricles were used for flow cytometry. Age and sex-matched, fresh-frozen LV samples embedded in Optimal Cutting Temperature (OCT, Tissue-Tek, Sakura Australia) compound were acquired from a separate cohort of ND and diabetic mice for histological analysis. For further information, see the methodology section in the publication within Chapter 3.

2.3.2 Aim 2: To assess the progressive cardiac cellular differences in the *db/db* mouse model of T2D – a time-course study.

Analogous to section 2.3.1, a range of physiological tests were conducted prior to euthanasia. Blood glucose measurements were performed fortnightly using a glucometer (Accu-Chek® Performa II, Roche Diagnostics). Percentage glycated haemoglobin (% HbA_{1c}) was measured at endpoint to assess long-term blood glucose handling (Cobas b 101 POC system, Roche Diagnostics). Intraperitoneal insulin tolerance testing was performed at end-point to determine insulin sensitivity *in vivo*. Whole-body composition analysis was performed at endpoint using an Echo-MRI™ 4-in-1 700 Analyser (EchoMRI, Houston, TX, USA). Endpoint echocardiography measurements were also performed to assess cardiac function *in vivo*, using a Phillips iE33 ultrasound machine with a 12-MHz sector transducer. For analysis, Doppler flow and tissue Doppler echocardiography were acquired to measure diastolic function, while M-mode echocardiography was utilised for assessment of systolic function.

For flow cytometry experiments, the thoracic cavity was exposed and right atrium was cut to allow for cardiac perfusion as described in Section 2.3.1. Following perfusion, cardiac ventricles (right & left ventricle, intra-ventricular septum) were isolated and placed in 5mL Eppendorf™ tubes with 3mL of ‘enzymatic digestion buffer’ (further detailed in Section 2.9). Cell suspensions from each sample were individually filtered through a 70µM cell strainer into a 15mL tube containing 10mL of phosphate buffered saline (PBS). Samples were then centrifuged at 200×g for 15-minutes without brakes to clear unwanted debris. The supernatant was then aspirated and cell pellets were resuspended in 200µl of 2% ‘HBSS buffer’, before staining with a specific antibody panel for flow cytometry. Cardiac non-myocyte cells were identified using the specific antibody panel (Table 2.2).

2.3.3 Aim 3: To interrogate the single-cell cardiac transcriptome using single-cell RNA sequencing in the dbdb mouse model of T2D-induced heart failure.

All animal related physiological tests were conducted as described in Section 2.3.1. For single-cell RNA sequencing, hearts were prepared following a previously detailed cardiac cell isolation protocol [249], with slight modifications (see Section 2.9 for more specific information regarding this Aim). Briefly, after successful heart digestion, cardiac single cell suspensions were collected for antibody/viability-dye staining and subsequent fluorescence-activated cell sorting (FACS), as described previously [225,234]. FACS sorted non-myocyte cardiac cells were manually counted prior to single-cell transcriptomic library preparation on the 10X Chromium console (10X Genomics). Following cell capture and lysis within oil droplets, cDNA was synthesised and amplified for 12 cycles according to manufacturer’s instructions (10X Genomics). Amplified cDNA was used to construct Illumina sequencing libraries that were each sequenced on one lane (per genotype) of an Illumina NovaSeq 6000. Sequencing data was processed by Cell Ranger pipeline version 5.0.0 (10X Genomics), prior to subsequent bioinformatic analyses in R Studio (further described in Section 2.10).

2.3.4 Aim 4: To assess the differences in circulating leukocytes from human blood in patients with diabetes: a preliminary clinical trial.

Blood samples were collected from elective patients diagnosed with T1D or T2D, referred from the Diabetes Clinical Research Laboratory within the Baker Heart and Diabetes Institute. Healthy non-diabetic (ND) controls were also recruited. Upon recruitment (see Chapter 6 for further information on recruitment and consent), whole blood flow cytometry was performed to detect an array of disparate leukocytes (See Table 2.1). Blood collection tubes (10ml EDTA Vacutainer) were labelled with a unique study identifier (‘BIT-number’) to ensure adequate blinding of diabetic and non-diabetic samples. Subsequently, blood was collected in 10ml EDTA Vacutainer tubes by investigators with an approved phlebotomy accreditation (Mr. Charles Cohen, Ms. Erin Boyle, Mr. Michael Rechtman), and placed in secondary zip-locked, sealed bags provided by Baker investigators (Mr. Charles Cohen, Dr. Miles De Blasio). Upon collection of whole blood, samples were double-blinded with randomly generated numbers (conducted by Dr. Darnel Prakoso), such

that experimental samples were unknown to the investigator performing experiments (Mr. Charles Cohen).

Table 2.1: Human blood flow cytometry antibody panel

Cell type identified	Primary	Clone	Conjugate/fluorophore
Pan B-cell	CD19	RA3-6B2	BD Horizon BV650
Dead cells	DAPI	-	-
Neutrophil	CD15	W6D3	BD Horizon BV421
Monocyte/neutrophil	CD16	3G8	PE/Cy5
Monocyte	CD14	63D3	APC
Pan leukocyte	CD45	2D1	APC/Cy7
Pan T-Cell	CD3	OKT3	PE
Th cells	CD4	OKT4	PE/Cy7
Tc cells	CD8a	RPA-T8	PerCP/Cy5.5
Antigen presenting cells	HLA-DR	G46-6	BUV395

Lists the antibody cocktail utilised for whole blood flow cytometry. Nine antibodies and 1 dye (DAPI) were used in this study to detect a range of leukocytes listed in column 1.

2.4 Animal monitoring

Regardless of the diabetic mouse models utilised in this project, diabetic mice require daily monitoring to ensure optimal health and wellbeing. Daily monitoring checks include (but are not limited to) observing classic murine symptoms of discomfort or stress; such as piloerection, hunched posture, reduced movement and/or social interaction. Both mouse models of diabetes include symptoms such as polyuria, which requires additional, fluid absorbing bedding in each cage (Pure-o' Cel®, ScottPharma Solutions Inc., MA, USA). Furthermore, both mouse models also typically exhibit polydipsia and polyphagia, hence food and water was changed daily. In the event that a mouse displayed any adverse events, or lost more than 5% of their body weight, animals were placed under more rigorous supervision. Aside from frequent observation, any animals fitting the aforementioned criteria received mashed chow (dependent on their diet), water-soaked cotton wool and were placed on a heat pad to ensure they recover as quickly as possible. If an animal did not improve, early euthanasia was performed with approval from the Alfred Alliance Animal Facility Veterinarian staff.

2.5 Blood glucose monitoring and HbA_{1c} measurement

Blood glucose levels were measured fortnightly via saphenous vein bleeds using a glucometer (Accu-Chek® Performa II, Roche Diagnostics, NSW, Australia). For STZ-HFD mice, blood glucose was first measured two weeks post induction of diabetes. For *db/db* mice, blood glucose was measured upon animal arrival. For both cohorts, mice were restrained inside a 50mL centrifuge tube containing breathing holes. Subsequently, the rear right leg was fully extended and fur was parted using Vaseline petroleum jelly (Unilever, Rotterdam, Netherlands), such that the saphenous vein was clearly visible. A 30-gauge needle was then used to puncture the vein, after which exposed blood was aspirated with a glucose strip attached to the glucometer (Accu-Chek® Performa II, Roche Diagnostics, NSW, Australia). Once blood glucose was successfully measured and documented, pressure was applied to the wound with a sterile gauze swab for approximately one minute to stop any bleeding. At endpoint, HbA_{1c} was measured to assess long-term blood glucose handling (information pertaining to animal euthanasia further discussed in Section 2.6). Approximately 2µL of whole blood was pipetted onto a commercially available HbA_{1c} microfluidic cassette and loaded into the hardware system for analysis (Cobas b 101 POC system, Roche, Basel, Switzerland). Acquired measurements were recorded as % HbA_{1c}.

2.6 Animal euthanasia and tissue collection

All mice used in this thesis were euthanised with high-dose ketamine/xylazine/atropine (KXA; 85:8.5:1mg/kg, i.p.), following subsequent exsanguination via cardiac puncture. For more information regarding cardiac perfusion and cardiac flow cytometry, see Section 2.7. In addition, the upper mid portion (~1mm thickness) of the LV, RV and intra-ventricular septum (IVC) was sliced using a 3D-printed apparatus to guide blades in a consistent manner (Figure 2.1). Sliced heart portions were embedded in OCT compound and stored at -80°C for immunohistochemical analysis. Once hearts were perfused and excised for flow cytometry and histology, tissues were collected for storage and further analysis.

For Aim 1, dissected tissues included; liver, spleen and tibias (right: for measurement to correct to organ weights [mm], left: flow cytometry). These tissues were all stored at -80°C for any impending analyses. For Aim 2, tissues excised included; kidneys, fat deposits (separated by loci), pancreas, lungs, gastrocnemius muscle, liver, spleen and tibias. Tissues stored at -80°C included; right kidney, spleen, liver, gastrocnemius, and pancreas. Small portions of the pancreas, liver and the left kidney were fixed in 10% neutral buffered formalin (NBF; Labserv, Pronalys Chemicals, Scoresby, Australia), and paraffin-embedded (conducted by Gribbles Pathology, VIC, Australia) for any relevant histological analysis.



Figure 2.1: Illustrates the technique used to obtain similar regions of the heart for histological analysis. Left: 3D-printed apparatus used for guiding blades, with remaining heart sample for flow cytometry. Right: LV, RV and IVC sliced and embedded in OCT for storage at -80°C .

2.7 Cardiac flow cytometry

For flow cytometry experiments, the thoracic cavity was exposed and right atria was cut to allow for cardiac perfusion (perfusate = PBS supplemented with 0.9mM CaCl_2 , 200mM KCl) as described previously [248]. Hearts were perfused via 30G hypodermic needles attached to a peristaltic pump at a rate of $4\text{mL}/\text{min}$ (Cole Palmer, IL, USA) for ~ 5 minutes, or until the blood within the liver had cleared sufficiently. Following perfusion, cardiac ventricles (right & left ventricle, intra-ventricular septum) were isolated and placed in 5mL Eppendorf™ tubes with 3mL of ‘enzymatic digestion buffer’ ($2\text{mg}/\text{mL}$ collagenase IV [Worthington Biochemical Corporation], $1.2\text{U}/\text{mL}$ dispase II [Sigma-Aldrich] in PBS supplemented with $0.9\text{mmol}/\text{L CaCl}_2$). To facilitate digestion, the tissue and *enzymatic digestion buffer* were incubated at 37°C for 45 minutes and triturated at 15-minute intervals during incubation. Next, cell suspensions from each sample were individually filtered through a $70\mu\text{m}$ cell strainer into a 15mL tube containing 10mL of PBS (supplemented with $0.9\text{mmol}/\text{L CaCl}_2$). Samples were then centrifuged at $200\times g$ for 15-minutes with centrifuge brakes deactivated, for debris clearance. The supernatant was aspirated and cell pellets were resuspended in $200\mu\text{L}$ of 2% FCS/HBSS buffer, before staining with a specific antibody panel for flow cytometry (listed below in Table 2.2 and described in [174,250]). Cardiac non-myocyte cells were identified using the specific antibody panel, after which the heart was excised and ventricles were used for flow cytometry.

2.8 Flow cytometry of whole blood, spleen and bone marrow

Whole blood was obtained by cardiac puncture at endpoint and stained using a leukocyte-specific antibody panel (Table 2.3). Bone marrow from the left tibia was flushed using PBS without Mg^{2+} and Ca^{2+} into 50mL centrifuge tubes. Spleens were manually dissociated and passed through a $35\mu\text{m}$ filter into 50mL centrifuge tubes to obtain a single cell suspension as previously described [113]. Blood, spleen and bone marrow were then subjected to red blood cell (RBC) lysis for 15 minutes at 4°C using an ammonium chloride based commercial lysis buffer (1X dilution, 555899,

Becton Dickinson, USA). After RBC lysis, the remaining stained cells were washed twice in 'Fx buffer' (1 X HBSS [Gibco™, NY, USA], 2% FCS). Between each wash, cells were centrifuged at 400×g for 5 minutes at 4°C. Cells were then resuspended in 200µl of Fx buffer containing 4',6-diamidino-2-phenylindole (DAPI [0.1µg/mL]); and filtered through 35µM mesh into 5mL polystyrene round-bottom tubes (352052, Falcon®, NY, USA) for flow cytometry.

Table 2.2 – Flow cytometry antibody panel utilised in myocardium from mice

Antibody Target/Dye	Cat #	Company	Clone	Staining pattern
CD31	740879	BD Biosciences	390	Endothelial cells
I-A/I-E (MHCII)	743876	BD Biosciences	2G9	B-cells, macrophages
CD11b	564443	BD Biosciences	M1/70	Myeloid cells
CD64 (a & b alloantigens)	740622	BD Biosciences	X54-5/7.1	Macrophages
CD146 (Mcam)	740827	BD Biosciences	ME-9F1	Mural cells
Ly6C	128012	Biolegend	HK1.4	Monocytes
CD59a	130-104-105	Miltenyi Biotec	REA287	Schwann cells
Ly6G	127648	Biolegend	1A8	Granulocytes
NK1.1	108716	Biolegend	PK136	Natural killer cells
CD39	143806	Biolegend	Duha59	Smooth muscle cells
CD90.2	105320	Invitrogen	30-H12	T-cells
CD45	557659	BD Biosciences	30-F11	Pan leukocytes
SYTOX™ Green Dead Cell Stain	S34860	Invitrogen	N/A	Dead cells/nuclear debris
eBioscience™ Calcein Blue AM Viability Dye	65-0855-39	Invitrogen	N/A	Metabolically active cells

Antibody cocktail utilised for flow cytometry of cardiac ventricles. 12 antibodies and 2 dyes (SYTOX green and Calcein blue) were used in this study to detect an array of cardiac non-myocytes. Note: cell types in column 5 are the identifiable cardiac non-myocyte cells and may not apply in different tissue contexts. For more detailed information regarding flow cytometry gating strategies and cellular identification, Chapter 3 (Additional file 1: Figure 2).

Table 2.3 – Flow cytometry antibody panel utilised in whole blood from mice

Antibody Target/Dye	Cat #	Company	Clone	Staining pattern
DAPI	D9542-5MG	Sigma-Aldrich	N/A	Dead cells
CD45R/B220	103241	BD Biosciences	RA3-6B2	B-cells
CD3ε	11-0033-81	BD Biosciences	500A2	T-cells
Gr1 (Ly6G/Ly6C)	552093	BD Biosciences	RB6-8C5	Monocytes & Neutrophils
CD115	135506	BD Biosciences	AFS98	Monocytes
CD4	116016	BD Biosciences	RM4-4	CD4 ⁺ T-cells
CD8	126612	BD Biosciences	YTS156.7.7	CD8 ⁺ T-cells
CD45	557659	BD Biosciences	30-F11	Pan leukocytes

Lists the antibody cocktail utilised for whole blood flow cytometry. 7 antibodies and 1 dye (DAPI) were used in this study to detect a range of leukocytes. Note: cell types in column 5 are the identifiable cells for the purpose of this study and may not apply in different contexts. For more detailed information regarding flow cytometry gating strategies and cellular identification, see Chapter 3 (Additional file 1: Figure 2).

2.9 Cardiac single-cell RNA sequencing

For single-cell RNA sequencing (scRNAseq) cardiac non-myocytes were prepared using a novel cardiac cell isolation protocol [251]. After euthanasia, the thoracic cavity was opened and the inferior *vena cava* was ligated, before injecting 7mL of cold ‘EDTA buffer’ [249,251] into the right ventricle for perfusion. Following perfusion, the atria were clamped using a haemostat and the heart was gently cut away from the thoracic cavity with curved Walton scissors. The hearts were subsequently cut away from the thoracic cavity taking care to keep the ventricles and atria intact. With the hearts clamped, the haemostat was then attached to a magnetic, 3D-printed platform such that the apex of each heart was facing up-ward (Figure 2.2) [251]. Next, a 30G hypodermic needle attached to a peristaltic pump (Cole Palmer, IL, USA) was inserted into the left-ventricular chamber, and allowed to perfuse *EDTA buffer* at 6mL/min for ~5 minutes. Once the heart had ‘cleared’, the perfusion rate was reduced to 4mL/min and the perfusate was changed to *enzymatic digestion buffer* [249,251], for ~15 minutes. All buffers were maintained at 37°C throughout the perfusion process.

After successful heart digestion, cardiac ventricles were excised (including the intra-ventricular septum) and gently dissociated with forceps before placing the tissue into 2mL of *enzymatic digestion buffer* and incubated for 10-minutes at 37°C. During incubation, the cell suspensions were triturated twice using sterilised Pasteur pipettes to ensure uniform tissue digestion. Next, digested cell suspensions were passed through a 177µm filter into a 15mL tube containing 5mL of cold ‘*stop buffer*’ [249,251]. Cardiac myocytes and debris were pelleted by conducting three 1-minute centrifugation spins at 50×g (4°C). The supernatant (cardiac non-myocyte fraction) was collected for antibody/viability-dye staining and consequent fluorescence-activated cell sorting (FACS) as described previously [225,234]. Live (SYTOX™ Green⁻), metabolically active (Vybrant™

DyeCycle™ Ruby⁺) non-myocyte cardiac cells were sorted by endothelial cells (CD31⁺), leukocytes (CD45⁺), and resident mesenchymal cells (CD31⁻CD45⁻) for cell counting.

Each major non-myocyte cell population were manually counted using a haemocytometer and were mixed (ECs; ~10%, RMCs and leukocytes; ~90%) and used for single cell transcriptomic library preparation on the 10X Chromium system. Approximately 12,000 cells were loaded into each well (lane 1: pooled *db/db* non-myocytes [*n*=4], lane 2: pooled *db/h* non-myocytes [*n*=3]) and processed using the Chromium Single Cell 3' v2 chemistry reagent kit (10X Genomics). Individual cells were captured and lysed within the 10X controller, after which cDNA was synthesised and amplified for a total of 12 cycles (as previously reported [234]). Amplified cDNA within encapsulated within single-cells were then sequenced on an Illumina NovaSeq 6000 system.

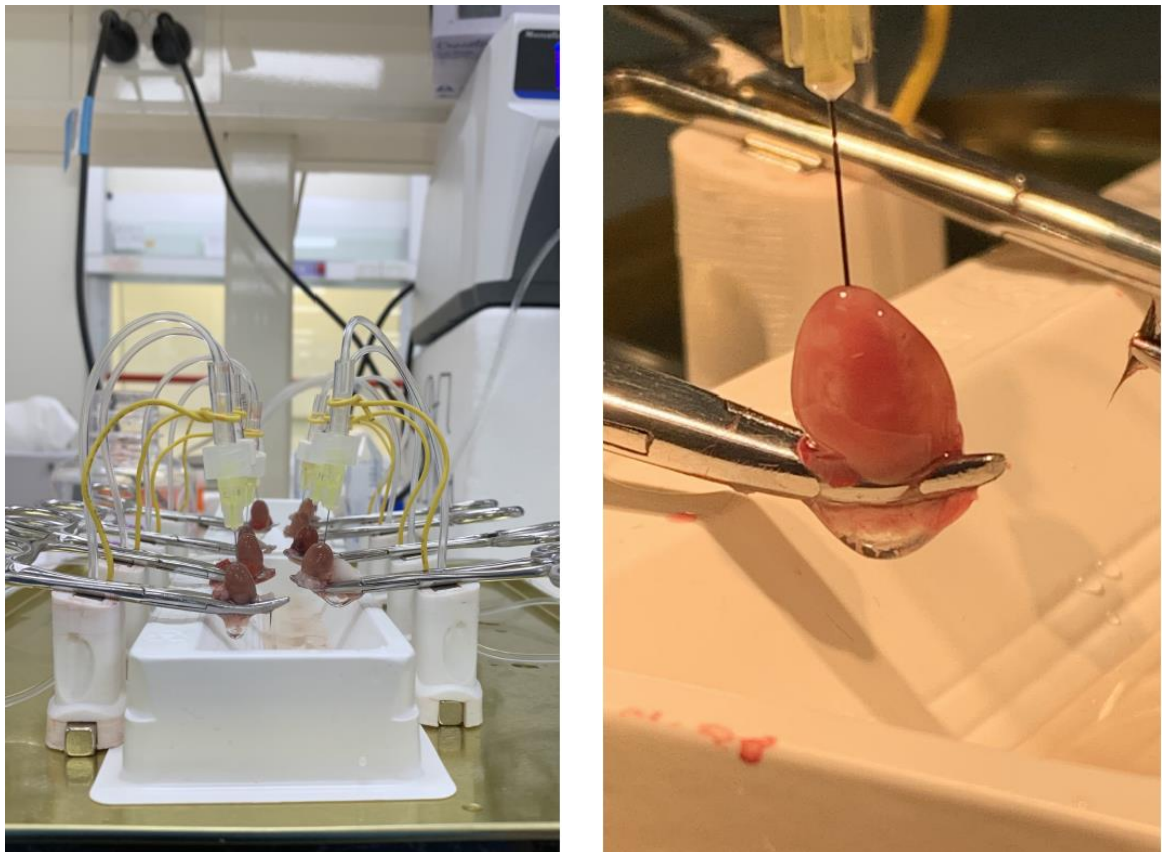


Figure 2.2: Illustrates the high-throughput cardiac perfusion technique as described in Section 2.9. Left: concomitant perfusion of 8 mouse hearts as described. Right: zoomed view of a single clamped, perfused heart. Figure adapted from Mclellan *et al* (2020), *Circulation*; 142:1448-1463 [234].

2.10 *In silico* analysis of single-cell RNA-sequencing data

Sequencing data was processed by Cell Ranger software version 5.0.0 (10X Genomics) prior to subsequent analysis. Raw sequencing data was deconvolved using Seurat suite version 3.2.0 pipeline. This pipeline converts Illumina basecall files to fastq formatted files, which aligns the sequencing reads to the reference *Mus Musculus* (mm10) transcriptome, and quantified the expression of transcripts within each cell. Analyses of processed scRNAseq data were then carried out in R studio version 4.1 using the Seurat suite. Pre-processing of scRNAseq data was conducted as previously described [234]. This yielded a total of 9,316 cardiac non-myocyte cells. Clustering of cells was primarily depicted via t-distributed stochastic neighbour embedding (tSNE) projection, which reduces highly complex data to two dimensions for interpretation. Cell types were annotated by querying established cell marker genes as described previously [225,234] and by considering the top-5 most highly-expressed genes in each cell cluster (of the top 1,000 most highly variable genes).

2.10.1 Differential gene expression analysis

Differential expression analysis was performed to identify differentially expressed (DE) genes between groups per cell type manner. Genes that have non-zero expression in >10% of cells in at least one of the experimental groups were considered in this analysis. The DE gene testing method ‘MASTcpmDetRate’ was used to identify DE genes between groups. This test is a modification of ‘MAST’ [252], considering cellular detection rate as a covariate, which has been successfully performed in a benchmark study for detecting differential expression from scRNA-seq [253]. To determine statistical significance of DE genes between experimental groups, the uncorrected *P* value threshold was set at < 0.01.

2.10.2 Gene ontology analysis

Gene Ontology (GO) enrichment analysis was performed using the ‘enrichGO’ function within the ‘clusterProfiler’ R package version 3.12.0 [254]. All GO analyses presented were mapped to reference genomes retrieved from <http://geneontology.org>. Enrichment analysis of GO Biological Process terms (GO-BP) was calculated by mapping our list of differentially expressed genes (uncorrected *P* value < 0.01) to the default background gene list for *Mus Musculus*, with minimum and maximum gene set sizes 10 and 500, respectively. Systematic similarities between GO terms were calculated using the ‘simplify’ function within the clusterProfiler R package. The GO-BP terms that had semantic similarity higher than the specific cut-off point of 0.7 were considered as redundant GO-BP terms and thus discarded from analysis. The Benjamini-Hochberg adjusted *P* value cut-off of 0.05 was used to determine statistically significant GO-BP terms (‘GO-BP’ abbreviated to ‘GO terms’ in Chapter 5). Of the statistically significant GO-BP terms identified in our analysis, more specific information was derived (further discussed in Chapter 5).

2.10.3 Ligand-receptor intercellular communication analysis

Intercellular communication between cardiac non-myocytes were inferred *in silico*, by obtaining mouse orthologs of human ligand-receptor pairs [255] from the ‘BioMart’ database (v.86), using

the biomaRt R package, as previously described [225]. If a detected ligand or receptor had a ‘non-zero expression’ value in more than 20% of cells in a given cell population, they were denoted as an ‘expressed’ ligand or receptor. To infer the cell-cell communication networks, I linked expressed ligands with their cognate receptors between and within major cell populations. The Circlize R package [256] was used to visualise the putative intercellular communication network in the *db/db* heart. The total number of communication signals transmitted and received by a certain cell population was also quantified (see Chapter 5).

2.10.4 Incorporation of bulk RNA-sequencing data

To validate our cardiac non-myocyte scRNAseq findings, I incorporated DE genes acquired from two additional, publically available bulk RNA sequencing (bulk RNA-seq) datasets [237,246] into our DE gene list and developed a proportional Venn diagram, using R packages, RVenn (v1.10), Euler (v6.10), VennDiagram (v1.6.20) and Venneuler (v1.1-0). DE genes from all datasets were filtered by *P* value ($P < 0.01$ for bulk RNA-seq, $P < 0.001$ for scRNAseq data). Common differentially expressed genes were identified using the ‘overlap’ function within RVenn. Differentially expressed gene lists were obtained and data was visualised using Venneuler. Subsequently, GO analysis (described in Section 2.10.2) was performed on each overlapping gene list derived from this analysis to produce biologically relevant pathways specific to each set of overlapping genes. For more information, see Chapter 5.

2.11 Immunofluorescence staining and confocal microscopy

In order to validate flow cytometric and scRNAseq data, I conducted immunofluorescence staining of fresh-frozen tissue embedded in OCT compound (as described in Figure 2.1). Heart sections were cut at 10µm on a cryostat (CM1950, Leica Biosystems), for histological staining. Briefly, frozen sections were incubated in 4% paraformaldehyde (PFA) for 10-minutes, before washing the tissue in Tris-EDTA solution (100mM Tris, 10mM EDTA) for 5-minutes. Fixed heart sections were then blocked (2% goat serum, 0.1% Triton, 0.05% Tween, 0.05% sodium azide in PBS) then subsequently washed in PBS-T (PBS supplemented with 0.5% Triton). After three consecutive washes, primary antibodies were added and allowed to incubate at room temperature for 2 hours. After incubation, three PBS-T washes were conducted prior to addition of specific secondary antibodies attached with a given fluorophore. Secondary antibodies were incubated for 1 hour at room temperature and washed twice in PBS-T. Primary and secondary antibodies vary in epitope target, species, clone and dilution depending on the study (see each Chapter for more information). Subsequently, sections were washed for 5 minutes in 4',6-diamidino-2-phenylindole (DAPI [0.1µg/mL]) to detect total nuclei in each sample. Slides were then dried and cover-slipped using Mowiol solution (containing 1,4-diazabicyclo-[2,2,2]-octane [DABCO; 2.5%])[257]. Prepared immunofluorescence cardiac micrographs were acquired at a 20X objective and tiled (3x3 fields of view unless otherwise stated) on a Nikon A1R confocal laser scanning microscope.

2.12 Cardiac Oil-red O staining

Oil-red O compound (ORO [$C_{26}H_{24}N_4O$], Sigma Aldrich) was used to assess the content of neutral cardiac lipids [258]. First, the ORO stock solution was prepared, containing 2.5g of ORO dissolved in 400mL of 99% isopropyl alcohol. The ORO stock solution was mixed for 2-hours using a magnetic stirrer to ensure the solution was thoroughly mixed. The ORO stock solution was consequently diluted in distilled water (1.5 parts ORO, 1 part distilled water) and left for 10 minutes at room temperature. The diluted ORO solution was then filtered twice through separate 45 μ m filters (Sartorius, Goettingen, Germany), to ensure no residual precipitates were present. Next, frozen cardiac sections (10 μ m thickness) were brought to room temperature. Using a hydrophobic barrier PAP pen (H-400, Vectorlabs, California, USA) a small hydrophobic chamber was traced around the section. Concomitantly, 200 μ l of filtered ORO solution was added to the section and allowed to incubate at room temperature for 5 minutes. All stained slides were then rinsed with distilled water for 30 minutes. Shortly after, slides were dried and cover-slipped, using Mowiol solution as the mounting medium. Stained, whole cardiac sections were imaged the following day, using a bright field scanning microscope (Aperio Scanscope AT Turbo, Monash Histology Platform) for analysis. Acquired images of cardiac cross-sections were exported to ImageJ for quantification of cardiac lipids, as previously described [258].

2.13 Body composition analysis

Body composition analysis was conducted using an EchoMRI™ 4-in-1 700 Analyser (EchoMRI, TX, USA) to quantify fat and lean mass, as well as free and total body water. All mice (Aim 1 and 2) were weighed prior to analysis. Animals were then gently guided into a specific plastic enclosure and inserted into the EchoMRI instrument for analysis. After each run (~30 seconds), mice were removed from the enclosure and placed in a fresh cage with their respective litter mates.

2.14 Intraperitoneal glucose (IPGTT) and insulin (IPITT) tolerance testing

At study endpoint, mice from Aim 1 underwent both an IPGTT and IPITT to assess glucose clearance and insulin sensitivity. Mice from Aim 2 only underwent an IPITT to determine the degree of insulin resistance. For both IPGTT and IPITT testing, animals were fasted for 5 hours before obtaining their fasting blood glucose levels, using the aforementioned glucometer.

2.14.1 IPGTT

After fasting blood glucose was taken (time 0), a single glucose bolus was administered i.p. to each mouse to assess the clearance rate of exogenous glucose (25% glucose [4 μ l/g], Baxter, Viaflex®). Blood glucose was then measured at 15-minute intervals in the first hour post bolus. Additional blood glucose measurements were taken at 120 and 150 minutes.

2.14.2 IPITT

The IPITT was conducted in a similar manner to the IPGTT above. Mice were fasted and their resting blood glucose was measured. However in this instance, a bolus of insulin was administered

via i.p. injection, to observe the changes in blood glucose over the same period of time. Insulin was diluted in isotonic saline (Humalog®, 10µl of 100U/ml; 3mL of saline) and injected i.p. at a dose of 0.3mg/kg. Synonymously, blood glucose was measured at 15-minute intervals in the first hour and also at 120 and 150 minutes post bolus. Mice were carefully monitored during this experiment, to assess the likelihood of a hypoglycaemic event (<2mmol/mol). As an additional precaution, a 1mL syringe was filled with 25% glucose solution for i.p. injection to assist in recovery of any apparent hypoglycaemic event.

2.15 Echocardiography for cardiac LV function *in vivo*

Echocardiography was conducted in mice (from Aims 1 and 2) under anaesthesia (Ketamine/Xylazine/Atropine [KXA], 80/8/0.96mg/kg, i.p.) at endpoint, with assistance from the Baker Heart and Diabetes Institute Preclinical Cardiology Microsurgery & Imaging Platform (PCMIP). A Philips iE33 ultrasound machine with a 15-MHz linear-array and 12MHz sector transducer (North Ryde, Australia) was used for all animals to assess the degree of cardiac functional impairment *in vivo*. Before acquisition, mice were anaesthetised and their thoracic area was shaved, after which ultrasound transmission gel was added to assist in optimal visualisation of raw echocardiography data.

2.15.1 Doppler echocardiography for diastolic function

Doppler flow echocardiography was used to assess cardiac transmitral flow velocity in each phase of diastole (Figure 2.3). The early phase (E wave) and the late atrial phase (A wave) of diastole were measured to determine the E:A ratio - an established measurement of LV diastolic function (Figure 2.3A) [17,18]. Other measurements of diastole were also measured including deceleration time (DT), isovolumic relaxation time (IVRT) and heart rate (HR; anaesthetised HR, Figure 2.3A). In a similar manner, tissue Doppler echocardiography was performed to examine the tissue motion of the mitral annulus. Peak mitral velocities were obtained from raw echocardiography traces and measured as indicated in Figure 2.3B (early phase = e', late atrial phase = a' wave). The e':a' and E/e' ratios were calculated and used as additional measures to assess diastolic function.

2.15.2 M-Mode echocardiography for systolic function

M-Mode echocardiography was used to measure any alterations in wall thicknesses between experimental mouse cohorts, and to determine any aberrances in systolic function (Figure 2.3C). M-mode derived measurements include; anterior (AWd) and posterior (PWd) wall thicknesses, left ventricular end-diastolic dimension (LVEDD), left ventricular end-systolic dimension (LVESD). Fractional shortening (FS) was also calculated ($\% FS = 100 \times [LVEDD - LVESD] / LVEDD$) as an index of LV systolic function. All echocardiographic analysis was blinded to the investigator under the supervision of the Baker Heart and Diabetes Institute PCMIP.

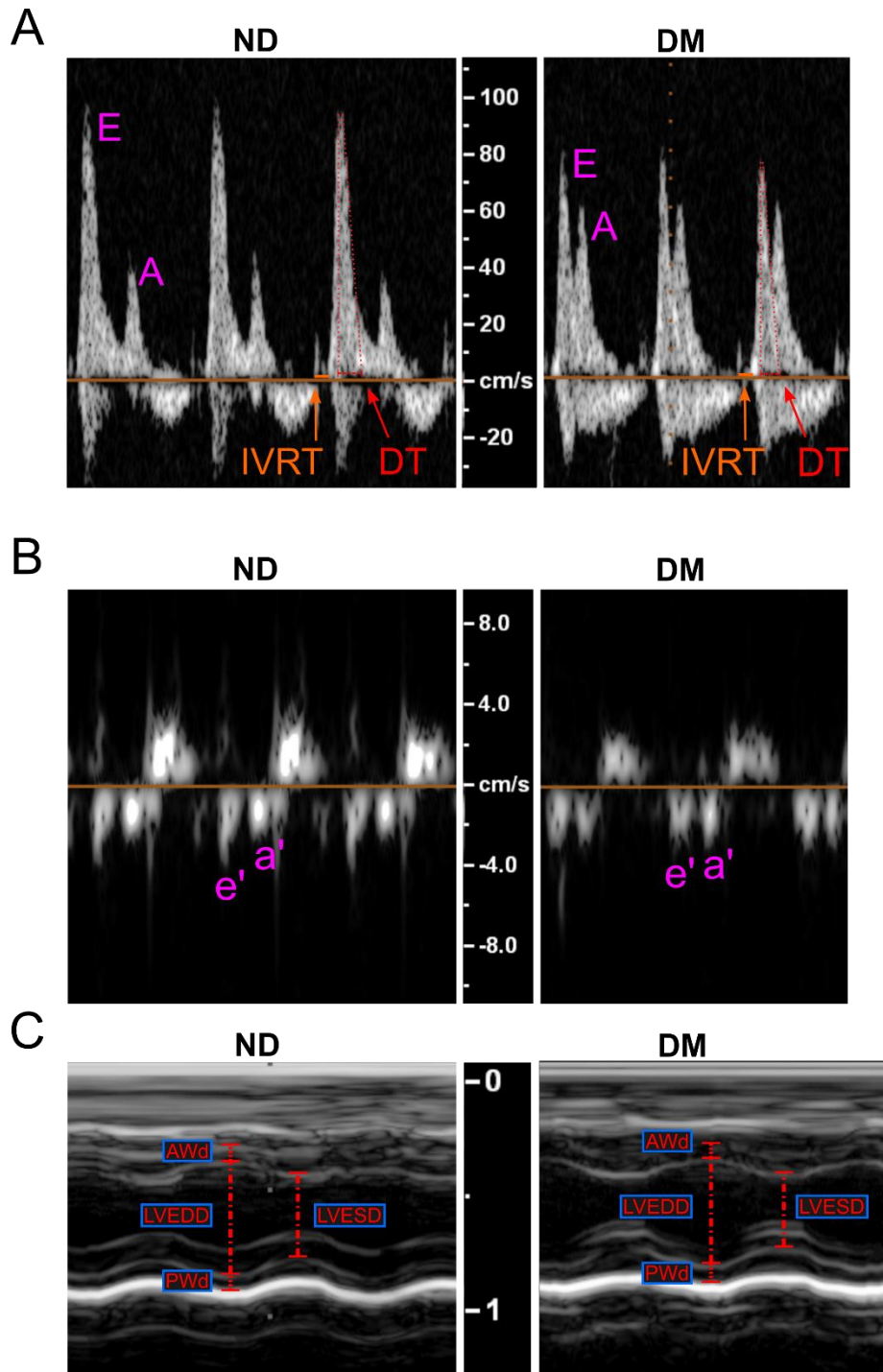


Figure 2.3: Representative echocardiography images including method of parameter measurement. E = blood flow during early phase of diastole, A = late atrial phase of diastole, e' = early mitral valve velocity during diastole, a' = late mitral valve velocity during diastole, IVRT = isovolumic relaxation time, DT = deceleration time, AWd = anterior wall dimension, LVEDD = LV end-diastolic dimension, PWd = posterior wall dimension, LVEDS = LV end-systolic dimension.

2.16 Statistical analyses

With the exception of Chapter 5 and 6, all data is presented as mean \pm standard error of the mean (SEM), where ' n ' represents the total number of animals per group. To mitigate batch effects, cardiac flow cytometry data was normalised to the mean of the ND values within each batch, such that the mean of each ND cell type was normalised to 1. Additionally, spanning-tree progression analysis for density-normalized events (SPADE; Cytobank Premium©, CA, USA) was conducted to validate the orthogonal flow cytometry gating strategies. SPADE is an algorithm that aids data visualisation of multi-parametric flow cytometry data, by clustering phenotypically similar cells determined by antibody affinity to its antigen (Figure 2.4). Node size corresponds to cellular abundance, node colour dictates the fold change from control (in this instance, comparing the mean proportions of *db/h* and *db/db* cell types), and node distance represents cellular phenotypic similarity (Figure 2.4). Live, metabolically active cells (SYTOX™ Green⁻, Calcein Blue⁺) from cardiac flow cytometry were concatenated and uploaded to Cytobank for SPADE analysis. For all SPADE analysis, between 100 – 200 target nodes were deemed sufficient for cellular identification and the event down-sampling target was set at 50%. Whole-blood flow cytometry data was normalised to total white-blood cell count, obtained from a Sysmex XS-1000i Hematology Analyzer, then subsequently batch normalised. Nuclei enumerated from immunofluorescence micrographs were quantified by QuPath software (v0.2.3), using the cell count function to quantify positive nuclei within each different fluorescent channel. Raw echocardiography traces were analysed using RadiAnt DICOM viewer software (v2020.2), after which quantification was performed in accordance with the PCMIP guidelines. All data (with exception of scRNAseq data) was illustrated and analysed statistically using GraphPad Prism (v8.1.2). Comparison of experimental groups was conducted using an unpaired *t*-test, whereby statistical significance was determined as $P < 0.05$. For more information regarding statistical analysis of scRNAseq data, see Section 2.10.

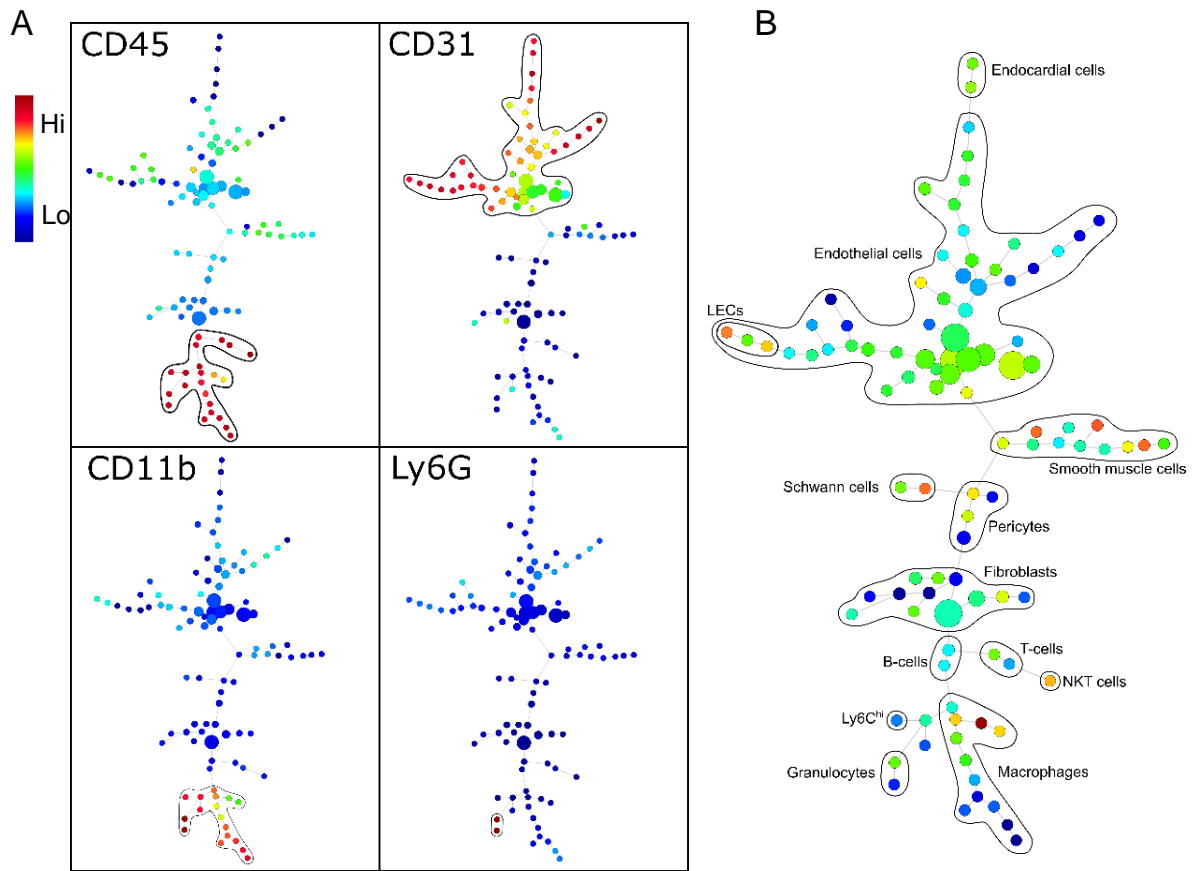


Figure 2.4: Identification of cell types from flow cytometry via SPADE dendrogram clustering

This image highlights the utility of SPADE for unbiased clustering and identification of cell types by antibody-antigen binding affinity. (A) Each SPADE in this image is identical, however each different SPADE has been heat-mapped according to a given antibody used in this experiment (only 4 have been shown for simplicity). CD45⁺ nodes represent leukocytes, CD31⁺ nodes characterise endothelial cells, CD11b⁺ nodes identify myeloid cells and Ly6G⁺ nodes – granulocytes (which are both unsurprisingly within the leukocyte cluster). This allows for identification of all detectable cells within entire non-myocyte fraction of the heart, which is depicted in (B). Annotated SPADE, presented as proportional log(% total ratio of live metabolically active cells). For this example, only 100 target nodes have been shown for pragmatic purposes.

Chapter 3

Determining the differences in cardiac cellularity in an established murine model of diabetic heart failure

3.1 Integrative commentary

This study makes an important new contribution to our understanding of how diabetes alters the cardiac cellular landscape. Using the STZ-HFD mouse model of diabetes, I found that resident mesenchymal cells in the heart were expanded with significantly elevated levels of fibroblasts and decreased levels of smooth muscle cells. I also document changes in the hematopoietic system, with systemic monocytosis and cellular alterations within the bone-marrow niche. This is the first study to compressively assess alterations in cardiac non-myocytes in parallel and offers a framework for understanding the cardiac cellular changes accompanying diabetes-induced diastolic dysfunction.

3.2 Declarations for Thesis chapter 3

This chapter has been published in *Cardiovascular Diabetology* and has adhered to all necessary guidelines for peer review. Therefore, this chapter is shown in within this thesis in PDF format, however this open access publication also includes the DOI for further information. The supplementary material is attached in this thesis, after the main manuscript (Additional file 1).

Main manuscript word count: 4,009.


Main Figures: 7

Supplementary Figures: 8

Supplementary Tables: 4

Declaration of candidate

I, Charles D. Cohen, declare that the above information is correct and is in line with the peer-reviewed publication version of the manuscript.

Signed: 

Charles D. Cohen

Date: 15/11/21

3.3 Diastolic Dysfunction in a Pre-Clinical Model of Diabetes is Associated with Changes in the Cardiac Non-myocyte Cellular Composition

Charles D. Cohen^{1,2,5}, Miles J. De Blasio¹, Man K. S. Lee³, Gabriella E. Farrugia², Darnel Prakoso¹, Crisdion Krstevski^{2,5}, Minh Deo¹, Daniel G. Donner^{4,6}, Helen Kiriazis^{4,6}, Michelle C. Flynn³, Taylah L. Gaynor^{2,5}, Andrew J. Murphy³, Grant R. Drummond⁵, Alexander R. Pinto^{2,5*}, Rebecca H. Ritchie^{1,5*}, 20:116, (2021).

**Equal contribution*

DOI: <https://doi.org/10.1186/s12933-021-01303-9>

¹Heart Failure Pharmacology, Drug Discovery Biology, Monash Institute of Pharmaceutical Sciences, Parkville, VIC; ²Cardiac Cellular Systems, ³Haematopoiesis and Leukocyte Biology, ⁴Preclinical Cardiology, Microsurgery & Imaging Platform, Baker Heart and Diabetes Institute, Prahran, VIC; ⁵Department of Physiology, Microbiology and Anatomy, La Trobe University, Bundoora, VIC, ⁶Baker Department of Cardiometabolic Health, The University of Melbourne, Parkville VIC 3010, Australia.

3.3.1 Statement of contributions


Name	Nature of contribution
Charles D. Cohen	Conceived & designed experiments. Performed animal experiments (including general monitoring, diabetes induction, assistance with echocardiography, tissue collection). Performed and heart and blood flow cytometry. Performed immunofluorescence staining and confocal imaging. Analysed flow cytometry data, interpreted results, prepared manuscript, edited and revised the manuscript.
Miles J. De Blasio	Conceived & designed experiments, assistance with animal work, edited and revised the manuscript.
Man K.S Lee	Assistance with systemic flow cytometry work, edited and revised the manuscript. Analysed bone marrow and spleen flow cytometry data for interpretation.
Gabriella E. Farrugia	Assistance with cardiac flow cytometry, edited and revised the manuscript.
Darnel Prakoso	Assistance with animal work and tissue collection, edited and revised the manuscript.
Crisdion Krstevski	Assistance with tissue and blood collection, edited and revised the manuscript.
Minh Deo	Assistance with animal work and tissue collection, revised the manuscript.
Daniel G. Donner	Conducted quality control of echocardiography analysis (initially analysed by CDC), edited and revised the manuscript.
Helen Kiriazis	Performed <i>in vivo</i> echocardiography (MJD, CDC assisting), edited and revised the manuscript.
Michelle C. Flynn	Performed bone marrow and spleen flow cytometry, edited and revised the manuscript.
Taylah L. Gaynor	Assistance with tissue collection. Edited and revised the manuscript.
Andrew J. Murphy	Assistance with conceiving systemic flow cytometry and data interpretation. Edited and revised the manuscript.
Grant R. Drummond	Assistance with conceiving experiments and providing intellectual input. Edited and revised the manuscript.
Alexander R. Pinto*	Conceived & designed experiments. Interpreted results, edited and revised the manuscript.
Rebecca H. Ritchie*	Conceived & designed experiments. Interpreted results, edited and revised the manuscript.

ORIGINAL INVESTIGATION

Open Access



Diastolic dysfunction in a pre-clinical model of diabetes is associated with changes in the cardiac non-myocyte cellular composition

Charles D. Cohen^{1,2,5}, Miles J. De Blasio¹, Man K. S. Lee³, Gabriella E. Farrugia², Darnel Prakoso¹, Crisdion Krstevski^{2,5}, Minh Deo¹, Daniel G. Donner^{4,6}, Helen Kiriazis^{4,6}, Michelle C. Flynn³, Taylah L. Gaynor^{2,5}, Andrew J. Murphy³, Grant R. Drummond⁵, Alexander R. Pinto^{2,5†} and Rebecca H. Ritchie^{1,5†} 

Abstract

Background: Diabetes is associated with a significantly elevated risk of cardiovascular disease and its specific pathophysiology remains unclear. Recent studies have changed our understanding of cardiac cellularity, with cellular changes accompanying diabetes yet to be examined in detail. This study aims to characterise the changes in the cardiac cellular landscape in murine diabetes to identify potential cellular protagonists in the diabetic heart.

Methods: Diabetes was induced in male FVB/N mice by low-dose streptozotocin and a high-fat diet for 26-weeks. Cardiac function was measured by echocardiography at endpoint. Flow cytometry was performed on cardiac ventricles as well as blood, spleen, and bone-marrow at endpoint from non-diabetic and diabetic mice. To validate flow cytometry results, immunofluorescence staining was conducted on left-ventricles of age-matched mice.

Results: Mice with diabetes exhibited hyperglycaemia and impaired glucose tolerance at endpoint. Echocardiography revealed reduced E:A and e'a' ratios in diabetic mice indicating diastolic dysfunction. Systolic function was not different between the experimental groups. Detailed examination of cardiac cellularity found resident mesenchymal cells (RMCs) were elevated as a result of diabetes, due to a marked increase in cardiac fibroblasts, while smooth muscle cells were reduced in proportion. Moreover, we found increased levels of Ly6C^{hi} monocytes in both the heart and in the blood. Consistent with this, the proportion of bone-marrow haematopoietic stem cells were increased in diabetic mice.

Conclusions: Murine diabetes results in distinct changes in cardiac cellularity. These changes—in particular increased levels of fibroblasts—offer a framework for understanding how cardiac cellularity changes in diabetes. The results also point to new cellular mechanisms in this context, which may further aid in development of pharmacotherapies to allay the progression of cardiomyopathy associated with diabetes.

Keywords: Cardiac cellularity, Diabetes, Flow cytometry, Echocardiography, Fibroblast

Background

Diabetes mellitus is a leading cause of death worldwide, with a total global prevalence exceeding 450 million individuals [1]. In 2015, diabetes was attributed to 12.8% of total all-cause mortality worldwide, providing a substantial socioeconomic burden and health concern [2, 3].

*Correspondence: alex.pinto@baker.edu.au; Rebecca.ritchie@monash.edu

[†]Alexander R. Pinto and Rebecca H. Ritchie Equal contribution

¹ Heart Failure Pharmacology, Drug Discovery Biology, Monash Institute of Pharmaceutical Sciences, 399 Royal Parade, Parkville, VIC 3052, Australia

² Cardiac Cellular Systems, Baker Heart and Diabetes Institute, 75 Commercial Road, Melbourne, VIC 3004, Australia

Full list of author information is available at the end of the article



© The Author(s) 2021. This article is licensed under a Creative Commons Attribution 4.0 International License, which permits use, sharing, adaptation, distribution and reproduction in any medium or format, as long as you give appropriate credit to the original author(s) and the source, provide a link to the Creative Commons licence, and indicate if changes were made. The images or other third party material in this article are included in the article's Creative Commons licence, unless indicated otherwise in a credit line to the material. If material is not included in the article's Creative Commons licence and your intended use is not permitted by statutory regulation or exceeds the permitted use, you will need to obtain permission directly from the copyright holder. To view a copy of this licence, visit <http://creativecommons.org/licenses/by/4.0/>. The Creative Commons Public Domain Dedication waiver (<http://creativecommons.org/publicdomain/zero/1.0/>) applies to the data made available in this article, unless otherwise stated in a credit line to the data.

Diabetes is associated with a significantly elevated risk of cardiovascular death and hospitalisation for heart failure (HF) [4, 5]. However, there remains no specific treatment for HF or its development in individuals with diabetes. HF in diabetes is often accompanied by impaired cardiac output, cardiac fibrosis, cardiomyocyte hypertrophy, cell death, and oxidative stress [6]. Diabetes also involves chronic and systemic inflammation [7, 8] with monocytosis and neutrophilia [7–9]. Despite extensive efforts to characterise diabetes-induced HF, inherent cellular mechanisms underpinning cardiac dysfunction in diabetes remain to be ascertained.

The mammalian heart consists of a diverse range of cell types [10]. Cardiac non-myocytes—comprised of endothelial cells (ECs), resident mesenchymal cells (RMCs) and leukocytes—outnumber myocytes, and are critical for maintaining homeostasis of the heart [10, 11]. While a number of recent studies have provided valuable new insights into the disparate roles of non-myocyte cells in cardiac homeostasis [10, 12, 13] and pathological remodelling [14–16], the cellular dynamics of non-myocytes during development of diabetes-induced heart failure remains unexplored. Using a recently published murine model of diabetes-induced cardiomyopathy [17], this study aimed to determine the difference in cardiac non-myocyte cellular proportions compared to non-diabetic mice. Here, we show that experimental diabetes impacts multiple cellular compartments in the heart, providing a framework for understanding the cellular dynamics and mechanisms driving development of diabetes-induced heart failure.

Research design and methods

Animal experiments

All animal-related experiments were approved by the Alfred Research Alliance (ARA) Animal Ethics Committee (Ethics number: E/1681/2016/B) and were performed in accordance with the National Health and Medical Research Council of Australia. FVB/N mice were sourced from the ARA Animal Services (provided in three separate cohorts). Mice had access to food and water *ad libitum* and were housed at 22 °C on a 12 h light/dark cycle. Male 6-week-old FVB/N mice were randomly allocated into the non-diabetic (ND, $n=7$) citrate vehicle control group fed standard chow diet, or diabetes mellitus (diabetes, $n=19$) which was induced by the combination of low-dose streptozotocin (STZ; cat# AG-CN2-0046, AdipoGen Life Sciences, NSW, Australia) and high-fat-diet (HFD; SF04-001, Specialty Feeds, WA, Australia, 43% total calculated digestible energy from lipids). STZ was administered by three consecutive daily intraperitoneal (i.p.) injections (55 mg/kg body weight in 0.1 mol/L citric acid vehicle, pH 4.5 [cat# 251275, Sigma-Aldrich,

USA]). Mice administered STZ were subsequently fed a HFD *ad libitum* for 26-weeks, as previously described [17]. Blood glucose levels were measured fortnightly via saphenous vein bleeds using a glucometer (Accu-Chek® Performa II, Roche Diagnostics, NSW, Australia). Intraperitoneal glucose and insulin tolerance tests were conducted at endpoint (26-weeks of diabetes) to assess glucose clearance and insulin resistance, as previously described [17]. Whole-body composition analysis was performed at endpoint using an Echo-MRI™ 4-in-1 700 Analyser (EchoMRI, Houston, TX, USA) to assess percentage fat mass and total lean mass. Percentage glycated haemoglobin (% HbA_{1c}) was also measured at endpoint to assess long-term blood glucose levels (Cobas b 101 POC system, Roche Diagnostics, NSW, Australia). Mice were euthanised by administration of Ketamine/Xylazine (85/8.5 mg/kg, i.p.) and subsequent cardiac exsanguination. As previously described [10–12], the thoracic cavity was exposed and right atrium was cut to allow for cardiac perfusion through the left-ventricular apex (PBS, 0.9 mM CaCl₂, 200 mM KCl), after which the heart was excised and ventricles were used for flow cytometry.

Echocardiography

Echocardiography was conducted in mice under anaesthesia (Ketamine/Xylazine/Atropine [KXA], 80/8/0.96 mg/kg, i.p.) at 26-weeks post diabetes (32-weeks of age) using a Philips iE33 ultrasound machine with a 15-MHz linear-array transducer. Analysis was conducted at the Baker Heart and Diabetes Institute and quality control was completed by technicians at the Pre-clinical Cardiology Microsurgery & Imaging Platform (PCMIP). Doppler flow echocardiography was used to assess cardiac transmitral flow velocity in each phase of diastole, where the early phase (E wave) and the late phase (A wave) were measured to determine the E:A ratio. Similarly, tissue Doppler was performed to examine the tissue motion of the mitral annulus (early phase = e', late phase = a' wave). M-mode echocardiography was conducted to assess left ventricle (LV) systolic function. Variables obtained from M-mode analysis included LV end-diastolic dimension (LVEDD) and LV end-systolic dimension (LVESD) to calculate fractional shortening (%FS = [(LVEDD-LVESD)/LVEDD] × 100).

Flow cytometry

Blood, spleen and bone marrow

Whole blood was obtained by cardiac puncture at endpoint and stained using a leukocyte-specific antibody panel (Additional file 1: Table S4). Bone marrow from the tibia and femur were flushed using PBS without Mg²⁺ and Ca²⁺ into 50 mL centrifuge tubes. Spleens were manually dissociated and passed through a 35 µm

filter into 50 mL centrifuge tubes to obtain a single cell suspension as previously described [7]. Blood, spleen and bone marrow were then subjected to red blood cell (RBC) lysis for 15 min at 4 °C using an ammonium chloride based commercial lysis buffer (1X dilution, 555899, Becton Dickinson, USA). After RBC lysis, the remaining stained cells were washed twice in 'F_x buffer' (1 X HBSS [Gibco™, NY, USA], 2% FCS). Between each wash, cells were centrifuged at 400 × g for 5 min at 4 °C. Cells were then resuspended in 200 µl of F_x buffer containing 4',6-diamidino-2-phenylindole (DAPI [0.1 µg/mL]); and filtered through 35 µm mesh into 5 ml polystyrene round-bottom tubes (352052, Falcon®, NY, USA) for flow cytometry. Gating strategies for each of the above cell suspensions are provided in Additional file 1: Figures S3–S5. For normalisation of flow cytometry data, 20 µl of blood was used to measure total white blood cell count using a Sysmex XS-1000i Hematology Analyzer.

Heart

High-dimensional flow-cytometry was performed on cardiac ventricles (comprising the LV, ventricular septum and right ventricle) from ND and mice with diabetes. Following perfusion, hearts were minced using curved scissors (14077-09, Walton, USA) as previously described [10], and transferred to 5 ml microfuge tubes for enzymatic digestion at 37 °C (2 mg/mL collagenase type IV [LS004188, Worthington Biochem, NJ, USA], 1 mg/mL Dispase II [04942078001, Roche, NSW, Australia] in 0.9 mM CaCl₂ in PBS). Cardiac non-myocyte cells were triturated three times at 15-min intervals using a Pasteur pipette to mechanically aid enzymatic digestion for a total of 45 min. Digested non-myocyte cardiac cells were then filtered through 75 µm nylon mesh into a 15 mL tube containing 10 mL of cold PBS (0.9 mM CaCl₂) and subjected to centrifugation (200 g, 15 min, 4 °C—no breaks) for debris clearance. The majority of the supernatant was aspirated and the remaining volume (~ 1 mL) was washed with a further 1 mL of F_x buffer supplemented with 0.9 mM CaCl₂. Cells were pelleted at 400 × g (4 min, 4 °C) and resuspended in 200 µl of F_x Buffer with Ca²⁺ to yield the single cell suspension of non-myocyte cardiac cells. Cells were then stained using the antibody panel designed for examining the non-myocyte fraction of the heart (Additional file 1: Table S5). Cells were strained through a 35 µm filter and flow cytometry was performed on a BD LSR Fortessa™ X-20 Special Order system located at the Baker Heart and Diabetes Institute.

Histological analysis

Age and sex-matched, fresh-frozen LV samples embedded in Optimal Cutting Temperature (OCT) compound were acquired from a separate cohort of ND and mice

with diabetes [17] for histological analysis. LV sections were cut (10 µm) on a cryostat (CM1950, Leica Biosystems) for staining (ND: *n* = 11, diabetes: *n* = 11). LV sections were co-stained with GATA4 (1:100, 14-9980-80, eBioScience™, Invitrogen, Australia) and PCMI1 (1:100, 19856-1-AP, ProteinTech Group, USA) antibodies to delineate the cell abundance of RMCs (PCMI⁺GATA4⁺ cells) as recently reported [12]. Serial sections were stained with DACH1 (1:100, 10914-1-AP, ProteinTech, USA) to quantify EC abundance [10, 12]. All immunofluorescence sections were counterstained with DAPI to identify total cell nuclei. Immunofluorescence micrographs of each LV sample were acquired at a 20X objective and tiled (3 × 3 fields of view) on a Nikon A1R confocal laser scanning microscope. Quantified values of immunofluorescence signal were normalised to total nuclei (DAPI⁺).

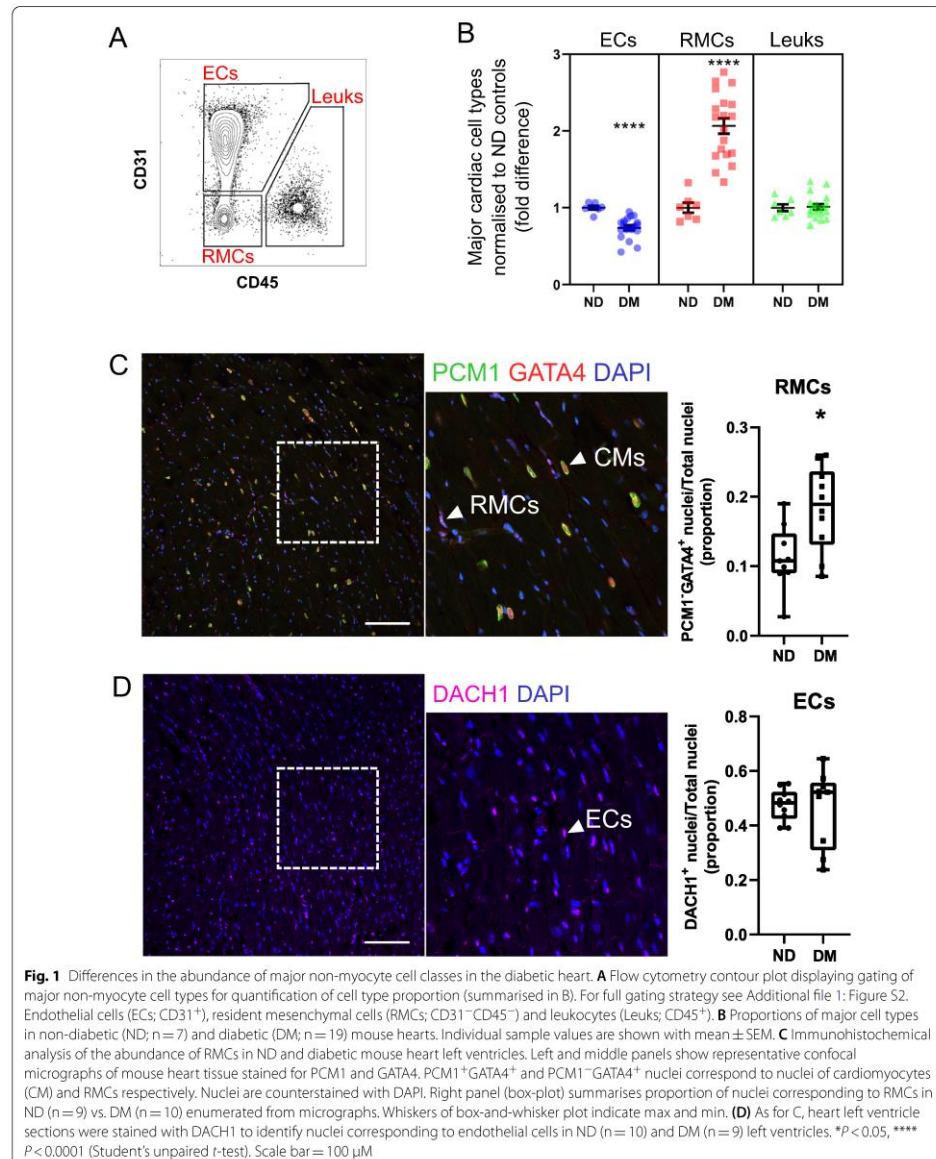
Statistical analysis

Flow cytometry data was analysed using FlowJo (v10.7.1) software. Raw cardiac flow cytometry data was normalised to the mean of the ND values within each batch, such that the mean of each ND cell type is equal to 1. Raw blood flow cytometry data was normalised to total white-blood cell count obtained from the hematology analyser, then subsequently batch normalised as aforementioned. Immunofluorescence micrographs were analysed by QuPath software (v0.2.3), using the cell count function to quantify nuclei. Echocardiography data was analysed using RadiAnt DICOM viewer software (v2020.2), after which quantification was performed in accordance with the PCMI guidelines. All data was illustrated and analysed statistically using GraphPad Prism (v8.1.2). Comparison of experimental groups was conducted using an unpaired *t*-test, whereby statistical significance was determined as *P* < 0.05.

Results

The STZ-HFD model recapitulates primary features of diabetes

The presence of diabetes was confirmed by a range of physiological tests prior to euthanasia. Consistent with our previous report [17], mice with diabetes exhibited significantly elevated blood glucose at endpoint (Additional file 1: Table S1). This was corroborated by measurement of glycated haemoglobin (% HbA_{1c}) at endpoint, which was significantly increased in mice with diabetes (*P* < 0.0001; Additional file 1: Table S1). In this study however, mice exhibiting diabetes did not gain more weight than their ND counterparts (Additional file 1: Table S1). This was recapitulated by the EchoMRI body composition analysis, showing no differences in lean or fat mass (Additional file 1: Table S1) between experimental



significantly increased in the myocardium of mice with diabetes (1.8-fold, Fig. 3B).

Content courtesy of Springer Nature, terms of use apply. Rights reserved.

groups. Impaired glucose tolerance was evident in mice with diabetes, indicating reduced clearing efficiency of systemic glucose, presented as the area under the curve (AUC, $P < 0.0001$, Additional file 1: Table S1). In contrast, there was no difference in the AUC from the insulin tolerance test between ND and mice with diabetes (Additional file 1: Table S1).

STZ-HFD mice exhibit LV diastolic dysfunction, but not systolic dysfunction

Echocardiography measurements of LV diastolic and systolic function were recorded *in vivo*, to determine the degree of cardiac functional impairment in mice with diabetes relative to their ND counterparts. Pulsed-wave Doppler echocardiography was conducted to measure mitral blood flow velocity during the early (E-wave) and late (A-wave) filling phases of diastole (Additional file 1: Fig. S1A). Heart rate (HR) tended to be elevated in mice with diabetes, but this did not reach statistical significance ($P = 0.07$; Additional file 1: Figure S1B). Although no differences were detected in the peak E wave (Additional file 1: Figure S1C), the peak A wave velocity was significantly elevated in mice with diabetes compared to ND mice ($P < 0.05$; Additional file 1: Figure S1D). Consequently, a significant reduction in E:A ratio (a hallmark feature of diastolic dysfunction) was observed in diabetic hearts vs. ND ($P < 0.05$, Additional file 1: Figure S1E). There were no differences in other measurements of diastolic function including deceleration time or isovolumic relaxation time (IVRT) between experimental groups (Additional file 1: Figure S1F, G, respectively).

To accompany transmitral blood flow, tissue Doppler echocardiography was used to assess the velocity of the mitral valve itself in each phase of diastole (e' = early phase, a' = late phase, Additional file 1: Figure S1H–L). Although the peak e' velocity was only modestly reduced ($P = 0.054$, Additional file 1: Figure S1I) and the peak a' velocity exhibited a minor increase ($P = 0.072$, Additional file 1: Figure S1J), the $e':a'$ ratio was significantly lower in mice with diabetes compared to ND mice ($P < 0.05$, Additional file 1: Figure S1K). There were no detectable changes in the E: e' ratio between cohorts (Additional file 1: Figure S1L).

M-Mode echocardiography was also performed to assess the difference in ventricular wall thickness and systolic function in mice with diabetes. The anterior wall thickness at diastole (AWd), LV end-diastolic dimension (LVEDD) and posterior wall thickness at diastole (PWd) were not different between groups (Additional file 1: Table S2). Interestingly, fractional shortening (% FS) was significantly elevated in mice with diabetes compared with ND mice ($P < 0.05$; Additional file 1: Table S2), consistent with a recent report in spontaneously type-1

diabetic (T1D) Akita mice [18]. Importantly however, diastolic dysfunction was observed in the absence of systolic dysfunction.

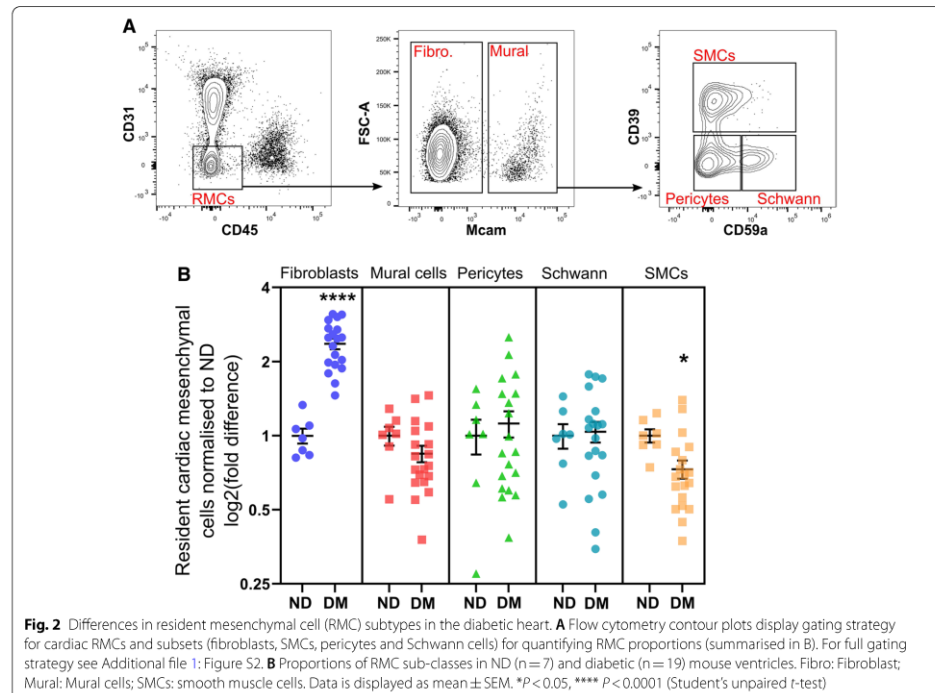
Diabetes alters the cardiac non-myocyte cellular composition

To assess differences in cardiac cellularity associated with diabetes-induced HF, we performed flow cytometric analysis of murine cardiac ventricles at study endpoint. Examination of viable single-cells (see Additional file 1: Figure S2A) revealed significant differences in endothelial cell (EC) and resident mesenchymal cell (RMC) proportions (0.26-fold decrease, twofold increase, respectively), indicating that diabetes alters the relative levels of cardiac non-myocyte cells (Fig. 1A, B). Conversely, leukocytes were at similar levels in ND and mice with diabetes (Fig. 1A, B).

Next, we sought to validate the proportional shifts in EC and RMC populations in diabetes observed by flow cytometry, with immunohistochemical analysis (Fig. 1C, D). To achieve this, we stained left ventricular sections of both cohorts with an antibody cocktail of GATA4 and PCM1 (Fig. 1C) or DACH1 (Fig. 1D), which we have previously employed to quantify proportions of RMCs and ECs [12]. These analyses revealed that RMC (PCM1⁺GATA4⁺) cell counts were significantly elevated in diabetic heart sections compared to ND counterparts ($P < 0.05$, Fig. 1C). Using the same approach for ECs, serial sections stained with DACH1 indicated no differences in EC abundance between experimental groups (Fig. 1D), suggesting that the proportional difference observed by flow cytometry is due to the increased RMCs [10].

Considering the proportion of RMCs were markedly elevated in the diabetic heart, a range of RMC subtypes were investigated from the initial RMC gate (Additional file 1: Fig. S2). Fibroblasts were significantly increased in diabetic hearts compared to ND (2.36-fold, $P < 0.0001$, Fig. 2B). In contrast, the proportion of smooth muscle cells (SMCs), were reduced in the diabetic cohort compared to ND controls (0.27-fold, $P < 0.05$, Fig. 2B). No major changes were observed in total mural cells, pericyte or Schwann cell populations (Fig. 2B).

While we did not detect any changes in total resident leukocyte proportions in diabetic mouse hearts compared to ND (Fig. 1B), diabetes has been previously associated with cardiac inflammation and systemic monocytosis [7, 19, 20]. To develop an overview of leukocyte diversity and abundance in diabetic hearts, we identified an array of leukocytes including myeloid and lymphoid cell populations and their subsets (Fig. 3A). There were no differences in cardiac leukocyte subsets between cohorts, except Ly6C^{hi} monocytes, which were



Circulating Ly6C^{hi} monocytes are elevated in diabetes

To confirm systemic monocytois, we quantified circulating leukocytes and their broad subtypes by flow cytometry. As shown previously [7], monocytes, particularly the Ly6C^{hi} subset, were significantly elevated in the blood of mice with diabetes (2.2-fold, 2.3-fold, respectively; $P < 0.05$ for both; Fig. 4B). Numbers of circulating neutrophils and Ly6C^{lo} monocytes were also marginally elevated in diabetic mice compared to their ND counterparts ($P = 0.09$, $P = 0.054$ respectively; Fig. 4B). By contrast, numbers of circulating lymphocytes (B and T-cells) did not differ between cohorts (Fig. 4C).

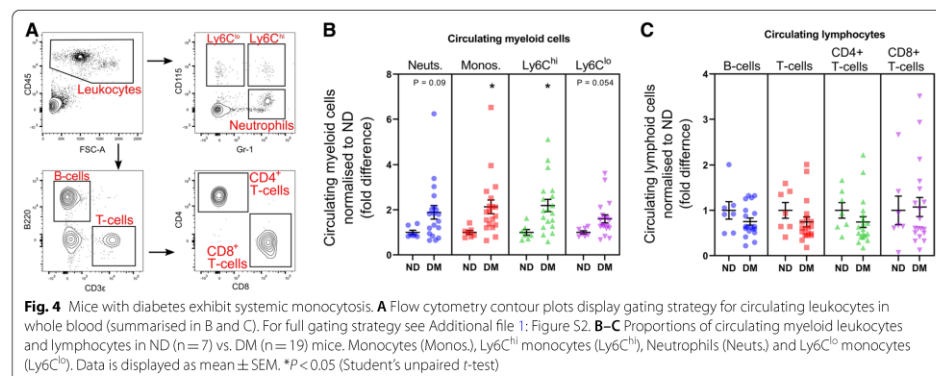
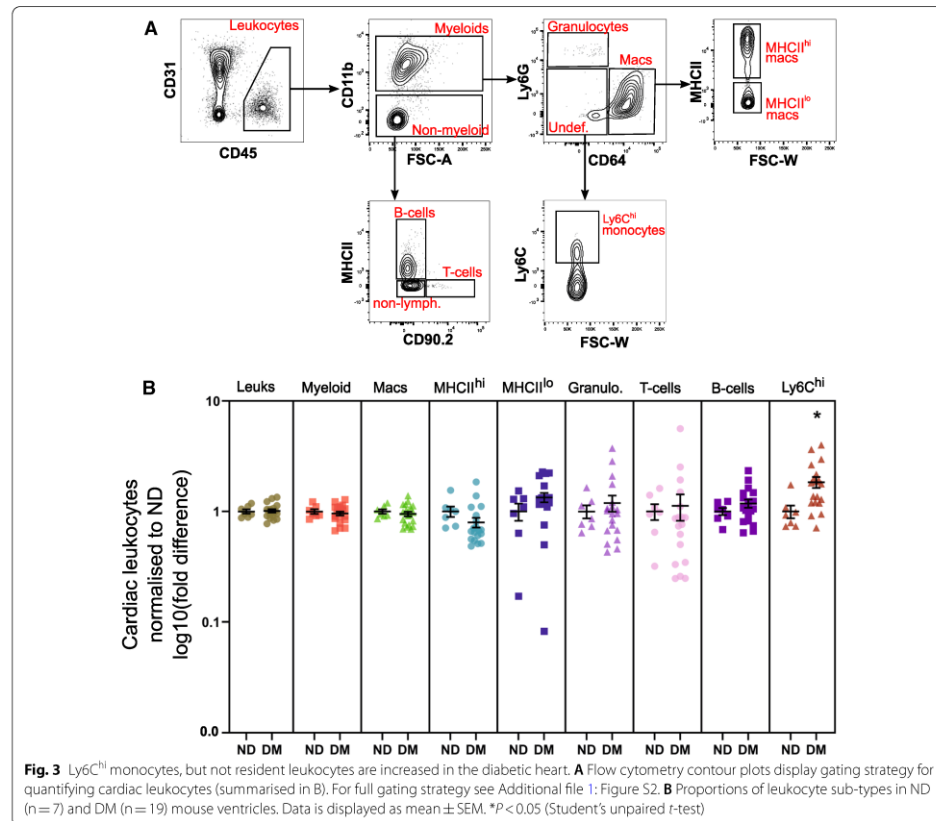
Systemic monocytois likely occurs via extramedullary myelopoiesis

To identify the potential sources of the observed monocytois in this model, we performed flow cytometry of the bone marrow and spleen. Within the bone marrow, LSKs (haematopoietic stem and progenitor cells; $[\text{Lin}^{-}\text{Sca1}^{+}\text{cKit}^{+}]$) were significantly increased in mice with diabetes (1.8-fold, $P < 0.01$, Fig. 5A). However,

bone-marrow derived common myeloid progenitors (CMP) and granulocyte-myeloid progenitors (GMP) were not different between experimental groups (Fig. 5A). Monocytes (both Ly6C^{hi} and Ly6C^{lo}) were significantly increased in the spleen in mice with diabetes compared to their ND controls (1.7-fold, 1.3-fold respectively, $P < 0.05$, Fig. 5B). These data suggest that the increased proportion of bone-marrow LSKs could be influencing these cells to mobilise to the spleen to undergo extramedullary myelopoiesis (Fig. 5C).

Discussion

The relationship between diabetes and HF remains poorly understood. Diabetes-associated cardiac remodelling—encompassing myocyte hypertrophy, fibrosis, oxidative stress and apoptosis [21] is well established. However, how the cardiac non-myocyte networks change in diabetes and contribute to this remodelling is unclear. Using a recently characterised mouse model of diabetes-induced cardiomyopathy [17], we aimed to determine how diabetes affects cardiac non-myocyte cell proportions and



Content courtesy of Springer Nature, terms of use apply. Rights reserved.

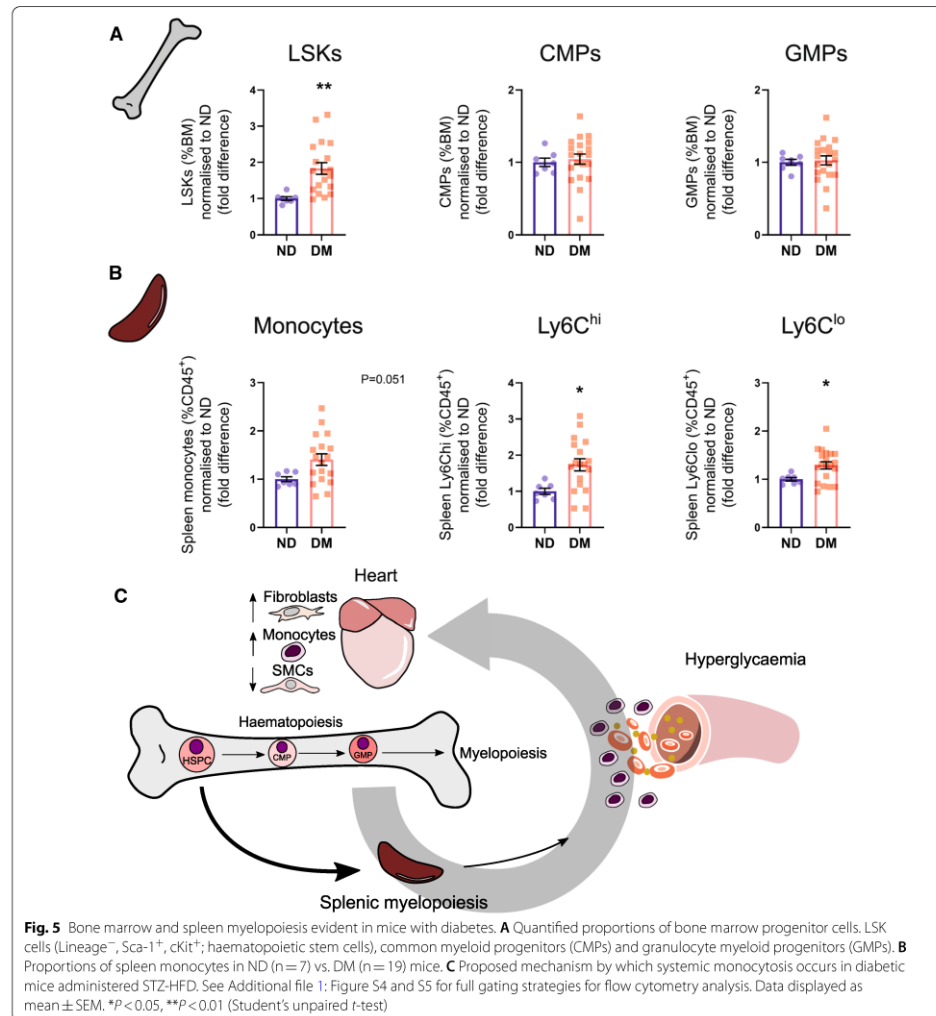


Fig. 5 Bone marrow and spleen myelopoiesis evident in mice with diabetes. **A** Quantified proportions of bone marrow progenitor cells. LSK cells (Lineage⁻, Sca-1⁺, cKit⁺; haematopoietic stem cells), common myeloid progenitors (CMPs) and granulocyte myeloid progenitors (GMPs). **B** Proportions of spleen monocytes in ND (n = 7) vs. DM (n = 19) mice. **C** Proposed mechanism by which systemic monocytois occurs in diabetic mice administered STZ-HFD. See Additional file 1: Figure S4 and S5 for full gating strategies for flow cytometry analysis. Data displayed as mean \pm SEM. * $P < 0.05$, ** $P < 0.01$ (Student's unpaired *t*-test)

abundance, to develop a framework for future mechanistic studies to consider. We revealed that with diabetes-associated diastolic dysfunction, proportions of cardiac fibroblasts are significantly increased in the myocardium. We also noted increased levels of Ly6C^{hi} monocytes and decreased levels of SMCs in diabetic hearts.

Numerous studies have implicated cardiac fibroblasts in diabetic cardiomyopathy, however their precise role in diabetes in vivo is still unknown. Cardiac fibroblasts are the primary cell type involved in deposition of extracellular matrix (ECM) in both states of acute injury or chronic stress [14, 15]. However, in these contexts, fibroblast gene expression and phenotype are distinct [22].

For example, in myocardial infarction (MI), fibroblasts rapidly differentiate into activated fibroblasts and myofibroblasts—both well-established drivers of cardiac ECM deposition [23]. Conversely, we have recently reported that myofibroblasts are absent during the development of chronic fibrosis in angiotensin II-induced cardiac remodelling [14]. Observations from the present study reveal that fibroblasts are the predominant non-myocyte cell type most dramatically affected by diabetes—suggesting an important role for fibroblasts in the development of diabetes-induced HF. Indeed, chronic hyperglycaemia is known to up-regulate various pro-fibrotic genes in the diabetic heart as a whole, including *Colla1*, *Postn*, *Timp-2* and *Ccn2* [17, 24, 25]. Furthermore, diabetes is associated with fibroblast-to-myofibroblast differentiation and ECM deposition [26, 27]. However, further research such as single-cell sequencing or targeted cell depletion experiments are needed to further elucidate the precise role of the cardiac fibroblast in diabetes and the regulatory mechanisms that drive these changes.

In the current study, we also observed an increase in monocyte numbers in the heart in diabetic mice, which is likely the result of increased systemic inflammation. In the non-injured heart, circulating leukocytes, such as monocytes primarily reside in the vascular lumens of cardiac capillaries [28], therefore reflecting changes occurring in the circulation. Systemic monocytosis is reported in both T1D and insulin resistant obese mice (i.e. leptin mutant *ob/ob* mice and diet-induced obese mice) [7, 8]. Consistent with systemic inflammation, the diabetic heart exhibits upregulation of pro-inflammatory cytokines such as TNF α , MCP-1 and IL-1 β [29–31]. Corresponding to the monocytosis, we also noted increased progenitor cells and splenic monocytes—the major site of secondary myelopoiesis [32]. Monocytosis is a well-established feature of diabetes and obesity/insulin resistance [33, 34]. However, in this model we only detected a significant increase in haematopoietic stem and progenitor cells (HSPCs), but not common myeloid progenitors (CMPs) or granulocyte-macrophage progenitors (GMPs) in the bone marrow. Given HSPCs can migrate to secondary myelopoietic sites, such as the spleen, to increase monocyte numbers [35–37], our findings suggest that this may be the primary mode of monocytosis observed in our model (Fig. 5C).

In contrast to the diabetes-induced increases in cardiac fibroblasts and monocyte numbers, we observed a decrease in SMC proportions. This was unexpected given hyperglycaemia has previously been associated with inhibition of aortic vascular SMC apoptosis in T1D patients, and in STZ-induced T1D mice [38, 39]. Conversely, metabolic syndrome and hypercholesterolaemia are both associated with increased apoptosis in aortic VSMCs of

mice and humans [33, 34]. Therefore, the precise mechanism leading to the reduction in SMC proportions in the hearts of STZ-HFD mice warrants further investigation.

Although there are a number of studies examining the role of individual cardiac cell types in diabetes, to our knowledge this is the first study to consider the entire cardiac non-myocyte network to understand differences in tissue cellularity. While novel technologies such as single-cell RNA sequencing have been successfully applied to tissues such as the pancreas [35, 36, 40], kidney [41, 42] and liver [43] in diabetes, detailed interrogation of the cellular heterogeneity in these tissue systems are lacking in this context. This study invites future research to consider cellular plasticity in diabetes to better understand the development of its associated pathologies.

Study limitations

While this study provides a basis for providing new understanding of the cardiac cellular dynamics in the context of diabetes, a number of limitations are noteworthy. First, cardiomyocytes were not considered in this study, as they are too large in diameter to pass through the flow cytometer available in our laboratories. Although cardiomyocytes are detectable by histology (PCM1⁺GATA4⁺ cells), they are often multi-nucleated, thus counting nuclei abundance is unlikely to yield accurate information. Furthermore, we did not measure morphological changes in cardiomyocyte size or deposition of myocardial fibrosis, despite there being no differences in our previous characterisation of this model [17]. Second, we only examined male mice in our study. Given that cardiac pathology is sex-specific in mice [44, 45] and in humans [46], cardiac cellular composition and gene expression are sexually-dimorphic [12, 14]. Future work should examine the impact of biological sex in the development of diabetic cardiomyopathy. Third, the STZ-HFD model used in this study did not yield a population of mice with elevated fat mass and body weight as expected [47]. Adiposity and obesity are important comorbidities contributing to pathology in experimental and clinical type-2 diabetes (T2D) [48, 49], albeit obesity is not essential for development of T2D [48, 49]. Importantly however, in this study mice with diabetes exhibited hyperglycaemia, impaired glucose tolerance and LV diastolic dysfunction, which are clinically relevant features of HF associated with diabetes. Furthermore, we were unable to ascertain whether the observed differences are attributed to the combination of STZ and HFD, or one of these individual insults. Future work using this model should consider the effect of STZ and HFD alone in addition to the combination of STZ-HFD to delineate the role of both factors in the development of diabetic HF. Lastly, this study did not consider how circulating populations

Road, Melbourne, VIC 3004, Australia. ³Haematopoiesis and Leukocyte Biology, Baker Heart and Diabetes Institute, Prahran, VIC, Australia. ⁴Preclinical Cardiology, Microsurgery & Imaging Platform, Baker Heart and Diabetes Institute, Prahran, VIC, Australia. ⁵Department of Physiology, Microbiology and Anatomy, La Trobe University, Bundoora, VIC, Australia. ⁶Baker Department of Cardiometabolic Health, The University of Melbourne, Parkville, VIC 3010, Australia.

Received: 18 March 2021 Accepted: 19 May 2021
Published online: 01 June 2021

References

- Raghavan S, Vassy JL, Ho YL, Song RJ, Gagnon DR, Cho K, et al. Diabetes mellitus-related all-cause and cardiovascular mortality in a national cohort of adults. *J Am Heart Assoc*. 2019. <https://doi.org/10.1161/JAHA.118.01295>.
- Ng ACT, Delgado V, Borlaug BA, Bax JJ. Diabetes: the combined burden of obesity and diabetes on heart disease and the role of imaging. *Nat Rev Cardiol*. 2020;18(4):291–304.
- Ogurtsova K, da Rocha Fernandes JD, Huang Y, Linnenkamp U, Guariguata L, Cho NH, et al. IDF Diabetes Atlas: Global estimates for the prevalence of diabetes for 2015 and 2040. *Diabetes Res Clin Pract*. 2017;128:40–50.
- Petar M, Mark C, Gerasimos S, Stefan D, Walter J, Boer D, et al. Type 2 diabetes mellitus and heart failure: a position statement from the Heart Failure Association of the European Society of Cardiology Type 2 diabetes mellitus and heart failure: a position statement from the Heart Failure Association of the European. *Eur J Heart Failure*. 2018;20:853–72.
- Rubler S, Dlugash J, Yuceoglu YZ, Kumral T, Branwood AW, Grishman A. New type of cardiomyopathy associated with diabetic glomerulosclerosis. *Am J Cardiol*. 1972;30:595–602.
- Ritchie RH, Dale AE. Basic mechanisms of diabetic heart disease. *Circ Res*. 2020;126:1501–25.
- Nagareddy PR, Murphy AJ, Stizaker RA, Hu Y, Yu S, Miller RG, et al. Hyperglycemia promotes myelopoiesis and impairs the resolution of atherosclerosis. *Cell Metab*. 2013;17:695–708.
- Nagareddy PR, Kraakman M, Masters SL, Stizaker RA, Gorman DJ, Grant RW, et al. Adipose tissue macrophages promote myelopoiesis and monocyte in obesity. *Cell Metab*. 2014;19:821–35.
- Wong SL, Demers M, Martinod K, Gallant M, Wang Y, Goldfine AB, et al. Diabetes primes neutrophils to undergo NETosis, which impairs wound healing. *Nat Med*. 2015;21:815–9.
- Pinto AR, Illykh A, Ivey MJ, Kuwabara JT, D'Antoni ML, Debuque R, et al. Revisiting cardiac cellular composition. *Circ Res*. 2016;118:400–9.
- Skelly DA, Squiers GT, McLellan MA, Bolisetti MT, Robson P, Rosenthal NA, et al. Single-cell transcriptional profiling reveals cellular diversity and intercommunication in the mouse heart. *Cell Rep*. 2018;22:600–10.
- Squiers GT, McLellan MA, Illykh A, Branca J, Rosenthal NA, Pinto AR. Cardiac cellularity is dependent upon biological sex and is regulated by gonadal hormones. *Cardiovasc Res*. 2020;cva265:1–25.
- Litviňuková M, Talavera-López C, Maatz H, Reichart D, Worth CL, Lindberg EL, et al. Cells of the adult human heart. *Nature*. 2020;588:466–72.
- McLellan MA, Skelly DA, Dona MSI, Squiers GT, Farrugia GE, Gaynor TL, et al. High-resolution transcriptomic profiling of the heart during chronic stress reveals cellular drivers of cardiac fibrosis and hypertrophy. *Circulation*. 2020;142:1448–63.
- Forté E, Skelly DA, Chen M, Daigle S, Morelli KA, Hon O, et al. Dynamic interstitial cell response during myocardial infarction predicts resilience to rupture in genetically diverse mice. *Cell Rep*. 2020;30:3149–3163.e6.
- Farbehi N, Patrick R, Dorison A, Xaymardan M, Janbandhu V, Wystub-Lis K, et al. Single-cell expression profiling reveals dynamic flux of cardiac stromal, vascular and immune cells in health and injury. *Elife*. 2019;8:1–39.
- Tate M, Prakoso D, Willis AM, Peng C, Deo M, Qin CX, et al. Characterising an alternative murine model of diabetic cardiomyopathy. *Front Physiol*. 2019;10:1–15.
- Tate M, Higgins GC, de Blasio MJ, Lindblom R, Prakoso D, Deo M, et al. The mitochondria-targeted methylglyoxal sequestering compound, MitoGamide, is cardioprotective in the diabetic heart. *Cardiovasc Drugs Ther*. 2019;33:669–74.
- Westermann D, Rutschow S, Jäger S, Linderer A, Anker S, Riad A, et al. Contributions of inflammation and cardiac matrix metalloproteinase activity to cardiac failure in diabetic cardiomyopathy: The role of angiotensin type 1 receptor antagonism. *Diabetes*. 2007;56:641–6.
- Chiu PY, Walder K, Horlock D, Williams D, Nelson E, Byrne M, et al. CXCR4 antagonism attenuates the development of diabetic cardiac fibrosis. *PLoS ONE*. 2015;10:1–13.
- Huynh K, Bernardo BC, McMullen JR, Ritchie RH. Diabetic cardiomyopathy: Mechanisms and new treatment strategies targeting antioxidant signaling pathways. *Pharmacol Ther*. 2014;142:375–415.
- Tallquist MD, Molkenin JD. Redefining the identity of cardiac fibroblasts. *Nat Rev Cardiol*. 2017;14:484–91.
- Krsteovski C, Cohen CD, Dona MSI, Pinto AR. New perspectives of the cardiac cellular landscape: mapping cellular mediators of cardiac fibrosis using single-cell transcriptomics. *Biochem Soc Trans*. 2020;48:2483–93.
- Hutchinson KR, Lord CK, West TA, Stewart JA. Cardiac fibroblast-dependent extracellular matrix accumulation is associated with diastolic stiffness in type-2 diabetes. *PLoS ONE*. 2013;8:e72080.
- Prakoso D, de Blasio M, Kiriazis H, Qian H, Deo M, Jap E, et al. Cardiac remodelling and inflammation associated with diabetic cardiomyopathy is mitigated by phosphoinositide 3-kinase P110α gene delivery (abstract). *Heart Lung Circ*. 2017;26:550. <https://doi.org/10.1016/j.hlc.2017.06.016>.
- Fowlkes V, Clark J, Fix C, Law BA, Morales MO, Qiao X, et al. Type II diabetes promotes a myofibroblast phenotype in cardiac fibroblasts. *Life Sci*. 2013;92:669–76.
- Sedgwick B, Riches K, Bageghni SA, O'Regan DJ, Porter KE, Turner NA. Investigating inherent functional differences between human cardiac fibroblasts cultured from nondiabetic and Type 2 diabetic donors. *Cardiovasc Pathol*. 2014;23:204–10.
- Epelman S, Lavine KJ, Randolph GJ. Origin and functions of tissue macrophages. *Immunity*. 2014;41:21–35.
- Jadhav A, Tiwari S, Lee P, Ndisang JF. The heme oxygenase system selectively enhances the anti-inflammatory macrophage-M2 phenotype, reduces pericardial adiposity, and ameliorated cardiac injury in diabetic cardiomyopathy in Zucker diabetic fatty rats. *J Pharmacol Exp Ther*. 2013;345:239–49.
- Qin CX, Sleaby R, Davidoff AJ, Bell JR, de Blasio MJ, Delbridge LM, et al. Insights into the role of maladaptive hexosamine biosynthesis and O-GlcNAcylation in development of diabetic cardiac complications. *Pharmacol Res*. 2017;116:45–56. <https://doi.org/10.1016/j.phrs.2016.12.016>.
- Kassan M, Choi SK, Galán M, Bishop A, Umezawa K, Trebak M, et al. Enhanced NF-κB activity impairs vascular function through PARP-1-, SP-1-, and COX-2-dependent mechanisms in type 2 diabetes. *Diabetes*. 2013;62:2078–87.
- Swirski FK, Nahrendorf M. Leukocyte behavior in atherosclerosis, myocardial infarction, and heart failure. *Science*. 2013;339:161–6.
- Clarke MCH, Figg N, Maguire JJ, Davenport AP, Goddard M, Littlewood TD, et al. Apoptosis of vascular smooth muscle cells induces features of plaque vulnerability in atherosclerosis. *Nat Med*. 2006;12:1075–80.
- Martínez-Hervás S, Vinué Á, Núñez L, Andrés-Blasco L, Piqueras L, Tomás-Real J, et al. Insulin resistance aggravates atherosclerosis by reducing vascular smooth muscle cell survival and increasing CX3CL1/CX3CR1 axis. *Cardiovasc Res*. 2014;103:324–36.
- Segerstolpe Å, Palasantza A, Eliasson P, Andersson EM, Andréasson AC, Sun X, et al. Single-cell transcriptome profiling of human pancreatic islets in health and type 2 diabetes. *Cell Metab*. 2016;24:593–607.
- Wang YJ, Schug J, Won KJ, Liu C, Naji A, Avrahami D, et al. Single-cell transcriptomics of the human endocrine pancreas. *Diabetes*. 2016;65:3028–38.
- Rai V, Quang DX, Erdos MR, Cusanovich DA, Daza RM, Narisu N, et al. Single-cell ATAC-Seq in human pancreatic islets and deep learning upscaling of rare cells reveals cell-specific type 2 diabetes regulatory signatures. *Mol Metab*. 2020;32:109–21.
- Ruiz E, Gordillo-Moscote A, Padilla E, Redondo S, Rodríguez E, Reguillo F, et al. Human vascular smooth muscle cells from diabetic patients are resistant to induced apoptosis due to high Bcl-2 expression. *Diabetes*. 2006;55:1243–51.
- Hall JL, Matter CM, Wang X, Gibbons GH. Hyperglycemia inhibits vascular smooth muscle cell apoptosis through a protein kinase C-dependent pathway. *Circ Res*. 2000;87:574–80.

Content courtesy of Springer Nature, terms of use apply. Rights reserved.

of cells such as mesenchymal stem cells may contribute to the cardiac RMC compartment. Future work will consider whether resident or circulating cell populations drive the expansion of fibroblasts in the diabetic heart.

Conclusion

Here we have profiled the differences in the cardiac non-myocyte network, observing that the cellular landscape of the heart changes in a murine model of diabetes. By quantifying proportional shifts in a wide array of cell types simultaneously, these results offer a framework for understanding the cellular mechanisms that may drive pathological remodelling of the heart during the development of diabetes-induced HF. Future research will determine the precise cellular and molecular mechanisms that drive increased fibroblast numbers and the impact of this for development of diabetic cardiomyopathy. Targeting the molecular pathways that drive these non-myocyte cellular changes may offer new therapeutic avenues to address the cardiac complications associated with diabetes.

Supplementary Information

The online version contains supplementary material available at <https://doi.org/10.1186/s12933-021-01303-9>.

Additional file 1: Table S1. Physiological endpoint characteristics of STZ-HFD-induced murine diabetes. **Table S2.** Endpoint M-Mode echocardiography for assessing cardiac systolic function in murine diabetes. **Table S3.** Organ weights. **Table S4.** Flow cytometry antibody panel utilised in whole blood from mice. **Table S5.** Flow cytometry antibody panel utilised in myocardium from mice. **Figure S1.** (A) Representative images of transmural annular blood flow via Doppler echocardiography. Quantified Doppler flow; (B) Anaesthetised heart rate (HR), (C) peak E-wave velocity, (D) A-wave velocity (E) E/A ratio, (F) deceleration time (DT) and (G) isovolumic relaxation time (IVRT). (H) Shows representative images for tissue Doppler echocardiography, quantified in figures I–L. (I) Peak e' velocity ($P=0.054$), (J) peak a' velocity ($P=0.072$), (K) e'a' ratio, (L) Ee'e' ratio. ND = non-diabetic, DM = diabetes mellitus. Data presented as mean \pm SEM and individual data points, and analysed using an unpaired t-test. Statistical significance was assumed at $P < 0.05$. **Figure S2.** Flow cytometry gating strategies – Heart. A) Illustrates the gating strategies used for identification of cardiac non-myocyte cell populations. Single, intact cells are first identified by the FSC-A/FSC-H gate. Next, cells are deemed 'live and metabolically active' by gating all SYTOX-Calcein+ events as indicated. Live, metabolically active cells were then identified based on their cell clustering to each respective antibody (listed on the x and y-axes). ECs = Endothelial cells, RMCs = Resident mesenchymal cells, Leuks = Leukocytes, Undefined = Undefined cells, Macs = Macrophages, MHClihi/lo = MHClihi/lo macrophages, Fibros = Fibroblasts, Mural = Mural cells, SMCs = Smooth Muscle Cells, Schwann = Schwann cells, FSC-A = forward scatter area, FSC-W = forward scatter width, FSC-H = forward scatter height. B) Depicts the total number of live, metabolically active cells acquired per sample (from flow cytometry), split by treatment (ND = non-diabetic, DM = diabetes mellitus). Data is presented as individual values. Each line indicates the median. $P = NS$ (Student's unpaired t-test). **Figure S3.** Flow cytometry gating strategies – Blood. Illustrates the gating strategies used for identification of circulating leukocyte populations. Single, intact cells are first identified by the FSC-A/FSC-H gate. Live cells were identified as DAPI- (4',6-diamidino-2-phenylindole), after which cells are assigned as described in Supplementary Figure 2. FSC-A = forward scatter area, FSC-W = forward scatter width, FSC-H

= forward scatter height. **Figure S4.** Flow cytometry gating strategies – Bone marrow. Illustrates the gating strategies used for identification of bone marrow progenitors. Lin- = lineage negative, HSPC = haematopoietic stem cell, LSK = lineage- cKit+ cells, FSC-H = forward scatter height. Lineage cocktail = CD3, CD19, CD2, B220, TER119, CD11b, Gr-1, CD8, CD4. **Figure S5.** Flow cytometry gating strategies – Spleen. Illustrates the gating strategies used for identification of splenic monocytes. SSC-A = side scatter area. **Figure S6.** Histological identification of resident mesenchymal cells. Representative micrograph of murine left-ventricle stained with PCMI and GATA4 antibodies, counter-stained with DAPI. Monochrome images (left) indicate the positive signals acquired for nuclei enumeration. Each channel is then merged and displayed in colour (right). **Figure S7.** Histological identification of endothelial cells. Representative micrograph of murine left-ventricle stained with DACH1 and counter-stained with DAPI. Monochrome images (left) indicate the positive signals acquired for nuclei enumeration. Both channels are then merged and displayed in colour (right). **Figure S8.** Chronic hyperglycaemia is evident in diabetic mice throughout study duration. Hyperglycaemia was first detected 2-weeks after the commencement of STZ-HFD administration, and remains elevated until endpoint (measured fortnightly). Data is presented as mean \pm SEM. Statistical significance was determined by a repeated measures ANOVA using a Tukey's multiple comparison post-hoc test. ** $P < 0.01$, *** $P < 0.001$, **** $P < 0.0001$.

Acknowledgements

We wish to acknowledge the Monash Micro-Imaging (MMI) facility for provision of instrumentation and training.

Authors' contributions

CDC, MJD, RHR, ARP, conceived the experiments, GD, MJD, AJM and MKSL provided intellectual input. CDC, ARP, MJD, GEF, CK, TLG, MCF, DP, MD performed experiments. HK, DD performed echocardiography imaging and assisted with quality control of echocardiography analysis. CDC wrote the manuscript under ARP and RHR's guidance. RHR, ARP, MJD, GD edited the manuscript. All co-authors read and approved the final manuscript.

Funding

CDC, CK and TLG are supported by the La Trobe University Postgraduate Research Scholarship (LTUPRS), Research Training Program Fees Off-set (RTP-Fo) Scholarship. CDC is supported by a Baker Institute 'Bright Sparks' Scholarship. TLG is supported by Defence Science Institute (DSI) RHD Grant. This work was supported by a project grant to RHR and MJD from the National Health and Medical Research Council (NHMRC) of Australia (APP1158013), and an NHMRC fellowship to RHR (APP1059960) and in part by an infrastructure grant from the Victorian Government of Australia. This work was also supported by an NHMRC Ideas Grant (GNT1188503) to ARP.

Availability of data and materials

The datasets used and/or analysed during the current study are available from the corresponding author on reasonable request.

Declarations

Ethics approval

All animal-related experiments were approved by the Alfred Research Alliance (ARA) Animal Ethics Committee (Ethics number: E/1681/2016/B) and were in accordance with NHMRC guidelines.

Consent for publication

Not applicable.

Competing interests

None.

Author details

¹Heart Failure Pharmacology, Drug Discovery Biology, Monash Institute of Pharmaceutical Sciences, 399 Royal Parade, Parkville, VIC 3052, Australia. ²Cardiac Cellular Systems, Baker Heart and Diabetes Institute, 75 Commercial

40. Veres A, Baron M, Shen-Orr SS, Klein AM, Melton DA, Faust AL, et al. A single-cell transcriptomic map of the human and mouse pancreas reveals inter- and intra-cell population structure. *Cell Syst*. 2016;3:346–360. e4. <https://doi.org/10.1016/j.cels.2016.08.011>.
41. Fu J, Akat KM, Sun Z, Zhang W, Schlondorff D, Liu Z, et al. Single-cell RNA profiling of glomerular cells shows dynamic changes in experimental diabetic kidney disease. *J Am Soc Nephrol*. 2019;30:533–45.
42. Wilson PC, Wu H, Kirita Y, Uchimura K, Ledru N, Rennke HG, et al. The single-cell transcriptomic landscape of early human diabetic nephropathy. *Proc Natl Acad Sci USA*. 2019;116:19619–25.
43. Xiong X, Kuang H, Ansari S, Liu T, Gong J, Wang S, et al. Landscape of intercellular crosstalk in healthy and NASH liver revealed by single-cell secretome gene analysis. *Mol Cell*. 2019;75:644–660.e5.
44. Alex L, Russo I, Holoborodko V, Frangogiannis NG. Characterization of a mouse model of obesity-related fibrotic cardiomyopathy that recapitulates features of human heart failure with preserved ejection fraction. *Am J Physiol Heart Circ Physiol*. 2018;315:H934–49.
45. Kessler EL, Rivaud MR, Vos MA, van Veen TAB. Sex-specific influence on cardiac structural remodeling and therapy in cardiovascular disease. *Biol Sex Differ*. 2019. <https://doi.org/10.1186/s13293-019-0223-0>.
46. Beale AL, Meyer PM, Marwick TH, Lam CSP, Kaye DM. Sex differences in cardiovascular pathophysiology why women are overrepresented in heart failure with preserved ejection fraction. *Circulation*. 2018;138:198–205.
47. Kahn SE, Cooper ME, del Prato S. Pathophysiology and treatment of type 2 diabetes: perspectives on the past, present, and future. *Lancet*. 2014;383:1068–83.
48. Yoon K-H, Lee J-H, Kim J-W, Cho J-H, Choi Y-H, Ko S-H, et al. Epidemic obesity and type 2 diabetes in Asia. *Lancet*. 2006;368:1681–8.
49. George AM, Jacob AG, Fogelfeld L. Lean diabetes mellitus: an emerging entity in the era of obesity. *World J Diabetes*. 2015;6:613.

Publisher's Note

Springer Nature remains neutral with regard to jurisdictional claims in published maps and institutional affiliations.

Ready to submit your research? Choose BMC and benefit from:

- fast, convenient online submission
- thorough peer review by experienced researchers in your field
- rapid publication on acceptance
- support for research data, including large and complex data types
- gold Open Access which fosters wider collaboration and increased citations
- maximum visibility for your research: over 100M website views per year

At BMC, research is always in progress.

Learn more biomedcentral.com/submissions



Content courtesy of Springer Nature, terms of use apply. Rights reserved.

3.5 Supplementary material

Additional file 1

Diastolic Dysfunction in a Pre-Clinical Model of Diabetes is Associated with Changes in the Cardiac Non-myocyte Cellular Composition

Cardiovascular diabetology

Charles D. Cohen^{1,2,5}, Miles J. De Blasio¹, Man K. S. Lee³, Gabriella E. Farrugia², Darnel Prakoso¹, Crisdion Krstevski^{2,5}, Minh Deo¹, Daniel G. Donner^{4,6}, Helen Kiriazis^{4,6}, Michelle C. Flynn³, Taylah L. Gaynor^{2,5}, Andrew J. Murphy³, Grant R. Drummond⁵, Alexander R. Pinto^{2,5*}, Rebecca H. Ritchie^{1,5*}.

¹Heart Failure Pharmacology, Drug Discovery Biology, Monash Institute of Pharmaceutical Sciences, Parkville, VIC; ²Cardiac Cellular Systems, ³Haematopoiesis and Leukocyte Biology, ⁴Preclinical Cardiology, Microsurgery & Imaging Platform, Baker Heart and Diabetes Institute, Prahran, VIC; ⁵Department of Physiology, Microbiology and Anatomy, La Trobe University, Bundoora, VIC, ⁶Baker Department of Cardiometabolic Health, The University of Melbourne, Parkville VIC 3010, Australia.

**Equal contribution*

Supplementary Table 1 – Physiological endpoint characteristics of STZ-HFD-induced murine diabetes

Parameters	ND	DM
<i>n</i>	7	19
Blood glucose (mmol/mol)	8.5±0.2	22.9±0.5****
HbA1c (%)	3.8±0.2	6.9±0.5**
Body Weight (g)	33.3±0.9	33.3±0.9
Fat mass (g)	8.48±2.0	7.51±3.9
Lean mass (g)	26.7±1.9	26.7±1.9
Glucose tolerance (AUC)	2396±163	4654±128****
Insulin tolerance (AUC)	471±29	540±80

Physiological parameters measured to assess the degree of diabetes-mellitus (DM) in STZ-HFD treated mice at endpoint. Data presented as mean ± SEM and analysed using an unpaired t-test. Statistical significance was assumed at $P < 0.05$, ** $P < 0.01$, **** $P < 0.0001$. AUC = area under the curve, DM = diabetes mellitus.

Supplementary Table 2 – Endpoint M-Mode echocardiography for assessing cardiac systolic function in murine diabetes

Parameters	ND	DM
<i>n</i>	7	19
Heart rate (bpm)	390±33	414±16
AWd (mm)	0.73±0.04	0.76±0.03
LVEDD (mm)	4.08±0.08	4.07±0.07
PWd (mm)	0.75±0.05	0.79±0.02
LVESD (mm)	2.86±0.06	2.6±0.08
Fractional shortening (%)	29.8±1.35	36.1±1.47*

Data presented as mean ± SEM and analysed using an unpaired t-test. Statistical significance was assumed at $P < 0.05$. AWd; anterior wall diastolic thickness, LVEDD; LV end diastolic dimension, PWd; posterior wall diastolic thickness, DM = diabetes mellitus.

Supplementary Table 3 – Organ weights

Organ	ND	DM
<i>n</i>	7	19
Tibial length (mm)	18.1±0.1	18.1±0.1
Heart weight (mg)	130.2±3.3	154.2±9.0
Liver weight (g)	1.5±0.05	2.1±1.1**
Spleen weight (mg)	99.5±3.6	121.7±8.5
Heart weight/tibial length	7.2±0.2	7.9±0.2
Liver weight/tibial length	84.7±2.7	107.7±3.8**
Spleen weight/tibial length	5.5±0.2	7.2±0.5

Represents the raw organ weights and weights relative to tibia length. Data are presented as mean ± SEM and analysed by unpaired t-test. * $P < 0.05$.

Supplementary Table 4 – Flow cytometry antibody panel utilised in whole blood from mice

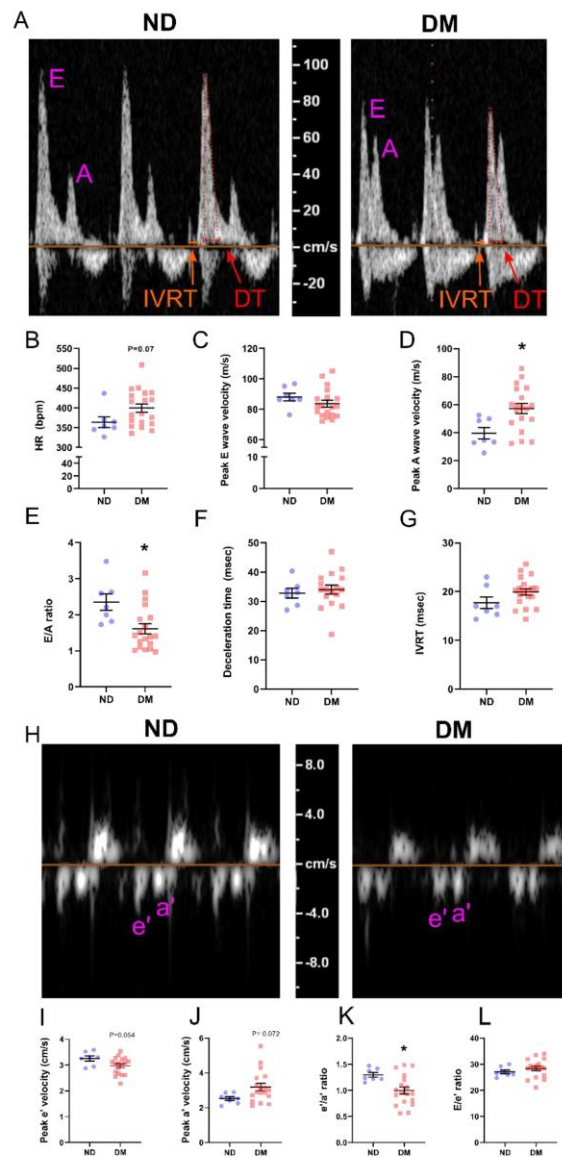
Antibody Target/Dye	Cat #	Company	Clone	Staining pattern
DAPI	D9542-5MG	Sigma-Aldrich	N/A	Dead cells
CD45R/B220	103241	BD Biosciences	RA3-6B2	B-cells
CD3e	11-0033-81	BD Biosciences	500A2	T-cells
Gr1 (Ly6G/Ly6C)	552093	BD Biosciences	RB6-8C5	Monocytes & Neutrophils
CD115	135506	BD Biosciences	AFS98	Monocytes
CD4	116016	BD Biosciences	RM4-4	CD4 ⁺ T-cells
CD8	126612	BD Biosciences	YTS156.7.7	CD8 ⁺ T-cells
CD45	557659	BD Biosciences	30-F11	Pan leukocytes

Lists the antibody cocktail utilised for whole blood flow cytometry. 7 antibodies and 1 dye (DAPI) were used in this study to detect a range of leukocytes. Note: cell types in column 5 are the identifiable cells for the purpose of this study and may not apply in different contexts. For more detailed information regarding flow cytometry gating strategies and cellular identification, see Supplementary Figure 3.

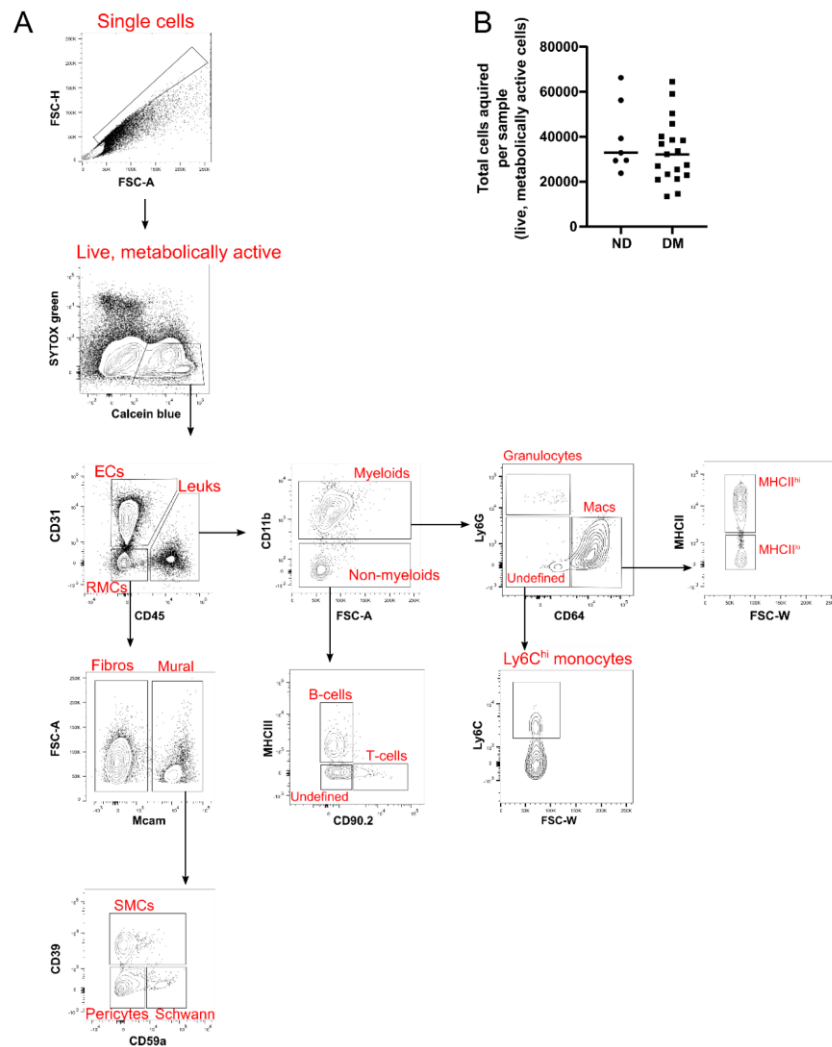
Supplementary Table 5 – Flow cytometry antibody panel utilised in myocardium from mice

Antibody Target/Dye	Cat #	Company	Clone	Staining pattern
CD31	740879	BD Biosciences	390	Endothelial cells
I-A/I-E (MHCII)	743876	BD Biosciences	2G9	B-cells, macrophages
CD11b	564443	BD Biosciences	M1/70	Myeloid cells
CD64 (a & b alloantigens)	740622	BD Biosciences	X54-5/7.1	Macrophages
CD146 (Mcam)	740827	BD Biosciences	ME-9F1	Mural cells
eBioscience™ Calcein Blue AM Viability Dye	65-0855-39	Invitrogen	N/A	Metabolically active cells
Ly6C	128012	Biolegend	HK1.4	Monocytes
CD59a	130-104-105	Miltenyi Biotec	REA287	Schwann cells
Ly6G	127648	Biolegend	1A8	Granulocytes
NK1.1	108716	Biolegend	PK136	Natural killer cells
CD39	143806	Biolegend	Duha59	Smooth muscle cells
SYTOX™ Green Dead Cell Stain	S34860	Invitrogen	N/A	Dead cells
CD90.2	105320	Invitrogen	30-H12	T-cells
CD45	557659	BD Biosciences	30-F11	Pan leukocytes

Lists the antibody cocktail utilised for flow cytometry of cardiac ventricles. 12 antibodies and 2 dyes (SYTOX green and Calcein blue) were used in this study to detect an array of cardiac non-myocytes. Note: cell types in column 5 are the identifiable cells for the purpose of this study and may not apply in different contexts. For more detailed information regarding flow cytometry gating strategies and cellular identification, see Supplementary Figure 2.

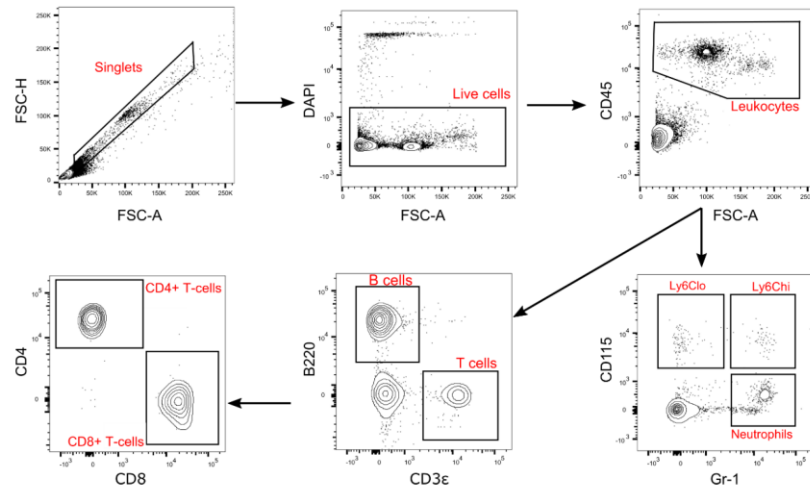


Supplementary Figure 1: (A) Representative images of transmitral annular blood flow via Doppler echocardiography. Quantified Doppler flow; (B) Anaesthetised heart rate (HR), (C) peak E-wave velocity, (D) A-wave velocity (E) E:A ratio, (F) deceleration time (DT) and (G) isovolumic relaxation time (IVRT). (H) Shows representative images for tissue Doppler echocardiography, quantified in figures I-L. (I) Peak e' velocity ($P=0.054$), (J) peak a' velocity ($P=0.072$), (K) e':a' ratio, (L) E:a' ratio. ND = non-diabetic, DM = diabetes mellitus. Data presented as mean \pm SEM and individual data points, and analysed using an unpaired t-test. Statistical significance was assumed at $P < 0.05$.



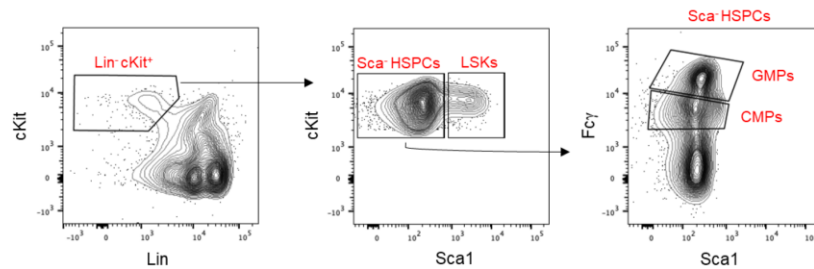
Supplementary Figure 2: Flow cytometry gating strategies – Heart

A) Illustrates the gating strategies used for identification of cardiac non-myocyte cell populations. Single, intact cells are first identified by the FSC-A/FSC-H gate. Next, cells are deemed 'live and metabolically active' by gating all SYTOX⁺Calcein⁺ events as indicated. Live, metabolically active cells were then identified based on their cell clustering to each respective antibody (listed on the x and y-axes). ECs = Endothelial cells, RMCs = Resident mesenchymal cells, Leuks = Leukocytes, Undefined = Undefined cells, Macs = Macrophages, MHCII^{hi/lo} = MHCII^{hi/lo} macrophages, Fibros = Fibroblasts, Mural = Mural cells, SMCs = Smooth Muscle Cells, Schwann = Schwann cells, FSC-A = forward scatter area, FSC-W = forward scatter width, FSC-H = forward scatter height. **B)** Depicts the total number of live, metabolically active cells acquired per sample (from flow cytometry), split by treatment (ND = non-diabetic, DM = diabetes mellitus). Data is presented as individual values. Each line indicates the median. $P = NS$ (Student's unpaired t -test).



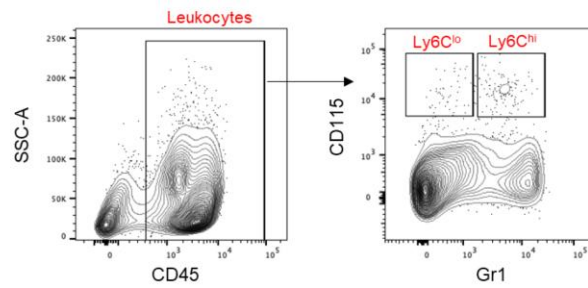
Supplementary Figure 3 – Flow cytometry gating strategies - Blood

Illustrates the gating strategies used for identification of circulating leukocyte populations. Single, intact cells are first identified by the FSC-A/FSC-H gate. Live cells were identified as DAPI⁺ (4',6-diamidino-2-phenylindole), after which cells are assigned as described in Supplementary Figure 2. FSC-A = forward scatter area, FSC-W = forward scatter width, FSC-H = forward scatter height.



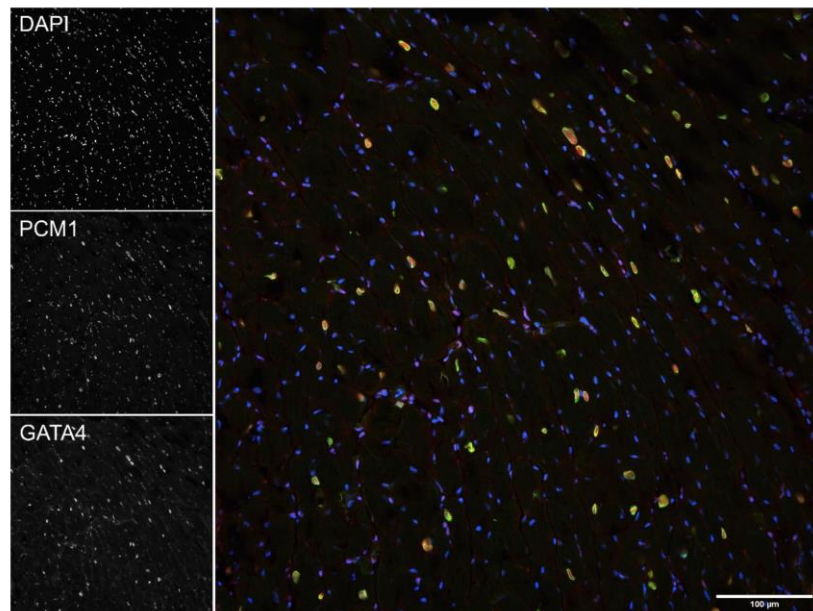
Supplementary Figure 4 –Flow cytometry gating strategies – Bone marrow

Illustrates the gating strategies used for identification of bone marrow progenitors. Lin⁻ = lineage negative, HSPC = haematopoietic stem cell, LSK = lineage⁻ cKit⁺ cells, FSC-H = forward scatter height. Lineage cocktail = CD3, CD19, CD2, B220, TER119, CD11b, Gr-1, CD8, CD4.



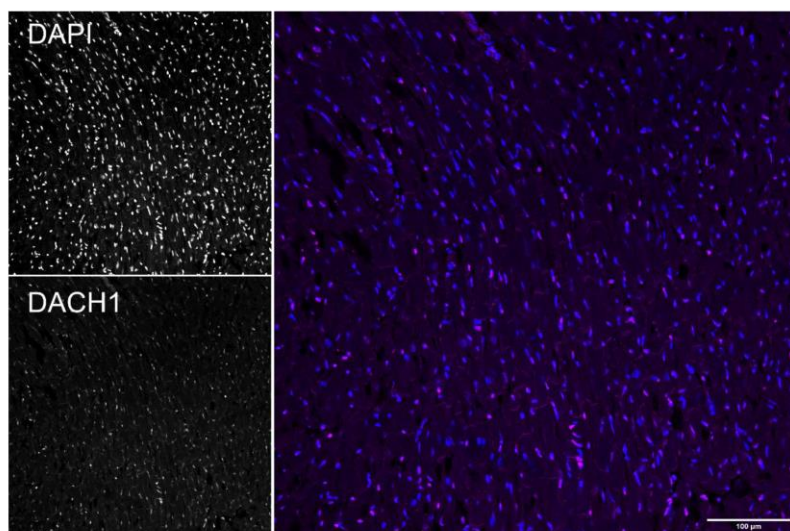
Supplementary Figure 5 – Flow cytometry gating strategies – Spleen

Illustrates the gating strategies used for identification of splenic monocytes. SSC-A = side scatter area.



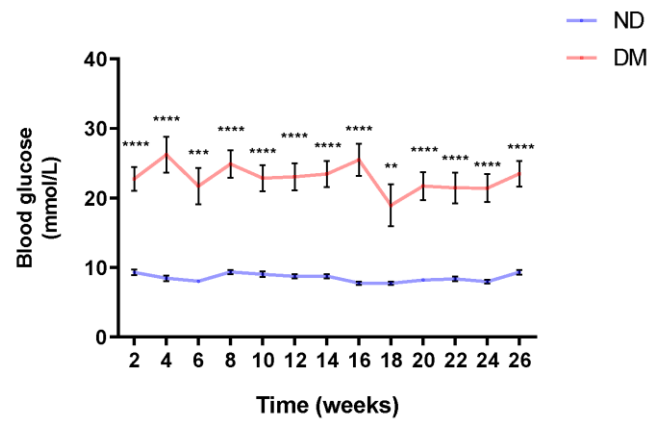
Supplementary Figure 6 – Histological identification of resident mesenchymal cells

Representative micrograph of murine left-ventricle stained with PCM1 and GATA4 antibodies, counter-stained with DAPI. Monochrome images (left) indicate the positive signals acquired for nuclei enumeration. Each channel is then merged and displayed in colour (right).



Supplementary Figure 7 – Histological identification of endothelial cells

Representative micrograph of murine left-ventricle stained with DACH1 and counter-stained with DAPI. Monochrome images (left) indicate the positive signals acquired for nuclei enumeration. Both channels are then merged and displayed in colour (right).



Supplementary Figure 8 – Chronic hyperglycaemia is evident in diabetic mice throughout study duration

Hyperglycaemia was first detected 2-weeks after the commencement of STZ-HFD administration, and remains elevated until endpoint (measured fortnightly). Data is presented as mean \pm SEM. Statistical significance was determined by a repeated measures ANOVA using a Tukey's multiple comparison post-hoc test. $**P < 0.01$, $***P < 0.001$, $****P < 0.0001$.

Chapter 4

Exploring the progressive differences in cardiac cellular composition in the *db/db* model of type-2 diabetes

4.1 Introduction

As discussed in the previous Chapter, type-2 diabetes (T2D) results in an increased risk of heart failure (HF) hospitalisation and mortality [260,261], accompanied by a number of cardiac morphological, cellular and molecular alterations [5,19,53,66]. Moreover, the development of T2D-induced HF represents a chronic, progressive phenotype of pathological cardiac remodelling [262]. As discussed in Chapter 3, the contribution of cardiac non-myocyte cells in the context of diabetes-induced cardiac dysfunction *in toto* remains understudied. Numerous mouse models of diabetes-induced HF exist, with many recapitulating the key characteristics of diabetes associated cardiac dysfunction [53,55,263–265].

Our group have previously characterised the functional and morphological alterations [53], and the non-myocyte cardiac cellular composition [5], in the STZ-HFD model of T2D, with diabetes inducing a fibrogenic, pro-inflammatory cardiac environment. However, these mice did not gain excessive weight - a common comorbidity of T2D. The leptin receptor deficient *db/db* mouse model (B6.BKS[D]-Lepr^{db}/J) is among the most commonly used rodent models that accurately recapitulates the T2D phenotype. This mouse model displays overt obesity, hyperglycaemia, hyperlipidaemia, hypercholesterolaemia and insulin resistance, all of which are relevant features of clinical T2D [247,266,267]. Building on the findings from Chapter 3, I selected the clinically relevant *db/db* mouse model of T2D to perform cardiac flow cytometry analogous to the STZ-HFD model. In addition, given that cardiac remodelling in T2D is chronic and progressive, I conducted a time-course study using cardiac flow cytometry, to assess the temporal cellular changes in this context. To date, there have been no studies assessing the progressive cellular changes in the cardiac cellular landscape in T2D-induced HF.

As such, three separate cohorts of male *db/db* mice and their heterozygote non-diabetic littermates (*db/h*) were aged to 10, 17 and 24-weeks of age for analysis. These time-points were chosen based on previous, unpublished preliminary work from our group, suggesting that commencement of cardiac dysfunction in *db/db* mice occurs at approximately 17-weeks of age. Analogous to Chapter 3, cardiac and whole blood flow cytometry were performed in each of these cohorts to determine the cellular shifts at different stages of T2D. Similarly to Chapter 3, a range of physiological tests were performed, including echocardiography to determine the degree of cardiac dysfunction in *db/db* mice. Importantly, detailed investigation of cardiac cellular heterogeneity in this context is warranted for application of novel technologies such as single-cell transcriptomics (Chapter 5).

4.2 Methodology

For a detailed description of this methodology, see Chapter 2, Section 2.7. All animal-related experiments were approved by the Alfred Research Alliance (ARA) Animal Ethics Committee (Ethics number: E/1880/2019/B) and were performed in accordance with the National Health and Medical Research Council of Australia guidelines. Male *db/db* mice ([B6.BKS(D)-Lepr^{db}/J], stock #000697) [13] and their heterozygous non-diabetic littermates (*db/h*) were obtained from The Jackson Laboratory (Bar Harbor ME, USA). Mice were underwent physiological assessment at each time point (10, 17, 24-weeks of age), after which euthanasia was performed (as described in Chapter 2, Section 2.6) to allow for tissue preparation and cardiac flow cytometry ($n = 8/\text{group}$ unless otherwise stated). Due to diabetic complications, mortality was higher in the 24-week old *db/db* cohort (with 2 premature *db/db* deaths), reducing the statistical power for some of our analyses. Raw cardiac flow cytometry data was processed using FlowJo (v10.5.3), where conventional gating strategies were performed as previously reported (Figure 4.1) [5,234,250]. Quantification of flow cytometry data was analysed statistically and illustrated using GraphPad Prism (v8.1.2), from raw flow cytometry data. To simplify visualisation of flow cytometry data, spanning-tree progression analysis for density-normalized events (SPADE; Cytobank Premium©, CA, USA) was conducted. Live, metabolically active cells (SYTOXTM Green⁻, Calcein Blue⁺) acquired from cardiac flow cytometry were merged into experimental groups (*db/db*, *db/h*) and uploaded to Cytobank for SPADE analysis. Pertaining to SPADE analyses, between 100 – 200 target nodes were chosen and the down-sampled events target was set at 50%. For more information regarding SPADE analysis, see Chapter 2, Section 2.16 and Figure 2.3.

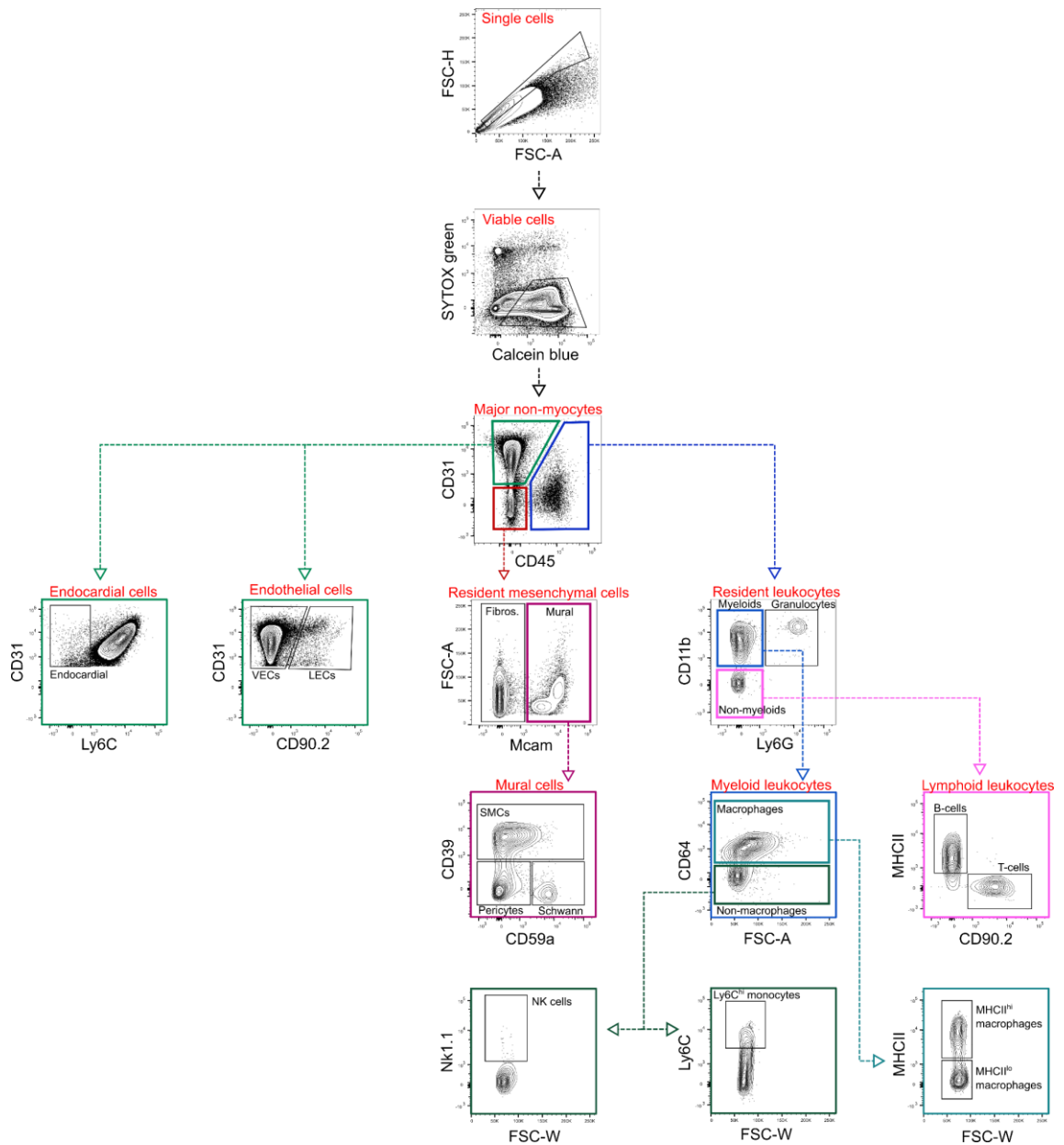


Figure 4.1: Conventional gating strategies for identification of cardiac non-myocyte cells. Single cells are first identified by the FSC-A/FSC-H gate. Next, cells are deemed ‘live and metabolically active’ by gating all SYTOX-Calcein+ events as indicated. Live, metabolically active cells were then identified based on their cell clustering to each respective antibody (listed on the x and y-axes). ECs = Endothelial cells, RMCs = Resident mesenchymal cells, Leuks = Leukocytes, Undefined = Undefined cells, Macs = Macrophages, MHCII^{hi/lo} = MHCII^{hi/lo} macrophages, Fibros = Fibroblasts, Mural = Mural cells, SMCs = Smooth Muscle Cells, Schwann = Schwann cells, FSC-A = forward scatter area, FSC-W = forward scatter width, FSC-H = forward scatter height.

4.3 Results

4.3.1 The systemic characteristics of *db/db* mice recapitulate features of clinical T2D

Each cohort of male *db/db* and *db/h* mice were culled at each respective endpoint for further analysis (Figure 4.2A). To confirm the T2D phenotype, a range of physiological tests were conducted upon euthanasia. All *db/db* mice exhibited hyperglycaemia as shown by elevated of glycated haemoglobin (% HbA1c) at each time-point, relative to their *db/h* control counterparts (Figure 4.2B, $P < 0.001$). In contrast to the model used in Chapter 3, *db/db* mice gained excessive weight at each time-point relative to *db/h* mice (Figure 4.2C, $P < 0.01$). Moreover, *db/db* mice displayed increased percentage fat mass (relative to total body weight) at each time-point, detected by EchoMRI body composition analysis (Figure 4.2D, $P < 0.0001$). Interestingly, lean mass (g) calculated by EchoMRI analysis was significantly reduced in *db/db* mice relative to *db/h* mice, at each time-point (Figure 4.2E, $P < 0.01$).

4.3.2 Cardiac dysfunction is evident in *db/db* mice *in vivo*

4.3.2.1 Pulsed-wave mitral Doppler echocardiography

Each mouse cohort also underwent echocardiography *in vivo* just prior to euthanasia, to assess the degree of cardiac functional impairment in *db/db* mice, relative to *db/h* controls. Pulsed-wave Doppler echocardiography was performed to determine mitral blood flow velocity in the early (E-wave) and late (A-wave) phase of diastole (Figure 4.3A-F). Anaesthetised heart rate (HR) was not different between experimental groups at any time-point (Figure 4.3A). Similarly, both the peak E-wave and peak A-wave were unaltered between experimental cohorts at each time point (Figure 4.3B-C). Consequently, there was no difference in the E/A ratio between experimental groups at any time-point (Figure 4.3D), contrary to findings from Chapter 3. Isovolumic relaxation time (IVRT) was unaltered between *db/db* and *db/h* mice at each time-point (Figure 4.3E). While deceleration time (DT) was also not different between experimental groups at 10-weeks and 17-weeks of age, DT increased in 24-week old *db/db* mice relative to controls (Figure 4.3F, $P < 0.05$). While unchanged at 10 and 24-weeks of age, the peak e' velocity was significantly decreased at 17-weeks of age in *db/db* mice (Figure 4.3G, $P < 0.01$). The peak a' velocity was unchanged at all time-points between experimental groups (Figure 4.3H). There were no statistically significant differences in the e'/a' ratio between experimental groups, despite a tendency for a reduced e'/a' ratio at 17 and 24-weeks (Figure 4.3I, both $P = 0.08$). The E/ e' ratio was unchanged in 10 and 24-week old mice, however was significantly increased in *db/db* mice relative to *db/h* controls at 17 weeks of age (Figure 4.3J, $P < 0.01$).

4.3.2.2 M-mode echocardiography

In addition to mitral flow velocity, M-Mode echocardiography was performed to infer any differences in ventricular wall thickness and chamber size between *db/db* and *db/h* mice. The cardiac anterior wall diastolic dimension (AWd) was unchanged between experimental groups, at every time-point (Figure 4.4A). The posterior wall diastolic dimension (PWd) was also not different

between experimental groups, at each time-point (Figure 4.4B). LV end-diastolic dimension (LVEDD) was significantly decreased at 17-weeks of age in *db/db* mice, but unaltered at 10 and 24-weeks of age between experimental groups (Figure 4.4C, $P < 0.01$). The LV end-systolic dimension (LVESD) was significantly decreased in *db/db* mice at 10 and 17-weeks of age, but unchanged at 24-weeks of age (Figure 4.4D, $P < 0.01$). Interestingly, percentage fractional shortening (% FS) was significantly increased in *db/db* mice at 17 and 24-weeks of age ($P < 0.05$), but unaltered in *db/db* mice at 10-weeks of age.

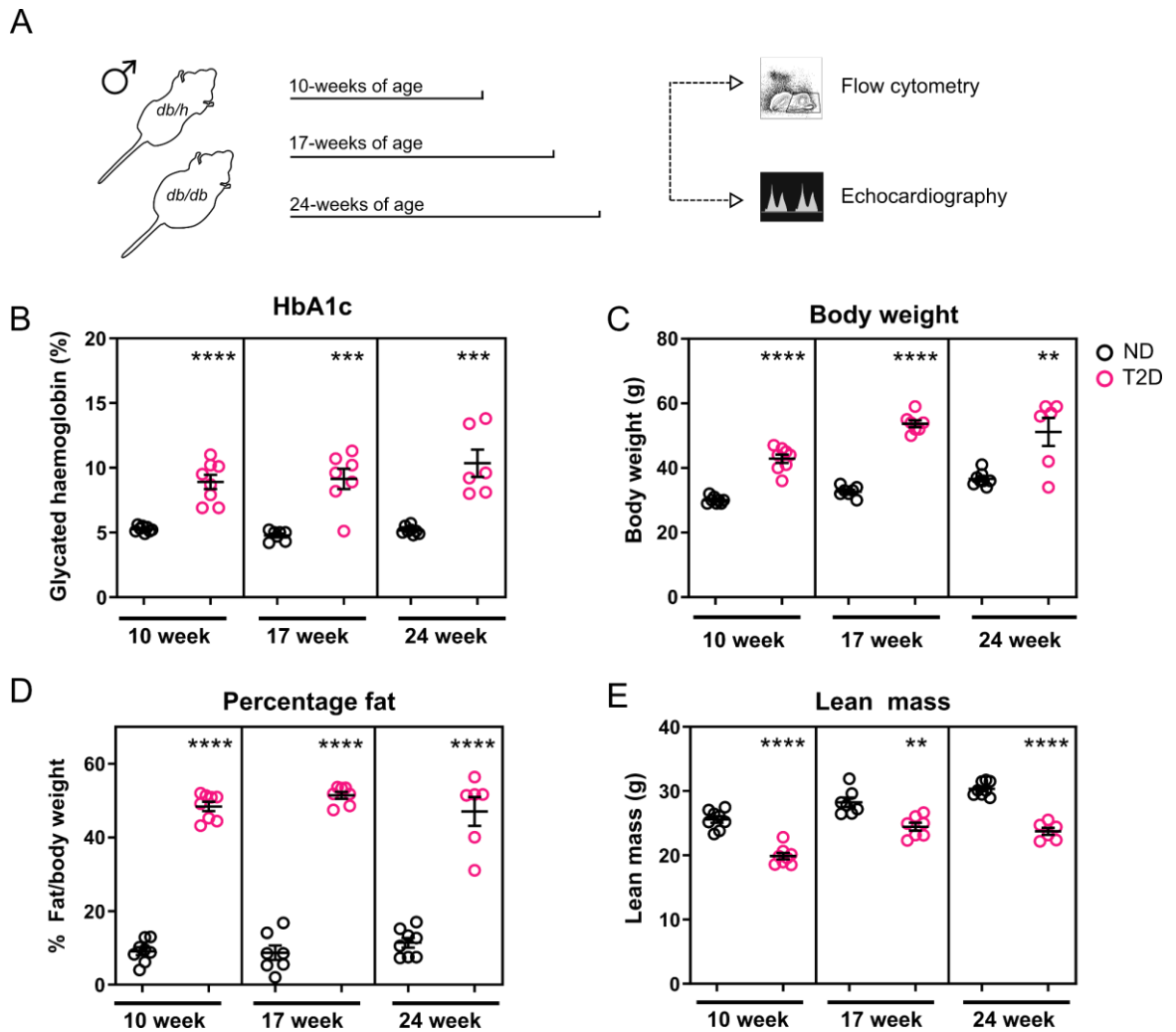


Figure 4.2: Systemic characteristics of *db/db* mice recapitulate clinical characteristics of T2D
(A) Schematic illustrating the experimental outline of the study. **(B)** The percentage of glycated haemoglobin (HbA1c) in T2D mice compared to ND mice at each time-point. **(C)** Body weight (grams) of T2D mice relative to their ND counterparts at each time-point. **(D)** Percentage fat derived from EchoMRI body composition analysis in T2D mice compared to ND mice. **(E)** Lean mass (grams) of T2D mice relative to their ND counterparts. ND, = non-diabetic (*db/h*) T2D = type-2 diabetes (*db/db*). Data presented as mean \pm SEM and individual data points. Statistical significance was achieved by an unpaired Student's *t*-test at each age for each cohort. * $P < 0.05$, ** $P < 0.01$, *** $P < 0.001$, **** $P < 0.0001$.

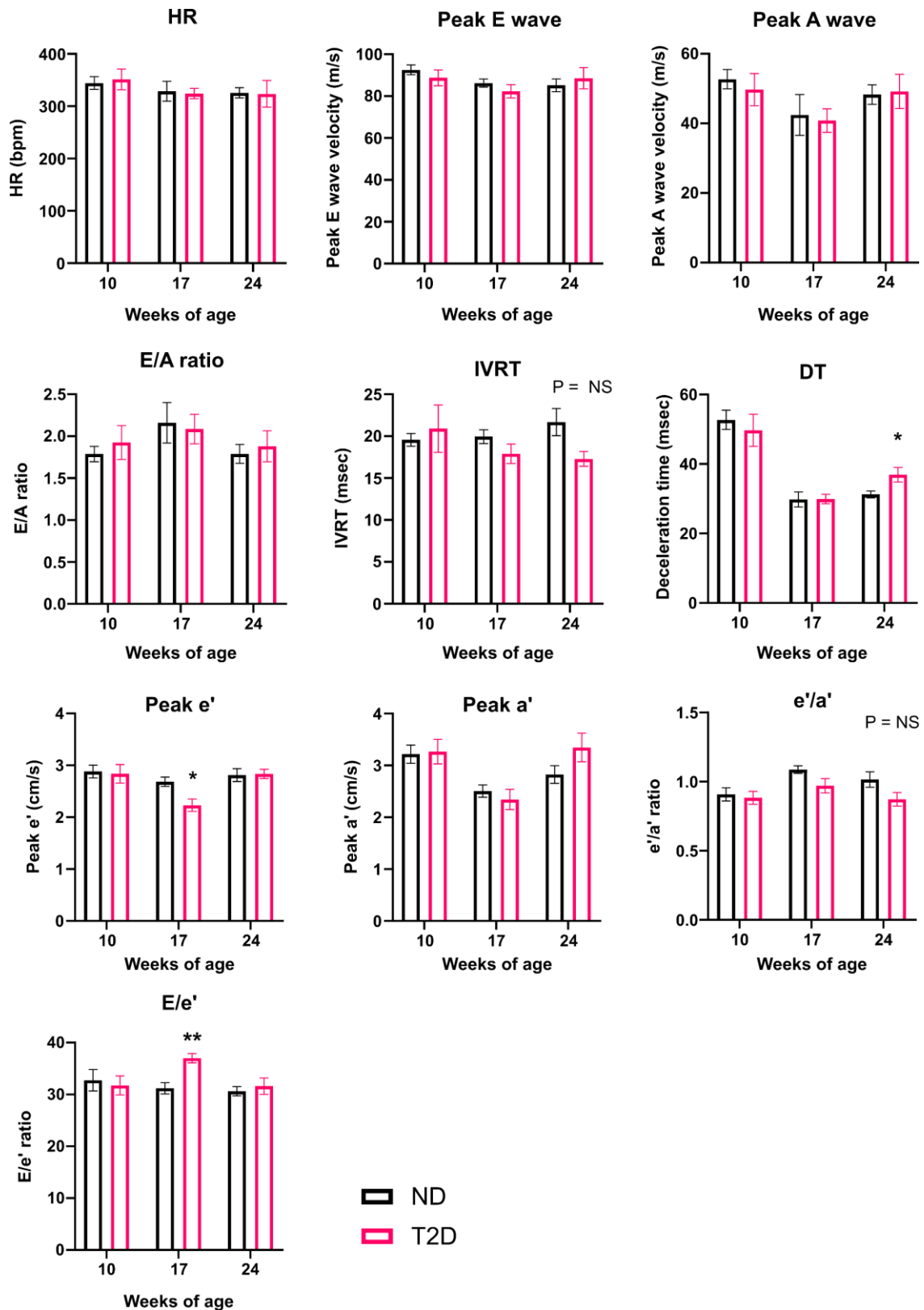


Figure 4.3: Doppler transmitral annular valve and blood flow in *db/h* and *db/db* mice

Doppler flow echocardiography acquiring mitral blood flow yielded; (A) anaesthetised heart rate (HR), (B) peak E-wave velocity (C) peak A-wave, (D) E/A ratio, (E) isovolumic relaxation time (IVRT) and (F) deceleration time. Mitral valve velocity obtained from tissue Doppler echocardiography generated; (G) the peak e' (H) the peak a' velocity, as well as the (I) e'/a' ratio. (J) E/e' ratio. Measurement of echocardiography parameters is highlighted in Chapter 2, Section 2.15. ND, = non-diabetic (*db/h*) T2D = type-2 diabetes (*db/db*). Data presented as mean \pm SEM and individual data points. Statistical significance was achieved by an unpaired Student's *t*-test comparing *db/h* vs. *db/db* at each time-point. * $P < 0.05$, ** $P < 0.01$.

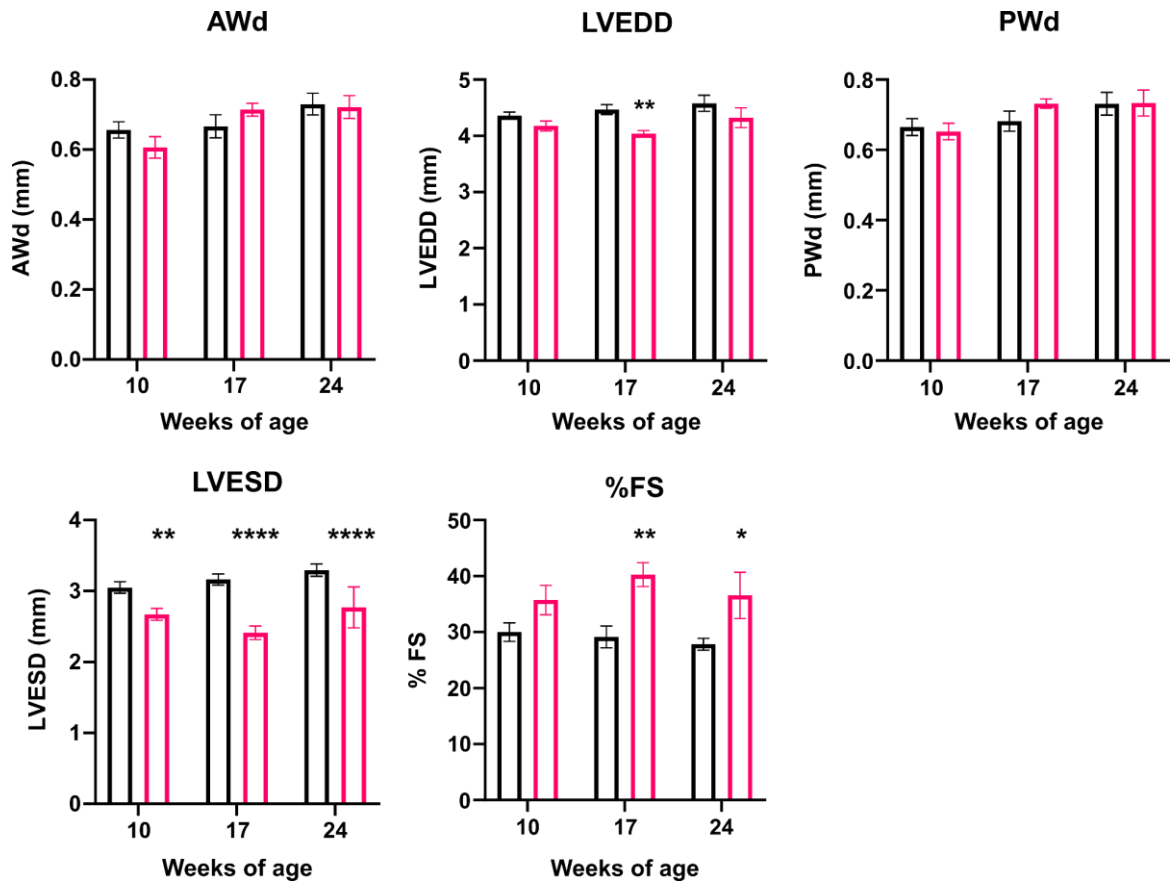


Figure 4.4: M-Mode echocardiography of *db/db* and *db/h* mice

(A) Cardiac anterior wall diastolic dimension (AWd). (B) Posterior wall diastolic dimension (PWd). (C) Left ventricular (LV) end-diastolic dimension (LVEDD). (D) LV end-systolic dimension (LVESD). (E) Percentage fractional shortening (% FS). This was calculated as indicated; $\%FS = [(LVEDD - LVESD) / LVEDD] \times 100$. Data is presented as mean \pm SEM and individual data points. Statistical significance was achieved by an unpaired Student's t-test comparing *db/h* vs. *db/db* at each time-point. * $P < 0.05$, ** $P < 0.01$. *** $P < 0.001$, **** $P < 0.0001$. ND = non-diabetic (*db/h*), T2D = type-2 diabetes (*db/db*).

4.3.3 Profiling the circulating leukocytes in *db/h* and *db/db* mice

Considering that T2D typically induces monocytosis and neutrophilia [113,114], I conducted flow cytometry on whole blood to measure the proportions of disparate circulating immune cells. At the 10-week time-point, there were no major differences in any circulating myeloid (Figure 4.5A) or lymphoid (Figure 4.5B) leukocytes between *db/db* or *db/h* mice. In 17-week old *db/db* mice however, monocytes were significantly elevated relative to *db/h* controls (Figure 4.5C, $P < 0.05$), which included both Ly6C^{hi} and Ly6C^{lo} monocyte subtypes (Figure 4.5C, $P < 0.05$). Neutrophil numbers were also significantly higher in *db/db* mice at this time-point relative to control mice (Figure 4.5C, $P < 0.05$), whereas there were no statistical differences in any lymphoid leukocyte cell type at this time-point (Figure 4.5D). At 24-weeks of age, there were no apparent alterations in circulating leukocytes, despite myeloid cells trending upward (Figure 4.5D-E, $P = \text{NS}$). This could be attributed, at least in part, to the lower animal numbers in the 24-week old *db/db* cohort (Section 4.2). In parallel, I next profiled the cardiac non-myocyte cellular landscape at each respective time-point by cardiac flow cytometry, to determine the cardiac cellular response to such systemic aberrances.

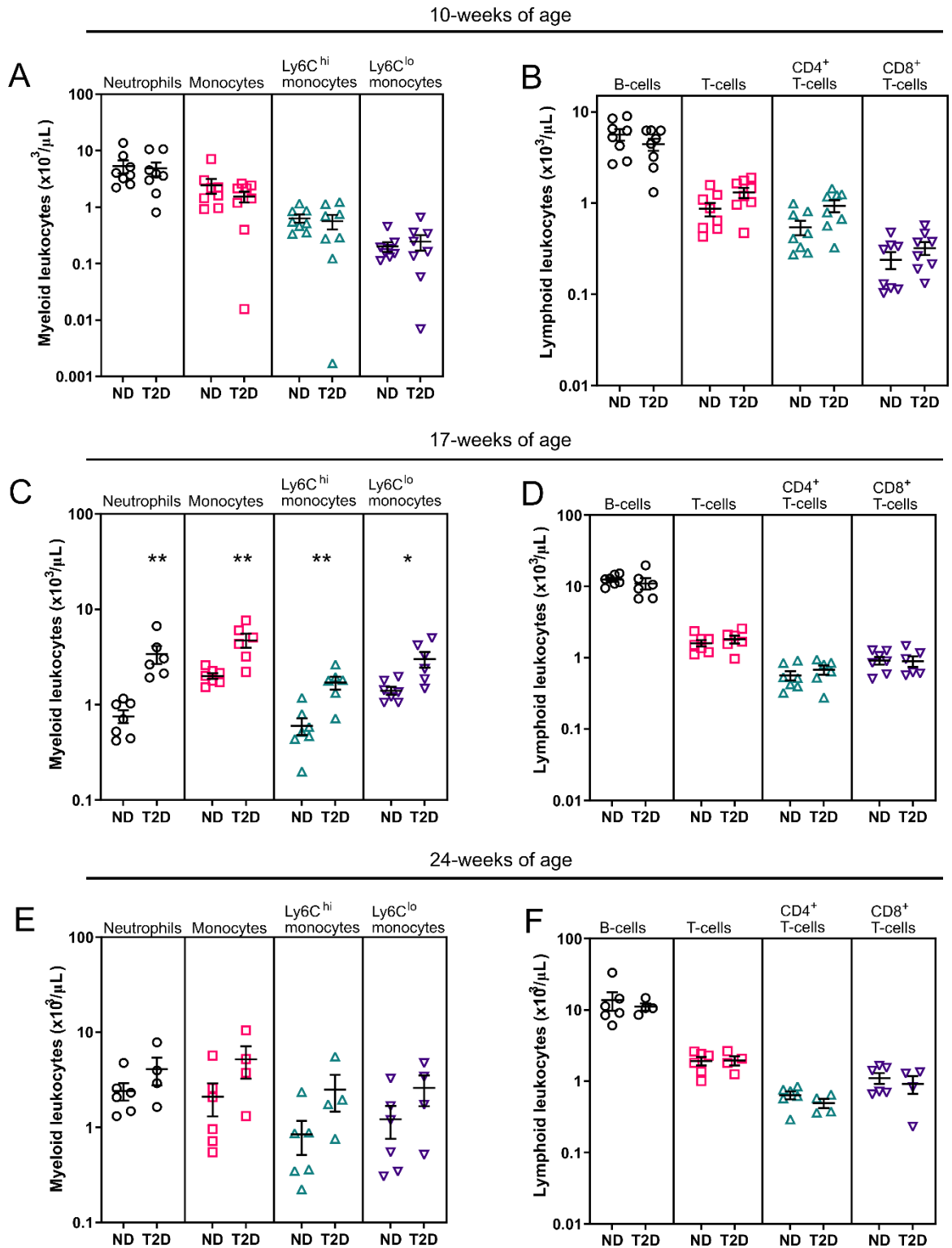


Figure 4.4: Circulating leukocytes in whole blood in *db/db* and *db/h* mice at each time-point (A) Circulating myeloid leukocytes and (B) lymphocytes in *db/h* and *db/db* mice at 10-weeks of age ($n = 8/\text{group}$). (C) Circulating myeloid cells and (D) lymphocytes at 17-weeks of age in *db/db* mice ($n = 6$) and *db/h* mice ($n = 7$). (E) Myeloid and (F) lymphoid leukocytes in *db/db* mice ($n = 4$) and *db/h* mice ($n = 6$). Data is presented as mean \pm SEM and individual data points. Statistical significance was achieved by an unpaired Student's *t*-test comparing *db/h* vs. *db/db* at each time-point. * $P < 0.05$, ** $P < 0.01$. ND = non-diabetic (*db/h*), T2D = type-2 diabetes (*db/db*).

4.3.4 The cardiac cellular composition of 10-week old *db/h* and *db/db* mice

To assess the effect of T2D on the murine cardiac cellular landscape in 10-week old mice, cardiac flow cytometry was performed on *db/db* and *db/h* mice, yielding viable non-myocyte cells. Live, metabolically active cells were manually gated (illustrated in Figure 4.1) and quantified as previously mentioned (Section 4.2). SPADE analysis of live, metabolically active cells was utilised to visualise the key differences in the non-myocyte cellular landscape between *db/db* and *db/h* control mice (Figure 4.6A). While vascular ECs (VECs) were unaltered, lymphatic ECs (LECs) were significantly reduced in *db/db* mice, relative to *db/h* controls (Figure 4.6B, $P < 0.001$). In contrast, endocardial cells were significantly elevated in the *db/db* myocardium at 10-weeks of age, compared to *db/h* controls (Figure 4.6B, $P < 0.05$). Within the resident mesenchymal cell (RMC) compartment, there were no major differences in cell proportions, with the exception of pericytes, which were significantly reduced in *db/db* hearts (Figure 4.6C). Within the leukocyte compartment, all leukocytes of the myeloid lineage were significantly reduced in the *db/db* myocardium, including macrophages, granulocytes and monocytes (Figure 4.6D, $P < 0.001$). Cardiac lymphocytes, however, were unaltered in the *db/db* heart (Figure 4.6D).

4.3.5 The cardiac cellular composition of 17-week old *db/h* and *db/db* mice

I next sought to determine the differences in cardiac cellularity in *db/db* relative to *db/h* mice at 17-weeks of age, considering that this time-point exhibits the greatest degree of cardiac functional impairment (as demonstrated in Figure 4.3-4.4). VEC, LEC, and endocardial cell levels did not differ between experimental groups (Figure 4.7B). Within the RMC compartment, I noted a significant increase in fibroblast and smooth muscle cell (SMC) numbers (Figure 4.7C, $P < 0.05$). Moreover, consistent with findings from 10-week old mice, pericytes were significantly reduced in *db/db* hearts (Figure 4.7C, $P < 0.01$). Of the cardiac leukocytes, resident macrophages were modestly reduced ($P = 0.06$, Figure 4.7D), which was likely driven by the attenuation of MHCII^{hi} macrophages ($P < 0.05$, Figure 4.7D). Conversely, MHCII^{lo} macrophage numbers were significantly augmented ($P < 0.01$, Figure 4.7D), possibly suggesting a switch in resident macrophage phenotype. In addition, Ly6C^{hi} monocytes were significantly elevated in *db/db* hearts, compared to their non-diabetic counterparts (Figure 4.7D, $P < 0.05$).

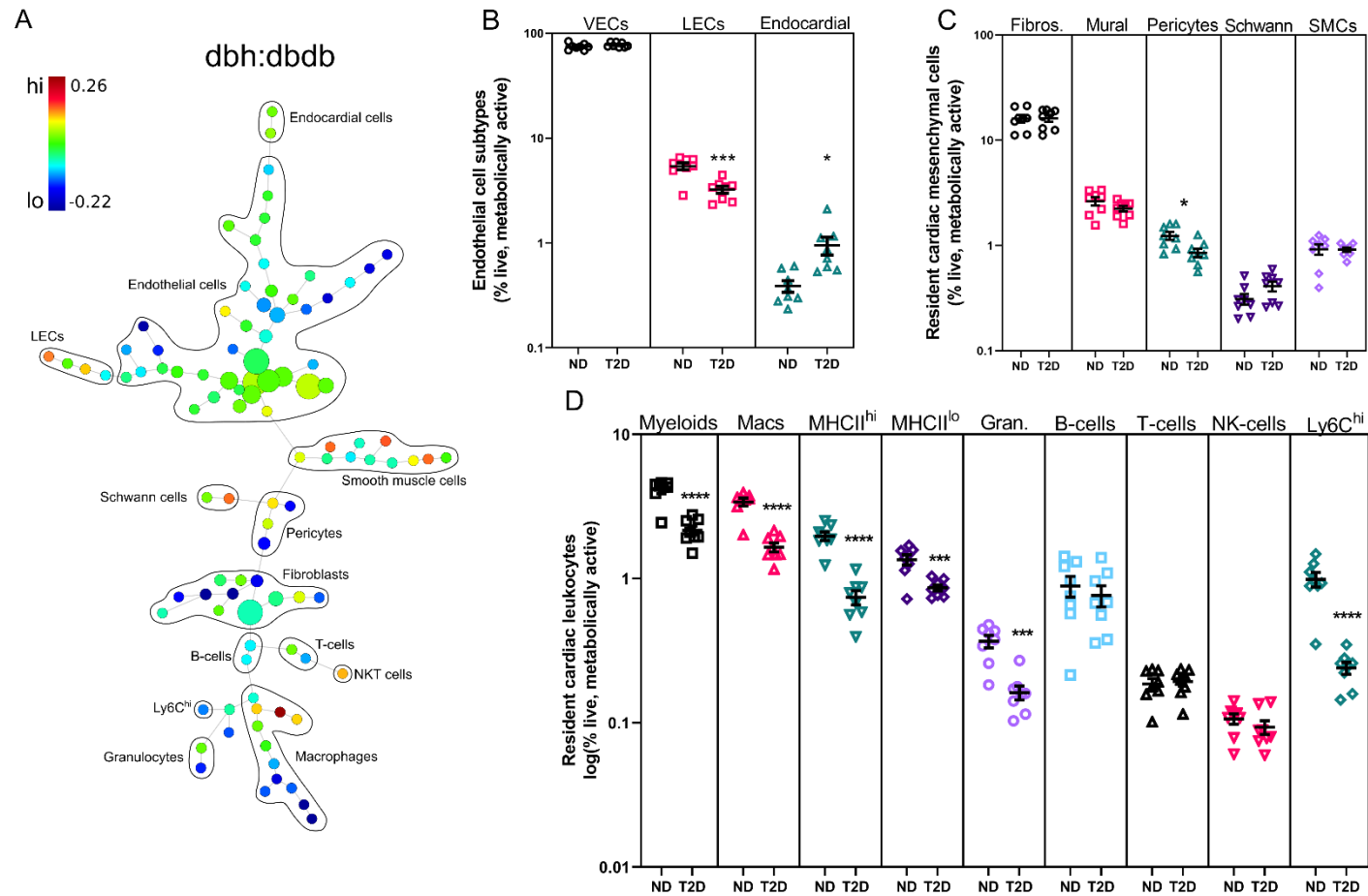


Figure 4.6: The cardiac cellular landscape in 10-weeks old *db/h* and *db/db* mice

(A) Ratiometric SPADE dendrogram, reflecting differences in the non-myocyte cellular landscape at 10-weeks of T2D. Heat mapping indicates the fold difference in *db/db* hearts relative to *db/h* hearts (100 target nodes, 50% down sampling). Manually gated and quantified data are displayed in B, C and D. (B) Cardiac endothelial cell (EC) subsets; vascular ECs (VECs) lymphatic ECs (LECs) and endocardial cells. (C) Resident mesenchymal cell (RMC) subsets; including fibroblasts (Fibros.), mural cells (Mural), pericytes, Schwann cells and smooth muscle cells (SMCs). (D) Cardiac leukocytes including; macrophages (Macs), MHCII^{hi/lo} macrophages, granulocytes (Gran.), B-cells, T-cells, NK-cells and Ly6C^{hi} monocytes (Ly6C^{hi}). Data is presented as mean \pm SEM with individual data points. Statistical significance was achieved by an unpaired Student's *t*-test comparing *db/h* vs. *db/db*. * $P < 0.05$, ** $P < 0.01$, *** $P < 0.001$, **** $P < 0.0001$. ND = non-diabetic (*db/h*); $n = 8$, T2D = type-2 diabetes (*db/db*); $n = 8$.

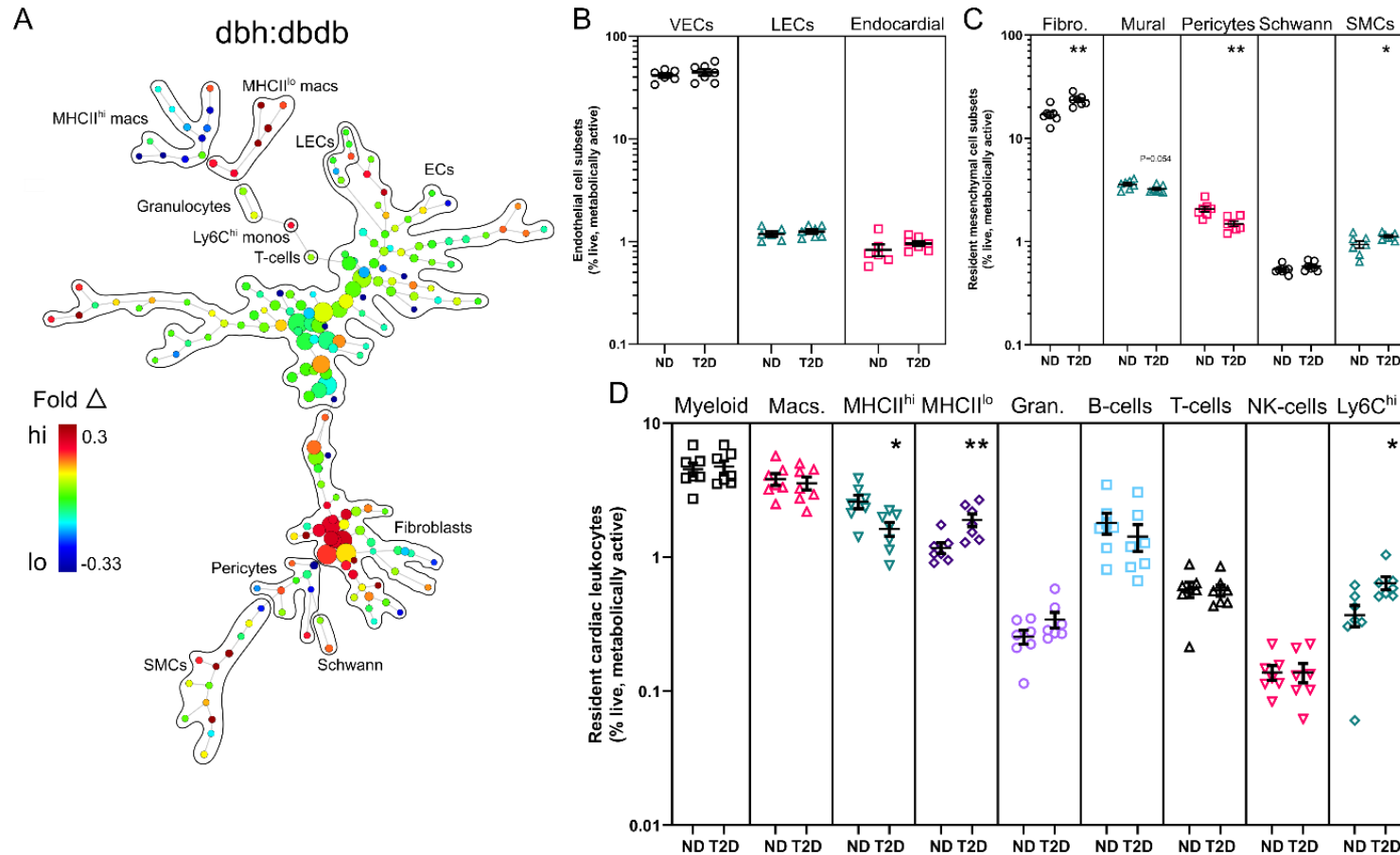


Figure 4.7: The cardiac cellular landscape of *db/db* mice at 17-weeks of age

(A) Ratiometric SPADE dendrogram, reflecting differences in the non-myocyte cellular landscape at 17-weeks of T2D. Heat mapping indicates the fold difference in *db/db* hearts relative to *db/h* hearts (200 target nodes, 50% down sampling). Proportions of viable cells were manually gated and quantified and are displayed in B,C,D. (B) Cardiac ECs, including; vascular ECs (VECs) lymphatic ECs (LECs) and endocardial cells (Endo.). (C) Resident mesenchymal cells (RMCs); including fibroblasts (Fibros.), mural cells (Mural), pericytes, Schwann cells and smooth muscle cells (SMCs). (D) Cardiac leukocytes including; macrophages (Macs), MHCII^{hi/lo} macrophages (MHCII^{hi/lo}), granulocytes (Gran.), B-cells, T-cells, NK cells and Ly6C^{hi} monocytes (Ly6C^{hi}). Data is presented as mean \pm SEM and individual data points. Statistical significance was achieved by an unpaired Student's *t*-test comparing *db/h* vs. *db/db*. * $P < 0.05$, ** $P < 0.01$. ND = non-diabetic (*db/h*); $n = 7$, T2D = type-2 diabetes (*db/db*); $n = 7$.

4.3.6 The cardiac cellular composition of 24-week old *db/h* and *db/db* mice

Given the distinct alterations in cardiac cellularity in *db/db* mice at 17-weeks of age, I again performed cardiac flow cytometry, in 24-week old *db/db* mice and their *db/h* controls, to observe the extent of the cellular changes with chronic diabetes. EC subset levels did not differ between experimental groups (Figure 4.8B). Similarly, within the RMC niche, I noted no statistically significant differences between experimental groups, despite a minor increase in Schwann cell levels with diabetes (Figure 4.8C, $P = 0.054$). Finally, of cardiac leukocytes, Ly6C^{hi} monocytes were significantly reduced in the *db/db* myocardium (Figure 4.8D, $P < 0.05$). There were no other differences detected in other leukocyte subtypes (Figure 4.8D). These data were interesting, as I expected more robust differences in cardiac cellularity, considering their age and cardiac dysfunction. Indeed, this cohort of *db/db* mice had a smaller sample size due to increased mortality, which reduced the statistical power of the data. Furthermore, I postulate that most cellular changes may have occurred prior to this time-point, and that the cardiac dysfunction is likely attributed to perturbed cardiomyocyte function.

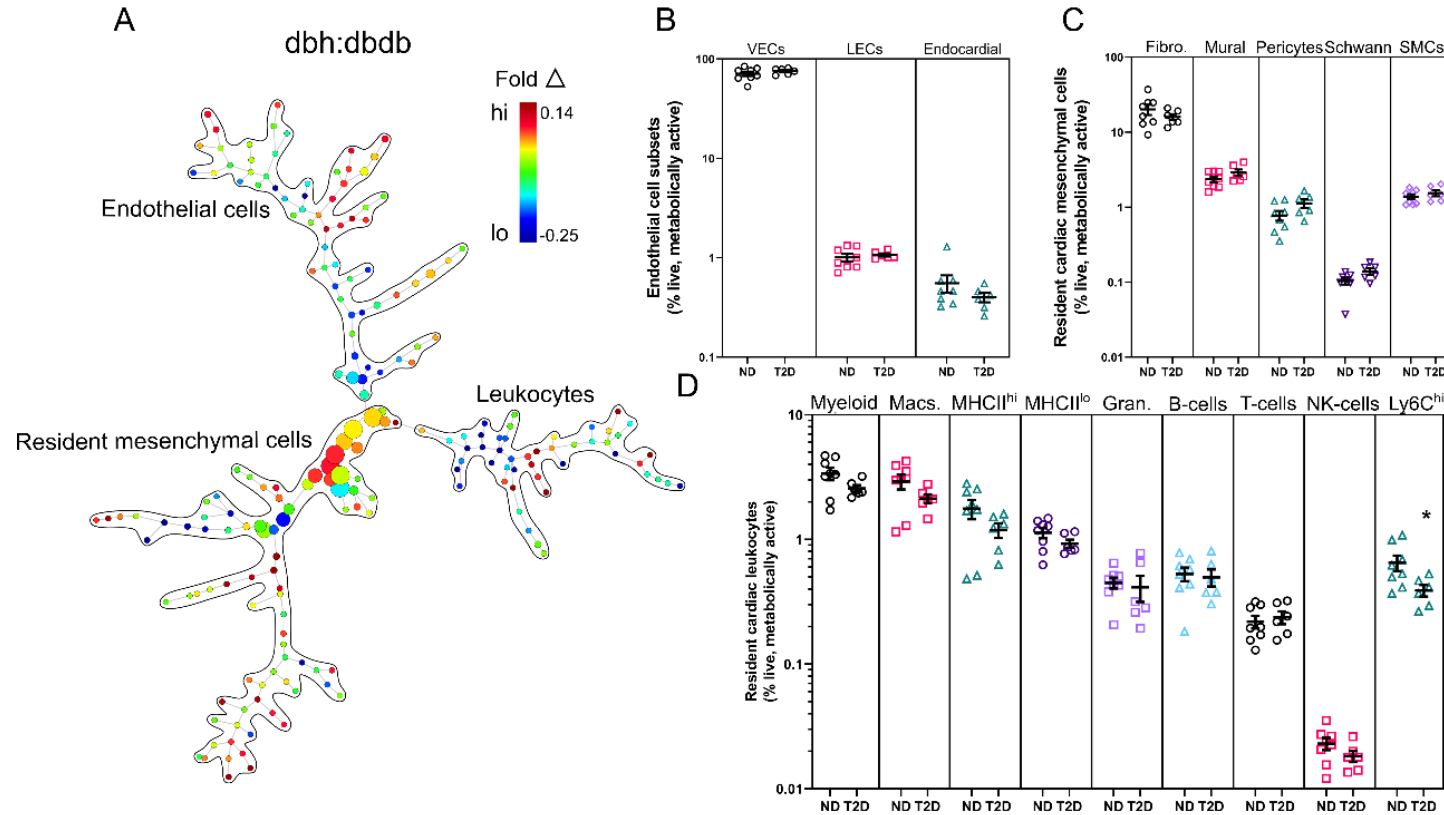


Figure 4.8: The cardiac cellular landscape of *db/db* mice at 24-weeks of age

(A) Ratiometric SPADE dendrogram, reflecting differences in the non-myocyte cellular landscape at 24-weeks of T2D. Heat mapping indicates the fold difference in *db/db* hearts relative to *db/h* hearts (100 target nodes, 50% down sampling). Proportions of viable cells were manually gated and quantified and are displayed in B,C,D. (B) Comprises cardiac ECs including, vascular ECs (VECs) lymphatic ECs (LECs) and endocardial cells (Endo.). (C) Resident mesenchymal cells (RMCs), including fibroblasts (Fibros.), mural cells (Mural), pericytes, Schwann cells and smooth muscle cells (SMCs). (D) Cardiac leukocytes including; macrophages (Macs), MHCII^{hi/lo} macrophages (MHCII^{hi/lo}), granulocytes (Gran.), B-cells, T-cells, NK cells and Ly6C^{hi} monocytes (Ly6C^{hi}). Data is presented as mean \pm SEM and individual data points. Statistical significance was achieved by an unpaired Student's *t*-test comparing *db/h* vs. *db/db* at each time-point. * $P < 0.05$, ND = non-diabetic (*db/h*); $n = 8$, T2D = type-2 diabetes (*db/db*); $n = 6$.

4.4 Discussion

While T2D and HF are strongly associated, the mechanisms driving cardiac dysfunction are still unclear. The diabetic heart phenotype has been characterised by augmented fibrosis, cardiomyocyte apoptosis and hypertrophy, as well as oxidative stress and inflammation [262]. In this thesis, I have also reported alterations in the non-myocyte cellular landscape in an alternate model of T2D-induced HF (Chapter 3), underscoring the importance of fibroblast expansion and systemic monocytosis in this context [5]. However, the temporal alterations in cardiac cellularity are yet to be described in murine T2D. Using the genetically-modified *db/db* mouse model of T2D [247], I highlight a number of non-myocyte cellular changes at each time-point analysed. Furthermore, I note 17-week old *db/db* mice exhibit similar non-myocyte cellular changes relative to the STZ-HFD model (Chapter 3), which were also accompanied by cardiac dysfunction. I reveal that 10-week old *db/db* hearts primarily undergo loss of cardiac myeloid leukocytes, accompanied by vascular remodelling. In addition, in 17-week old *db/db* mice I observed increased fibroblast and Ly6C^{hi} monocyte levels, also accompanied by similar differences in vascular cells. Surprisingly, there were no major cardiac non-myocyte cellular differences at 24-weeks of age, with the exception of a reduction in Ly6C^{hi} monocytes. Importantly, alterations in the cardiac non-myocyte cellular landscape are age-dependent and influenced by the array of circulating stressors that comprise T2D.

4.4.1 Systemic characteristics in male *db/db* mice recapitulate clinical features of T2D

Male *db/db* mice recapitulate key features of human T2D, corroborating the validity of this model to study T2D [247,263]. Indeed, all *db/db* mice in this study exhibited chronic hyperglycaemia indicated by significantly augmented HbA1c levels [268]. Distinct from the mouse model in Chapter 3, body weight was significantly elevated in *db/db* mice, accompanied by a marked increase in percentage fat mass and attenuated lean mass relative to body weight. This was unsurprising, although important – considering a major comorbidity of T2D is obesity, which in turn is associated with insulin resistance [43].

Moreover, both HF and obesity are associated with chronic, systemic inflammation [269]. In this study, *db/db* mice displayed significant monocytosis and neutrophilia at 17-weeks of age, despite no indication of this in *db/db* mice at 10 or 24-weeks of age. Inflammation is a known contributor of HF in humans, as highlighted in the CANTOS trial, demonstrating that pharmacological inhibition of IL-1 β prevents hospitalisation for HF [270]. Moreover, clinical T2D is also associated with low-grade systemic inflammation, characterised by elevated circulating pro-inflammatory cytokine levels [271,272]. This is also consistent with murine models of T1D, obesity and T2D, which display systemic monocytosis and neutrophilia, driven by haematopoiesis [5,113,273]. Consistent with previous clinical and pre-clinical studies, I implicate systemic inflammation as a likely driver of impaired cardiac function in murine T2D.

4.4.2 Cardiac dysfunction is most evident in 17-week old *db/db* mice

A key characteristic of T2D-induced HF is diastolic dysfunction, which was only evident in 17-week old *db/db* mice. These mice display a cardiac phenotype similar to clinical cardiomyopathy in patients with obesity and T2D [274,275], indicated by impaired cardiac filling capacity in diastole. Insights from echocardiography studies in patients with diabetes document left-ventricular (LV) diastolic dysfunction, inferred by reduced E/A and e'/a' ratios as well as an augmented E/e' ratio [276,277]. Other important measurements of impaired transmitral LV filling in diabetes include prolonged DT and IVRT [277] (Chapter 1, Section 1.2.1), although these were not altered in the present study, except for an increase in DT in 24-week old *db/db* mice.

Similar degrees of cardiac dysfunction have been documented in other animal models of diabetes. STZ-induced T1D mice typically display reduced E/A and e'/a' ratios accompanied by prolonged DT and IVRT [264,278]. The combination of STZ and high-fat diet (HFD) in mice also induces similar patterns of cardiac dysfunction, as described in Chapter 3 and previously reported [53]. While cardiac dysfunction in *db/db* mice has been reported, echocardiographic parameters in these studies are variable. Conventional echocardiographic analysis of *db/db* mice at 12, 24 and 30-weeks of age all display a reduced E/A ratio, with no alterations in DT, IVRT, nor any systolic parameters [279]. In contrast, a more recent study reported no difference in E/A ratios in 8-week and 24-week old *db/db* mice, but display a reduced e'/a' ratio and an increased E/e' ratio at 24-weeks of age [263]. While reports regarding cardiac dysfunction in *db/db* mice are variable, here, I note increased LV filling pressure in 17-week old *db/db* mice inferred from an elevated E/e' ratio, which is the preferred echocardiographic parameter for determining diastolic dysfunction [280]. No other time-point displayed any detectable degree of cardiac dysfunction.

M-mode echocardiography of LV diastolic and systolic chamber size and wall thickness also indicated reduced LVEDD and LVESD measurements, accompanied by an increase in % FS in 10 and 17-week old *db/db* mice. These reductions in LV end systolic and diastolic diameters in *db/db* mice, accompanied by increased fractional shortening are characteristic of concentric cardiac hypertrophy. Concentric cardiac hypertrophy is typically induced by hypertension [281], which is also an established characteristic of the *db/db* mouse [56,263]. This is important considering perturbed LV filling pressure in diabetes is not usually isolated and can occur concomitantly with variable degrees of systolic dysfunction [274]. This may suggest that male *db/db* mice initially undergo a compensatory increase in cardiac contractility in the face of impaired diastole, prior to development of overt HF.

Collectively, I demonstrate that 17-week old *db/db* mice exhibit the greatest degree of cardiac dysfunction in this study, suggesting that this is the optimal time-point to investigate cardiac remodelling in this model. Moreover, I postulate that *db/db* mice at this time-point exhibit early-onset diastolic dysfunction with concomitant HFpEF, which was inferred by an increase in

fractional shortening. It is however, important to note that cellular and molecular changes in the diabetic myocardium are likely to precede cardiac morphological and functional changes.

4.4.3 The differences in cardiac cellularity in *db/h* and *db/db* mice are age-dependent

Considering parallel investigation of non-myocyte cells is understudied in the diabetic heart, cardiac flow cytometry was performed at the three different time-points (10, 17 and 24 weeks of age) to determine the progressive differences in cardiac cellularity that may contribute to cardiac dysfunction in this context. Cell-specific analyses in the context of diabetes have traditionally focused on cardiomyocyte, EC and fibroblast signalling and function *in vitro* (discussed in Section 4.1). In our previous publication, we note an increase in fibroblast and Ly6C^{hi} monocyte levels, accompanied by a decrease in SMCs in the STZ-HFD model of diabetic cardiomyopathy [5]. Here, I observed a number of consistent cellular alterations in the *db/db* myocardium at 17-weeks of age, namely an increase in fibroblasts and Ly6C^{hi} monocytes. We also observed a number of unique cellular changes in the *db/db* heart at this time-point, characterised by decreased pericytes and MHCII^{hi} macrophage levels, and elevated SMCs and MHCII^{lo} macrophages. Importantly, these alterations occurring at 17-weeks of T2D exist in the presence of cardiac dysfunction, which is comparable to Chapter 3. However, it is also vital to consider the alterations that may occur before the onset of cardiac dysfunction.

Within the cohort of 10-week old *db/db* mice, I observed cellular changes associated with lymphatic dysfunction. Indeed, LECs decrease in proportion in the *db/db* myocardium at this time-point. Impaired lymphatic function is a common feature of metabolic diseases, such as T2D [282,283]. Lymphatic vessel barrier permeability is compromised in 20-week old *db/db* mice *in vivo*, accompanied by attenuated nitric oxide (NO) signalling [284] – an established abnormality in the diabetic heart [66]. Consistently, mice fed a HFD also display lymphatic leakiness, accompanied by reduced lymphatic vessel density *in vivo* [285]. In contrast, patients with T2D display enhanced lymphatic vessel density in the dermis dictated by LEC proliferation, suggesting lymphangiogenesis [286]. While the literature pertaining to LECs is mixed, reduced levels of LECs at 10-weeks of *db/db*-induced T2D may suggest commencement of cardiac lymphatic dysfunction.

I also noted an increase in endocardial cells in *db/db* mice at 10-weeks of age, which could be induced by a number of factors. Endocardial cells form the innermost layers of the heart chamber wall and contribute to a vast array of physiological functions. Moreover, endocardial cells display distinct heterogeneity and are capable of differentiating into a vast array of cardiac cells during development and possibly in disease [287,288]. Initial histological analysis of diabetic hamster hearts suggested that endocardial cells undergo a series of cellular morphological changes, with evidence of endoplasmic reticulum dysfunction and sub-endocardial expansion [289]. Endocardial cell shape and arrangement is also impaired in the face of haemodynamic abnormalities such as shear stress [290]. Moreover, mounting evidence suggests that endocardial cells undergo cellular trans-differentiation into mesenchymal cells in response to certain stimuli, such as hyperglycaemia

and TGF- β signalling [287]. Hence, endocardial trans-differentiation could explain the increase in RMC levels in both STZ-HFD and *db/db*-induced cardiomyopathy, although is yet to be comprehensively elucidated in the diabetic heart.

Perhaps the most surprising finding in 10-week old *db/db* hearts was a significant reduction in cardiac myeloid, but not lymphoid leukocytes. In contrast, CV and metabolic disease typically display increased leukocyte levels, which generally originate from within the bone marrow prior to release into the circulation [291] (Chapter 1, Section 1.3). Cardiac myeloid leukocytes are the primary interstitial non-myocyte cells responsible for undergoing phagocytosis and clearing excess debris within a given tissue [292]. There are no studies to date that report loss of cardiac myeloid leukocytes; however, there are concurrent variables to consider in the *db/db* heart. First, *db/db* mice generally exhibit cardiomyocyte hypertrophy [19,263], which could in turn reduce the proportion of leukocytes by reducing the interstitial area in which they reside. In addition, *db/db* mice consistently display elevated circulating lipids and cholesterol, in addition to hyperglycaemia [247]. Given the severely obese phenotype of *db/db* mice, myeloid leukocyte loss in this context could be explained by the accumulation of lipid-laden macrophages, which are commonly described in atherosclerosis [135]. However, hyperglycaemia alone tends to provoke a pro-inflammatory response by macrophages, promoting pro-inflammatory cytokine release and leukocyte chemotaxis [293,294]. This finding was unexpected and has not been previously reported, making interpretation difficult. However, future work should consider myeloid leukocyte dynamics in diabetic heart disease, using techniques such as lineage tracing (further elaborated in Chapter 7) to empirically determine the cogency of this paradigm.

In addition to myeloid cell loss, cardiac pericytes were attenuated in both 10-week and 17-week old *db/db* mice, suggesting pericyte dysfunction and possible death. Pericytes are a ubiquitous vessel-associated mural cell subset responsible for maintaining vascular integrity by supporting EC and SMC function [295]. Impaired pericyte function is associated with the pathogenesis of microvascular disease including retinopathy, nephropathy, neuropathy and peripheral artery disease in patients with T2D [296,297]. Pericyte loss is most widely characterised in diabetic retinopathy and is associated with local vascular dysfunction [298]. In the early stages of human diabetic retinopathy, hyperglycaemia perturbs pericyte function, induced by inflammation, ROS generation and apoptosis [299,300]. Pericyte apoptosis in diabetic patients is correlated with augmented mitogen-activated protein kinase (MAPK) and protein kinase C (PKC) signalling [301]. As vascular dysfunction progresses in the diabetic retina, hypoxia induces vasculogenesis and neovascularisation as an endogenous compensatory mechanism to improve blood flow [299–302]. Similar reports have been documented in other diabetic complications including nephropathy and neuropathy, which are associated with similar mechanisms [297]. More recent histological examination of human diabetic myocardial explants report pericyte loss, coinciding with impaired contractility of myocardial biopsies *ex vivo* [303]. While the literature pertaining to cardiac

pericytes in diabetes is limited, loss of myocardial pericytes may allude to cardiac vascular remodelling in diabetic heart.

Corroborating this, I also observed increased proportions of SMCs in 17-week old *db/db* mice. This is contrary to our findings from the previous Chapter. As discussed in Chapter 3, the literature pertaining to SMC behaviour in diabetes-induced HF is unclear. Hyperglycaemia alone inhibits the initiation of SMC apoptosis via PKC and B-cell lymphoma 2 (Bcl-2) signalling [304–306]. However, in rodent models of hypercholesterolaemia and atherosclerosis, SMCs undergo apoptosis and dysregulated proliferation, accompanied by increased leukocyte chemotaxis [307,308]. Because T2D induces both hyperglycaemia and hypercholesterolaemia, the precise role and contribution of each comorbidity on SMC function is yet to be distinguished.

Consistent with the previous Chapter, 17-week old *db/db* mice had elevated cardiac fibroblast and Ly6C^{hi} monocyte numbers. Fibroblast expansion is generally indicative of cardiac fibrosis, which is consistent with the commencement of cardiac dysfunction at this time-point. Fibroblast accumulation is often indicative of fibrogenesis and ECM remodelling [309], with different cardiac stressors resulting in disparate types of cardiac fibrosis [76]. For example, cardiac fibroblasts in murine myocardial infarction (MI) rapidly differentiate into myofibroblasts [233,245], resulting in replacement fibrosis and scar formation [76]. In contrast, angiotensin II-induced HF in mice is associated with diffuse fibrosis within the interstitial and perivascular spaces, dictated by augmented novel fibroblast levels [234]. While fibroblast heterogeneity and function is yet to be assessed in T2D *in vivo*, diabetes-induced cardiac fibrosis is typically interstitial and perivascular, representing cardiac remodelling similar to angiotensin II-induced HF. Analogous to Chapter 3, increased monocyte levels in the diabetic heart were accompanied by systemic monocytosis, exclusively in 17-week old *db/db* mice. While I was unable to determine the source of monocytosis in this study, a recent report has confirmed that monocytosis in *db/db* mice originates from enhanced haematopoiesis and splenic myelopoiesis prior to mobilisation of monocytes into the circulation [310]. These results underscore the importance of leukocyte dysregulation and systemic inflammation in diabetes-induced HF, as an additional consideration for future research in this field.

The resident cardiac macrophage phenotype in the myocardium of 17-week old *db/db* mice was also altered, characterised by a reduction in MHCII^{hi} macrophages, and an increase in MHCII^{lo} macrophages. Considering the plasticity of resident macrophages [188] and the presence of systemic monocytosis and inflammation, I postulate that local cardiac macrophages are actively changing their phenotype in response to the inflammatory environment, providing a basis for future studies to interrogate. In contrast, reports pertaining to the diabetic heart implicate macrophages in pathogenic cardiac inflammation, suggesting that macrophages stimulate the release of pro-inflammatory cytokines and chemokines [179,278,311,312]. Certainly, in the context of acute CV stress such as MI, cardiac macrophages enhance chemotaxis and induce inflammation [233,245]. However, cardiac macrophages can also play cardioprotective roles in homeostasis and disease by

various means, including the release of key trophic factors, such as interleukin 34 (IL34) and colony stimulating factor 1 (CSF1) [161,164,187,225,313]. Hence, it remains to be definitively determined if macrophages play a protective, or pathogenic role in the diabetic heart.

Surprisingly, there were no cardiac non-myocyte cellular alterations in 24-week old *db/db* mice relative to *db/h* controls, with the exception of reduced myocardial monocytes. Given the cellular changes observed at 17-weeks of age, I anticipated that *db/db* mice would exhibit an exaggerated pathogenic cellular response relative to 17-week old mice. Furthermore, 24-week old *db/db* mice still display some characteristics of cardiac dysfunction, despite the lack of cellular changes. It could be postulated that all non-myocyte cellular alterations have ceased, and cardiomyocyte dysfunction is the primary driver of their impaired cardiac function. However, this set of data is difficult to interpret, given their higher mortality rate at 24-weeks of age, which may compromise the statistical power of this cohort.

4.4.4 Study Limitations

While this study provides novel insights into the development of T2D-induced HF, a number of limitations are notable. First, the 24-week mouse cohort was likely subject to survival bias. Of the 24-week old *db/db* mice, we incurred two deaths due to severe diabetic complications. This, at least in part, could explain the lack of difference in the measured parameters in *db/db* mice of this age.

Second, it is important to consider the confounding effect of global leptin receptor truncation in the development and pathogenesis of HF in *db/db* mice. A number of studies suggest that leptin signalling is essential for cardiomyocyte function. Disruption of leptin signalling is sufficient to induce cardiac hypertrophy in mice independent of body weight, suggesting leptin or its components have a direct anti-hypertrophic effect [314]. Moreover, cardiomyocyte-specific leptin receptor depletion worsens myocyte hypertrophy, contractile function and survival, while leptin repletion reverses these effects [315].

Third, I did not measure the degree of insulin resistance of *db/db* mice in this study. It is however, well established that insulin resistance is evident in *db/db* mice [247,267,316]. While no assays relevant to insulin resistance were conducted in this cohort of mice, there is transcriptomic evidence implicating insulin resistance in 17-week old *db/db* mice (further discussed in Chapter 5).

Fourth, as aforementioned, systolic function appeared to be greater in *db/db* mice relative to *db/h* mice, determined by echocardiography analysis. However, as discussed (Chapter 1, Section 1.2), numerous echocardiography parameters are load-dependent. Indeed, *db/db* mice tend to display an augmented end-diastolic pressure volume relationship (EDPVR) [317], suggesting that readings from *db/db* mouse echocardiograms may be confounded by myocardial preload. This may also explain why a clear process of functional pathogenesis was not clearly identified. Nevertheless, this limitation poses an important future direction for future work using these technologies, to more accurately assess cardiac dysfunction in murine T2D (further discussed in Section 4.4.5).

Fifth, I also acknowledge that the sole use of male mice in this study, as well as the lack of cardiomyocyte analysis are significant limitations, consistent with our limitations in Chapter 3. Cardiac pathology is sex-specific in mice and humans [229,250,263,318]. As such, future work should incorporate female mice to decipher any apparent sexual dimorphisms in the context of diabetic HF. In addition, exclusion of myocytes from analysis in Chapter 3 and 4 was unavoidable, as the cytometric approaches utilised preclude larger cells from analysis. This limitation applies to most high-throughput single-cell technologies, due to their reliance on microfluidic systems that are often too small in diameter to fit larger, potentially hypertrophic cells. Importantly, the focus of these studies was to characterise the non-myocyte differences, as there are numerous studies characterising cardiomyocyte abnormalities (Chapter 1, Section 1.2.2, 1.2.3).

Lastly, while outside the scope of this dissertation, it is important to consider the role of other systemic organs in the pathogenesis of heart disease elicited from T2D. Indeed, diabetes is the leading cause of renal failure, which can have a number of off-target effects, on multiple organ systems [319]. Specifically, the kidney releases a myriad of molecular mediators in the face of hyperglycaemia, including hormones and cytokines, leading to vascular and cardiac dysfunction [320,321]. Moreover, haemodynamic perturbations resulting from global renal damage further exacerbate cardiovascular damage [322]. While I did not investigate diabetes-associated renal aberrances in this thesis, investigation of the cardio-renal axis using these methodologies poses an exciting future direction.

4.4.5 Future considerations studying mouse models of diabetic heart disease

While *db/db* mice displayed cardiac dysfunction most prominently at 17-weeks of age, it is important to discuss the suitability of each model used in this thesis, for studying diabetic heart disease. Of note, STZ-HFD treated mice (Chapter 3) appeared to exhibit more pronounced diastolic dysfunction relative to *db/db* mice, with perturbations in peak A wave velocity, E/A, e'/a' ratios. In contrast, *db/db* mice (at any age) did not display overt alterations in mitral flow velocity, although 17-week old *db/db* mice displayed reduced passive ventricular filling (peak e' wave). The reduction in passive ventricular filling in this cohort of *db/db* mice was also accompanied by an augmented ratio of passive LV filling relative to myocardial relaxation – the preferred load-independent measure of diastolic dysfunction [33]. While STZ-HFD mice tend to display more conspicuous diastolic dysfunction, these parameters may be confounded by myocardial load, which should be hemodynamically assessed in future studies. Interestingly, both murine models of T2D showed enhanced systolic function. Both STZ and HFD treatment alone can display altered LV haemodynamic measurements in mice, including increases in EDVPR and Tau [323,324], which are associated with increased LV pressure and artefactual increases in fractional shortening [325]. The same has been observed in *db/db* mice, whereby end-diastolic pressure is increased and arterial elastance is reduced [326], signifying augmented preload and attenuated afterload, respectively [325]. Therefore, 17-week old *db/db* mice are the recommended model for studying the emergence

of diastolic dysfunction in murine T2D, given the load-independent detection of diastolic dysfunction at 17-weeks of age. It is thus critically important that future work examining cardiac function in T2D mice considers the haemodynamic aberrances in these models, to more accurately assess the degree of cardiac functional impairment.

4.4.6 Additional strategies to address the mechanisms dictating altered cardiac cellularity

The common cardiac cellular alterations in both STZ-HFD and *db/db* mice primarily involve increased fibroblast and monocyte levels, which warrant further robust, cell-specific analyses to specifically address the mechanisms inducing these changes. For instance, introducing fibrogenic stimuli to isolated cultures of cardiac fibroblasts harvested from diabetic mice is an informative approach to determine the basic mechanisms that may induce fibroblast expansion. This has been performed in *db/db* mice, whereby fibroblast stimulation with TGF- β does not elicit fibroblast differentiation, but rather is associated with development of matricellular-like cells [263]. While TGF- β is inhibited by cartilage intermediate layer protein (CILP), acting as a negative feedback loop [327], *Cilp* has been associated with the development of chronic cardiac fibrosis [234]. Thus, it would be interesting to investigate the dual role of TGF- β and CILP *in vitro* to determine if this feedback loop is governing the expansion of cardiac fibroblasts in the diabetic heart. Similarly, *in vivo* approaches using fibroblast-specific transgenic mice, such as the PDGFR α ^{GFP} mouse line [328], would be a useful tool for tracking fibroblast fate, activation and dynamics of expanding cardiac fibroblasts over time in mice with diabetes. Specifically, tissue-specific Cre-lox conditional knock-down of fibrogenic genes such as *Cilp* or *Tgf β 1* are viable options for interrogating the mechanisms inducing fibroblast hyperplasia in diabetic mice. The same can be described for monocytes and macrophages, which is further discussed in Section 5.4.8.

In addition, while this study design yielded insights into the temporal pathogenesis of cardiac dysfunction in T2D, each time-point was comprised of a different cohort of animals, providing difficulty assessing time as a variable. If performing additional time-course experiments, future studies are encouraged to adopt a ‘paired’ experimental approach, whereby the same mice are followed-up over a given time period using non-invasive assessments. For example, by performing a prospective cardiac MRI study, temporal perturbations in matched cohorts of mice would provide more robust insights relating to cardiac dysfunction in this context. Further, it would also be pertinent to investigate cardiac fibrosis levels via basic histology—such as Masson’s Trichrome—to determine when fibrosis contributes to functional impairments in this context. Although it is also worth noting that these studies present with their own limitations, primarily relating to premature euthanasia. Notwithstanding, use of cell-specific experimental techniques and improvement of experimental design to consider temporal changes will further aid in determining the mechanisms dictating cellular composition changes identified in this thesis.

4.5 Conclusions

Taken together, this study highlights the age-dependent, cellular changes that contribute to cardiac dysfunction in the *db/db* mouse model of T2D. Early cellular changes in the *db/db* heart are dictated by significant reductions in LECs, pericytes, and all cardiac myeloid cells, accompanied by an increase in endocardial cells. In 17-week old *db/db* mice, fibroblasts, SMCs and Ly6C^{hi} monocytes are augmented, while pericytes remain reduced relative to *db/h* control mice. Moreover, macrophage polarisation is altered in the *db/db* myocardium, with attenuated levels of MHCII^{hi} macrophages and elevated MHCII^{lo} macrophages. There were no major differences in cardiac cellularity in *db/db* mice at 24-weeks of age. Importantly, 17-week old *db/db* mice exhibit consistent cellular differences in accompanied by cardiac dysfunction, relative to the STZ-HFD mouse model used in the previous Chapter. This study encourages future research to consider cardiac cellular composition in diabetes-induced HF, particularly when applying other single-cell technologies such as single-cell RNA sequencing.

Chapter 5

Single-cell transcriptomic analysis of the T2D mouse heart

5.1 Introduction

Considering that the diabetic heart undergoes numerous non-myocyte cellular changes, I next sought to investigate any transcriptomic alterations within individual non-myocytes, which may be driving the observed cellular changes. To achieve this, I performed cardiac single-cell RNA sequencing (scRNAseq) in a separate, age-matched cohort, of *db/db* mice and their *db/h* littermates. Single-cell transcriptomics allows for inference of cellular diversity and phenotypic states in tissue systems, by examining an array of individual cell transcriptomes. High-throughput scRNAseq of multiple cells is typically achieved by ‘droplet-based’ sequencing [329], whereby cells within a single-cell suspension are encapsulated in reagent filled oil droplets. This yields isolated, cell-specific cDNA, which is subsequently amplified and sequenced prior to *in silico* data analysis [222].

In recent years, scRNAseq has provided unprecedented detail regarding the phenotypes and circuitry of disparate cardiac cell types. For example, recent studies have identified novel players in cardiac fibrosis and ECM maintenance [76]. In acute cardiac injury (MI), emergence of protagonists such as macrophages and myofibroblasts dictate the initiation and progression of cardiac remodelling [233,245]. However, in chronic AngII-induced HF, cardiac scRNAseq revealed that fibrosis induction is not facilitated by myofibroblasts, but rather induced by other novel fibrogenic fibroblasts, such as ‘Fibroblast-*Cilp*’ and ‘Fibroblast-*Thbs4*’ [234]. Moreover, a recent study also highlighted the importance of transcriptional regulator ‘MEOX1’ in activated cardiac fibroblasts in MI, suggesting it alters fibroblast plasticity by acting as a ‘switch’ initiating the expression of fibrogenic genes [330]. Similar methodologies have been applied to healthy human donor hearts [331,332], providing useful insights into cellular and molecular dynamics relative to findings from various rodent models in both health and disease [225,233,234,245]. However, scRNAseq technology is yet to be applied to study the impact of diabetes on the heart, providing a distinct gap in our knowledge regarding the molecular underpinnings that govern cardiac dysfunction in this context.

To address this, scRNAseq was performed on *db/db* and *db/h* mouse hearts at 17-weeks-of-age, to develop a comprehensive cardiac cellular atlas in experimental T2D associated with the appropriate degree of cardiac dysfunction (Chapter 4, Figure 4.2-3). In this Chapter, I identify a concerted diabetes-induced response for cardiac remodelling and infer possible mechanisms for the cellular changes described in Chapter 4. Activation of unexpected gene expression programs, as well as those corresponding to well-established pathways associated with the phenotype of the diabetic heart, were identified. I also observed cellular changes in the *db/db* heart that corroborate the cytometric findings from the Chapter 3 and 4. Moreover, I incorporate our current dataset with two, publicly available bulk RNA sequencing datasets to determine common molecular pathways in the

diabetic heart. These findings provide a robust framework for future studies to consider, and may aid in identifying new therapeutic avenues to address the cardiac complications associated with diabetes.

5.2 Research Design and Methods

For a detailed description of this methodology, see Section 2.9 and 2.10 within Chapter 2 of this thesis. All animal-related experiments were approved by the Alfred Research Alliance (ARA) Animal Ethics Committee (Ethics number: E/1880/2019/B) and were performed in accordance with the National Health and Medical Research Council of Australia (NH&MRC) guidelines. Male *db/db* mice ([B6.BKS(D)-Lepr^{db}/J], stock #000697) [247] and their heterozygous non-diabetic controls (*db/h*) were obtained from The Jackson Laboratory (Bar Harbor ME, USA). Mice were monitored until 17-weeks of age, after which euthanasia was performed (as described; Chapter 2, Section 2.9) to allow for tissue preparation and scRNAseq ($n = 4/\text{group}$). In this project, utility of 4 animals per group was deemed sufficient to regress out the effects of statistical outliers, based on previous studies [225,234]. One mouse was excluded from analysis when performing tissue preparation for scRNAseq, due to insufficient perfusion and digestion. As such, the updated n values for this Aim were, *db/h* = 3, *db/db* = 4. Single-cell suspensions of non-myocyte cells were pooled together by genotype. Cells were then manually counted using a haemocytometer (as described in Chapter 2) and subsequently underwent library preparation as performed previously [234]. For information pertaining to *in silico* analyses, see Chapter 2, Section 2.10. Regarding dataset integration analysis (Chapter 2, Section 2.10.4), external datasets were obtained from the Gene Expression Omnibus (GEO) repository ('Akita' dataset identifier: GSE66577. Bulk RNAseq *db/db* dataset identifier: GSE36875).

5.3 Results

5.3.1 Single-cell transcriptomic profiling reveals extensive heterogeneity of non-myocytes

To examine the cell-specific, transcriptomic changes that occur in the diabetic heart, scRNAseq was performed on *db/h* and *db/db* mouse hearts to develop a comprehensive atlas of the cardiac cellome. Cardiac non-myocyte scRNAseq and histology was conducted in *db/db* and *db/h* mice at 17-weeks of age, in parallel with the cohort from the previous Chapter. Bioinformatic analysis of raw scRNAseq data revealed a distinct array of non-myocyte cell types in both *db/db* and *db/h* mice (9,316 individual cells Figure 5.1B). Cell types were annotated by querying typical cellular marker genes and by considering the top-5 most distinct genes in each cell cluster (Figure 5.1C, Chapter 2 Section 2.10). The non-myocyte cells within the dataset were then systematically identified by querying gene expression for fibroblasts (*Pdgfra*, *Col1a1*), pericytes (*Vtn*, *Kcnj8*), endothelial cells (ECs; *Peacam1*, *Ly6c1*), smooth muscle cells (SMCs; *Myh11*, *Acta2*), endocardial cells (*H19*, *Tmem108*), epicardial cells (*Upk3b*, *Kr19*), and a number of immune cells (including macrophages, B-cells, T-cells, eosinophils/basophils, NK-cells, DC-like cells and granulocytes (Figure 5.1B-C). *In silico* clustering parameters identified eight fibroblast subsets (Figure 5.1B). Reflecting the

increase in fibroblasts determined in the previous chapter using flow cytometry, here, I found a relative increase in total fibroblasts in *db/db* mouse hearts compared to *db/h* mice (Chapter 4 Figure 4.6; Chapter 5 Figure 5.5-5.8). Other cell types rarely described in the heart also included $\gamma\delta$ T-cells (*Tcr γ -C1*, *Cd3g*) NK-cells (*Klrk1*, *Nkg7*), and Schwann cells (*Kcna1*, *Gfra3*).

5.3.2 Cardiac differential gene expression indicates cell-specific and broad transcriptomic patterns

Next, I sought to identify the top 10 differentially expressed genes in each cell type in *db/db* hearts relative to their *db/h* counterparts (described in Chapter 2, Section 2.10.1). While the top 3 Gene Ontology (GO) terms associated with up-regulated genes in the *db/db* heart suggest highly cell-specific gene expression patterns in T2D, down-regulated gene expression patterns represent a global concerted effort for protein folding (Figure 5.2C-D). Among the many differentially expressed genes in the *db/db* heart, up-regulated genes included *Angptl4* (fibroblasts), *Ccr2* (macrophages), *Cntrl* (T-cells), *Ncbp3* (Pericytes) and *Ppar γ* (ECs), displayed in Figure 5.2A. Gene expression for mitogen-activated protein kinase (MAPK) related proteins were also exclusively increased in *db/db* fibroblasts, including *Egfr* and *Ackap12* (Figure 5.2A). GO analysis of up-regulated genes (Figure 5.2A) revealed a complex array of cell-specific biological processes, including cell migration (ECs), angiogenesis (ECs), regulation of small GTPases (lymphatics, endocardial, pericytes, fibroblasts, epicardial cells) and WNT protein signalling (endocardial, fibroblasts; Figure 5.2C). Of the differentially expressed genes that were down-regulated (Figure 5.2B), genes of note included *Hspa1a/b*, *Hspa5*, *Hspa8*, *Hspe1*, *Hsph1*, which were all significantly reduced in a number of cardiac non-myocyte cell types (Figure 5.2D). In addition, genes encoding for anti-inflammatory complement proteins *C1qb*, *C1qc* were significantly down-regulated in macrophages and DC-like cells. GO analysis of the top down-regulated genes (Figure 5.2B) indicated a combined effort by nearly all cardiac non-myocyte cells to orchestrate protein folding and to regulate the unfolded protein response (Figure 5.2D).

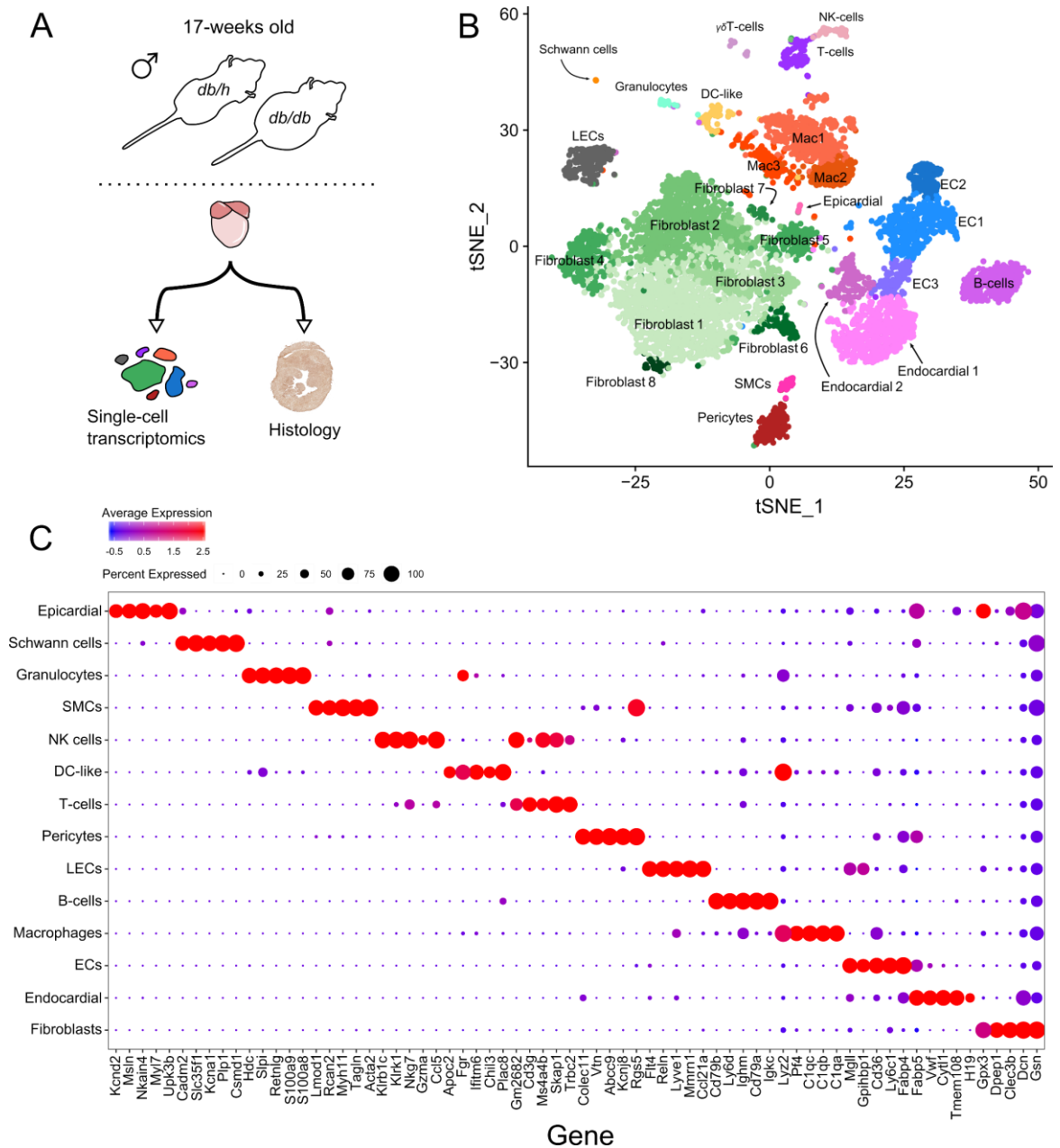


Figure 5.1: Analysis of the T2D (*db/db*) mouse heart cellulome

(A) Schematic indicating the analyses conducted on the *db/db* and *db/h* mouse hearts. Single-cell RNA sequencing was performed in 17-week old male *db/db* ($n=4$) and *db/h* ($n=3$) mouse hearts. Flow cytometry and echocardiography (previously discussed in Chapter 4) and histology were also performed, in a separate cohort of age-matched *db/db* mice with their respective *db/h* control counterparts ($n = 8/\text{group}$). (B) Merged t-SNE projection of all captured cardiac, non-myocyte cells analysed in *db/h* and *db/db* mice. (C) Dot plot illustrating the top-5 most highly expressed genes within each cell cluster. Dot size indicates the relative proportions of cells expressing a given gene and dot colour indicates the relative average expression level.

5.3.3 Cardiac non-myocytes increase ligand and receptor expression in a cell-specific manner

To profile deeper into the single cell transcriptomic profile of the diabetic heart, I investigated the intercellular communication by mapping genes encoding for ligands and their cognate receptors expressed by major cell populations (Figure 5.3). To illustrate this, a chord plot was developed to visualise the overall cell-cell communication in *db/db* hearts (Figure 5.3A). Quantification of the total number of connections in *db/h* and *db/db* mice for each broad non-myocyte cell type, suggests that numerous cell types increase their cell-cell communication (Figure 5.3B). To gain further insight into the biological relevance of the augmented cellular cross-talk, I mapped the top 3 GO terms for up-regulated and down-regulated receptors and ligands in each broad non-myocyte cell type (Figure 5.3C&D, respectively). GO terms enriched in up-regulated genes corresponding to receptors, indicated positive regulation of the MAPK cascade in fibroblasts (Figure 5.3C). Key genes corresponding to MAPK regulation in fibroblasts included the insulin receptor *Insr*, MAPK cell-surface receptor *Egfr*, and MAPK transcriptional regulator *Notch2* [333]. In addition, GO terms related to up-regulated receptors in ECs were associated with increased cell migration, chemotaxis, angiogenesis and vasculogenesis (Figure 5.3C); suggesting mobilisation of circulating cells is facilitated by ECs in the diabetic heart. Among the many genes regulating these terms, were vascular endothelial growth factor (VEGF) receptor encoded by *Kdr*, cell-surface ligand transporter *Cd36*, cell-surface adhesion molecule CD31, and VEGF-related cell-surface protein encoded by *Nrp1* [334].

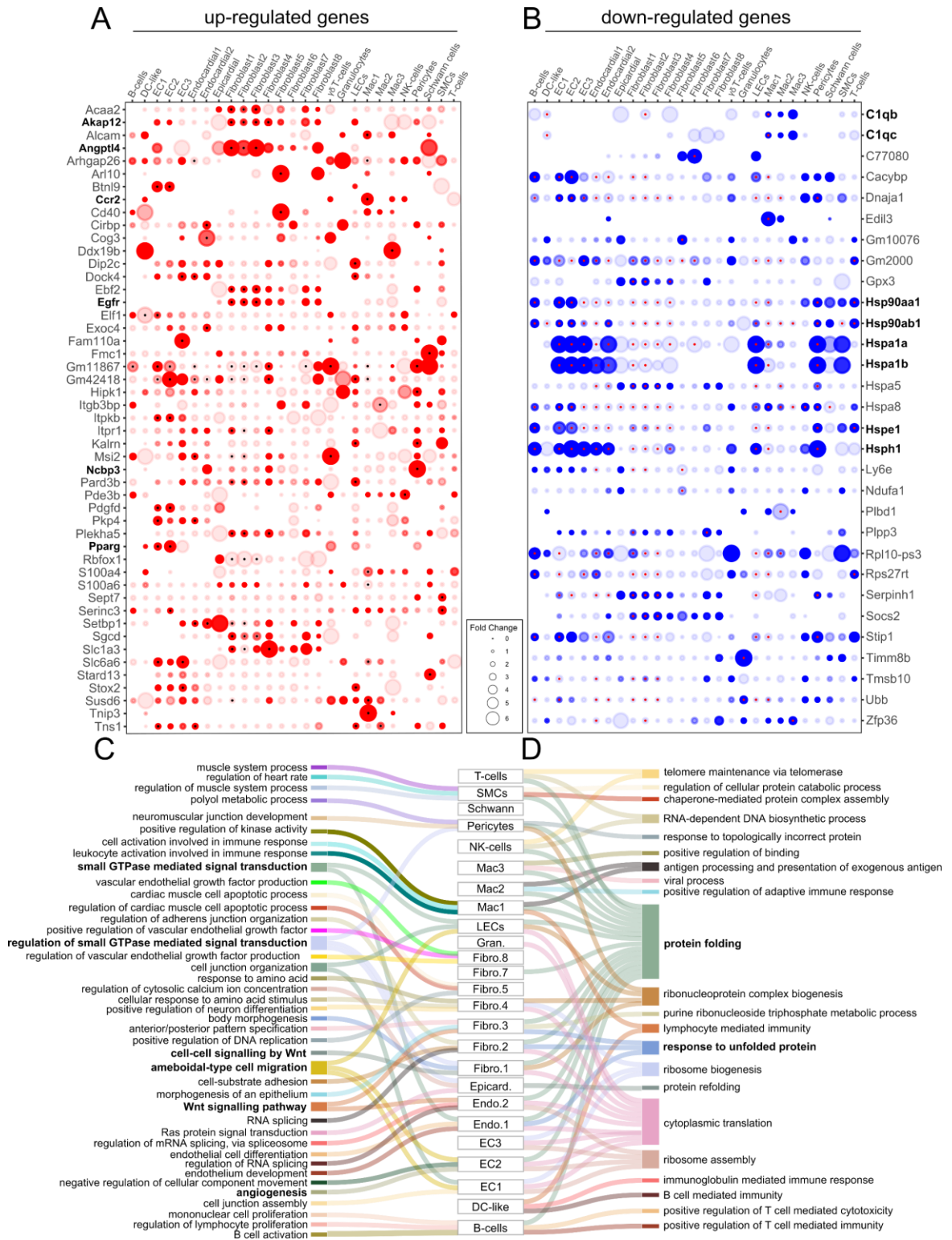


Figure 5.2: Differentially expressed genes in the *db/db* heart

(A) Dot plot illustrating the top 10 up-regulated genes in *db/db* hearts relative to *db/h* counterparts. (B) Down-regulated gene expression patterns within *db/db* hearts relative to *db/h* counterparts. Dot colour is relative to the average expression within each cell cluster. Dot size indicates fold change (red = increased, blue = decreased) in *db/db* non-myocyte cells relative to *db/h* control cells. Black points within the centre of coloured dots indicate a statistical difference in gene expression in *db/db* hearts relative to *db/h* controls (uncorrected $P < 0.001$). The Sankey plot illustrates the top-3 gene ontology (GO) terms for up-regulated genes (C) and down-regulated genes (D) in each cell type (corrected $P < 0.05$).

Consistent with up-regulated receptors, GO terms enriched in up-regulated genes corresponding to ligands in fibroblasts indicated angiogenesis and extracellular matrix (ECM) organisation (Figure 5.3D). In this context, genes associated with angiogenesis included lipoprotein lipase (LPL) inhibitor *Angptl4* [240], anti-inflammatory cell adhesion molecule *Anxa1* [335] and transforming growth factor-beta (TGF- β) growth factor super-family member *Bmp4* [336]. In addition, genes corresponding to ECM organisation primarily comprised collagen genes, including *Col14a1*, *Col1a1*, *Col4a5*, *Col5a2*, and *Col5a3* [337]. Analogous to genes encoding their receptors, genes for up-regulated ligands in ECs are also associated with increased chemotaxis and cell migration (Figure 5.3D). Genes associated with these GO terms included chemokine ligand *Cxcl12* [338], VEGF-related growth factor *Pdgfb* [334] and mast cell growth factor *Kitl* [339]. Interestingly, genes encoding receptors and ligands in lymphatic ECs (LECs) are associated with negative chemotaxis GO terms, with genes such as endothelin receptor type-B *Ednrb* [340] as well as semaphorin encoding genes including *Sema3a* and *Sema6a*, which have recently implicated in atherosclerosis [341]. GO terms encompassing downregulated genes encoding ligands and receptors in the *db/db* heart were most evident in fibroblasts, macrophages and LECs (Figure 5.3E-F). GO terms relating to downregulated genes encoding receptors implicate a role for endocytosis and positive regulation of MAPK signalling (Figure 5.3E). Down-regulated genes encoding for receptors in fibroblasts linked with positive regulation of MAPK signalling (Figure 5.3E) include MHC class II-related cell-surface molecules *Cd74* and *Cd81* [342,343] as well as cell-surface tyrosine-kinase protein *Ret* [344]. Down-regulated receptor encoding genes contributing to endocytosis in fibroblasts included *Cd81*, chemokine receptor *Ackr3* [345] and cell-surface protein *Cd63* [346].

Additionally, macrophages down-regulated ligand gene expression related to leukocyte proliferation and myeloid leukocyte differentiation (Figure 5.3E). Among the downregulated genes corresponding to receptors in macrophages, genes regulating the aforementioned processes included *Cd74*, *Cd81* and macrophage growth factor *Csf1r* [225]. Of the down-regulated genes corresponding to ligands, fibroblasts further implicate a role for endocytosis (Figure 5.3F). Genes associated with fibroblast endocytosis included cholesterol receptors *ApoE*, *Lpl* [347,348] and complement protein 3 *C3* [164], alluding to extracellular lipid and cholesterol influx. Additionally, in LECs, downregulated genes pertaining to ligands in the *db/db* heart were also associated with chemotaxis and leukocyte migration (Figure 5.3F). Genes of note in this context included *Anxa1*, chaperone protein *Calr* [349] and adhesion cell-surface molecule *Cd34* [350]. Macrophage gene expression also contributes to receptors for chemotaxis, with genes downregulated including cell-surface receptor *App* [351], chemokine ligand *Ccl4* [352] and cytokine ligand *Il1b* [353]. Furthermore, macrophage ligands also regulate ERK1&2 signalling (Figure 5.3F), with similar genes downregulated including *App*, *Ccl4* and additional chemokine *Ccl7* [354]. Together, increased leukocyte trafficking, augmented ligands for ECM remodelling and fibroblast endocytosis may suggest that cells are responding to circulating factors such as hyperglycaemia and hyperlipidaemia – key characteristics of the *db/db* mouse model of T2D.

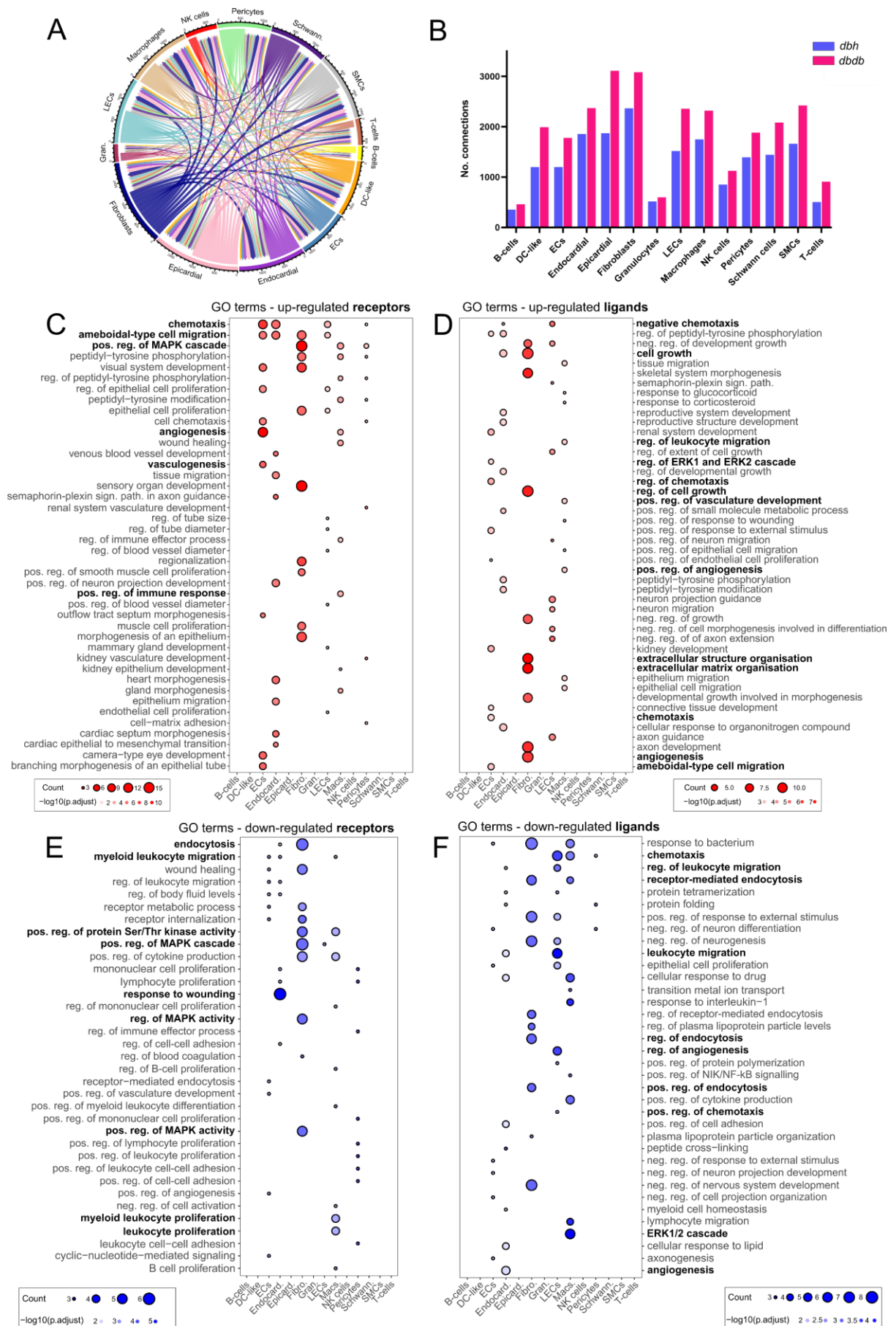


Figure 5.3: Intercellular communication is increased in the T2D (*db/db*) heart
(A) Chord plot illustrating cell-cell communications between cardiac cell types. (*Continued*).

Figure 5.3 continued: (B) Quantified chord plot showing increased intercellular communication most cardiac cell types in *db/db* hearts. GO terms enriched in genes corresponding to up-regulated receptors **(C)** and to up-regulated ligands **(D)** in *db/db* hearts relative to *db/h* controls. GO terms enriched in genes corresponding to down-regulated receptors **(E)** and to down-regulated ligands **(F)** in *db/db* hearts relative to *db/h* controls.

5.3.4 Identifying key genes that regulate cardiac lipid accumulation

Given the severely obese phenotype of *db/db* mice, and transcriptomic markers suggesting stress from circulating factors (such as hyperlipidaemia), histological analysis and further *in silico* analyses were conducted to determine the extent of cardiac lipotoxicity. First, to determine the presence of excess lipids in the *db/db* heart, frozen cardiac cross-sections (left ventricle [LV], intra-ventricular septum [IVS], right ventricle [RV]) were histologically stained with Oil Red O, as previously described [258] (Figure 5.4A). Enumeration of lipid droplets in micrographs of entire cardiac cross-sections indicated significantly augmented lipid content in the myocardium of *db/db* hearts, confirming dysregulation of lipid homeostasis ($P < 0.0001$, Figure 5.4B). I next sought to determine the gene expression patterns associated with the increased myocardial lipid content, by filtering our previously generated GO term list (see Chapter 2 Section 2.10.2) for lipid-related GO terms. Of the up-regulated genes in the *db/db* heart, GO terms related to lipid processing were most highly enriched in fibroblasts and macrophages (Figure 5.4C). Up-regulated genes of note in fibroblasts corresponding to this GO term included MAPK cell-surface receptor *Egfr*, secreted factor *Angptl4* and low density lipoprotein (LDL) receptor *Ldlr*. Similarly, in macrophages, up-regulated genes related to lipid processing included *Ldlr*, as well as *Cd36* and *Anxa1*, among others. Within ECs, up-regulated genes involved in lipid metabolism included *Pparγ*, *Cd36* and *Flt1*: a gene encoding a member of the vascular endothelial growth factor (VEGF) receptor family [334]. Down-regulated genes were also linked to lipid-related GO terms, albeit this was only evident in a subpopulation of macrophages (Figure 5.4D). Downregulated genes of note in this instance included critical reverse cholesterol transporters *Abca1* and *Cd36*, as well as oxidised LDL cholesterol scavenger receptor *Cxcl16*, which may suggest intracellular cholesterol accumulation in macrophages. These data underscore the importance lipotoxicity as a key characteristic of murine T2D-induced HF, with novel gene expression patterns regulating excess lipid deposition. However, I also note a number of cellular changes, consistent with previous findings discussed in Chapter 3 and 4. In particular, increased fibroblast numbers and a shift in macrophage heterogeneity.

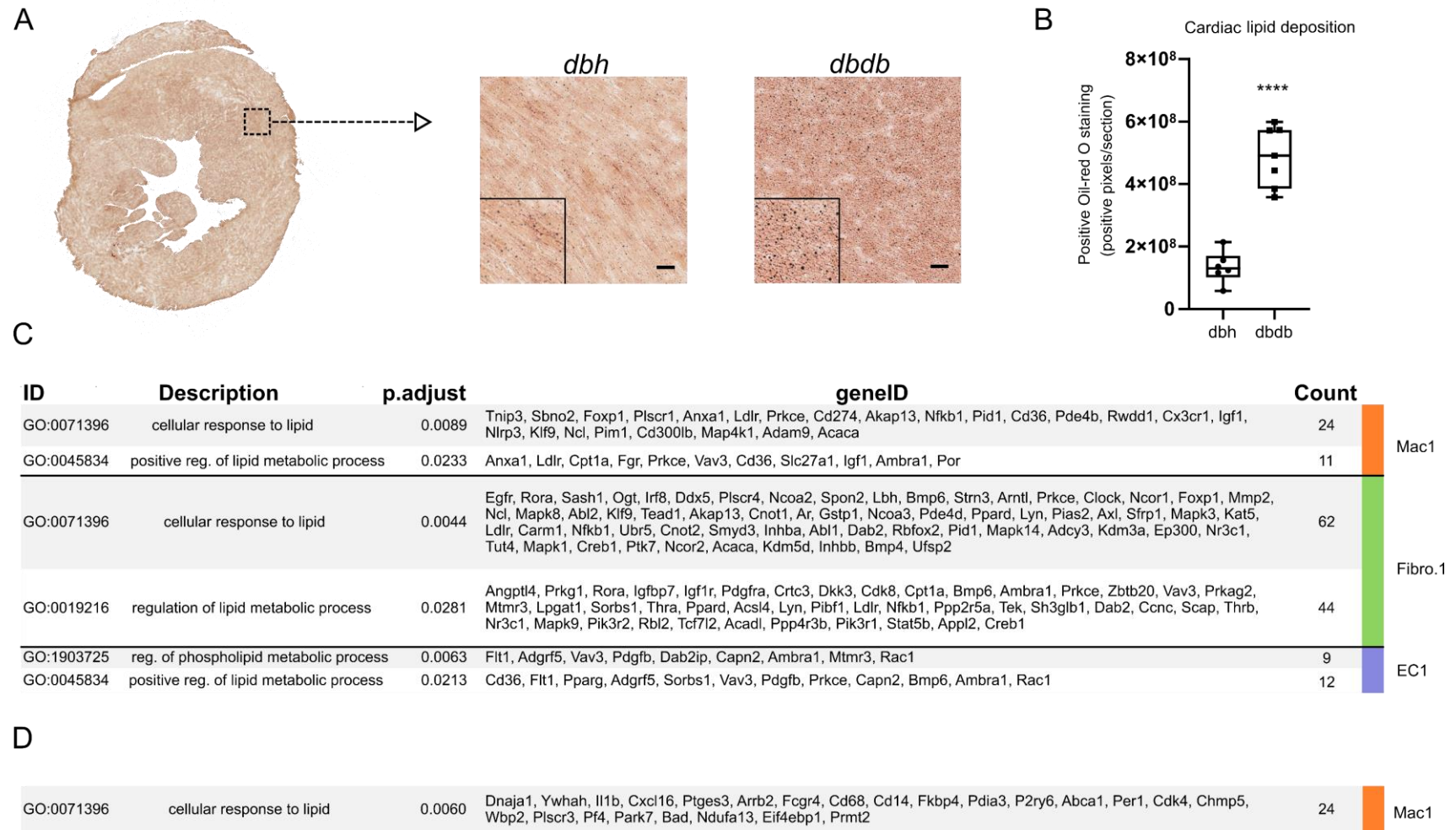


Figure 5.4: Lipotoxicity in the *db/db* heart is associated with cell-specific gene expression patterns

(A) Micrograph of an entire heart ventricle cross-section stained with Oil-red O (ORO), with adjacent representative images for *db/h* and *db/db* mice. (B) Enumerated ORO droplets indicating lipid accumulation in the *db/db* heart. (C) Up-regulated genes in *db/db* hearts mapped to GO terms corresponding to lipid processing (D) Downregulated genes in *db/db* hearts, mapped to lipid processing GO terms. Mac1 = Macrophage subset 1. Fibro.1 = Fibroblast subset 1. EC1 = Endothelial cell subset 1. *p.adjust* = adjusted *P* value for GO analysis. Micrograph scale bar = 50µm. **** *P* < 0.0001.

5.3.5 Revealing the expanding fibroblast subsets in the T2D (*db/db*) heart

While the quantity of fibrogenic collagen ligands released from *db/db* fibroblasts increase (Figure 5.3D), the top-3 GO terms were not enriched in up-regulated genes encoding ECM remodelling (Figure 5.2C), suggesting that other factors might be dictating fibroblast expansion (Figure 5.5). In order to better understand what genes distinguish expanding fibroblasts in murine T2D, fibroblasts from *db/db* hearts were isolated from other cells types *in silico*, to perform more detailed analyses. To confirm their cellular phenotype, I queried typical fibroblast markers, such as *Colla1* and *Col8a1* (Figure 5.5B). Notably, some fibroblast subtypes were associated with pro-fibrogenic genes, such as transcriptional fibroblast regulator *Meox1*, *Postn* and *Ccn2* (Figure 5.5B). I also identify novel fibroblast sub-types recently reported [233,234], including Fibroblast-*Wif1* (Fibroblast6) and Fibroblast-*Cilp* (Fibroblast3). In addition, I observed an increase in specific fibroblast subtypes in the *db/db* heart relative to their *db/h* counterparts (Figure 5.5C-D). Of the 8 transcriptionally distinct fibroblast subtypes, Fibroblast1, Fibroblast2 and Fibroblast3 were increased, with no major differences in other fibroblast levels (Figure 5.5D). To gain further insight, GO analysis was performed exclusively on the expanding fibroblast subtypes, to delineate potential drivers of this expansion.

5.3.6 Expanding fibroblasts do not exhibit transcriptomic signatures related to fibrosis

In silico isolation of cardiac fibroblasts exclusively from *db/db* mice allowed for more detailed analysis to be performed in the fibroblast subtypes of interest. In order to determine what gene expression programs may be altering fibroblast levels in the *db/db* heart, I obtained the top marker genes in each fibroblast cluster (described in Chapter 2.10), then mapped these to the top 20 GO terms, to yield biologically relevant information for each expanding fibroblast subtype (Figure 5.6). Surprisingly, GO terms associated with the gene list from the Fibroblast1 cluster indicate no transcriptional evidence to suggest ECM organisation or fibrosis (Figure 5.6A, adjusted *P* value [*p.adjust*] = NS) despite increasing in number (Figure 5.5D). Indeed, GO terms associated with gene expression in Fibroblast2 cells also indicated no transcriptional patterns suggesting ECM remodelling of the *db/db* heart (Figure 5.6B, *p.adjust* = NS). Lastly, GO terms pertaining to Fibroblast3 gene expression were also not associated with ECM remodelling and do not suggest they contribute to cardiac fibrosis (Figure 5.6C, *p.adjust* = NS). It is important to note that while other GO terms are present in these fibroblast clusters, none of these clusters yielded statistically significant GO terms, determined by the adjusted *P* value (Figure 5.6).

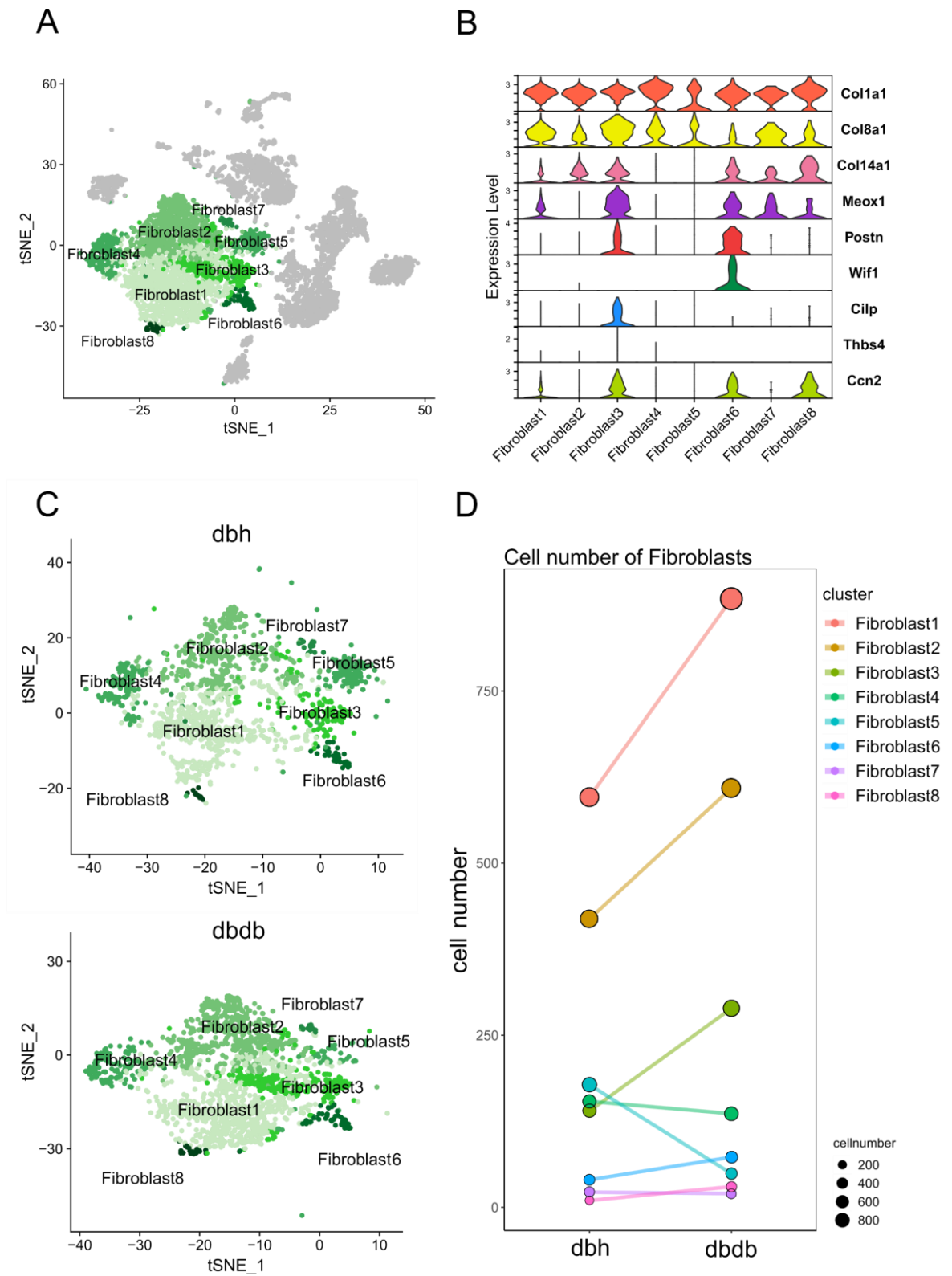


Figure 5.5: Fibroblast sub-setting identifies fibrogenic and expanding fibroblasts in T2D

(A) tSNE projection depicting all cells considered in our analysis, coloured by detected fibroblast subtypes. (B) Violin-plot indicating common fibroblast markers and known fibrogenic genes in each fibroblast cluster. (C) tSNE projection of fibroblasts isolated *in silico*, in *dbh* and *db/db* mouse hearts. (D) Drumstick plot enumerating the cell number within each fibroblast cluster.

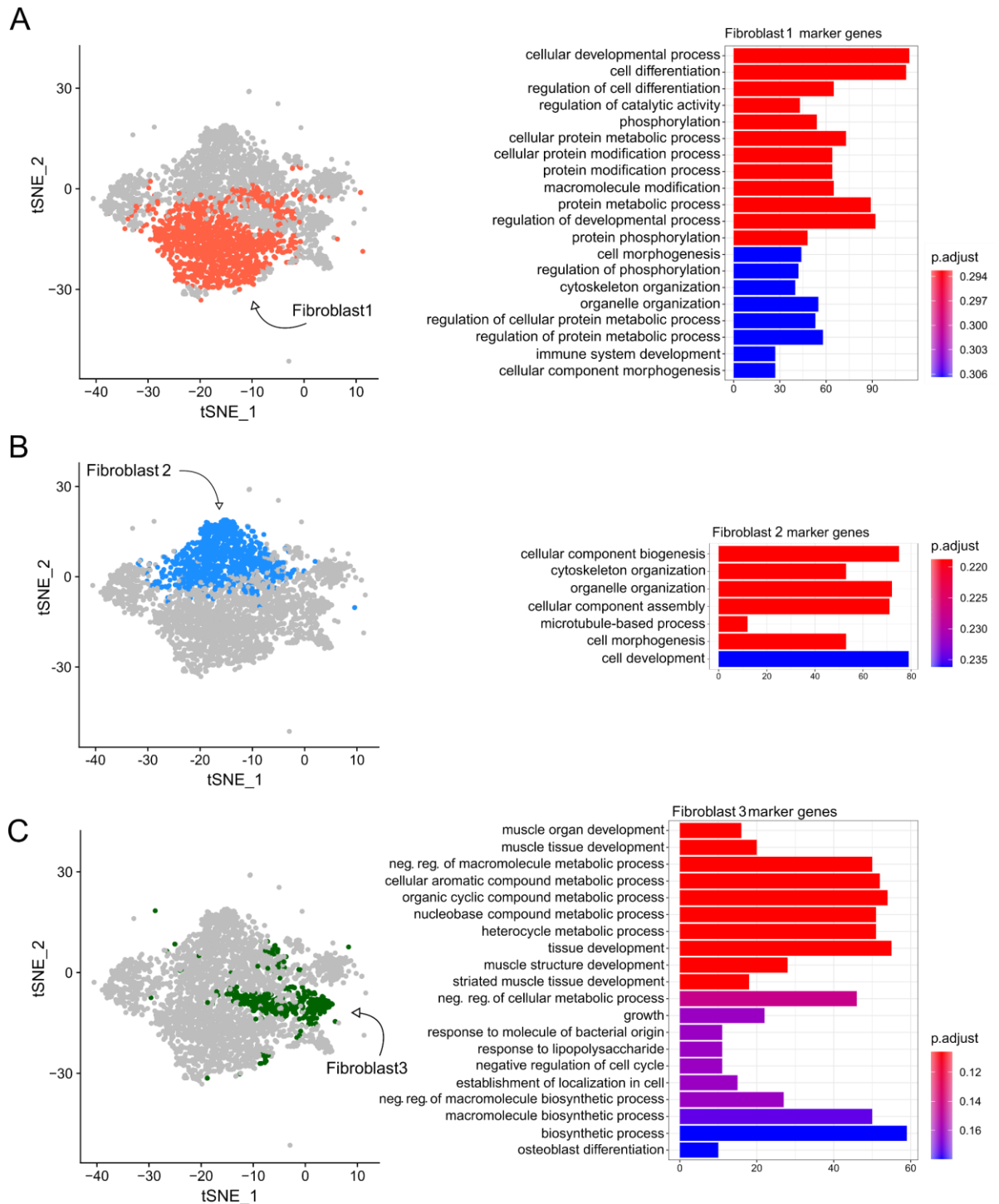


Figure 5.6: Expanding fibroblasts do not exhibit typical characteristics of ECM remodelling

(A) The top-20 GO terms enriched in genes from Fibroblast1 compared to gene lists from other fibroblast subtypes. The x-axis indicates the number of genes mapped to a given GO term, which are displayed on the y-axis. The bar colour indicates the adjusted P value ('p.adjust') from *in silico* GO enrichment analysis. (B) GO terms mapped from Fibroblast2 relative to all other fibroblast subtypes. There were no more than 7 GO terms associated with the gene expression patterns in Fibroblast2. (C) Top 20 GO terms enriched in genes in Fibroblast3 compared to all other fibroblasts as described in A and B. Statistical significance of GO terms was achieved by conducting a Benjamini-Hochberg correction as described in Chapter 2 (Section 2.10.2).

5.3.7 Identification and comparison of cardiac macrophage subtypes in *db/h* and *db/db* mice

Using a similar approach, I isolated cardiac macrophages from *db/h* mice *in silico*, to decipher any relevant gene expression patterns that govern the apparent alteration in the cardiac macrophage polarisation (Figure 5.7, Chapter 4; Figure 4.6D). A total of 3 transcriptionally distinct macrophages were identified in our analysis (Figure 5.7A). To confirm their phenotype, cells were mapped to common macrophage marker genes (Figure 5.7B). Indeed, the cells exhibit typical macrophage marker genes, such as *Csf1r*, *Mrc1* and *H2-Ab1* (which encodes for the MHC II protein). After *in silico* isolation of macrophages, these cells were split by genotype, for further analysis (Figure 5.7C). While all macrophages generally decrease in number in this analysis, I noted a substantial loss of Macrophage3 (Figure 5.7B). This is further depicted in Figure 5.7C, illustrating the extent of the loss of this macrophage subtype, relative to other macrophage subtypes.

5.3.8 Macrophage subtype 3 exhibits a reduced capability to perform reverse cholesterol transport

Analogous to Section 5.4.7, GO enrichment analysis was performed on each macrophage cluster to determine any gene expression patterns that were linked with the substantial loss in Macrophage3 (Figure 5.7). First, I performed GO analysis of genes that were more highly expressed in Macrophage3 (Figure 5.8A). Interestingly, there were no statistically significant GO terms within this macrophage cluster, nor did any GO terms suggest a possible mechanism for cell loss (Figure 5.8B). Conversely, when I performed GO analysis from genes that were more highly expressed in Macrophage1 and 2, compared to genes within Macrophage3, I noted a number of significant GO terms, including response to external stimulus, defence response, and importantly, transport (Figure 5.8B). Among genes that were more highly expressed in Macrophage1 and 2, were those that corresponded to reverse cholesterol transport receptors (Figure 5.8C). However, virtually no transcripts for these genes were detected in Macrophage3 cells (Figure 5.8C). Given that *db/db* mice exhibit systemic hypercholesterolaemia [355], the lack of intrinsic cellular machinery to expel excess intracellular cholesterol offers a potential mechanism for the loss of the macrophage 3 subpopulation.

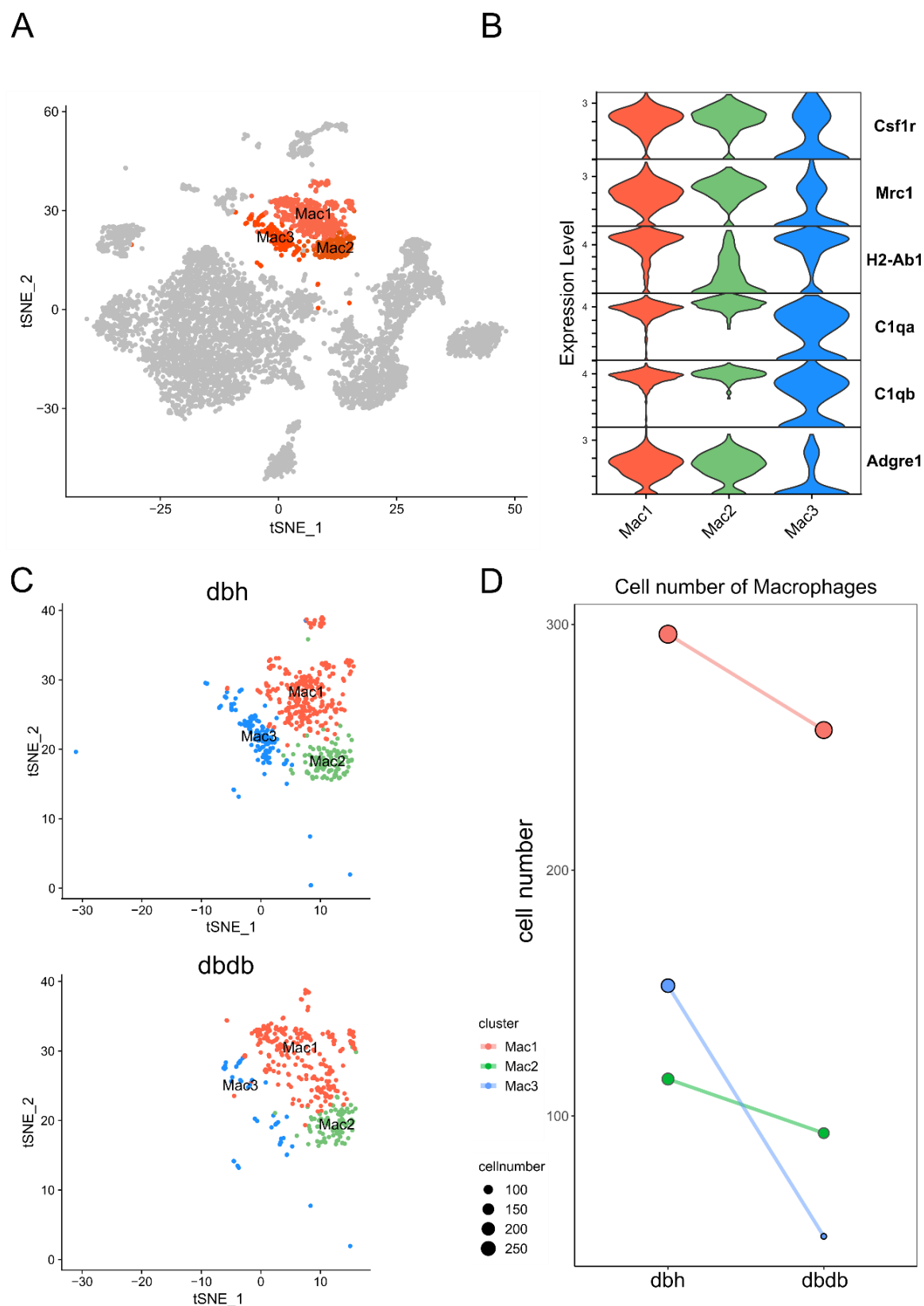


Figure 5.7: A subset of cardiac resident macrophages are lost in *db/db* hearts

(A) tSNE projection depicting all cells considered in our analysis, coloured by macrophage subtypes. (B) Violin-plot mapping established macrophage markers and confirming the macrophage cellular phenotype (C) tSNE projection of macrophages isolated *in silico*, in *db/h* and *db/db* mouse hearts. (D) Drumstick plot enumerating the cell number within each macrophage cluster from this analysis.

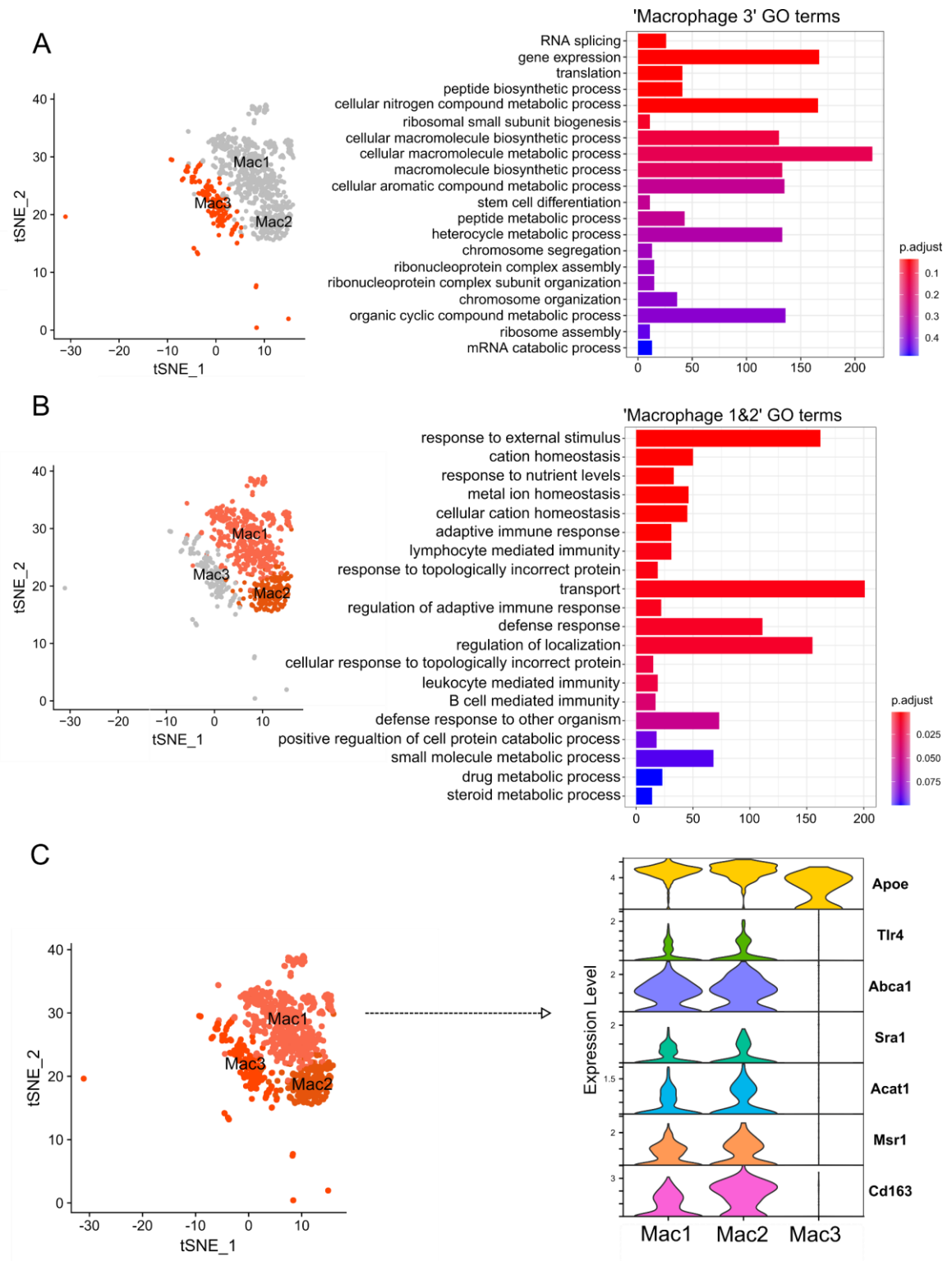


Figure 5.8: ‘Macrophage3’ exhibits a reduced capability to perform reverse-cholesterol efflux
(A) Lists the top 20 GO terms enriched in genes from Macrophage3 compared to gene lists from the other two macrophage subtypes. The x-axis indicates the number of genes mapped to a given GO term, which themselves are displayed on the y-axis. The bar colour indicates the adjusted *P* value (‘p.adjust’) from *in silico* GO enrichment analysis. **(B)** Top 20 GO terms enriched in genes from Macrophage1 and 2, compared to Macrophage3. **(C)** Violin plot considering all *db/h* macrophages, mapped to expression of key reverse cholesterol efflux genes. Statistical significance of GO terms was achieved by conducting a Benjamini-Hochberg correction as described in Chapter 2 (Section 2.10.2). Note: this figure only presents macrophages from *db/h* mice.

5.3.9 Identifying common molecular pathways in the diabetic heart

To determine common mechanisms driving the pathological remodelling of the heart in disparate diabetes models I compared differentially expressed gene lists generated from our scRNAseq pipeline, with those from cardiac bulk RNAseq datasets from unaffiliated studies [237,246] (Figure 5.9A). Datasets were obtained from the Gene Expression Omnibus (GEO) repository ('Akita' dataset identifier: GSE66577, bulk RNAseq *db/db* dataset identifier: GSE36875). GO terms associated with the 23 overlapping genes in all three datasets underscores the importance of angiogenesis, ECM regulation and lipid metabolism in the diabetic heart (Figure 5.9B). Common genes between genetically T1D *Ins2^{Akita}* (Akita) mice and *db/db* scRNAseq emphasized the role of ECM organisation in both type-1 and type-2 murine diabetes (Figure 5.9C). GO terms generated from *db/db* bulk RNAseq genes and *db/db* scRNAseq genes included positive regulation of MAPK and hydrolase activity, as well as angiogenesis and cell migration. Considering our scRNAseq dataset only contains non-myocyte cells, it is likely that the aforementioned comparison highlights common non-myocyte biological processes in murine T2D. Finally, I also sought to determine the overlapping genes between the Akita and *db/db* bulk RNA datasets. GO terms corresponding to these overlapping genes indicated an array of processes also including in lipid, carbohydrate and acyl-CoA metabolism (Figure 5.9E).

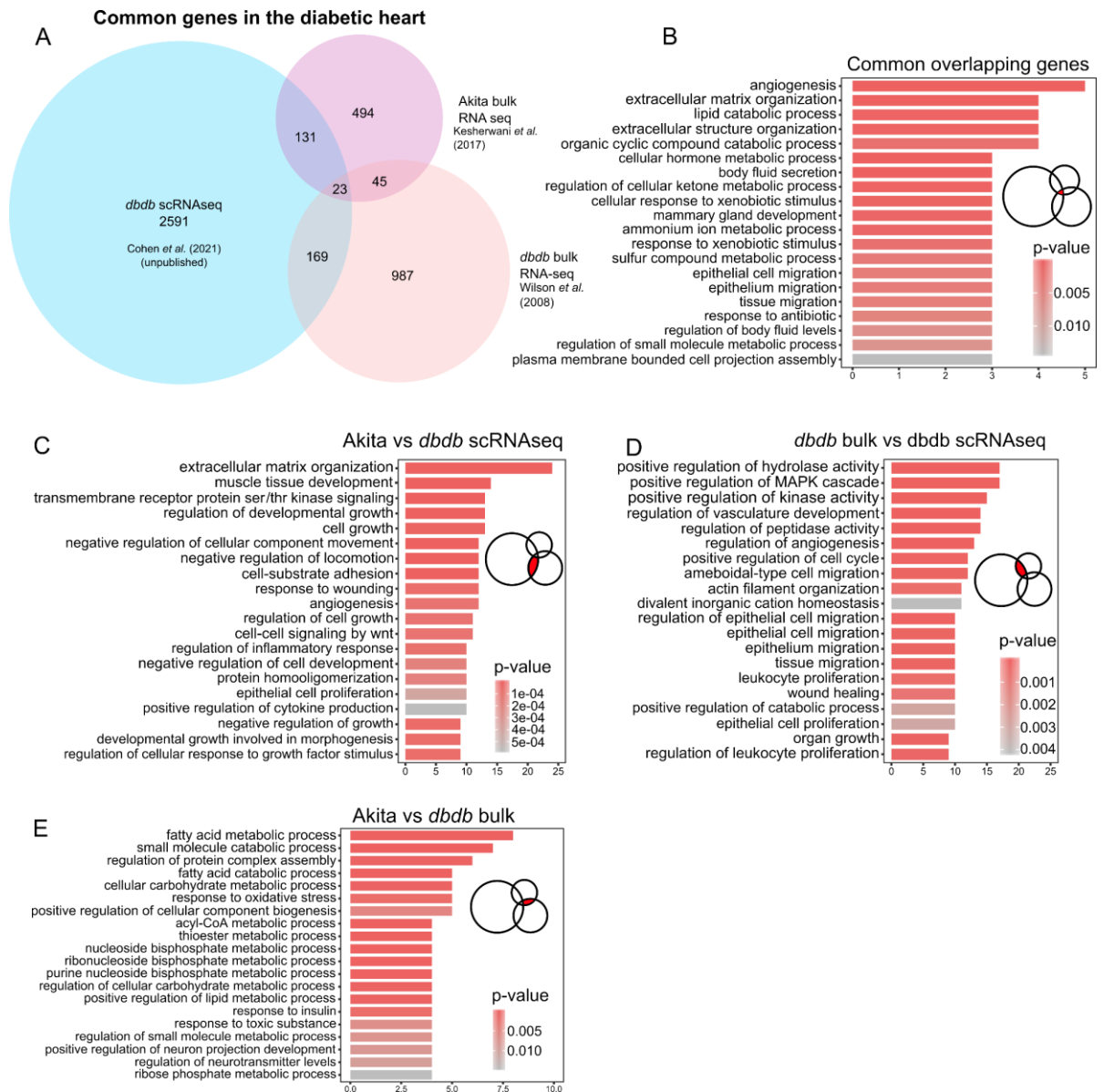


Figure 5.9: Incorporation of bulk RNA sequencing datasets highlights common molecular pathways in the diabetic heart

(A) Proportional Venn diagram illustrating unique and common differentially expressed genes in our scRNAseq dataset relative to two publically-available bulk RNAseq datasets of the diabetic heart. Gene lists were derived from each overlap and subsequently underwent GO enrichment analysis. (B) Between all datasets analysed, there were 23 common genes. GO analysis revealed the top 20 common biological functions (y-axis) and the collection of genes corresponding to each GO term (x-axis). (C) GO analysis of bulk RNAseq genes in the T1D Akita mouse heart relative to our *db/db* scRNAseq dataset. (D) GO analysis pertaining to common genes in the *db/db* bulk RNAseq dataset compared to the *db/db* scRNAseq dataset, highlighting key non-myocyte differentially expressed genes. (E) GO analysis of genes common in Akita and *db/db* hearts, from bulk RNAseq. Datasets were obtained from the Gene Expression Omnibus (GEO) repository. ‘Akita’ dataset identifier: GSE66577. Bulk RNAseq *db/db* dataset identifier: GSE36875.

5.4 Discussion

While single-cell technologies allow for improvements in our understanding of the cellular and molecular dynamics in cardiac homeostasis and disease, this is the first study to apply this technology in the context of murine T2D. Using the established *db/db* model of T2D-induced cardiac dysfunction (discussed in Chapter 4), I highlight a number of novel cellular and molecular alterations within the cardiac milieu. Using a previously described strategy [234] I produced a high-resolution atlas of the *db/db* cellulome, with a number of cell-specific and broad transcriptomic alterations. Among these, include up-regulated genes programs relevant to cell migration (ECs, LECs), chemotaxis (ECs, LECs), angiogenesis (fibroblasts, ECs, LECs), augmented MAPK signalling (fibroblasts) and regulation of leukocyte function (macrophages). Down-regulated genes in *db/db* non-myocytes encode a broader response prompting protein folding. I also noted excess lipid deposition in *db/db* hearts, with transcriptomic signatures corresponding to dysregulated lipid and cholesterol metabolism in fibroblasts, macrophages and ECs. While I observed an increase in fibroblast levels using scRNAseq (consistent with findings from Chapter 3 and 4), the data suggests that cardiac fibrosis is not a key feature at this stage of diabetes-induced HF. Moreover, I noted a shift in macrophage subset proportions, with one MHCII^{hi} macrophage subtype virtually absent in our *db/db* dataset. Lastly, two existing bulk RNAseq datasets examining the diabetic heart [237,246] were incorporated with our current scRNAseq dataset, to delineate common molecular pathways in this context. Together, these data provide a novel insights into the non-myocyte cellular and molecular changes that occur in T2D and provide a valuable resource for future studies to utilise.

5.4.1 Fibroblast expansion is apparent in murine T2D without evidence of ECM remodelling

In this study I observed an expansion of 3 fibroblast subtypes, however differing from recent reports [233,234,245], there is little transcriptomic evidence associated with extensive cardiac fibrosis or ECM organisation. The increase in certain fibroblast levels is also corroborated by our cardiac flow cytometry findings (Chapter 3 and 4). This finding is intriguing, considering that echocardiography data suggests cardiac dysfunction (Chapter 4, Section 4.32), which usually occurs concomitantly with fibrosis. Genes up-regulated in fibroblasts, such as *Egfr* provide a possible mechanism facilitating cell growth and proliferation [356]. EGFR is a cell surface tyrosine kinase receptor regulating MAPK signal transduction—a known contributor to cardiac fibroblast activation and fibrosis in diabetes [357–359]. In the heart, EGFR typically activates small guanosine triphosphate (GTP) molecules such as the Ras proto-oncogene [360] leading to MEK and ERK1/2 signal transduction, ultimately initiating cell growth and proliferation in both development and pathology [361,362]. Indeed, GO enrichment analysis of differentially expressed *db/db* genes also revealed that fibroblasts up-regulate genes related to regulation of small GTPases. Moreover, GO terms associated with differentially expressed genes encoding receptors in fibroblasts confirm positive regulation of MAPK signalling, further substantiating the involvement of this pathway in diabetic fibroblasts. Additionally, down-regulated ligands and receptors are associated with endocytosis and

response to external stimulus GO terms, which may indicate extracellular influx of various factors such as glucose, lipids and cholesterol.

Various characteristics of the diabetic milieu such as hyperglycaemia, hyperlipidaemia and hyperinsulinaemia can stimulate the MAPK cascade in the heart, particularly its down-stream signalling components p38 and ERK1/2. While little is known in the human context, mice with T1D exhibit augmented phosphorylation of p38, which is associated with up-regulation of fibrogenic gene expression and cardiac dysfunction [363]. In the same study, pharmacological inhibition of p38 improved fibrosis and cardiac function *in vivo* [363]. Increased ERK1/2 activation within the MAPK pathway is also implicated in fibroblast activation. Stimulation of murine fibroblasts with high glucose *in vitro* increased both phosphorylation of ERK1/2 and p38, which are associated with fibroblast expansion and increased collagen I and III synthesis [364,365]. Furthermore, increased ERK1/2 phosphorylation is also associated with impaired cardiac function, further underscoring its importance in the pathogenesis of HF in diabetes [366]. In T2D mice, these pathways are also described in the heart. Indeed, phosphorylation of p38 and ERK1/2 proteins were significantly increased in *db/db* hearts in the presence of diastolic dysfunction [367].

However, the role of MAPK differs in disparate cell types [361]. Increased ERK1/2 phosphorylation in hyperglycaemic T1D mice can stimulate opposing effects such as apoptosis in ECs from murine mesenteric arteries [368]. Moreover, peripheral blood mononuclear cells (PBMCs) from human patients with acute hyperglycaemia also enhances MAPK activation [369], facilitating the release of pro-inflammatory cytokines and inflammation via p38 signalling [370]. Notably, in this study ligands related to ERK1/2 signalling are downregulated in macrophages despite increased MAPK activity in fibroblasts, suggesting macrophages are dampening inflammation. The functional divergence of MAPK signalling in disparate cell types emphasises the need for cell-specific analyses, to decipher which cells are pathologically susceptible to this pathway.

Here, simultaneous examination of all non-myocyte cells in the diabetic heart suggests that MAPK activation occurs almost exclusively in fibroblasts, which may contribute to their expansion. However, MAPK-related ligands are also downregulated in cardiac macrophages, suggesting highly variable functions of this cascade. While the MAPK pathway is implicated in fibroblast activation and fibrosis, the phosphorylation status of individual MAPK members have not been assessed here. Hence, the precise mechanism initiating fibroblast expansion in the *db/db* heart remains unclear.

5.5.2 Lipotoxicity in *db/db* mice is a contributing feature driving impaired cardiac function

It is well established that obesity and insulin resistance are essential comorbidities governing ectopic lipid accumulation and lipotoxicity in T2D [371], however its contribution to cardiac dysfunction in diabetes remains unclear. In this study, I confirm substantial myocardial lipid deposition histologically. *In silico* filtering of genes based on their enrichment in lipid-related GO terms indicated that fibroblasts, macrophages and ECs are the key non-myocyte cells responding to

dyslipidaemia. Among the many differentially expressed genes in the *db/db* heart, genes most indicative of lipotoxicity include *Pparγ* (ECs), *Angptl4* (fibroblasts) and *Ldlr* (macrophages).

The nuclear receptor PPAR γ (peroxisome proliferator-activated receptor gamma) is understudied in the diabetic heart, however its primary role involves regulating lipid and glucose metabolism [34]. In fact, pharmacological PPAR γ agonists such as thiazolidinedione agents are often used in clinical T2D to increase insulin sensitivity, by preferentially facilitating glucose flux into cells, rather than free fatty acids (FFAs) [373]. Indeed, genetic overexpression of PPAR γ in diabetes-induced HF results in preferential glucose utilisation for energy metabolism [374]. Although cardiac energy metabolism relies primarily on FFA oxidation, even minor perturbations in substrate utilisation can progress to impaired cardiac function [56,375]. Given that ECs are generally early responders to systemic abnormalities, this data suggests that PPAR γ is responding to lipid stress in murine T2D and encourages glucose influx into ECs to compensate. Interestingly, PPAR γ expression is positively correlated with the secretion of angiopoietin-like protein 4 (ANGPTL4 - encoded by *Angptl4*), suggesting their cellular and molecular cross-talk in lipid metabolism [376,377].

ANGPTL4 is a nutrient partitioning molecule responsible for redirecting triglycerides away from adipose tissues, toward functional organs for energy utilisation, rather than for storage [347]. ANGPTL4 does this by inhibiting the action of LPL; which itself catalyses the hydrolysis of absorbed triglycerides, for organ energy storage. ANGPTL4 is most highly expressed in adipose and skeletal myocytes, however remains expressed at lower levels in other organs, including the heart [378]. As such, overexpression of ANGPTL4 ultimately leads to raised plasma triglycerides [240,347,379], but also serves as a marker for cellular and organ lipid stress. In addition to the heightened expression of *Angptl4*, GO terms encoding downregulated receptors in *db/db* fibroblasts are associated endocytosis, which may also suggest that fibroblasts are attempting to further dampen lipid influx by reducing the available receptors facilitating this. Together, these data implicate dysregulated lipid and cholesterol influx within *db/db* myocardial fibroblasts as potential drivers of murine T2D-induced HF.

Although yet to be described in the diabetic heart, a number of studies investigate macrophage dynamics in the setting of hypercholesterolaemia and atherosclerosis [380]. In this study, macrophages up-regulate lipid metabolism genes including phospholipid binding protein *Anxa1*; intermediate fatty acid substrates, *Acaca*; and cholesterol efflux receptor, *Ldlr*, among others. Annexin-A1 (ANXA1 - encoded by *Anxa1*) is widely reported as an anti-inflammatory protein, inhibiting the actions of a number of inflammatory cytokines [381]. More importantly, ANXA1 mediates intracellular lipid and cholesterol trafficking and metabolism in macrophages [382]. Further, ANXA1 can act in tandem with ATP-binding cassette transporter ABCA1 (further discussed in Section 5.5.4) to further facilitate cholesterol efflux in macrophages [383]. While

ANXA1 induces cardioprotective effects in atherosclerosis and in MI [384,385], the precise mechanism of ANXA1 in cardiac pathology, including HF in diabetes, remains unclear.

Acetyl-CoA carboxylase (encoded by *Acaca*) is an intermediate, rate-limiting metabolite of fatty acid synthesis [386,387]. As such, increased expression of *Acaca* in macrophages is likely indicative of increased fatty acid synthesis in macrophages. Indeed, *Acaca* has been used previously as a marker for intracellular hepatic lipid stress in diabetic patients with fatty liver disease [388]. Moreover, increased expression of *Acaca* has been described in lipid-laden macrophages isolated from human tumour biopsies, further implicating its role in macrophage homeostasis [389]. However, its specific role in regulating tissue resident macrophage lipogenesis is yet to be comprehensively assessed.

Lastly, it is unsurprising to observe augmented expression of *Ldlr* in *db/db* macrophages, given that the fundamental role of the LDL receptor (encoded by *Ldlr*) is reverse cholesterol efflux [390]. The LDL receptor is known to increase its expression and translocation to the cell surface in the context of high cholesterol via a complex intracellular pathway [391]. Indeed, knockout of the LDL receptor aggravates atherosclerotic plaque burden and foam cell accumulation in mice fed a Western diet [392], highlighting the importance of LDL-mediated cholesterol efflux in macrophage homeostasis. Here, I provide novel insights into fibroblast and macrophage behaviour in *db/db* mouse hearts, underscoring the importance of lipid and cholesterol accumulation and reverse cholesterol transport. However, this data may suggest that some macrophage subtypes are more susceptible than others, to the accumulation of intracellular cholesterol, which is discussed below.

5.4.4 A subtype of cardiac macrophages are unable to perform reverse cholesterol efflux in the *db/db* heart

Expanding on cardiac macrophages in murine T2D, our data suggests substantial resident macrophage loss, dictated by lack of gene expression for critical reverse cholesterol transporters. As aforementioned, *Ldlr* increases its gene expression in Macrophage1, which is counterintuitive when considering the possible mechanism of macrophage loss is likely related to lipid and/or cholesterol toxicity. However, LDL is not the sole reverse cholesterol transporter in macrophages [393]. In fact, key reverse cholesterol transporters in macrophages include; ABCA1, CD163 (encoded by *Cd163*), Msr1/SR-A (encoded by *Msr1* and *Sra1*), TLR4 (encoded by *Tlr4*) and ApoE (encoded by *ApoE*) [394–398]. These transporters, in addition to the LDL receptor, collectively govern macrophage viability in the face of hypercholesterolaemia – a major comorbidity in T2D.

Hindered reverse cholesterol transport in diabetes has been known for decades. In STZ-induced T1D mice, mRNA yielded from peritoneal macrophages and the liver exhibited significantly reduced expression of ABCA1 [399]. Indeed, *db/db* peritoneal macrophages reduce their mRNA expression of ABCA1 homolog ‘ABCG1’, which is accompanied by a 2-fold increase in intracellular cholesterol levels [400]. Although in this study ABCG1 expression is undetected in

cardiac *db/db* macrophages, ABC transporters are tissue-specific [401,402], which may explain its absence.

Aberrant cholesterol efflux is extensively studied in atherosclerosis, which report similar findings to macrophage behaviour in the *db/db* heart. Principally, atherosclerosis is also driven by elevated circulating lipids and cholesterol, resulting in augmented monocyte-derived macrophage recruitment to susceptible vessel areas [403]. In this context, macrophages engulf excess cholesterol, however exhibit hindered efferocytosis intracellular cholesterol, subsequently leading to lipid-laden macrophages known as foam cells [135]. Ultimately, accumulation of foam cells and other associated factors leads to unstable plaque formation, obstruction of vessels and a cascade of pathophysiological responses [135,403]. Genetic ablation of ABCA1 and ABCG1 either separately [404] or concomitantly [405] is sufficient enough to accelerate plaque occlusion and foam cell formation, highlighting their importance in regulating cellular cholesterol levels. Moreover, hyperglycaemia alone in T1D increases myelopoiesis and impairs resolution of atherosclerotic lesions [113]. Likewise, the monocytosis-driven increase in cardiac Ly6C^{hi} monocytes described in Chapter 4 could be further exacerbating the local inflammatory milieu, analogous to atherosclerosis. Considering our data *in toto*, it is reasonable to speculate that cholesterol-induced macrophage toxicity is another key feature of the diabetic heart, mimicking macrophage loss in atherosclerosis. As such, it was pertinent to investigate the effect of these findings on vascular homeostasis in the *db/db* heart.

5.4.5 Angiogenesis and dysregulated leukocyte trafficking are characteristics of the *db/db* heart

Considering the impairments in cardiac of monocytes and macrophages, I also noted a complex, cell-specific role for chemotaxis, cell migration and impaired lymphatic drainage in *db/db* hearts. Specific to ECs, among the top-3 GO terms for up-regulated genes were both angiogenesis and EC differentiation. Moreover, GO terms corresponding to up-regulated ligands include chemotaxis and EC proliferation, further corroborated by GO terms for up-regulated receptors, again suggesting chemotaxis, angiogenesis, as well as vasculogenesis. This data is consistent with numerous reports in the context of diabetes, which highlight a role for compensatory, ischaemia-induced neovascularisation. This is most commonly described in diabetic retinopathy, where hyperglycaemia reduces retinal capillary density, leading to disproportionately enhanced angiogenesis and ultimately retinal hypoxia [3]. In the context of CV disease, diabetes is also associated with augmented angiogenesis and dysregulated vascular remodelling. Diabetic patients with early-phase HF have historically exhibited coronary microvessel occlusion and compensatory angiogenesis, by facilitating the formation of coronary collateral vessels [406–408]. Coronary collateral vessels are vascular connections between arterioles that undergo arteriogenesis and formation of new vascular branches, in response to myocardial ischaemia and hypoxia [409]. Indeed, more recent reports have demonstrated dysregulated angiogenesis in rodent T1D [410] as

well as human patients with T2D undergoing heart transplantation [411]. Murine T1D-induced angiogenesis is associated with abnormal redox protein signalling suggesting concomitant cardiac capillary rarefaction [410]. Human T2D explants are also associated with capillary rarefaction and interestingly, pericyte loss [411], which has also been described in diabetic retinopathy [412] and is consistent with our data in Chapter 4. Together, these studies implicate vascular rarefaction in diabetic heart disease as a key feature governing cardiac dysfunction. I propose that compensatory angiogenesis is occurring in the *db/db* heart as an initial phase of vascular remodelling. This could be partly attributed to vessel occlusion by lipid-laden cardiac macrophages [135], similar to atherosclerosis. However, it is important to note that the precise mechanism for neovascularisation in diabetes remains unknown. Further, it is still unclear whether this compensatory angiogenesis in diabetes is affected by a particular comorbidity, or a combination of the stressors that define T2D.

Abnormal angiogenesis and neovascularisation could also contribute to increased cell migration, which were observed in *db/db* macrophages, ECs and endocardial cells. Cardiac macrophages in *db/db* mice up-regulate expression of *Ccr2*, encoding for the cognate receptor of monocyte chemoattractant protein-1 (MCP-1), a key chemotaxis mediator for monocytes [262,413,414]. Increased *Ccr2* is positively correlated with leukocyte homing and recruitment in the diabetic heart [262,413]. Corroborating this, I previously demonstrate an increase in cardiac Ly6C^{hi} monocyte levels within the *db/db* myocardium (Chapter 4, Section 4.35). Although while encouraging monocyte chemotaxis, *db/db* macrophages also downregulate *C1q* genes encoding for complement protein C1q – a secreted protein that dampens inflammation and enhances macrophage phagocytic activity [164]. This may suggest that macrophages are concomitantly attempting to dampen inflammation, particularly given the pronounced monocytosis and neutrophilia that we observe in this model (Chapter 4, Section 4.33).

Other adhesion molecules also appeared to be dictating chemotaxis and cell migration in ECs, such as chemoattractant *Cxcl12* and CD31 encoded by *Pecam1*. The C-X-C motif ligand 12 (CXCL12, encoded by *Cxcl12*) is strongly associated with T2D-induced nephropathy [415], however less is known regarding its function in the diabetic heart. Conversely, it is well documented that CXCL12 can attract myeloid progenitors such as monocytes in the context of MI and myocardial ischaemia [338]. However, comparable to the MAPK pathway discussed in Section 5.5.1, CXCL12 is linked to opposing functions such as maintenance of EC homeostasis [416], highlighting its multimodal function. It is proposed that CXCL12 is acting as a chemoattractant for circulating leukocytes in ECs, however the off target effects resulting from this remain unclear. The CD31 protein, a ubiquitous marker of ECs, also exhibits chemoattractant functions. Indeed, CD31 facilitates transmigration of monocytes across the EC monolayer *in vitro* [417]. Again, while less is known regarding CD31 perturbations in the diabetic heart, diabetic retinopathy is associated with reduced abundance of CD31, accompanied by retinal EC loss [418,419]. I also observed increases in established inflammatory proteins relevant to the diabetic heart such as TGFβ, IL-1β and TNFα

[262], however gene expression for these existed at comparatively lower levels. It is becoming increasingly important to consider vascular and leukocyte dynamics in diabetic heart disease, given the presence of local and systemic inflammation coupled with dysregulated angiogenesis. Given that gene expression patterns in the *db/db* myocardium suggest enhanced cell migration, it is also important to consider how this affects the drainage capacity of the cardiac lymphatic system.

Accordingly, I observed a concerted response by *db/db* cardiac LECs to reduce cell migration and chemotaxis, suggesting reduced leukocyte trafficking and hindered LEC function. The cardiac lymphatic network forms a delicate plexus of vessels dispersed diffusely, with impairments in cardiac contractility sufficient to impair LEC function [420]. Here, *db/db* LECs express up-regulated ligand genes are associated with negative chemotaxis, while down-regulated ligand genes correspond to leukocyte migration and chemotaxis. Whilst not among the most highly expressed differentially expressed genes in our dataset, expression of pro-survival transcription factor *Prox1* was up-regulated in LECs, which is indicative of extrinsic LEC stress [420,421]. Whether LECs are dysfunctional, or merely compensating for excessive leukocyte chemotaxis remains to be determined. However, it has been documented that increased nitric oxide production in *db/db* hearts increases LEC permeability and dysfunction [422]. Moreover, in clinical and pre-clinical obesity, cardiac ectopic fat deposition is associated with impaired lymphatic function, by perturbed mechanical shear stress and via paracrine communications [423]. Consequently, chronically dysregulated LEC function is characterised by impaired lymphatic pumping and lymphoedema [421,424,425]. While in this study, I was unable to empirically test lymphatic function in the *db/db* myocardium, I highlight a role for impaired leukocyte trafficking in LECs, which may be associated with dysregulated cardiac lymphatic function.

5.4.6 Gene expression programs are distinct between murine models of T1D and T2D

Lastly, determination of common dysregulated genes in the heart of diabetic mice from unaffiliated studies, point to common biological pathways that may broadly induce cardiac remodelling. Akita mice (see Chapter 1, Table 1.1)—bearing a single base pair substitution in the *Ins2* gene—exhibited genes corresponding primarily to ECM organisation and muscle tissue development, which may suggest that hyperglycaemia alone is the prominent feature inducing cardiac remodelling in the diabetic heart. This is further substantiated by both *db/db* datasets, which do not share genes corresponding to ECM remodelling, but rather, relate to MAPK signalling and vasculature development, including angiogenesis. This seminal transcriptomic data integration implies that hyperglycaemia in murine T1D is the driving force behind ECM remodelling in the diabetic heart, rather than the myriad of additional comorbidities present in murine T2D, underscoring the multifaceted nature of T2D. Future transcriptomic and proteomic studies using multiple models of diabetes in parallel are warranted to determine the validity of these observations.

5.4.7 Limitations

Despite highlighting a number of novel paradigms in this study, I acknowledge a number of limitations that can improve future work in this context. First, cardiomyocytes were not considered due to their size, limiting our capability to infer important information regarding their involvement in diabetes-induced cardiac remodelling. This limitation applies to most high-throughput single-cell technologies, due to their reliance on microfluidic systems that are often too small in diameter to fit larger, potentially hypertrophic cells. However as mentioned in Chapter 4, Section 4.4.4, cardiomyocyte gene expression in this context is widely studied, providing some insight into their contribution.

Second, while I elude to increased MAPK cascade signalling, we have not conducted proteomic analysis in this study. Accordingly, I was unable to determine the phosphorylation status of individual MAPK members, making it difficult to determine the primary activated signalling cascade. This encourages future studies to consider phosphoproteomic analysis of fibroblasts in experimental T2D.

Third, I did not yield any specific information pertaining to spatial gene expression, to assess the physical cellular relationships and gene expression loci. Spatial transcriptomics is an emerging field, allowing for measurement of high-resolution, spatially resolved transcriptomic information from tissues *in situ*. This however is also accompanied with its own limitations, with comparatively lower resolution than scRNAseq [426]. In addition, this study did not include any other histological analyses to validate our scRNAseq data. This further impedes our ability to spatially resolve the scRNAseq data acquired, inviting future research to address.

Finally, I also acknowledge that the sole use of male mice in this study is a significant limitation. As previously discussed, cardiac pathology is sex-dependent in mice and humans [225,229,250,318]. Therefore, future work should incorporate female mice to decipher any apparent sexual dimorphisms in the context of T2D-induced HF.

5.4.8 Future prospects

While this work provides mechanistic insights into cardiac cellular and molecular alterations, these data would benefit from additional validation studies. Indeed, systemic monocytoxis, genes corresponding to cell migration and alterations in resident macrophage populations signify the importance of investigating monocyte and macrophage behaviour in the context of diabetic heart disease. Indeed, this could be empirically tested by a number of means. Pharmacological siRNA knock-down of the CCR2 receptor at various time-points in mice with T2D would provide valuable insights into the role of CCR2-induced monocyte recruitment, given that this approach reduces cardiac monocyte recruitment post MI [427]. Additionally, utility of clodronate-loaded liposomes eliciting systemic monocyte depletion in this context would assist in determining the role of circulating monocytes. Moreover, transgenic murine models capable of marking monocytes and/or

macrophages could be another useful approach for verifying their role in diabetes-induced cardiac complications. For example, lineage tracing experiments using the CCR2^{RFP} mouse line [428] in mice with diabetes would provide additional mechanistic insights into monocyte trafficking into cardiac tissue. Regardless, this Chapter presents seminal findings regarding cell-specific gene expression patterns and provides mechanistic information pertaining to cardiac cellularity changes in T2D.

5.5 Conclusion

This is the first study to incorporate cardiac single-cell transcriptomics in murine T2D-induced cardiac dysfunction (primarily via reduced e' velocity), revealing a concerted diabetes-induced cellular response for remodelling the heart. I have identified diabetes-induced up-regulation of pathways involving dysregulation of vascular homeostasis and lipid metabolism, as well as augmented inflammation, in cell specific contexts. I also identify other unexpected characteristics in the diabetic heart, including impaired protein folding and leukocyte trafficking in lymphatic vessels. While this work offers a comprehensive framework for understanding the cardiac non-myocyte cellular and molecular dynamics in T2D, further analyses of the cardiac cell networks in diabetes-induced HF are warranted. Our next steps include extending this framework to the female diabetic heart to decipher any apparent sexual dimorphisms and to determine the gene regulatory elements that govern the observed gene expression differences. Targeting the pathways that drive these changes may offer new therapeutic avenues to address the cardiac complications associated with diabetes.

Chapter 6

Profiling circulating leukocytes in diabetic patients: a pilot study

6.1 COVID-19 pandemic disclaimer

Due to the global COVID-19 pandemic, recruitment of patients for blood profiling was halted in 2020. This led to the premature cessation of the study as the data was unblinded and then analysed, hindering us from any further recruitment of patients. The statistical power of this study was significantly compromised and as such, this study is presented as pilot data.

6.2 Introduction

Diabetes is associated with elevated circulating leukocyte counts in the clinic [115–119]; however, the contribution of phenotypically distinct human leukocytes in pathogenesis of diabetic complications remains understudied. Insights from pre-clinical studies suggest that systemic inflammation in T2D is characterised primarily by monocytosis and neutrophilia [5,113,273]. Similar findings have been reported in patients with diabetes, with the most pronounced alterations occurring in innate immune cells, such as monocytes [119,139]. However, this information is often derived from differential white blood cell (WBC) counts using clinical haematology analysers [119,429–431], which provide inexpensive and rapid information regarding circulating WBCs. These systems only identify cells based on cell size and gross morphology and do not provide information about cellular activation state. While haematology analysers are clinically useful, they cannot accurately discriminate between all circulating cell types, particularly the more subtle alterations that may occur in diabetes [432,433]. Rodent studies have allowed for precise detection and tracing of specific leukocytes using flow cytometric and cell-sorting approaches in various models of disease, including diabetes [5,113,310,434]. Given that clinical T2D is associated with ‘sub-clinical’ inflammation and murine T2D induces monocytosis and neutrophilia (via flow cytometry), more sensitive approaches are warranted to determine the relative proportions of circulating leukocytes and their subtypes in the human context.

Using flow cytometry, murine monocytes are phenotypically separated by cell surface expression of Ly6C, which exhibit differing functions depending on their cell-surface antigen density (Chapter 3 & 4). The same concept can also be applied to the human context, except monocytes are typically divided into three subtypes; CD14⁺CD16⁻ (classical), CD14⁺CD16⁺ (intermediate) and CD14⁻CD16⁺ (non-classical) [435]. Classical monocytes in humans are thought to be phenotypically equivalent to Ly6C^{hi} monocytes in mice, while non-classical monocytes exhibit phenotypic similarity to Ly6C^{lo} monocytes [436]. Intermediate monocytes have been implicated in clinical pathogenic inflammation in the context of sepsis and atherosclerosis [437], however are yet to be comprehensively quantified in patients with T2D.

Given the mounting evidence implicating systemic inflammation in T2D and its associated complications, I performed multicolour flow cytometry in blood from human non-diabetic

participants and patients with diagnosed type-1 diabetes (T1D) or T2D. I postulated that diabetes in humans is associated with differences in circulating leukocytes, particularly monocytes and neutrophils, relative to normoglycaemic controls. Therefore, the aims of this study were to (1) establish any differences in relative abundances of disparate leukocytes in each patient group and (2) to determine if the observed alterations from pre-clinical models accurately reflect the circulating leukocyte profiles of diabetic patients, using a similarly designed flow cytometry antibody panel.

6.3 Methodology

6.3.1 Experimental design

For a detailed description of the experimental design, see Chapter 2, Section 2.3.4. Briefly, ethics approval was granted by the Alfred Hospital Research and Ethics Committee (HREC; approval number: 564/18). All elective patients referred by A/Prof Neale Cohen (Head of Clinical Diabetes, Baker Heart & Diabetes Institute) were invited on the day of their routine visit, to participate in the study. Participants who agreed to take part in the study were then given the opportunity to read and sign the informed consent document and provide informed consent if they were willing to participate, prior to blood collection. Subsequently, 14 mL of blood was collected by designated investigators with an approved phlebotomy accreditation (Mr. Charles Cohen, Ms. Erin Boyle, Mr. Michael Rechtman). Approximately 4 mL of blood was utilised for Full Blood Examination (FBE; Melbourne Pathology) to allow for flow cytometry data normalisation (similar to that performed in Chapter 3 & 4). A separate blood sample (~10mL) was also collected for flow cytometric analysis. Whole-blood flow cytometry was performed, whereby red blood cells were lysed (Chapter 2, Section 2.8), prior to antibody staining of pertinent leukocytes (Chapter 2, Table 2.1). Raw flow cytometry data was processed using Flow Jo (v10.5.3), normalised to total WBCs (derived from FBE values) and subsequently analysed and illustrated using GraphPad Prism (v8.1.2). A visual outline of the study methodology is also illustrated in Chapter 1, Figure 1.3.

6.3.2 Participant enrolment and statistical power

Previous studies performing flow cytometry of human blood have reported that sample sizes of ~30 participants per group were sufficient to detect statistically significant alterations of relevant cell types [438,439]. Although, these (and other) studies have used greater sample sizes to count leukocytes (>100 patients per group) [119,429,431], the majority of these studies employed automated cell counting which is less precise than flow cytometry [440]. Therefore, I based the statistical power calculation from studies using flow cytometry [438,439], to yield the appropriate sample size to detect any changes in circulating leukocytes. Based on an expected difference of approximately 20% (power 80%, $P = 0.05$) in leukocyte levels, the power calculation projected that 30 participants per group (i.e. 30 ND, T1D and T2D participants) would be sufficient to accurately detect any change using flow cytometry. Unfortunately, we were unable to reach the desired number of subjects per group to achieve sufficient statistical power in this study, due to the COVID-19

pandemic. As a result, recruitment was halted in 2020 and all existing data was unblinded and analysed. This in turn led to complete study cessation, due to the likelihood of sampling bias after data unblinding.

6.4 Results

6.4.1 Participant characteristics

Due to the premature discontinuation of this study, a total of only 31 participants (13 males and 18 females) were recruited for flow cytometric profiling of circulating leukocytes. Of these patients, 9 were non-diabetic (ND), 14 had established T1D and 7 were diagnosed with T2D (Table 6.1). We noted a significant age disparity between each patient group, with ND patients being younger than T1D patients, who in turn were younger than the T2D patients (Table 6.1, $P < 0.01$ for all comparisons). This confounder is a possible explanation for the lack of difference observed in the automated WBC count, given that ageing is generally associated with immunosenescence [441] (FBEs, Table 6.1). Glycated haemoglobin (HbA1c) levels in both T1D and T2D patients were significantly elevated relative to ND participants (Table 6.1, $P < 0.01$).

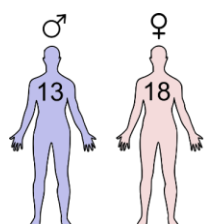
	Participant details	ND	T1D	T2D
	<i>n</i>	14	9	8
	Age	29 ± 6 ^{#†}	40 ± 14 ^{*†}	62 ± 5 ^{*#}
	Sex (M/F)	5/9	4/5	5/3
	HbA1c (%)	5.2 ± 0.5	7.3 ± 0.7 [*]	8.2 ± 2.1 [*]
	FBE (x 10 ⁹ /L)	7.0 ± 1.0	6.6 ± 1.6	8.1 ± 2.1

Table 6.1: Participant details from recruited patients, grouped by diagnosis. A total of 31 patients were included in this study. Data are shown as mean ± SD and was analysed statistically using a one-way ANOVA and a Tukey's *post hoc* test. * $P < 0.01$ vs. ND, # $P < 0.01$ vs. T1D, † $P < 0.01$ vs. T2D.

6.4.2 Circulating myeloid cells

Considering the previous evidence of systemic monocytosis and neutrophilia in T2D, myeloid cells were first gated and quantified (Figure 6.1A). Total leukocytes (CD45⁺ cells) detected by flow cytometry were not different between the patient groups (Figure 6.1B), consistent with the FBE count of total leukocytes (Table 6.1). While numbers of antigen-presenting cells (APCs; CD45⁺HLA-DR⁺), including monocytes and B-cells, were not different between ND and T2D patients, they were significantly reduced in patients with T2D relative to T1D participants (Figure 6.1B, $P < 0.05$). Additionally, while neutrophil (CD45⁺CD16⁺CD15⁺) numbers were similar between ND and T2D patients, they were significantly reduced in patients with T1D relative to ND participants (Figure 6.1B, $P < 0.05$). Classical monocytes (CD45⁺HLA-DR⁺CD14⁺) also followed a comparable trend to neutrophils, with no difference between ND and T1D participants, but a shift towards a decrease in cell numbers in T2D relative to T1D participants (Figure 6.1B, $P = 0.07$). There were no differences in intermediate (CD45⁺HLA-DR⁺CD14⁺CD16⁺) or non-classical

(CD45⁺HLA-DR⁺CD14⁺CD16⁺) monocytes between each patient group (Figure 6.1B). Hence, while our findings are not consistent with previous reports of monocytosis and neutrophilia in T2D, they imply that there was an overall reduction of APCs and neutrophils in T2D, relative to T1D patients.

6.4.3 Circulating lymphoid cells

The circulating lymphocyte profile was next characterised in each patient group using the illustrated gating strategies (Figure 6.2A). B-cells (CD45⁺HLA-DR⁺CD19⁺) were (non-significantly) reduced in T2D patients relative to T1D patients (Figure 6.2B, $P = 0.052$), which was likely a major contributor driving the overall reduction in APCs (Section 6.4.2, Figure 6.1B). The relative abundance of T-cells (CD45⁺CD3⁺) was not different between any of the patient groups (Figure 6.2B). Moreover, T-helper (Th; CD45⁺CD3⁺CD4⁺) and cytotoxic T-cells (Tc; CD45⁺CD3⁺CD8⁺) did not differ in any patient group (Figure 6.2B).

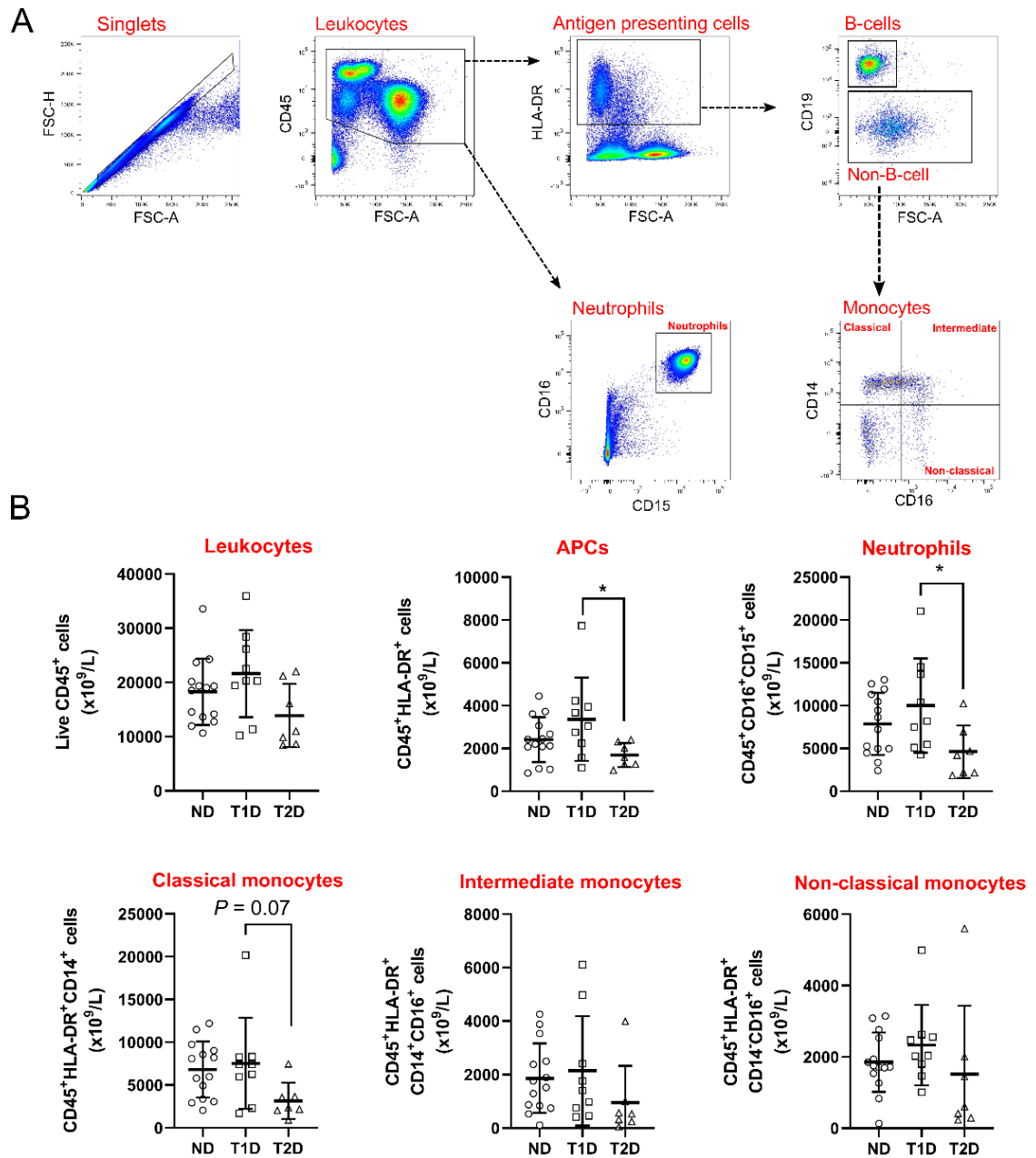


Figure 6.1: Immunophenotyping human circulating myeloid cells

(A) Illustrates the flow cytometric gating strategies employed to detect myeloid cells in human blood. (B) Quantified circulating myeloid leukocytes in each patient group. ND = non-diabetic, T1D = type-1 diabetes, T2D = type-2 diabetes, HLA-DR = HLA Class II Histocompatibility Antigen. Data is presented as mean \pm SD and individual data points. Statistical significance was determined using a one-way ANOVA and a Tukey's multiple comparison *post hoc* test. * $P < 0.05$.

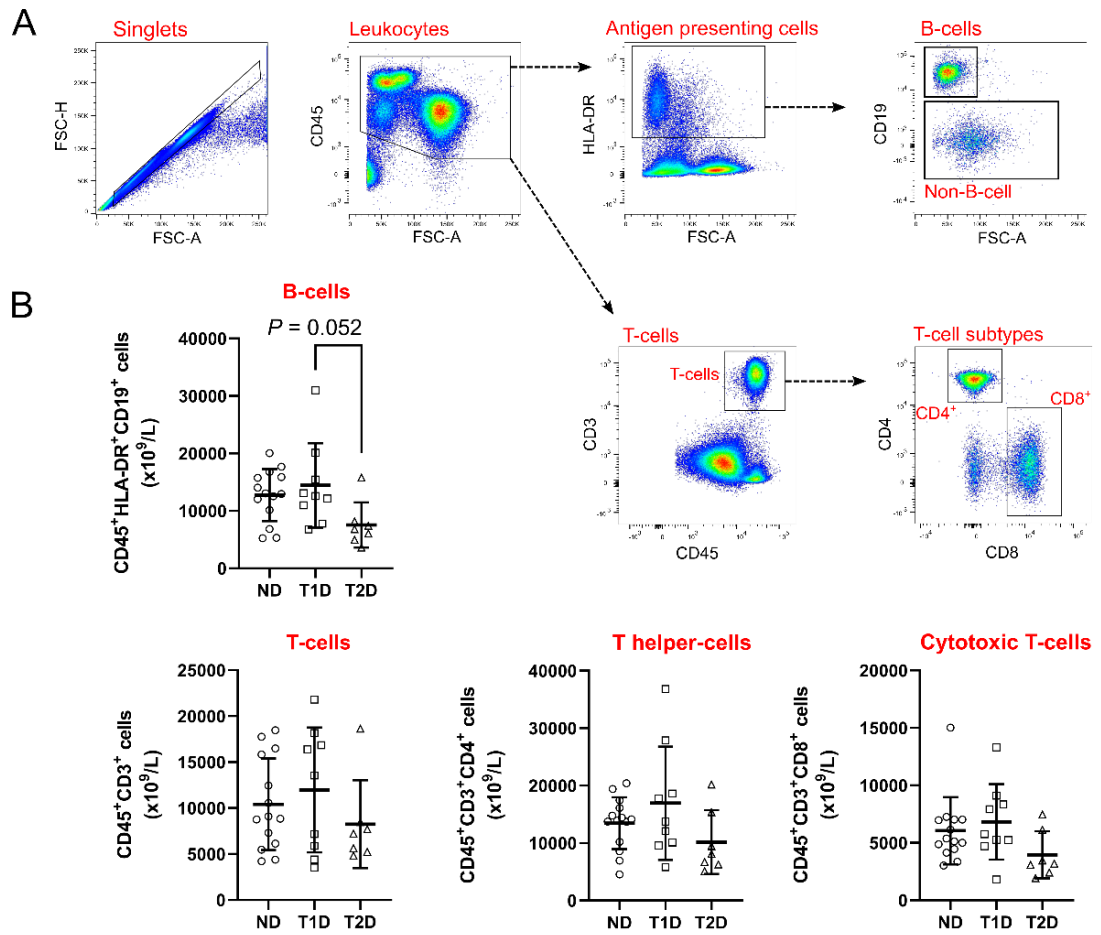


Figure 6.2: Immunophenotyping human circulating lymphoid cells

(A) Illustrates the flow cytometric gating strategies utilised to detect lymphocytes in human blood. (B) Quantified circulating lymphoid leukocytes in each patient group. ND = non-diabetic, T1D = type-1 diabetes, T2D = type-2 diabetes, HLA-DR = HLA Class II Histocompatibility Antigen. Data is presented as mean \pm SD and individual data points. Statistical significance was determined using a one-way ANOVA and a Tukey's multiple comparison *post hoc* test.

6.5 Discussion

Dysregulated immune cell function is implicated in the pathogenesis of diabetic complications, however the specific human leukocyte subtypes that contribute to these complications remain understudied. This study aimed to characterise the circulating leukocyte profiles of human ND and diabetic patients and to elucidate any consistencies congruent with pre-clinical models of T2D. While this study was underpowered for testing our hypotheses, a number of findings were noteworthy. Indeed, we observed a reduction in APCs and neutrophils in T2D patients relative to T1D participants, which contradicts much of the current literature. However, there were also very significant confounding factors in this study including the difference in age of each of the groups, which may have affected our results. Nevertheless, I provide a number of considerations for future studies to utilise when performing flow cytometric analysis of WBCs in diabetic patients.

6.5.1 Preliminary insights into the circulating leukocyte profile of diabetic patients

Despite the premature cessation of the study (Section 6.1), I noted reduced total APCs in T2D patients relative to T1D patients, which was likely driven by lower abundances of both antigen-presenting B-cells and monocytes. This was surprising given that insulin resistance and obesity (common comorbidities of T2D) are well known drivers of systemic inflammation, which is orchestrated by both the innate and adaptive arms of the immune system [136]. B-cells become more active in T2D relative to ND patients secreting various pro-inflammatory and chemotactic molecules, including IL-6, TNF- α and IgG [201]. Indeed, adoptive B-cell transfer in high-fat fed, B-cell-deficient mice exacerbates insulin resistance in visceral adipose tissue, while B-cell depletion improves insulin sensitivity [442]. However, T1D is also associated with augmented and dysfunctional B-cells [443], which are associated with pancreatic β -cell dysfunction [444,445]. Furthermore, comprehensive interrogation of B-cell subtypes in T1D patients revealed that the follicular B-cell subtype is decreased, while marginal zone B-cells are increased, highlighting the need for B-cell subtype analyses in clinical diabetes [446]. Considering I observed lower levels of B-cells in T2D patients relative to T1D patients, more specific analyses of B-cells is warranted in both types of diabetes to determine their role in the development of diabetic complications.

Antigen-presenting classical monocytes also appeared to be slightly reduced in T2D patients compared to T1D patients, which was surprising considering our pre-clinical findings [135]. As alluded to earlier in this dissertation, a distinct characteristic of T2D is monocytosis, accompanied by dysregulated monocyte function [115–119]. Indeed, CD14⁺ monocyte abundance and vascular adherence properties are impaired in poorly controlled diabetes (irrespective of diabetes ‘type’) [447], which is also associated with endoplasmic reticulum stress and dysregulated intercellular signalling [448]. Moreover, monocytes in obese individuals exhibit altered monocyte polarisation toward a non-classical phenotype, detected by increased CD16⁺ cell-surface expression [449]. Increased numbers of CD14⁺CD16⁺ monocytes have also been observed in hypercholesterolaemic patients with coronary artery disease [450,451], suggesting their potential involvement in cardiac

remodelling. However, in this thesis, I was unable to definitively determine any major differences in monocyte levels between participant groups. Nevertheless, phenotypically distinct monocyte subsets are becoming recognised protagonists mediating the pathogenesis of diabetic complications. While my results do not necessarily reflect the current literature, this may relate to confounders such as ageing-induced immunosenescence or patient medications (further discussed in Section 6.5.2), which provides important considerations for future studies of this nature.

Intriguingly, I also observed reduced circulating neutrophil levels in T2D patients, relative to T1D patients, which certainly contrasts pre-clinical evidence for neutrophilia in T2D [113,119]. Indeed, a number of studies in murine T2D suggest a role for systemic neutrophilia [5,273]. Moreover, an elevated neutrophil-lymphocyte ratio is a characteristic of clinical T2D, which is generally driven by elevated neutrophils [452]. Additionally, diabetes induces neutrophil activation and is associated with increased deposition of neutrophil extracellular traps (NETs) and rates of amputation [121]. However, reduced neutrophil levels in diabetes are also associated with increased peripheral neutrophil consumption and neutrophil tissue retention [453], which may, in part, explain the reduction in neutrophils in T2D patients relative to T1D participants. Interestingly, recent transcriptomic analysis of neutrophils isolated from T2D patients reveals distinct gene expression patterns corresponding to gene ontology (GO) terms related to myeloid leukocyte activation, inflammation and chemotaxis [454]. Considering the variance in circulating neutrophil numbers in clinical diabetes, more comprehensive studies are warranted to determine the precise role of neutrophils in diabetic complications. However, the discrepancy in the literature regarding neutrophil perturbations may result from a number of confounders, such as discoveries in differing stages of diabetes, different patient ethnicities and age-related immunosenescence.

6.5.2 Experimental limitations and considerations for future studies

While we observed differences in circulating leukocyte abundances in T2D patients relative to T1D participants, there were a number of limitations to consider. First, we noted a number of confounding variables related to sample size. Indeed, the small sample size and inadequate statistical power indicates that all findings in this study must be interpreted with caution (Section 6.3.2).

Upon unblinding of patient data, we observed considerable age disparities across patient groups, which is likely to have hampered data interpretation. Typically with larger sample sizes, key clinical characteristics such as age and sex are usually statistically corrected for [455], although this was redundant in this instance given the sample size. Importantly, ageing induces an array of systemic alterations affecting many components of the immune system, which is reflected by the increased incidence of bacterial and viral infections in the elderly [441,456]. Specifically, the efficacy of macrophage and neutrophil phagocytosis diminishes with age, which is also accompanied by delayed and dysfunctional intrinsic cytokine release [457,458]. Similarly, dendritic cells also exhibit reduced uptake of pathological antigens, as well as a reduction in cell-surface co-stimulatory

receptors necessary for T-cell recruitment [459,460]. The T-cell receptor repertoire is also reduced at least two-fold in the elderly [461], which may reduce the capability of T-cell recognition of antigens, particularly on APCs [441]. Given that patients with T2D are far older than the both the ND controls and T1D participants, it is likely that the observed changes align more with an ageing phenotype, rather than the T2D phenotype. Hence, this limitation is a critical confounder to consider and may, in part, explain some of the inconsistencies with the literature and my pre-clinical findings (Chapter 3 & 4).

Another possible explanation for these results relate to patients medications in the T2D cohort, given that T1D patients were only receiving daily exogenous insulin and ND participants were not receiving any regular medications. Patients with T2D however, were receiving a combination of treatments, including metformin, empagliflozin, pioglitazone and linagliptin. These medications are associated with dampening of inflammation in T2D [462–466], despite the mechanisms remaining unclear. For instance, T2D patients receiving empagliflozin exhibit reduced levels of circulating inflammatory markers including C-reactive protein (CRP) and myeloperoxidase (MPO) [465]. Similar findings have been reported in *db/db* mice receiving Western diet, whereby exogenous empagliflozin administration reduces gene expression of pro-inflammatory cytokines, and increases gene expression of anti-inflammatory cytokines in the heart [464]. However, regardless of any of these medications, the precise, cell-specific mechanisms by which these medications exert their anti-inflammatory effects remains understudied. With a larger sample size, multivariate analyses could be used to determine if different medications influence leukocyte counts; however in the present study, we cannot rule out the possibility that this variable contributed to data bias.

Pertaining to the flow cytometry methodology, a recent study using high-resolution mass cytometry has further optimised monocyte detection, proposing that improvements can be made to the current the antibody panel. While traditional bi-axial gating of CD14/CD16 monocytes is an accurate determinate of monocyte phenotypes, gating selection can be arbitrary and lead to inter-subset contamination of intermediate monocytes with classical and non-classical monocytes [467]. With the addition of markers such as CD36, CCR2, and CD11c, more precise separation of human monocytes can be performed [467], which should be taken into consideration in the future when designing antibody panels to analyse human monocytes.

This study provides a basis for future clinical studies, seeking to determine the differences in circulating leukocytes in human patients with diabetes. Indeed, there are a number of improvements that can be made to substantiate the validity of these findings. Importantly, the data from this study highlights the need for a larger sample size than initially anticipated from our initial power calculation. By utilising the data from this pilot study, we are better equipped to develop a more accurate power calculation to observe differences in disparate leukocytes, using this methodology. Using the same power calculation parameters used in this study (expected difference = 20%, power 80%, $P = 0.05$), we can revise the required values used to determine the sample size, using the

means and standard deviation (SD) from this study. For example, using the means and SDs of ND and T1D CD45⁺ leukocytes from this study (18256 ± 6118 vs. 21629 ± 8036 respectively), the updated power calculation suggests cohort sizes of at least 52 participants per group. This approach can also be extended further to consider more specific leukocytes, dependent on the primary endpoint question. Despite the confounders in this study, I provide useful information to improve the study design of any future work using this methodology.

6.6 Conclusions

In this Chapter, we endeavoured to profile the circulating leukocyte populations in patients with diabetes to corroborate findings from the current literature, and to establish any consistencies with pre-clinical findings. On the contrary, we noted reduced APCs and neutrophils in T2D patients relative to non-diabetic controls, accompanied by minor decreases in B-cells and classical monocytes. Indeed, there were a number of noteworthy limitations, primarily relating to sample size, age disparities and patient medications. Therefore, the findings from this study must be interpreted with caution due to the presence of a number of confounding variables primarily related to premature study cessation. Although unable to complete this study under optimal requirements, I provide a number of feasible considerations for future clinical studies of this nature to build upon.

Chapter 7

General Discussion

7.1 Overview

The diabetic heart has been studied for over 50 years [468,469], which has led to significant advancements in our understanding of this pathology. However, there remains a clear knowledge gap regarding the precise molecular and cellular dynamics in diabetes-induced heart failure (HF), which is reflected by the lack of specific treatment options. Type-2 diabetes (T2D) is strongly associated with impaired cardiac function and worsened CV outcomes [468–470], which is associated with cardiac fibrosis, cardiomyocyte dysfunction, ROS generation and inflammation [262]. These conventional characteristics of HF in diabetes are established, although the precise cellular and molecular pathophysiology remains unresolved. The cardiac cellular composition has recently been reappraised in homeostasis and disease, which has been facilitated by utility of single-cell technologies [174,225]. However, prior to the body of work in this thesis, these analyses were yet to be applied to the heart in the setting of diabetes-induced HF.

The primary objectives of this dissertation were to investigate the changes in cardiac cellular composition in murine T2D-induced HF and to determine the cell-specific, transcriptomic signatures that may contribute to these changes. In two disparate models of T2D (Chapter 3 and 4), I demonstrate both common and distinct cardiac non-myocyte cellular changes for diabetes-induced remodelling (Figure 7.1). Moreover, we identify both cell-specific and broad gene expression patterns in non-myocyte cells from *db/db* and *db/h* mice from single-cell transcriptomics. These results also corroborate the aforementioned flow cytometry results, implicating cardiac fibroblast expansion and macrophage dysfunction in the development of HF. While the human pilot study data (Chapter 6) does not corroborate the flow cytometric pre-clinical findings (Chapter 3 and 4), these are confounded by a number of variables and should be interpreted with caution. Therefore, I implicate a role for systemic monocytosis and neutrophilia in the development of T2D complications, including HF. *In toto*, these findings provide a foundation for future studies to build on and may aid in identification of novel cellular and/or molecular targets for pharmacological manipulation.

7.2 Degrees of cardiac dysfunction in T2D-induced HF

Whilst both mouse models of T2D used in this thesis do not completely recapitulate clinical T2D, both the streptozotocin high-fat diet (STZ-HFD) and 17-week old *db/db* mouse models exhibited similar cardiac functional impairments. While the parameters measured by echocardiography were different between models, cardiac function is similarly hindered in both models of T2D. STZ-HFD mice displayed left-ventricular (LV) diastolic dysfunction in the form of reduced mitral valve velocity and blood flow in the early phase of diastole (Chapter 3, Section 3.3). Similarly, 17-week old *db/db* mice display comparable diastolic dysfunction, with reduced early mitral annulus velocity

and a consequent increase in the E/e' ratio (Chapter 4, Section 4.4.2). Indeed, both 17-week old *db/db* and STZ-HFD mice exhibit echocardiographic parameters suggestive of increased LV resistance and stiffening [471,472]. However, 10 and 24-week old *db/db* mice did not display any major functional abnormalities of note.

7.3 Cardiac non-myocyte cellular alterations that characterise the diabetic heart

A comprehensive understanding of the cardiac cellular landscape is crucial for studying cardiac biology and pathophysiology, however this has yet to be comprehensively surveyed in the diabetic heart. Cardiac non-myocytes are a highly plastic, heterogeneous collection of cells that are essential for maintenance of homeostasis and myocyte function in the mammalian heart [174,225,473]. As discussed in Chapter 1 (Section 1.4) detection of cardiac non-myocyte cells has been streamlined by optimisation of cardiac digestion, flow cytometric and histological protocols [473]. In this thesis, I have demonstrated that basal cardiac cellular composition is altered in two established models of murine T2D with concomitant HF.

7.3.1 Fibroblast expansion in STZ-HFD and 17-week old *db/db* mice

Consistent with the comparable degree of cardiac dysfunction, a prominent feature of diabetes-induced remodelling uncovered by my work is fibroblast hyperplasia. Both STZ-HFD mice and 17-week old *db/db* mice exhibit increased fibroblast levels in the myocardium (Figure 7.1), suggesting that augmented fibroblast levels are positively correlated with cardiac dysfunction in T2D. However, the specific expanding fibroblast phenotype is yet to be elucidated in this context. For example, in the infarcted heart, fibroblasts rapidly differentiate and proliferate into myofibroblasts, facilitating replacement fibrosis [76,245,474]. In contrast, mice with hypertensive HF initiated by chronic angiotensin-II infusion exhibit fibroblast expansion, but do not constitute a classical myofibroblast phenotype [234]. In this thesis, I noted cardiac fibroblast hyperplasia, accompanied by augmented fibroblast-specific MAPK signalling and endocytosis in the absence of myofibroblast development (Figure 7.1 & 7.2B).

Indeed, fibroblast levels were elevated in STZ-HFD and *db/db*-induced HF, although analysis of cardiac fibroblasts from single-cell RNA sequencing (scRNAseq) suggests little evidence for ECM remodelling and cardiac fibrosis (Chapter 5). Here, I implicate a number of diabetes-specific gene expression patterns in cardiac fibroblasts that may explain their expansion. In particular, fibroblasts increase mitogen-activated protein kinase (MAPK) pathway signalling. Given that *Egfr* is significantly elevated in *db/db* fibroblasts exclusively, activation of MAPK likely occurs via the *Egfr*-encoding cell surface protein epidermal growth factor receptor (EGFR). While this is well-described in the diabetic heart as a whole [366,475], this is the first report of fibroblast-specific MAPK activation, during simultaneous examination of all non-myocyte cells in the diabetic heart. EGFR intrinsically activates guanosine triphosphate (GTP) molecules, such as the Ras proto-oncogene, inducing intracellular ERK1/2 signalling, which ultimately initiates cell growth and proliferation [361,362]. Corroborating this, gene expression patterns in 17-week old *db/db* mice

correspond to small GTPase signal transduction – a downstream process in the MAPK cascade [362]. Moreover, up-regulated genes in 17-week old *db/db* mice encode for receptors in fibroblasts are associated with augmented MAPK signalling.

Down-regulated genes in 17-week old *db/db* hearts were associated with response to external stimuli and endocytosis GO terms, which may suggest an intrinsic compensatory response to external stress. Numerous extrinsic factors can initiate activation of the MAPK cascade, including glucose, lipids and cholesterol [362]. As discussed (Chapter 5), hyperglycaemia is sufficient to activate MAPK signalling, which primarily initiates p38 and ERK1/2 intracellular pathways [78,364,366]. The same has been demonstrated in kidney biopsies from T2D patients, suggesting that increased MAPK-p38 signalling is a primary feature contributing to renal fibrosis [476]. Supporting this, MAPK activation in *db/db* mouse kidneys is associated with increased phosphorylation of p38 and consequent downstream ERK signalling [476,477]. However, the highest differentially expressed gene within fibroblasts is angiopoietin-like protein 4 (*Angptl4*), which may suggest that fibroblasts attempt to compensate for excess circulating lipids (Figure 7.2I), by up-regulating nutrient partitioning protein ANGPTL4. This protein is generally responsible for directing free-fatty acids to alternative sites for metabolism, which may indirectly suggest cardiac fibroblast lipotoxicity. Furthermore, genes downregulated for ligands and receptors in fibroblasts correspond to regulation of endocytosis, which eludes to a fibroblast-specific compensatory mechanism to reduce intrinsic lipids. While there are many reports of hyperglycaemia-induced fibroblast activation in diabetic complications, single-cell analyses have provided more detailed information regarding the cellular dynamics in T2D-induced HF. Therefore, I propose that the range of circulating factors established in the *db/db* mouse (Figure 7.2A) initiate pathological fibroblast hyperplasia via MAPK cascade signalling and fibroblast lipotoxicity. While diabetes ultimately leads to cardiac fibrosis [20,77,478], further research is required to confirm the mechanism of action dictating elevated fibroblast levels in the diabetic heart, considering the multifactorial nature of T2D comorbidities.

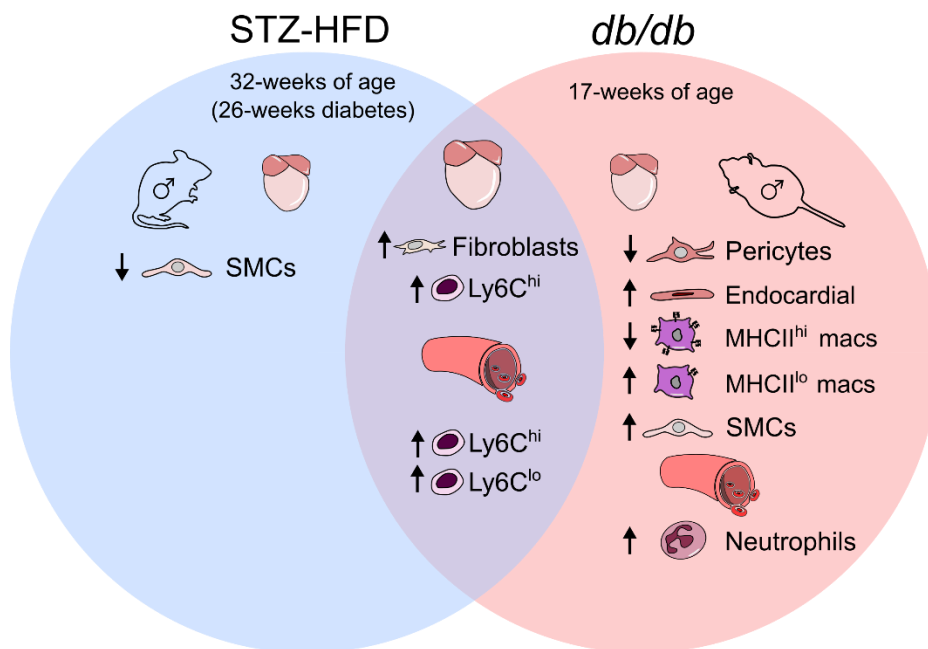


Figure 7.1: Similarities and differences in cardiac cellularity in two mouse models of T2D

(A) Illustrates the cardiac cellular alterations yielded from flow cytometry in the STZ-HFD and (B) in the *db/db* mouse model of T2D. Common cellular alterations include increased fibroblast levels, and inflammatory monocytes (both in the heart and blood). Distinct alterations are indicated A & B respectively. STZ-HFD = blue circle, *db/db* = pink circle.

7.3.2 Cardiac vascular alterations

There were a number of cellular alterations corresponding to vascular abnormalities, which was initially identified by aberrant gene expression in *db/db* endothelial cells (ECs; Chapter 5). Although EC proportions were unaltered in both murine models of T2D (Chapter 3 & 4), scRNAseq revealed gene expression patterns corresponding to increased extrinsic stress, chemotaxis and dysregulated angiogenesis (Figure 7.2C, D, E). EC dysfunction is a widely reported paradigm in diabetes and is an important characteristic of its associated pathologies [262]. Indeed, gene expression of peroxisome proliferator-activated receptor gamma (PPAR γ) is distinctly upregulated in ECs. As mentioned (Chapter 5), PPAR γ preferentially facilitates glucose flux into cells, rather than lipids. Given that free-fatty acids are the primary source of cardiac energy [374], increased expression of PPAR γ may suggest an EC-specific compensatory response to extrinsic lipid stress, in a similar fashion to fibroblasts (Figure 7.2I). Genes encoding ligands and receptors in ECs also correspond to augmented chemotaxis, suggesting cell migration into the myocardium is, in part, catalysed by altered EC gene expression. A number of chemotactic genes contributed to this, including *Cxcl12* and *Cd31* (further discussed in Chapter 5). Moreover, macrophages highly express *Ccr2*, which is likely further driving cellular chemotaxis and migration, particularly of monocytes (elucidated in Section 7.3.3). In addition, genes encoding both ligands and receptors also suggest a role for dysregulated angiogenesis and cardiac vascular remodelling. As discussed, is appreciated that diabetes induces disproportionate angiogenesis in the heart (and other organs) to compensate for external stress, vessel occlusion and hypoxia (refer to Chapter 5). This is generally initiated by

initial capillary rarefaction and consequent hypoxia, which in turn stimulates enhanced, disproportionate angiogenesis [406,408,409]. Using information generated from scRNAseq of *db/db* ECs relative to *db/h* controls, I note a number of EC-specific abnormalities that are likely to contribute to the development and progression of diabetes-induced HF.

Endocardial cells increased in number exclusively in 10-week old *db/db* hearts (Figure 7.1) and displayed similar transcriptomic patterns to cardiac ECs for cell migration in 17-week old *db/db* mice, relative to *db/h* controls (Figure 7.2F). Endocardial cells are highly dynamic and respond to a variety of stressors [288]. In diabetes however, the literature regarding endocardial cell dynamics is limited, providing a novel avenue for future studies. Hyperlipidaemic diabetic hamsters exhibit alterations in endocardial morphology and permeability, accompanied by accumulation of macrophage-derived foam cells within the sub-endocardial layer [289]. Macrophage-derived foam cell accumulation is synonymous with the development to atherosclerosis [135], which emphasises the significance of macrophage lipid metabolism in the development of HF in T2D. *In silico* analyses of 17-week old *db/db* endocardial cells further corroborates this, suggesting that gene expression patterns are linked with cell migration (Figure 7.2F). Furthermore, the endocardial gene signature in *db/db* mice is also associated with augmented Wnt-related integration site (WNT) signalling (Figure 7.2F). WNTs are a family of glycoprotein ligands regulating numerous processes, including cellular adhesion, migration and differentiation [479]. Specifically, the canonical WNT pathway plays a critical role in fibroblast differentiation in the heart [480]. This may point to an alternative mechanism driving fibroblast hyperplasia (Section 7.3.1), whereby endocardial cells increase WNT ligand communication with fibroblasts, initiating endocardial-fibroblast transdifferentiation. However, more comprehensive analyses, such as endothelial-specific ‘Cre-lox’ lineage tracing studies [287,481], are required to definitively determine this. Thus, data from this thesis implicates endocardial cell dysfunction in the development of T2D-induced HF and requires further interrogation.

Alterations in lymphatic endothelial cell (LEC) number and gene expression were also noted in 10 and 17-week old *db/db* hearts respectively, alluding to lymphatic dysfunction. Numerous clinical studies have demonstrated that obesity poses a significant risk of lymphatic dysfunction [482–484]. Moreover, a recent study has shown that both humans and mice consuming high-fat diet display aberrant mesenteric lymphangiogenesis and lymphatic ‘leakiness’ [482]. Mouse models of diabetes also show perturbed lymphatic permeability and function in the retina and in peripheral vessels [284,285,485], further implicating this paradigm in as a characteristic of T2D. In this thesis, proportions of LECs were increased in 10-week old *db/db* mice, although were unaltered in 17-week old *db/db* mice relative to *db/h* controls. There were no apparent alterations in LEC proportions in the STZ-HFD model of diabetes. This may suggest that LECs may initially undergo cell death and lymphatic dysfunction, however subsequently initiate an intrinsic pro-survival response to compensate. Indeed, elevated expression of pro-survival transcription factor *Prox1* was

observed in 17-week old *db/db* mice, which may suggest lymphangiogenesis is occurring in response to the initial reduction in LECs at 10-weeks of murine T2D. Moreover, 17-week old *db/db* mice yield gene expression patterns in cardiac LECs corresponding to negative chemotaxis (Figure 7.2E), which may suggest that LECs also initiate a compensatory response to lymphoedema. These data may indicate that LECs are initially reduced due to extrinsic stressors, which is followed by an intrinsic compensatory mechanism to counteract these factors that characterise murine T2D (Figure 7.2A). While more specific analyses of cardiac LEC dynamics are warranted, cardiac lymphatic dysfunction may act as a potential driver of cardiac functional impairment in T2D.

Similarly, myocardial pericytes were reduced in both 10 and 17-week old *db/db* mice relative to *db/h* littermates (Figure 7.1). Pericytes are perivascular cells juxtaposed to endothelial and smooth muscle cells and are critical for maintaining vascular integrity in homeostasis and disease [486]. Loss of pericytes has been extensively studied in diabetes-induced microvascular complications, including retinopathy, nephropathy and peripheral artery disease [297,304,487]. Pericyte loss in diabetic retinopathy also leads to vascular destabilisation and subsequent capillary rarefaction [296]. This is one of the first signs of diabetic retinopathy and is considered to represent early microvascular remodelling in T2D [297]. This, in part, could explain the initiation of possible capillary rarefaction in the heart, ultimately triggering disproportionate angiogenesis. While further analyses of pericytes are required, I propose pericyte loss is an additional abnormality contributing to cardiac vascular dysfunction in murine T2D.

Cardiac smooth muscle cells (SMCs) were also altered in both models of T2D (Figure 7.1). While STZ-HFD mice (Chapter 3) exhibited decreased levels of smooth muscle cells (SMCs), 17-week old *db/db* mice displayed increased SMC levels (Chapter 4). The pathogenesis of vasculopathy in T2D is complex, and the mechanism by which this occurs is unclear. As discussed (Chapter 3 & 4), hyperglycaemia tends to inhibit SMC apoptosis, whereas models of metabolic syndrome (including T2D) stimulate SMC apoptosis (Chapter 3 and 4). For example, hyperglycaemia inhibits apoptosis in cultured human and rat vascular SMCs (vSMCs), via PKC and B-cell lymphoma 2 (Bcl-2) signalling [305,306]. In contrast, rodent models of atherosclerosis augment vSMC apoptosis, proliferation and leukocyte chemotaxis [307,308]. Due to the opposing results in the disparate mouse models used, it is difficult to interpret the SMC dynamics from data in this thesis. However, it is expected that SMCs in STZ-HFD mice undergo apoptosis as a result of chronic consumption of HFD, considering that hyperlipidaemia is associated with vSMC apoptosis [488]. Comparatively, the increase in SMCs in 17-week old *db/db* mice is likely attributable to chronic hyperglycaemia, particularly given that *db/db* mice consumed only regular chow diet. Because T2D is associated with a heterogeneous array of comorbidities, the cardiac SMC phenotype may vary depending on the respective contribution of each pathological comorbidity. While the disparate mouse models of T2D exhibit contrasting differences in SMCs, these findings further underscore a role for vascular remodelling in the diabetic heart.

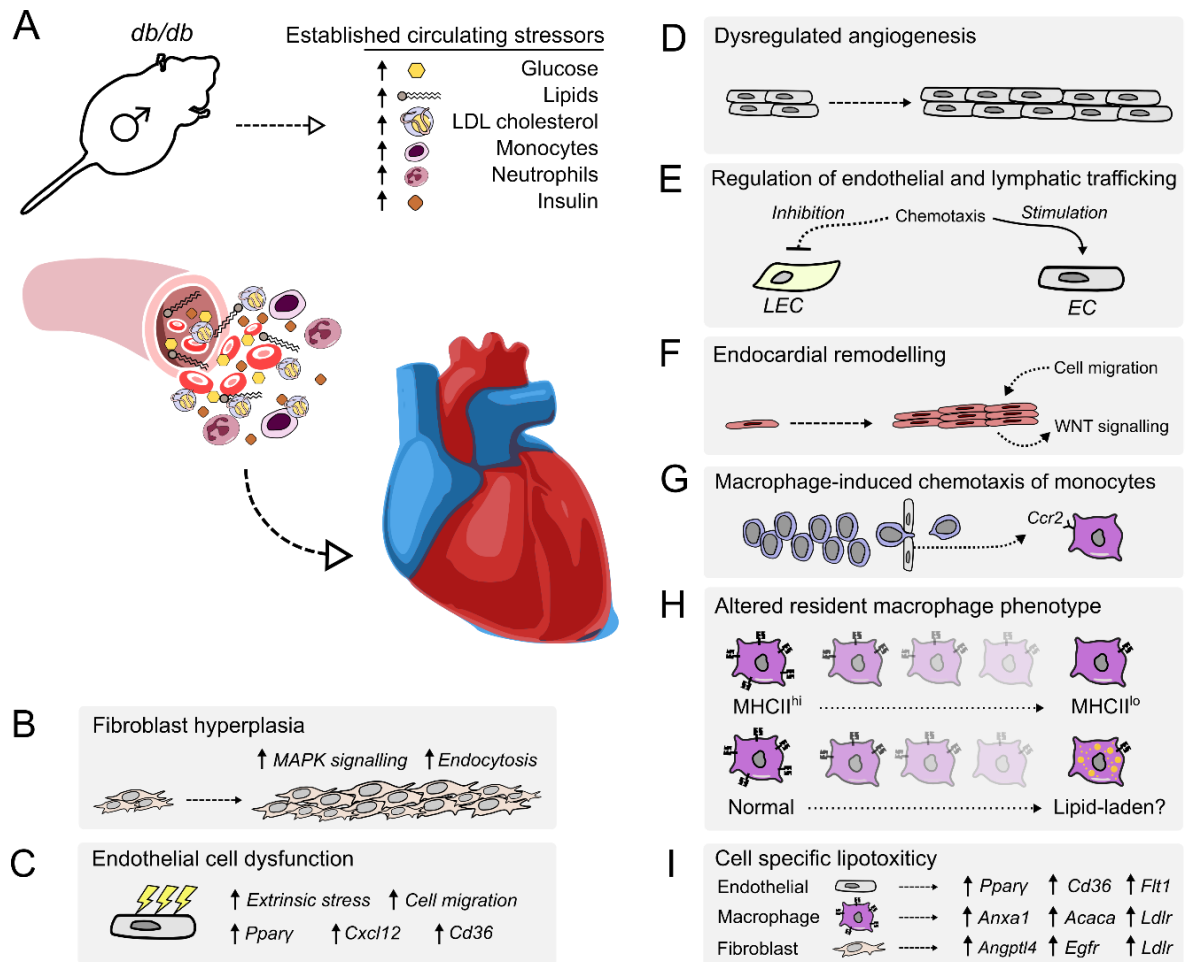


Figure 7.2: Defining the major non-myocyte abnormalities that comprise the *db/db* heart

(A) Illustrates the array of major extrinsic stressors in *db/db* mice that may contribute to cardiac remodelling. Important features of the non-myocyte milieu within the diabetic heart involve (B) fibroblast hyperplasia, (C) endothelial cell dysfunction, (D) disproportionate pathological angiogenesis, (E) perturbed endothelial and lymphatic chemotaxis, (F) endocardial remodelling, (G) macrophage-induced monocyte chemotaxis, (H) alterations in cardiac resident macrophages and (I) cell-specific lipotoxicity.

7.3.3 The contribution of the immune system

Accompanying cardiac vascular alterations, this thesis also reveals important contributions of leukocytes in the development of HF in the context of murine T2D. While inflammation is a recognised feature of metabolic syndrome and T2D [115–119], less is known regarding the contribution of specific leukocytes in the pathogenesis of HF in this context. Both murine models used commonly exhibited systemic monocytosis (Figure 7.1), highlighting the importance of circulating monocytes in the pathogenesis of T2D-induced HF. In addition, neutrophilia was distinct to 17-week old *db/db* mice (Chapter 4), although STZ-HFD mice displayed a minor trend toward increased neutrophil levels (Chapter 3). Interestingly, there were no detectable alterations in circulating lymphocyte numbers, despite these being implicated in a number of complications associated with T2D [213,216,442].

Circulating and local cardiac monocytes were elevated in both models of T2D-induced HF, suggesting that monocytes are likely infiltrating into the myocardium, from the circulation (Figure 7.1). Cardiac monocyte recruitment in diabetes is facilitated by upregulated chemokine expression, particularly monocyte chemoattractant protein 1 (MCP-1; the canonical ligand for CCR2) [489]. Augmented expression of MCP-1 in cardiac macrophages is implicated in circulating monocyte recruitment in both ischaemic cardiomyopathy and myocardial infarction [76,245,474]. Moreover, elevated plasma MCP-1 levels are correlated with an increased risk of developing vascular inflammation and coronary artery disease [490,491]. While no study to date has reported alterations in MCP-1 signalling in the diabetic heart, knockout of its canonical receptor CCR2 improves cardiac dysfunction and degree of fibrosis [492], suggesting a role for MCP-1/CCR2 signalling. The mammalian myocardium is enriched in resident macrophages within the interstitium [164], which are primarily responsible for inter-organ debris clearance and chemotaxis of monocytes [135]. Interestingly, macrophages from 17-week old *db/db* mice exhibited significantly increased expression of *Ccr2* (encoding CCR2), suggesting that cardiac macrophage-mediated monocyte recruitment is a feature of the diabetic heart (Figure 7.2G).

Indeed, resident cardiac macrophages in 17-week old *db/db* mice display an alternate phenotype relative to *db/h* control mice. This was initially identified by flow cytometry, whereby major histocompatibility complex II (MHCII) density on local cardiac macrophages was altered in 17-week old *db/db* mice (Figure 7.1). This was also corroborated by scRNAseq analyses, whereby the MHCII^{hi} ‘Macrophage 3’ subset reduced in number in the *db/db* myocardium. More detailed *in silico* analyses suggests that Macrophage 3 gene expression patterns lack the capability to perform reverse cholesterol efflux, which is particularly important in the context of murine T2D (Figure 7.2A). This may imply that a subtype of cardiac macrophages are susceptible to hypercholesterolaemia in T2D, which in turn instigates local macrophage cell death. Moreover, *db/db* cardiac macrophages also increase gene signatures associated with lipotoxicity, suggesting extrinsic lipid stress is an additional contributor to macrophage loss (Figure 7.2I). These findings,

are analogous to the development of atherosclerosis and coronary artery disease [403], whereby excess cholesterol and lipid influx results in the formation of lipid-laden foam cells [135]. In diabetes, less is known regarding macrophage dynamics in the heart, however multiple reports suggest reductions in reverse cholesterol transporters in macrophages isolated from other organs (Chapter 5). Thus, from the data presented in this thesis, I postulate that cardiac macrophages play a cardioprotective role by engulfing excess vascular debris in the heart as a result of T2D. Chronically, this is likely to overwhelm the phagocytic capacity of cardiac macrophages, which may induce enhanced macrophage-mediated monocyte chemotaxis into the myocardium.

Considering the pronounced inflammation encompassing murine T2D, I also attempted to extend this to the human context by performing whole blood flow cytometry in patients with diabetes relative to normoglycaemic controls (Chapter 6). Contrary to the majority of the literature, I noted marginally reduced B-cells, neutrophils and monocytes in patients with T2D, relative to non-diabetic participants. However, as discussed this clinical study was interrupted due to the COVID-19 pandemic restrictions, preventing any further recruitment. This consequently led to premature study cessation, resulting in low sample sizes and other related confounders, given that the data was blinded to the investigators. Thus, the data from this Chapter should be interpreted as pilot data only, for future work to investigate.

7.4 Future directions

This thesis provides a number of novel concepts pertaining to HF in the context of murine T2D, providing a comprehensive framework for future studies to build upon. Indeed, these studies ought to be extended to females to decipher any apparent sexual dimorphisms that may exist in the pathogenesis of HF in T2D. As discussed throughout this dissertation, future work should also consider cardiomyocytes in this context, given that they are the primary functional cell in the heart. Moreover, given the complexity of HF in T2D, more rigorous genomic approaches are also warranted to characterise the cellular dynamics and gene regulatory elements that govern the observed differences in cellularity and gene expression in cardiac non-myocytes.

Importantly, there is little evidence to date that has utilised the vast array of genetic tools currently available for studying mouse genetics and biology, in the context of the diabetic heart. For instance, utility of cre-*loxP* recombination is widespread in mouse biology, allowing for precise, cell-specific information regarding gene expression [493]. This technology has also been adapted for diverse range of other genetic functions, including fate-mapping of developmental ontogeny of differentiating cell types [494], making it a desirable validation tool. Indeed, utility of fluorescently labelled, fibroblast-specific mouse lines (such as the *Colla1*-GFP strain [495]) would be particularly useful in the context of T2D-induced HF, to determine the temporal dynamics of cardiac fibroblasts in T2D. However, in the diabetic heart, these experiments are limited and have been restricted to cardiomyocytes rather than the entire cardiac cellular milieu. In attempt to recapitulate cardiomyocyte characteristics in the context of T2D, cardiomyocyte-specific knockdown of glucose

transporter type 4 (GLUT4) impairs myocyte contractility as a result of unbalanced substrate utilisation [496,497]. More sophisticated analyses have been performed in murine diabetic retinopathy, whereby conditional knock-out of vascular endothelial growth factor (VEGF) within retinal Müller cells improves vascular permeability, suggesting a cell-specific, pathogenic role for VEGF in the retina [498]. Nevertheless, there remains an urgent demand for more robust cell-specific analyses of the diabetic heart, particularly to complement findings including those presented in this thesis. Incorporation of these techniques in parallel with approaches such as scRNAseq and flow cytometry will provide more detailed information regarding cell history, transcriptional elements and transition state – heralding an exciting avenue for future research.

The methodologies applied in this thesis should also be extended to additional models of T2D, considering the variable and multifaceted nature of this disease. While, in this thesis, I used a combination of STZ and HFD to induce murine T2D, it would be particularly pertinent to catalogue the cardiac cellular milieu of mice receiving high-fat diet alone, as well as mice receiving streptozotocin alone. Given that *db/db* mice consume standard chow diet, it would also be prudent to consider alternative diets capable of inducing T2D, such as the ‘Western diet’, which is typically high in fat, sucrose and cholesterol [499].

In the era of single cell technologies, it is also pertinent to consider other high-resolution techniques to further explain the differences in cardiac cellularity and transcriptome. Considering the involvement of lipids and cholesterol in murine T2D, utility of plasma and tissue lipidomics may yield important insights into the lipid profiles of T2D mice and how they affect cardiac function. Similarly, proteomic analyses cardiac tissue would be beneficial to determine whether the observed gene expression patterns are congruent with protein expression and whether proteins are affected by post-translational modifications in this context.

Finally, it would be of particular interest to observe the effects of novel pharmaceutical agents that have reported improved clinical cardiovascular outcomes. These primarily include glucagon-like peptide-1 (GLP-1) agonists and sodium glucose transport 2 (SGLT2) inhibitors, whereby both of these agents reduce the outcomes of major cardiovascular events and hospitalisation for HF [500,501]. While these agents are showing immense promise in clinical HF associated with T2D, the precise mechanism by which they exert their cardioprotective effects remains unclear. As such, utility of sensitive analyses such as single-cell transcriptomics may provide valuable insights into the complex biological responses to these novel agents.

7.5 Conclusions

Taken together, this thesis offers a new perspective for understanding the cellular and molecular mediators of diabetes-induced cardiac pathology. Using high-dimensional flow cytometry, I found that both models of T2D display marked differences in cardiac cellularity compared to their non-diabetic controls. Specifically, shared hallmarks include increased resident mesenchymal cells,

fibroblasts and infiltrating monocytes in both models of T2D. I also show disparate alterations in cardiac cellularity between the different models of T2D. Importantly however, these alterations point to common themes regulating the diabetes-induced cardiac pathophysiology: including vascular remodelling, fibroblast hyperplasia and immune cell dysfunction. Single-cell transcriptomic analysis of *db/db* mouse hearts revealed a concerted diabetes-induced cellular response driving cardiac pathological remodelling, congruent with the cellular findings. I identified a diabetes-induced up-regulation of pathways contributing to established features of diabetic cardiomyopathy such as dysregulation of vascular homeostasis and lipid metabolism, as well as augmented inflammation, in cell specific contexts. We also identified novel characteristics in the diabetic heart, including perturbed angiogenesis and cellular trafficking within lymphatic vessels. In conclusion, this thesis provides a comprehensive framework for understanding the cellular and molecular aberrances that dictate the pathophysiology of the heart in the context of T2D. Future studies should aim to extend this framework in order to offer new therapeutic avenues to mitigate the cardiovascular complications associated with T2D.

Chapter 8

References

1. Jia G, DeMarco VG, Sowers JR. Insulin resistance and hyperinsulinaemia in diabetic cardiomyopathy. *Nature Reviews Endocrinology*. 2016;12:144–53.
2. Khan JN, Wilmot EG, Leggate M, Singh A, Yates T, Nimmo M, et al. Subclinical diastolic dysfunction in young adults with Type 2 diabetes mellitus: A multiparametric contrast-enhanced cardiovascular magnetic resonance pilot study assessing potential mechanisms. *European Heart Journal Cardiovascular Imaging*. 2014;15:1263–9.
3. Gerstein HC, Werstuck GH. Dysglycaemia, vasculopenia, and the chronic consequences of diabetes. *Lancet Diabetes Endocrinology*. 2013.
4. Yoon K-H, Lee J-H, Kim J-W, Cho JH, Choi Y-H, Ko S-H, et al. Epidemic obesity and type 2 diabetes in Asia. *The Lancet*. 2006;368:1681–8.
5. Cohen CD, de Blasio MJ, Lee MKS, Farrugia GE, Prakoso D, Krstevski C, et al. Diastolic dysfunction in a pre-clinical model of diabetes is associated with changes in the cardiac non-myocyte cellular composition. *Cardiovascular Diabetology*. 2021;20:116.
6. Cho NH, Shaw JE, Karuranga S, Huang Y, da Rocha Fernandes JD, Ohlrogge AW, et al. IDF Diabetes Atlas: Global estimates of diabetes prevalence for 2017 and projections for 2045. *Diabetes Research and Clinical Practice*. 2018;138:271–81.
7. Fernandes J da R, Ogurtsova K, Linnenkamp U, Guariguata L, Seuring T, Zhang P, et al. IDF Diabetes Atlas estimates of 2014 global health expenditures on diabetes. *Diabetes Research and Clinical Practice*. 2016;117:48–54.
8. Nolan CJ, Damm P, Prentki M. Type 2 diabetes across generations: from pathophysiology to prevention and management. *The Lancet*. 2011;378:169–81.
9. Roglic G, Norris SL. Medicines for Treatment Intensification in Type 2 Diabetes and Type of Insulin in Type 1 and Type 2 Diabetes in Low-Resource Settings : Synopsis of the World Health Organization Guidelines on Second- and Third-Line Medicines and Type of Insulin for the Control of Blood Glucose Levels in Nonpregnant Adults With Diabetes Mellitus. *Annals of Internal Medicine*. 2018;169:394–7.
10. Roth GA, Johnson C, Abajobir A, Abd-Allah F, Abera SF, Abyu G, et al. Global, Regional, and National Burden of Cardiovascular Diseases for 10 Causes, 1990 to 2015. *Journal of the American College of Cardiology*. 2017;70:1–25.
11. Remme WJ, Swedberg K. Guidelines for the diagnosis and treatment of chronic heart failure. *European Heart Journal*. 2001;22:1527–60.
12. McMurray JJV, Gerstein HC, Holman RR, Pfeffer MA. Heart failure: A cardiovascular outcome in diabetes that can no longer be ignored. *The Lancet Diabetes and Endocrinology*. 2014;2:843–51.
13. Pogossova N. Costs associated with cardiovascular disease create a significant burden for society and they seem to be globally underestimated. *European Journal of Preventive Cardiology*. 2019;26:1147–9.

14. Squire I, Cardoso JS, Merkely B, Martinez F, Starling RC, Desai AS, et al. Risk Related to Pre-Diabetes Mellitus and Diabetes Mellitus in Heart Failure With Reduced Ejection Fraction Insights From Prospective Comparison of ARNI With ACEI to Determine. *Circulation Heart Failure*. 2016;1:1–12.
15. Tauschmann M, Thabit H, Bally L, Allen JM, Hartnell S, Wilinska ME, et al. Closed-loop insulin delivery in suboptimally controlled type 1 diabetes: a multicentre, 12-week randomised trial. *The Lancet*. 2018;392:1321–9.
16. Nimri R, Muller I, Atlas E, Miller S, Fogel A, Bratina N, et al. MD-logic overnight control for 6 weeks of home use in patients with type 1 diabetes: Randomized crossover trial. *Diabetes Care*. 2014;37:3025–32.
17. Weisman A, Bai JW, Cardinez M, Kramer CK, Perkins BA. Effect of artificial pancreas systems on glycaemic control in patients with type 1 diabetes: a systematic review and meta-analysis of outpatient randomised controlled trials. *The Lancet Diabetes and Endocrinology*. 2017;5:501–12.
18. Buse JB, Wexler DJ, Tsapas A, Rossing P, Mingrone G, Mathieu C, et al. 2019 Update to: Management of Hyperglycemia in Type 2 Diabetes, 2018. A Consensus Report by the American Diabetes Association (ADA) and the European Association for the Study of Diabetes (EASD). *Diabetes Care*. 2020;43:487–93.
19. Huynh K, Kiriazis H, Du X, Love JE, Jandeleit-Dahm KA, Forbes JM, et al. Coenzyme Q10 attenuates diastolic dysfunction, cardiomyocyte hypertrophy and cardiac fibrosis in the db/db mouse model of type 2 diabetes. *Diabetologia*. 2012;55:1544–53.
20. Huynh K, McMullen JR, Julius TL, Tan JW, Love JE, Cemerlang N, et al. Cardiac-specific IGF-1 receptor transgenic expression protects against cardiac fibrosis and diastolic dysfunction in a mouse model of diabetic cardiomyopathy. *Diabetes*. 2010;59:1512–20.
21. Huynh K, Kiriazis H, Du XJ, Love JE, Gray SP, Jandeleit-Dahm KA, et al. Targeting the upregulation of reactive oxygen species subsequent to hyperglycemia prevents type 1 diabetic cardiomyopathy in mice. *Free Radical Biology and Medicine*. 2013;60:307–17.
22. Prakoso D, de Blasio M, Kiriazis H, Qian H, Deo M, Jap E, et al. Cardiac remodelling and inflammation associated with diabetic cardiomyopathy is mitigated by phosphoinositide 3-kinase P110 α gene delivery (Abstract). *Heart, Lung and Circulation*. 2017;26:S50.
23. Schannwell CM, Schneppenheim M, Perings S, Plehn G, Strauer BE. Left ventricular diastolic dysfunction as an early manifestation of diabetic cardiomyopathy. *Cardiology*. 2002;98:33–9.
24. Bajraktari G, Koltai MS, Ademaj F, Rexhepaj N, Qirko S, Ndrepepa G, et al. Relationship between insulin resistance and left ventricular diastolic dysfunction in patients with impaired glucose tolerance and type 2 diabetes. *International Journal of Cardiology*. 2006;110:206–11.
25. Boyer JK, Thanigaraj S, Schechtman KB, Pérez JE. Prevalence of ventricular diastolic dysfunction in asymptomatic, normotensive patients with diabetes mellitus. *American Journal of Cardiology*. 2004;93:870–5.
26. Zile MR, Brutsaert DL. New concepts in diastolic dysfunction and diastolic heart failure: Part I: Diagnosis, prognosis, and measurements of diastolic function. *Circulation*. 2002;105:1387–93.

27. Levelt E, Rodgers CT, Clarke WT, Mahmood M, Ariga R, Francis JM, et al. Cardiac energetics, oxygenation, and perfusion during increased workload in patients with type 2 diabetes mellitus. *European Heart Journal*. 2016;37:3461–9.
28. von Bibra H, Hansen A, Dounis V, Bystedt T, Malmberg K, Rydén L. Augmented metabolic control improves myocardial diastolic function and perfusion in patients with non-insulin dependent diabetes. *Heart*. 2004;90:1483–4.
29. Nagueh SF. Left Ventricular Diastolic Function: Understanding Pathophysiology, Diagnosis, and Prognosis With Echocardiography. *JACC: Cardiovascular Imaging*. 2020;13:228–44.
30. Nishimura RA, Abel MD, Hatle LK, Tajik AJ. Assessment of diastolic function of the heart: background and current applications of doppler echocardiography. Part II. Clinical studies. *Mayo Clinic Proceedings*. 1989;64:181–204.
31. Jellis CL, Sacre JW, Wright J, Jenkins C, Haluska B, Jeffriess L, et al. Biomarker and imaging responses to spironolactone in subclinical diabetic cardiomyopathy. *European Heart Journal*. 2014;15:776–86.
32. Mizushige K, Yao L, Noma T, Kiyomoto H, Yu Y, Hosomi N, et al. Alteration in left ventricular diastolic filling and accumulation of myocardial collagen at insulin-resistant prediabetic stage of a type II diabetic rat model. *Circulation*. 2000;101:899–907.
33. Park J-H, Marwick TH. Use and Limitations of E/e' to Assess Left Ventricular Filling Pressure by Echocardiography. *Journal of Cardiovascular Ultrasound*. 2011;19:169.
34. Kass DA. Clinical evaluation of left heart function by conductance catheter technique. *European Heart Journal*. 1992;13:57-64.
35. Weiss JL, Frederiksen JW, Weisfeldt ML. Hemodynamic determinants of the time course of fall in canine left ventricular pressure. *Journal of Clinical Investigation*. 1976;58:751–60.
36. Connelly KA, Prior DL, Kelly DJ, Feneley MP, Krum H, Gilbert RE. Load-sensitive measures may overestimate global systolic function in the presence of left ventricular hypertrophy: a comparison with load-insensitive measures. *American Journal of Physiology: Heart Circulatory Physiology*. 2006;290:1699–705.
37. Chirinos JA, Bhattacharya P, Kumar A, Proto E, Konda P, Segers P, et al. Impact of diabetes mellitus on ventricular structure, arterial stiffness, and pulsatile hemodynamics in heart failure with preserved ejection fraction. *Journal of the American Heart Association*. 2019;8.
38. Paterson DI, Wells G, Erthal F, Mielniczuk L, O'Meara E, White J, et al. OUTSMART HF: A Randomized Controlled Trial of Routine Versus Selective Cardiac Magnetic Resonance for Patients with Non-Ischemic Heart Failure (IMAGE-HF 1B). *Circulation*. 2020;141:818–827.
39. Diamant M, Lamb HJ, Groeneveld Y, Endert EL, Smit JWA, Bax JJ, et al. Diastolic dysfunction is associated with altered myocardial metabolism in asymptomatic normotensive patients with well-controlled type 2 diabetes mellitus. *Journal of the American College of Cardiology*. 2003;42:328–35.
40. Liu X, Yang ZG, Gao Y, Xie LJ, Jiang L, Hu BY, et al. Left ventricular subclinical myocardial dysfunction in uncomplicated type 2 diabetes mellitus is associated with impaired myocardial perfusion: A contrast-enhanced cardiovascular magnetic resonance study. *Cardiovascular Diabetology*. 2018;17.

41. Camici PG, Tschöpe C, di Carli MF, Rimoldi O, van Linthout S. Coronary microvascular dysfunction in hypertrophy and heart failure. *Cardiovascular Research*. 2020; 116:806-816.
42. Wu CK, Lee JK, Hsu JC, Su MYM, Wu YF, Lin TT, et al. Myocardial adipose deposition and the development of heart failure with preserved ejection fraction. *European Journal of Heart Failure*. 2019; 22:445-454
43. Ng ACT, Delgado V, Borlaug BA, Bax JJ. Diabetes: the combined burden of obesity and diabetes on heart disease and the role of imaging. *Nature Reviews Cardiology*. 2020; 18:291-304.
44. Zou C, Li W, Pan Y, Khan ZA, Li J, Wu X, et al. 11 β -HSD1 inhibition ameliorates diabetes-induced cardiomyocyte hypertrophy and cardiac fibrosis through modulation of EGFR activity. *Oncotarget*. 2017;8: 96263-96275.
45. Feng B, Chen S, George B, Feng Q, Chakrabarti S. miR133a regulates cardiomyocyte hypertrophy in diabetes. *Diabetes/Metabolism Research and Reviews*. 2010;26:40-49.
46. Ritchie RH, Delbridge LMD. Cardiac hypertrophy, substrate utilization and metabolic remodelling: Cause or effect? *Clinical and Experimental Pharmacology and Physiology*. 2006;33:159-66.
47. He A, Fang W, Zhao K, Wang Y, Li J, Yang C, et al. Mast cell-deficiency protects mice from streptozotocin-induced diabetic cardiomyopathy. *Translational Research*. 2019;208:1-14.
48. Malhotra a, Penpargkul S, Fein FS, Sonnenblick EH, Scheuer J. The effect of streptozotocin-induced diabetes in rats on cardiac contractile proteins. *Circulation Research*. 1981;49:1243-50.
49. Furman B. Streptozotocin-Induced Diabetic Models in Mice and Rats. *Current Protocols in Pharmacology*. 2015;70:1-20.
50. Like AA, Rossini AA. Streptozotocin-induced pancreatic insulinitis: new model of diabetes mellitus. *Science*. 1976;193:415-7.
51. Pulinilkunnil T, Kienesberger PC, Nagendran J, Sharma N, Young ME, Dyck JRB. Cardiac-specific adipose triglyceride lipase overexpression protects from cardiac steatosis and dilated cardiomyopathy following diet-induced obesity. *International Journal of Obesity*. 2014;38:205-15.
52. Hua Y, Zhang Y, Dolence J, Shi GP, Ren J, Nair S. Cathepsin K knockout mitigates high-fat diet-induced cardiac hypertrophy and contractile dysfunction. *Diabetes*. 2013;62:498-509.
53. Tate M, Prakoso D, Willis AM, Peng C, Deo M, Qin CX, et al. Characterising an alternative murine model of diabetic cardiomyopathy. *Frontiers in Physiology*. 2019;10:1-15.
54. de Blasio MJ, Huynh K, Qin C, Rosli S, Kiriazis H, Ayer A, et al. Therapeutic targeting of oxidative stress with coenzyme Q10 counteracts exaggerated diabetic cardiomyopathy in a mouse model of diabetes with diminished PI3K (p110a) signaling. *Free Radical Biology and Medicine*. 2015;87:137-47.
55. Basu R, Oudit GY, Wang X, Zhang L, Ussher JR, Lopaschuk GD, et al. Type 1 diabetic cardiomyopathy in the Akita (Ins2WT/C96Y) mouse model is characterized by lipotoxicity and diastolic dysfunction with preserved systolic function. *American Journal of Physiology Heart and Circulatory Physiology*. 2009;297:2096-108.

56. Daniels A, van Bilsen M, Janssen BJA, Brouns AE, Cleutjens JPM, Roemen THM, et al. Impaired cardiac functional reserve in type 2 diabetic db/db mice is associated with metabolic, but not structural, remodelling. *Acta Physiologica*. 2010;200:11–22.
57. Belke DD, Swanson EA, Dillmann WH. Decreased sarcoplasmic reticulum activity and contractility in diabetic db/db mouse heart. *Diabetes*. 2004;53:3201–8.
58. Lee M, Gardin JM, Lynch JC, Smith V-E, Tracy RP, Savage PJ, et al. Diabetes mellitus and echocardiographic left ventricular function in free-living elderly men and women: The Cardiovascular Health Study. *American Heart Journal*. 1997;133:36–43.
59. Dawson A, Morris AD, Struthers AD. The epidemiology of left ventricular hypertrophy in type 2 diabetes mellitus. *Diabetologia*. 2005;48:1971–9.
60. Devereux RB, Roman MJ, Paranicas M, O MJ, Lee ET, Welty TK, et al. Impact of Diabetes on Cardiac Structure and Function The Strong Heart Study. *Circulation*. 2000;101:2271–2276.
61. Fischer VW, Barner HB, Leskiw ML. Capillary basal laminar thickness in diabetic human myocardium. *Diabetes*. 1979;28:713–9.
62. Devereux RB, Alonso DR, Lutas EM, Gottlieb GJ, Sachs I, Reichek N. Echocardiographic Assessment of Left Ventricular Hypertrophy: Comparison to Necropsy Findings. *The American Journal of Cardiology*. 1986;57:450–8.
63. Frustaci A, Kajstura J, Chimenti C, Jakoniuk I, Leri A, Maseri A, et al. Myocardial Cell Death in Human Diabetes. *Circulation Research*. 2000;87:1123–32.
64. Olivetti G, Melissari M, Balbi T, Quaini F, Cigola E, Sonnenblick EH, et al. Myocyte cellular hypertrophy is responsible for ventricular remodelling in the hypertrophied heart of middle aged individuals in the absence of cardiac failure. *Cardiovascular Research*. 1994;28.
65. Ritchie RH, Quinn JM, Cao AH, Drummond GR, Kaye DM, Favaloro JM, et al. The antioxidant tempol inhibits cardiac hypertrophy in the insulin-resistant GLUT4-deficient mouse in vivo. *Journal of Molecular and Cellular Cardiology*. 2007;42:1119–28.
66. Huynh K, Bernardo BC, McMullen JR, Ritchie RH. Diabetic cardiomyopathy: Mechanisms and new treatment strategies targeting antioxidant signaling pathways. *Pharmacology and Therapeutics*. 2014;142:375–415.
67. Nakagami H, Morishita R, Yamamoto K, Yoshimura S, Taniyama Y, Aoki M, et al. Phosphorylation of p38 Mitogen-Activated Protein Kinase Downstream of Bax-Caspase-3 Pathway Leads to Cell Death Induced by High D-Glucose in Human Endothelial Cells. *Diabetes*. 2001;50:1472–81.
68. Cai L, Li W, Wang G, Guo L, Jiang Y, Kang YJ. Hyperglycemia-Induced Apoptosis in Mouse Myocardium. 2002;51.
69. Federici M, Hribal M, Perego L, Ranalli M, Caradonna Z, Perego C, et al. High Glucose Causes Apoptosis in Cultured Human Pancreatic Islets of Langerhans. *Diabetes*. 2001;50:1290–301.
70. Smart EJ, Li X. Hyperglycemia : Cell death in a cave. *Biochimica et Biophysica Acta*. 2007;1772:524–6.
71. Maria C, Volpe O, Henrique P, Martins P, Nogueira-machado JA. Cellular death , reactive oxygen species (ROS) and diabetic complications. *Cell Death and Disease*. 2018;9:1–9.

72. Gray SP, Jha JC, Kennedy K, Bommel E van, Chew P, Szyndralewicz C, et al. Combined NOX1/4 inhibition with GKT137831 in mice provides dose-dependent reno- and atheroprotection even in established micro- and macrovascular disease. *Diabetologia*. 2017;60:927–37.
73. Anvari E, Wikström P, Walum E, Welsh N. The novel NADPH oxidase 4 inhibitor GLX351322 counteracts glucose intolerance in high-fat diet- treated C57BL/6 mice. *Free Radical Research*. 2015;49:1308–18.
74. Shimizu M, Umeda K, Sugihara N, Yoshio H, Ino H, Takeda R, et al. Collagen remodelling in myocardia of patients with diabetes. *Journal of Clinical Pathology*. 1993;46:32–6.
75. Hinderer S, Schenke-Layland K. Cardiac fibrosis – A short review of causes and therapeutic strategies. *Advanced Drug Delivery Reviews*. 2019;146:77–82.
76. Krstevski C, Cohen CD, Dona MSI, Pinto AR. New perspectives of the cardiac cellular landscape: mapping cellular mediators of cardiac fibrosis using single-cell transcriptomics. *Biochemical Society Transactions*. 2020;48:2483–93.
77. van Linthout S, Seeland U, Riad A, Eckhardt O, Hohl M, Dhayat N, et al. Reduced MMP-2 activity contributes to cardiac fibrosis in experimental diabetic cardiomyopathy. *Basic Research in Cardiology*. 2008;103:319–27.
78. Westermann D, Rutschow S, Jäger S, Linderer A, Anker S, Riad A, et al. Contributions of inflammation and cardiac matrix metalloproteinase activity to cardiac failure in diabetic cardiomyopathy: The role of angiotensin type 1 receptor antagonism. *Diabetes*. 2007;56:641–6.
79. Tate M, Grieve D, Ritchie R. Are targeted therapies for diabetic cardiomyopathy on the horizon? *Clinical Science*. 2017;131:897–915.
80. Aronson D. Cross-linking of glycated collagen in the pathogenesis of arterial and myocardial stiffening of aging and diabetes. *Journal of Hypertension*. 2003;21:3–12.
81. Westermann D, van Linthout S, Dhayat S, Dhayat N, Schmidt A, Noutsias M, et al. Tumor necrosis factor- α antagonism protects from myocardial inflammation and fibrosis in experimental diabetic cardiomyopathy. *Basic Research in Cardiology*. 2007;102:500–7.
82. Bugger H, Abel ED. Rodent models of diabetic cardiomyopathy. *Disease Models & Mechanisms*. 2009;2:454–66.
83. Chen S, Puthanveetil P, Feng B, Matkovich SJ, Dorn GW, Chakrabarti S. Cardiac miR-133a overexpression prevents early cardiac fibrosis in diabetes. *Journal of Cellular and Molecular Medicine*. 2014;18:415–21.
84. Kawaguchi M, Techigawara M, Ishihata T, Asakura T, Saito F, Kazuhira M, et al. A comparison of ultrastructural changes on endomyocardial biopsy specimens obtained from patients with diabetes mellitus with and without hypertension. *Heart Vessels*. 1997;12:267–74.
85. Nunoda S-I, Genda A, Sugihara N, Nakayama A, Mizuno S, Takeda R. Quantitative approach to the histopathology of the biopsied right ventricular myocardium in patients with diabetes mellitus. *Heart and Vessels*. 1985;1:43–7.
86. Ying C, Liu T, Ling H, Cheng M, Zhou X, Wang S, et al. Glucose variability aggravates cardiac fibrosis by altering AKT signalling path. *Diabetes & Vascular Disease Research*. 2017;14:1–9.

87. Hutchinson KR, Lord CK, West TA, Stewart JA. Cardiac fibroblast-dependent extracellular matrix accumulation is associated with diastolic stiffness in type-2 diabetes. *PLoS ONE*. 2013;8.
88. Ma H, Li SY, Xu P, Babcock SA, Dolence EK, Brownlee M, et al. Advanced glycation endproduct (AGE) accumulation and AGE receptor (RAGE) up-regulation contribute to the onset of diabetic cardiomyopathy. *Journal of Cellular and Molecular Medicine*. 2009;13:1751–64.
89. Chiu CY, Yang R sen, Sheu ML, Chan DC, Yang TH, Tsai KS, et al. Advanced glycation end-products induce skeletal muscle atrophy and dysfunction in diabetic mice via a RAGE-mediated, AMPK-down-regulated, Akt pathway. *Journal of Pathology*. 2016;238:470–82.
90. Forbes JM, Cooper ME. Mechanisms of diabetic complications. *Physiological Reviews*. 2013;93:137–88.
91. Candido R, Forbes JM, Thomas MC, Thallas V, Dean RG, Burns WC, et al. A breaker of advanced glycation end products attenuates diabetes-induced myocardial structural changes. *Circulation Research*. 2003;92:785–92.
92. Berg TJ, Snorgaard O, Faber J, Torjesen PA, Hildebrandt P, Mehlsen J, et al. Serum levels of advanced glycation end products are associated with left ventricular diastolic function in patients with type 1 diabetes. *Diabetes Care*. 1999;22:1186–90.
93. Brunvand L, Heier M, Brunborg C, Hanssen KF, Fugelseth D, Stensaeth KH, et al. Advanced glycation end products in children with type 1 diabetes and early reduced diastolic heart function. *BMC Cardiovascular Disorders*. 2017;17.
94. Shen X, Zheng S, Metreveli NS, Epstein PN. Protection of cardiac mitochondria by overexpression of MnSOD reduces diabetic cardiomyopathy. *Diabetes*. 2006;55:798–805.
95. Ceriello A, Mercuri F, Quagliaro L, Assaloni R, Motz E, Tonutti L, et al. Detection of nitrotyrosine in the diabetic plasma: Evidence of oxidative stress. *Diabetologia*. 2001;44:834–8.
96. Piconi L, Quagliaro L, Assaloni R, da Ros R, Maier A, Zuodar G, et al. Constant and intermittent high glucose enhances endothelial cell apoptosis through mitochondrial superoxide overproduction. *Diabetes/Metabolism Research and Reviews*. 2006;22:198–203.
97. Tan Y, Ichikawa T, Li J, Si Q, Yang H, Chen X, et al. Diabetic downregulation of Nrf2 activity via ERK contributes to oxidative stress-induced insulin resistance in cardiac cells in vitro and in vivo. *Diabetes*. 2011;60:625–33.
98. Hiranandani N, Bupha-Intr T, Janssen PML. SERCA overexpression reduces hydroxyl radical injury in murine myocardium. *American Journal of Physiology Heart and Circulatory Physiology*. 2006;291:H3130-5.
99. Mohazzab-H KM, Kaminski PM, Agarwal R, Wolin MS. Potential role of a membrane-bound NADH oxidoreductase in nitric oxide release and arterial relaxation to nitroprusside. *Circulation Research*. 1999;84:220–8.
100. Zhou G, Li X, Hein DW, Xiang X, Marshall JP, Prabhu SD, et al. Metallothionein Suppresses Angiotensin II-Induced Nicotinamide Adenine Dinucleotide Phosphate Oxidase Activation, Nitrosative Stress, Apoptosis, and Pathological Remodeling in the Diabetic Heart. *Journal of the American College of Cardiology*. 2008;52:655–66.

101. Serpillon S, Floyd BC, Gupte RS, George S, Kozicky M, Neito V, et al. Superoxide production by NAD(P)H oxidase and mitochondria is increased in genetically obese and hyperglycemic rat heart and aorta before the development of cardiac dysfunction. The role of glucose-6-phosphate dehydrogenase-derived NADPH. *American Journal of Physiology-Heart and Circulatory Physiology*. 2009;297:153–62.
102. Huaqing Z, Shen E, Jianmin L, Arnold M, Wan L, Peng T. Myocardial Remodeling in a Mouse Model of Type 1 Diabetes. *Diabetes*. 2010;59:2033–42.
103. Indo HP, Davidson M, Yen HC, Suenaga S, Tomita K, Nishii T, et al. Evidence of ROS generation by mitochondria in cells with impaired electron transport chain and mitochondrial DNA damage. *Mitochondrion*. 2007;7:106–18.
104. Ritchie RH, Love JE, Huynh K, Bernardo BC, Henstridge DC, Kiriazis H, et al. Enhanced phosphoinositide 3-kinase(p110 α) activity prevents diabetes-induced cardiomyopathy and superoxide generation in a mouse model of diabetes. *Diabetologia*. 2012;55:3369–81.
105. Gutierrez J, Ballinger SW, Darley-USmar VM, Landar A. Free radicals, mitochondria, and oxidized lipids: The emerging role in signal transduction in vascular cells. *Circulation Research*. 2006;99:924–32.
106. Taye A, Abouzied MM, Mohafez OMM. Tempol ameliorates cardiac fibrosis in streptozotocin-induced diabetic rats: Role of oxidative stress in diabetic cardiomyopathy. *Naunyn-Schmiedeberg's Archives of Pharmacology*. 2013;386:1071–80.
107. Sharma A, Fonarow GC, Butler J, Ezekowitz JA, Felker GM. Coenzyme Q10 and heart failure. *Circulation: Heart Failure*. 2016;9.
108. Nishida K, Otsu K. Inflammation and metabolic cardiomyopathy. 2018;389–98.
109. Dick SA, Epelman S. Chronic heart failure and inflammation. *Circulation Research*. 2016;119:159–76.
110. Sugimura R, Jha DK, Han A, Soria-Valles C, da Rocha EL, Lu YF, et al. Haematopoietic stem and progenitor cells from human pluripotent stem cells. *Nature*. Nature Publishing Group; 2017;545:432–8.
111. Orkin SH, Zon LI. Hematopoiesis: An Evolving Paradigm for Stem Cell Biology. *Cell*. 2008;132:631–44.
112. Masopust D, Soerens AG. Tissue-Resident T Cells and Other Resident Leukocytes. 2019; 37:521-546.
113. Nagareddy PR, Murphy AJ, Stirzaker RA, Hu Y, Yu S, Miller RG, et al. Hyperglycemia promotes myelopoiesis and impairs the resolution of atherosclerosis. *Cell Metabolism*. 2013;17:695–708.
114. Nagareddy PR, Kraakman M, Masters SL, Stirzaker RA, Gorman DJ, Grant RW, et al. Adipose tissue macrophages promote myelopoiesis and monocytosis in obesity. *Cell Metabolism*. 2014;19:821–35.
115. Schmidt MI, Duncan BB, Sharrett AR, Lindberg G, Savage PJ, Offenbacher S. Markers of inflammation and prediction of diabetes mellitus in adults (Atherosclerosis Risk in Communities study): a cohort study. *The Lancet*. 1999;353:1649–52.

116. Ford ES. Leukocyte Count , Erythrocyte Sedimentation Rate , and Diabetes Incidence in a National Sample of US Adults. *American Journal of Epidemiology*. 2002;155:57–64.
117. Ohshita K, Yamane K, Hanafusa M, Mori H, Mito K, Okubo M, et al. Elevated White Blood Cell Count in Subjects With Impaired Glucose Tolerance. *Diabetes Care*. 2004;27:491–6.
118. Woo SJ, Ahn SJ, Ahn J, Park KH, Lee K. Elevated Systemic Neutrophil Count in Diabetic Retinopathy and Diabetes : A Hospital-Based Cross-sectional Study of 30,793 Korean Subjects. *Investigative Ophthalmology & Visual Science*. 2011;52:7697–703.
119. Menart-houtermans B, Ruth R, Nowotny B, Rosenbauer J, Koliaki C, Kahl S, et al. Leukocyte Profiles Differ Between Type 1 and Type 2 Diabetes and Are Associated With Metabolic Phenotypes : Results From the German Diabetes Study (GDS). *Diabetes Care*. 2014;37:2326–33.
120. Lee RH, Bergmeier W. Sugar makes neutrophils RAGE: Linking diabetes associated hyperglycemia to thrombocytosis and platelet reactivity. *Journal of Clinical Investigation*. American Society for Clinical Investigation; 2017. 127(6):2040–3.
121. Wong SL, Demers M, Martinod K, Gallant M, Wang Y, Goldfine AB, et al. Diabetes primes neutrophils to undergo NETosis, which impairs wound healing. *Nature Medicine*. 2015;21:815–9.
122. Huang J, Xiao Y, Zheng P, Zhou W, Wang Y, Huang G, et al. Distinct neutrophil counts and functions in newly diagnosed type 1 diabetes, latent autoimmune diabetes in adults, and type 2 diabetes. *Diabetes/Metabolism Research and Reviews*. 2019;35:1–10.
123. Friedman GD, Klatsky AL, Siegelaub AB. The leukocyte count as a predictor of myocardial infarction. *The New England Journal of Medicine*. 1974;290:1275–8.
124. Madjid M, Awan I, Willerson JT, Casscells SW. Leukocyte Count and Coronary Heart Disease Implications for Risk Assessment. *Journal of the American College of Cardiology*. 2004;44:1945–56.
125. Rogacev KS, Seiler S, Zawada AM, Reichart B, Herath E, Roth D, et al. CD14++CD16+ monocytes and cardiovascular outcome in patients with chronic kidney disease. *European Journal of Cardiology*. 2011;32:84–92.
126. Rogacev KS, Cremers B, Zawada AM, Ms C, Seiler S, Binder N, et al. CD14++ CD16+ Monocytes Independently Predict Cardiovascular Events A Cohort Study of 951 Patients Referred for Elective Coronary Angiography. *Journal of the American College of Cardiology*. 2012;60:1512–20.
127. Manabe I, Inflammation AT, Syndrome M. Chronic Inflammation Links Cardiovascular, Metabolic and Renal Diseases. 2011;75:2739–2748.
128. Goldfine AB, Shoelson SE, Goldfine AB, Shoelson SE. Therapeutic approaches targeting inflammation for diabetes and associated cardiovascular risk Find the latest version : Therapeutic approaches targeting inflammation for diabetes and associated cardiovascular risk. 2017;127:83–93.
129. Shirazi LF, Bissett J, Romeo F, Mehta JL. Role of Inflammation in Heart Failure. *Current Atherosclerosis Reports*; 2017;27.
130. Sun J, Sukhova GK, Wolters PJ, Yang M, Kitamoto S, Libby P, et al. Mast cells promote atherosclerosis by releasing proinflammatory cytokines. *Nature Medicine*. 2007;13:719–24.

131. Constantinides P. Mast Cells and Susceptibility to Experimental Atherosclerosis. *Science*. 1953;117:505–6.
132. Drechsler M, Megens RTA, van Zandvoort M, Weber C, Soehnlein O. Hyperlipidemia-triggered neutrophilia promotes early atherosclerosis. *Circulation*. 2010;122:1837–45.
133. Ross R. Atherosclerosis — An Inflammatory Disease. *New England Journal of Medicine*. 1999;340:115–26.
134. Swirski FK, Nahrendorf M. Leukocyte behavior in atherosclerosis, myocardial infarction, and heart failure. *Science*. 2013;339:161–6.
135. Flynn MC, Pernes G, Lee MKS, Nagareddy PR, Murphy AJ. Monocytes, macrophages, and metabolic disease in atherosclerosis. *Frontiers in Pharmacology*. 2019;10.
136. Bajpai A, Tilley DG. The Role of Leukocytes in Diabetic Cardiomyopathy. *Frontiers in Physiology*. 2018;9:1–12.
137. Fadini GP, Menegazzo L, Scattolini V, Gintoli M, Albiero M, Avogaro A. A perspective on NETosis in diabetes and cardiometabolic disorders. *Nutrition, Metabolism and Cardiovascular Diseases*. 2016;26:1–8.
138. Pecoraro RE, Reiber GE, Burgess EM. Pathways to diabetic limb amputation. Basis for prevention. *Diabetes Care*. 1990;13:513–21. A
139. Vulesevic B, Sirois MG, Allen BG, de Denu S, White M. Subclinical Inflammation in Heart Failure: A Neutrophil Perspective. *Canadian Journal of Cardiology*. 2018;34:717–25.
140. Qin CX, May LT, Li R, Cao N, Rosli S, Deo M, et al. Small-molecule-biased formyl peptide receptor agonist compound 17b protects against myocardial ischaemia-reperfusion injury in mice. *Nature Communications*. 2017;8:1–13.
141. Chia S, Nagurney JT, Brown DFM, Raffel OC, Bamberg F, Senatore F, et al. Association of Leukocyte and Neutrophil Counts With Infarct Size, Left Ventricular Function and Outcomes After Percutaneous Coronary Intervention for ST-Elevation Myocardial Infarction. *American Journal of Cardiology*. 2009;103:333–7.
142. Guasti L, Dentali F, Castiglioni L, Maroni L, Marino F, Squizzato A, et al. Neutrophils and clinical outcomes in patients with acute coronary syndromes and/or cardiac revascularization: A systematic review on more than 34,000 subjects. *Thrombosis and Haemostasis*. 2011;106:591–9.
143. Horckmans M, Ring L, Duchene J, Santovito D, Schloss MJ, Drechsler M, et al. Neutrophils orchestrate post-myocardial infarction healing by polarizing macrophages towards a reparative phenotype. *European Heart Journal*. 2017;38:187–97.
144. Marshall JS. Mast-cell responses to pathogens. *Nature Reviews Immunology*. 2004;4:787–99.
145. Franco CB, Chen CC, Drukker M, Weissman IL, Galli SJ. Distinguishing Mast Cell and Granulocyte Differentiation at the Single-Cell Level. *Cell Stem Cell*. 2010;6:361–8.
146. Triggiani M, Patella V, Staiano RI, Granata F, Marone G. Allergy and the cardiovascular system. *Clinical and Experimental Immunology*. 2008;153:7–11.

147. Janicki JS, Brower GL, Levick SP. The Emerging Prominence of the Cardiac Mast Cell as a Potent Mediator of Adverse Myocardial Remodeling. Hughes MR, McNagny KM, editors. *Methods in Molecular Biology*. 2015;1220:121–39.
148. Lombardi A, Roberto V, Cere E, di Pasquale G. Silent acute myocardial infarction following a wasp sting. *Italian Heart Journal*. 2003;9:638–41.
149. Wagdi P, Mehan VK, Burgi H, Salzmann C. Acute myocardial infarction after wasp stings in a patient with normal coronary arteries.
150. Liao CH, Akazawa H, Tamagawa M, Ito K, Yasuda N, Kudo Y, et al. Cardiac mast cells cause atrial fibrillation through PDGF-A - Mediated fibrosis in pressure-overloaded mouse hearts. *Journal of Clinical Investigation*. 2010;120:242–53.
151. Liu J, Divoux A, Sun J, Zhang J, Clément K, Glickman JN, et al. Genetic deficiency and pharmacological stabilization of mast cells reduce diet-induced obesity and diabetes in mice. *Nature Medicine*. 2009;15:940–5.
152. Wernersson S, Pejler G. Mast cell secretory granules: Armed for battle. *Nature Reviews Immunology*. 2014;14:478–94.
153. Mackins CJ, Kano S, Seyedi N, Schäfer U, Reid AC, Machida T, et al. Cardiac mast cell-derived renin promotes local angiotensin formation, norepinephrine release, and arrhythmias in ischemia/reperfusion. *Journal of Clinical Investigation*. 2006;116:1063–70.
154. Krystel-Whittemore M, Dileepan KN, Wood JG. Mast cell: A multi-functional master cell. *Frontiers in Immunology*. 2016;6.
155. Heikkilä HM, Lätti S, Leskinen MJ, Hakala JK, Kovanen PT, Lindstedt KA. Activated mast cells induce endothelial cell apoptosis by a combined action of chymase and tumor necrosis factor- α . *Arteriosclerosis, Thrombosis, and Vascular Biology*. 2008;28:309–14.
156. Leskinen MJ, Heikkilä HM, Speer MY, Hakala JK, Laine M, Kovanen PT, et al. Mast cell chymase induces smooth muscle cell apoptosis by disrupting NF- κ B-mediated survival signaling. *Experimental Cell Research*. 2006;312:1289–98.
157. Wood JG, Mattioli LF, Gonzalez NC. Systemic hypoxia increases leukocyte emigration and vascular permeability in conscious rats. *The Journal of Applied Physiology*. 1999;87:1561–8.
158. Chen W, Werner F, Illerhaus A, Knopp T, Völker K, Potapenko T, et al. Stabilization of Perivascular Mast Cells by Endothelial CNP (C-Type Natriuretic Peptide). *Arteriosclerosis, Thrombosis, and Vascular Biology*. 2020;40:682–696.
159. Leatham EW, Bath PMW, Tooze JA, Camm AJ. Increased monocyte tissue factor expression in coronary disease. *British Heart Journal*. 1995;73:10–3.
160. Hanazawa S, Kawata Y, Takeshita, A, Kumada H, Okithu M, Tanaka S, et al. Expression of Monocyte Chemoattractant Protein 1 (MCP-1) in Adult Periodontal Disease: Increased Monocyte Chemotactic Activity in Crevicular Fluids and Induction of MCP-1 Expression in Gingival Tissues. *Infection and Immunity*. 1993;61:5219–24.
161. Gordon S, Pluddeman A, Martinez Estrada F. Macrophage heterogeneity in tissues: phenotypic diversity and functions. *Immunological Review*. 2014;262:36–55.

162. Bradshaw EM, Raddassi K, Elyaman W, Orban T, Gottlieb PA, Kent SC, et al. Monocytes from patients with type-1 diabetes spontaneously secrete proinflammatory cytokines inducing Th17 cells. *The Journal of Immunology*. 2009;183:4432–9.
163. Jagannathan-Bogdan M, McDonnell ME, Shin H, Rehman Q, Hasturk H, Apovian CM, et al. Elevated proinflammatory cytokine production by a skewed T-cell compartment requires monocytes and promotes inflammation in type-2 diabetes. *The Journal of Immunology*. 2010;186:1162–72.
164. Pinto AR, Paolicelli R, Salimova E, Gospocic J, Slonimsky E, Bilbao-Cortes D, et al. An abundant tissue macrophage population in the adult murine heart with a distinct alternatively-activated macrophage profile. *PLoS ONE*. 2012;7.
165. Ehses JA, Perren A, Eppler E, Ribaux P, Pospisilik JA, Maor-Cahn R, et al. Increased Number of Islet-Associated Macrophages in Type 2 Diabetes. *Diabetes*. 2007;56:2356–70.
166. Richardson SJ, Willcox A, Bone AJ, Foulis AK, Morgan NG. Islet-associated macrophages in type 2 diabetes. *Diabetologia*. 2009;52:1686–8.
167. Zinselmeyer BH, Vomund AN, Saunders BT, Johnson MW, Carrero JA, Unanue ER. The resident macrophages in murine pancreatic islets are constantly probing their local environment, capturing beta cell granules and blood particles. *Diabetologia*. 2018;61:1374–83.
168. Klessens CQF, Zandbergen M, Wolterbeek R, Bruijn JA, Rabelink TJ, Bajema IM, et al. Macrophages in diabetic nephropathy in patients with type 2 diabetes. *Nephrology Dialysis Transplantation*. 2017;32:1322–9.
169. Hooke DH, Gee DC, Atkins RC. Leukocyte analysis using monoclonal antibodies in human glomerulonephritis. *Kidney International*. 1987;31:964–72.
170. Yang N, Isbel NM, Nikolic-Paterson DJ, Li Y, Ye R, Atkins RC, et al. Local macrophage proliferation in human glomerulonephritis. *Kidney International*. 1998;54:143–51.
171. Curat CA, Wegner V, Sengenès C, Miranville A, Tonus C, Busse R, et al. Macrophages in human visceral adipose tissue: Increased accumulation in obesity and a source of resistin and visfatin. *Diabetologia*. 2006;49:744–7.
172. Trim W, Turner JE, Thompson D. Parallels in Immunometabolic Adipose Tissue Dysfunction with Ageing and Obesity. *Frontiers in Immunology*. 2018;9:1–22.
173. Morris DL, Singer K, Lumeng CN. Adipose tissue macrophages: phenotypic plasticity and diversity in lean and obese states. *Current Opinion in Clinical Nutrition and Metabolic Care*. 2011;14:341–6.
174. Pinto AR, Ilinykh A, Ivey MJ, Kuwabara JT, D’Antoni ML, Debuque R, et al. Revisiting cardiac cellular composition. *Circulation Research*. 2016;118:400–9.
175. Pinto AR, Godwin JW, Rosenthal NA. Macrophages in cardiac homeostasis, injury responses and progenitor cell mobilisation. *Stem Cell Research*. 2014;13:705–14.
176. Sager HB, Hulsmans M, Lavine KJ, Moreira MB, Heidt T, Courties G, et al. Proliferation and Recruitment Contribute to Myocardial Macrophage Expansion in Chronic Heart Failure. *Circulation Research*. 2016;119:853–64.

177. Kain D, Amit U, Yagil C, Landa N, Naftali-Shani N, Molotski N, et al. Macrophages dictate the progression and manifestation of hypertensive heart disease. *International Journal of Cardiology*. 2016;203:381–95.
178. Carai P, Leeuwen REW van, Custers K, Peters T, Hazebroek M, Stöger L, et al. Macrophage MicroRNA-155 Promotes Cardiac Hypertrophy and Failure. *Circulation*. 2013; 128:1420–1432.
179. Tate M, Robinson E, Green BD, Mcdermott BJ, Grieve DJ. Exendin-4 attenuates adverse cardiac remodelling in streptozocin- induced diabetes via specific actions on infiltrating macrophages. *Basic Research in Cardiology*. 2016;111:1–13.
180. Schilling JD, Machkovech HM, Kim AHJ, Schwedwener R, Schaffer JE. Macrophages modulate cardiac function in lipotoxic cardiomyopathy. *American Journal of Physiology-Heart and Circulatory Physiology*. 2012;303:H1366–73.
181. Leor J, Rozen L, Zuloft-Shani A, Feinberg MS, Amsalem Y, Barbash IM, et al. Ex vivo activated human macrophages improve healing, remodeling, and function of the infarcted heart. *Circulation*. 2006;114.
182. Shiraishi M, Shintani Y, Shintani Y, Ishida H, Saba R, Yamaguchi A, et al. Alternatively activated macrophages determine repair of the infarcted adult murine heart. *Journal of Clinical Investigation*. American Society for Clinical Investigation; 2016;126:2151–66.
183. Hulsmans M, Clauss S, Xiao L, Aguirre AD, King KR, Hanley A, et al. Macrophages Facilitate Electrical Conduction in the Heart. *Cell*. 2017;169:510-522.e20.
184. Hucker WJ, McCain ML, Laughner JJ, Iaizzo PA, Efimov IR. Connexin 43 expression delineates two discrete pathways in the human atrioventricular junction. *Anatomical Record*. 2008;291:204–15.
185. Yoo S, Dobrzynski H, Fedorov V v., Xu SZ, Yamanushi TT, Jones SA, et al. Localization of Na⁺ channel isoforms at the atrioventricular junction and atrioventricular node in the rat. *Circulation*. 2006;114:1360–71.
186. Nisbet AM, Camelliti P, Walker NL, Burton FL, Cobbe SM, Kohl P, et al. Prolongation of atrio-ventricular node conduction in a rabbit model of ischaemic cardiomyopathy: Role of fibrosis and connexin remodelling. *Journal of Molecular and Cellular Cardiology*. 2016;94:54–64.
187. Chen B, Frangogiannis NG. Macrophages in the Remodeling Failing Heart. *Circulation Research*. 2016;119:776–8.
188. Khallou-Laschet J, Varthaman A, Fornasa G, Compain C, Gaston AT, Clement M, et al. Macrophage plasticity in experimental atherosclerosis. *PLoS ONE*. 2010;5.
189. McArdle S, Buscher K, Ghosheh Y, Pramod AB, Miller J, Winkels H, et al. Migratory and Dancing Macrophage Subsets in Atherosclerotic Lesions. *Circulation Research*. 2019;125:1038–51.
190. Masopust D, Soerens AG. Tissue-Resident T Cells and Other Resident Leukocytes. *Annual Review of Immunology*. 2019;37:521-546.
191. Gall A, Treuting P, Elkon KB, Loo YM, Gale M, Barber GN, et al. Autoimmunity Initiates in Nonhematopoietic Cells and Progresses via Lymphocytes in an Interferon-Dependent Autoimmune Disease. *Immunity*. 2012;36:120–31.

192. Salomon B, Lenschow DJ, Rhee L, Ashourian N, Singh B, Sharpe A, et al. B7/CD28 Costimulation Is Essential for the Homeostasis of the CD4⁺CD25⁺ Immunoregulatory T Cells that Control Autoimmune Diabetes. *Immunity*. 2000;12:431–40.
193. Putnam AL, Brusko TM, Lee MR, Liu W, Szot GL, Ghosh T, et al. Expansion of Human Regulatory T-Cells From Patients With Type 1 Diabetes. *Diabetes*. 2009;58:652–62.
194. Viglietta V, Baecher-Allan C, Weiner HL, Hafler DA. Loss of Functional Suppression by CD4⁺ CD25⁺ Regulatory T Cells in Patients with Multiple Sclerosis. *The Journal of Experimental Medicine*. 2004;199:971–9.
195. Miyara M, Ito Y, Sakaguchi S. TREG-cell therapies for autoimmune rheumatic diseases. *Nature Reviews Rheumatology*. 2014;10:543–51.
196. Morena D'alise A, Auyeung V, Feuerer M, Nishio J, Fontenot J, Benoist C, et al. The defect in T-cell regulation in NOD mice is an effect on the T-cell effectors. *Proceedings of the National Academy of Sciences of the United States of America*. 2008;105:19857-19862.
197. Glick AB, Wodzinski A, Fu P, Levine AD, Wald DN. Impairment of regulatory T-Cell function in autoimmune thyroid disease. *Thyroid*. 2013;23:871–8.
198. Mazumder PK, O'Neill BT, Roberts MW, Buchanan J, Yun UJ, Cooksey RC, et al. Impaired cardiac efficiency and increased fatty acid oxidation in insulin-resistant ob/ob mouse hearts. *Diabetes*. 2004;53:2366–74.
199. Dong F, Zhang X, Yang X, Esberg LB, Yang H, Zhang Z, et al. Impaired cardiac contractile function in ventricular myocytes from leptin-deficient ob/ob obese mice. *Journal of Endocrinology*. 2006;188:25–36.
200. Saraiva RM, Minhas KM, Zheng M, Pitz E, Treuer A, Gonzalez D, et al. Reduced neuronal nitric oxide synthase expression contributes to cardiac oxidative stress and nitroso-redox imbalance in ob/ob mice. *Nitric Oxide - Biology and Chemistry*. 2007;16:331–8.
201. Winer DA, Winer S, Shen L, Wadia PP, Yantha J, Paltser G, et al. B cells promote insulin resistance through modulation of T cells and production of pathogenic IgG antibodies. *Nature Medicine*. 2011;17:610–7.
202. Tobin LM, Mavinkurve M, Carolan E, Kinlen D, O'Brien EC, Little MA, et al. NK cells in childhood obesity are activated, metabolically stressed, and functionally deficient. *JCI Insight*. 2017;2:1–9.
203. Michelet X, Dyck L, Hogan A, Loftus RM, Duquette D, Wei K, et al. Metabolic reprogramming of natural killer cells in obesity limits antitumor responses. *Nature Immunology*. 2018;19:1330–40.
204. Ogasawara K, Hamerman JA, Hsin H, Chikuma S, Bour-Jordan H, Chen T, et al. Impairment of NK cell function by NKG2D modulation in NOD mice. *Immunity*. 2003;18:41–51.
205. Lee IF, Qin H, Priatel JJ, Tan R. Critical role for IFN- γ in natural killer cell-mediated protection from diabetes. *European Journal of Immunology*. 2008;38:82–9.
206. Qin H, Lee IF, Panagiotopoulos C, Wang X, Chu AD, Utz PJ, et al. Natural killer cells from children with type 1 diabetes have defects in NKG2D-dependent function and signaling. *Diabetes*. 2011;60:857–66.

207. Flodström M, Maday A, Balakrishna D, Cleary MM, Yoshimura A, Sarvetnick N. Target cell defense prevents the development of diabetes after viral infection. *Nature Immunology*. 2002;3:373–82.
208. Poirot L, Benoist C, Mathis D. Natural killer cells distinguish innocuous and destructive forms of pancreatic islet autoimmunity. *Proceedings of the National Academy of Sciences of the United States of America*. 2004;101:8102–8107.
209. Angkananard T, Anothaisintawee T, McEvoy M, Attia J, Thakkinstian A. Neutrophil Lymphocyte Ratio and Cardiovascular Disease Risk: A Systematic Review and Meta-Analysis. *BioMed Research International*. 2018:1–11.
210. Vaduganathan M, Ambrosy AP, Greene SJ, Mentz RJ, Subacius HP, Maggioni AP, et al. Predictive value of low relative lymphocyte count in patients hospitalized for heart failure with reduced ejection fraction. *Circulation: Heart Failure*. 2012;5:750–8.
211. Chiurciu V, Leuti A, Saracini S, Fontana D, Finamore P, Giua R, et al. Resolution of inflammation is altered in chronic heart failure and entails a dysfunctional responsiveness of T lymphocytes. *FASEB Journal*. 2019;33:909–16.
212. Wei Z, Spizzo I, Diep H, Drummond GR, Widdop RE, Vinh A. Differential phenotypes of tissue-infiltrating T cells during angiotensin II-induced hypertension in mice. *PLoS ONE*. 2014;9:e114895.
213. Bansal SS, Ismahil MA, Goel M, Patel B, Hamid T, Rokosh G, et al. Activated T lymphocytes are essential drivers of pathological remodeling in ischemic heart failure. *Circulation: Heart Failure*. 2017;10.
214. Madhumitha H, Mohan V, Deepa M, Babu S, Aravindhan V. Increased Th1 and suppressed Th2 serum cytokine levels in subjects with diabetic coronary artery disease. 2014;13.
215. Mombaerts P, Iacomini J, Johnson RS, Herrup K, Tonegawa S, Papaioannou O VE. RAG-1-Deficient Mice Have No Mature B and T Lymphocytes. *Cell*. 1992;66:869–77.
216. Abdullah CS, Li Z, Wang X, Jin ZQ. Depletion of T lymphocytes ameliorates cardiac fibrosis in streptozotocin-induced diabetic cardiomyopathy. *International Immunopharmacology*. 2016;39:251–64.
217. Khanna S, Biswas S, Shang Y, Collard E, Azad A, Kauh C, et al. Macrophage dysfunction impairs resolution of inflammation in the wounds of diabetic mice. *PLoS ONE*. 2010;5.
218. Huang J, Xiao Y, Zheng P, Zhou W, Wang Y, Huang G, et al. Distinct neutrophil counts and functions in newly diagnosed type 1 diabetes, latent autoimmune diabetes in adults, and type 2 diabetes. *Diabetes/Metabolism Research and Reviews*. 2019;35:e3064.
219. Nag A. Study of non-muscle cells of the adult mammalian heart: a fine structural analysis and distribution. *Cytobios*. 1980;28:41–61.
220. Mohenska M, Tan NM, Tokolyi A, Furtado MB, Costa MW, Perry AJ, et al. 3D-cardiomics: A spatial transcriptional atlas of the mammalian heart. *Journal of Molecular and Cellular Cardiology*. 2022;163:20–32.
221. Linscheid N, Santos A, Poulsen PC, Mills RW, Calloe K, Leurs U, et al. Quantitative proteome comparison of human hearts with those of model organisms. *PLoS Biology*. 2021;19.

222. Tang F, Barbacioru C, Wang Y, Nordman E, Lee C, Xu N, et al. mRNA-Seq whole-transcriptome analysis of a single cell. *Nature Methods*. 2009;6:377–82.
223. Tang F, Barbacioru C, Wang Y, Nordman E, Lee C, Xu N, et al. mRNA-Seq whole-transcriptome analysis of a single cell. *Nature Methods*. 2009;6:377–82.
224. Klein AM, Mazutis L, Akartuna I, Tallapragada N, Veres A, Li V, et al. Droplet barcoding for single-cell transcriptomics applied to embryonic stem cells. *Cell*. 2015;161:1187–201.
225. Skelly DA, Squiers GT, McLellan MA, Bolisetty MT, Robson P, Rosenthal NA, et al. Single-cell transcriptional profiling reveals cellular diversity and intercommunication in the mouse heart. *Cell Reports*. 2018;22:600–10.
226. Ramilowski JA, Goldberg T, Harshbarger J, Kloppman E, Lizio M, Satagopam VP, et al. A draft network of ligand-receptor-mediated multicellular signalling in human. *Nature Communications*. 2015;6.
227. Lavin Y, Mortha A, Rahman A, Merad M. Regulation of macrophage development and function in peripheral tissues. *Nature Reviews Immunology*. 2015;15:731–44.
228. Nam J, Onitsuka I, Hatch J, Uchida Y, Ray S, Huang S, et al. Coronary veins determine the pattern of sympathetic innervation in the developing heart. *Development*. 2013;140:1475–85.
229. Beale AL, Meyer PMD, Marwick TH, Lam CSP, Kaye DM. Sex differences in cardiovascular pathophysiology why women are overrepresented in heart failure with preserved ejection fraction. *Circulation*. 2018;138:198–205.
230. Buenrostro JD, Giresi PG, Zaba LC, Chang HY, Greenleaf WJ. Transposition of native chromatin for fast and sensitive epigenomic profiling of open chromatin, DNA-binding proteins and nucleosome position. *Nature Methods*. 2013;10:1213–8.
231. Gladka MM, Molenaar B, de Ruiter H, van der Elst S, Tsui H, Versteeg D, et al. Single-Cell Sequencing of the Healthy and Diseased Heart Reveals Cytoskeleton-Associated Protein 4 as a New Modulator of Fibroblasts Activation. *Circulation*. 2018;138:166–80.
232. Ruggiero A, Chen SN, Lombardi R, Rodriguez G, Marian AJ. Pathogenesis of hypertrophic cardiomyopathy caused by myozenin 2 mutations is independent of calcineurin activity. *Cardiovascular Research*. 2013;97:44–54.
233. Farbehi N, Patrick R, Dorison A, Xaymardan M, Janbandhu V, Wystub-Lis K, et al. Single-cell expression profiling reveals dynamic flux of cardiac stromal, vascular and immune cells in health and injury. *Elife*. 2019;8:1–39.
234. McLellan MA, Skelly DA, Dona MSI, Squiers GT, Farrugia GE, Gaynor TL, et al. High-resolution transcriptomic profiling of the heart during chronic stress reveals cellular drivers of cardiac fibrosis and hypertrophy. *Circulation*. 2020;142:1448–63.
235. Travers JG, Kamal FA, Robbins J, Yutzey KE, Blaxall BC. Cardiac fibrosis. *Circulation Research*. 2016;1021–40.
236. Palevski D, Levin-Kotler LP, Kain D, Naftali-Shani N, Landa N, Ben-Mordechai T, et al. Loss of macrophage Wnt secretion improves remodeling and function after myocardial infarction in mice. *Journal of the American Heart Association*. 2017;6.

237. Keshewani V, Shahshahan HR, Mishra PK. Cardiac transcriptome profiling of diabetic Akita mice using microarray and next generation sequencing. *PLoS ONE*. 2017;12.
238. Ornitz DM, Itoh N. The fibroblast growth factor signaling pathway. *Wiley Interdisciplinary Reviews: Developmental Biology*. 2015;4:215–66.
239. Sweetwyne MT, Murphy-Ullrich JE. Thrombospondin1 in tissue repair and fibrosis: TGF- β -dependent and independent mechanisms. *Matrix Biology*. 2012;31:178–86.
240. Gusarova V, O'Dushlaine C, Teslovich TM, Benotti PN, Mirshahi T, Gottesman O, et al. Genetic inactivation of ANGPTL4 improves glucose homeostasis and is associated with reduced risk of diabetes. *Nature Communications*. 2018;9.
241. Singh AK, Aryal B, Chaube B, Rotllan N, Varela L, Horvath TL, et al. Brown adipose tissue derived ANGPTL4 controls glucose and lipid metabolism and regulates thermogenesis. *Molecular Metabolism*. 2018;11:59–69.
242. Catoire M, Alex S, Paraskevopoulos N, Mattijssen F, Evers-Van Gogh I, Schaart G, et al. Fatty acid-inducible ANGPTL4 governs lipid metabolic response to exercise. *Proceedings of the National Academy of Sciences of the United States of America*. 2014;111.
243. Chen TC, Benjamin DI, Kuo T, Lee RA, Li ML, Mar DJ, et al. The glucocorticoid-Angptl4-ceramide axis induces insulin resistance through PP2A and PKC ζ . *Science Signaling*. 2017;10.
244. Faulkner A, Dang Z, Avolio E, Thomas AC, Batstone T, Lloyd GR, et al. Multi-Omics Analysis of Diabetic Heart Disease in the db/db Model Reveals Potential Targets for Treatment by a Longevity-Associated Gene. *Cells*. 2020;9.
245. Forte E, Skelly DA, Chen M, Daigle S, Morelli KA, Hon O, et al. Dynamic interstitial cell response during myocardial infarction predicts resilience to rupture in genetically diverse mice. *Cell Reports*. 2020;30:3149-3163.e6.
246. Wilson KD, Li Z, Wagner R, Yue P, Tsao P, Nestorova G, et al. Transcriptome alteration in the diabetic heart by rosiglitazone: Implications for cardiovascular mortality. *PLoS ONE*. 2008;3.
247. Coleman DL. Obese and Diabetes: Two Mutant Genes Causing Diabetes-Obesity Syndromes in Mice*. *Diabetologia*. 1978;14:141-148.
248. Pinto AR, Chandran A, Rosenthal NA, Godwin JW. Isolation and analysis of single cells from the mouse heart. *Journal of Immunological Methods*. 2013;393:74–80.
249. Ackers-Johnson M, Li PY, Holmes AP, O'Brien SM, Pavlovic D, Foo RS. A Simplified, Langendorff-Free Method for Concomitant Isolation of Viable Cardiac Myocytes and Nonmyocytes from the Adult Mouse Heart. *Circulation Research*. 2016;119:909–20.
250. Squiers GT, McLellan MA, Ilinykh A, Branca J, Rosenthal NA, Pinto AR. Cardiac cellularity is dependent upon biological sex and is regulated by gonadal hormones. *Cardiovascular Research*. 2020;cva265:1–25.
251. Farrugia GE, McLellan MA, Weeks KL, Matsumoto A, Cohen CD, Krstevski C, et al. A protocol for rapid and parallel isolation of myocytes and non-myocytes from multiple mouse hearts. *STAR Protocols*. 2021;2:1–17.

252. Finak G, McDavid A, Yajima M, Deng J, Gersuk V, Shalek AK, et al. MAST: A flexible statistical framework for assessing transcriptional changes and characterizing heterogeneity in single-cell RNA sequencing data. *Genome Biology*. 2015;16.
253. Sonesson C, Robinson MD. Bias, robustness and scalability in single-cell differential expression analysis. *Nature Methods*. 2018;15:255–61.
254. Yu G, Wang LG, Han Y, He QY. ClusterProfiler: An R package for comparing biological themes among gene clusters. *OMICS: A Journal of Integrative Biology*. 2012;16:284–7.
255. Ramilowski JA, Goldberg T, Harshbarger J, Kloppman E, Lizio M, Satagopam VP, et al. A draft network of ligand-receptor-mediated multicellular signalling in human. *Nature Communications*. 2015;6.
256. Gu Z, Gu L, Eils R, Schlesner M, Brors B. Circlize implements and enhances circular visualization in R. *Bioinformatics*. 2014;30:2811–2.
257. Schneider CA, Rasband WS, Eliceiri KW. NIH Image to ImageJ: 25 years of image analysis. *Nature Methods*. 2012;9:671–5.
258. Mehlem A, Hagberg CE, Muhl L, Eriksson U, Falkevall A. Imaging of neutral lipids by oil red O for analyzing the metabolic status in health and disease. *Nature Protocols*. 2013;8:1149–54.
259. Galderisi M, Anderson KM, Wilson PWF, Levy D. Echocardiographic evidence for the existence of a distinct diabetic cardiomyopathy (The Framingham Heart Study). *The American Journal of Cardiology*. 1991;68:85–9.
260. Rosengren A, Edqvist J, Rawshani A, Sattar N, Franzén S, Adiels M, et al. Excess risk of hospitalisation for heart failure among people with type 2 diabetes. *Diabetologia*. 2018;61:2300–9.
261. Gaede P, Lund-Andersen H, Parving H-H, Pedersen O. Effect of a Multifactorial Intervention on Mortality in Type 2 Diabetes. 2008;358:580-91.
262. Ritchie RH, Abel DE. Basic mechanisms of diabetic heart disease. *Circulation Research*. 2020;126:1501–25.
263. Alex L, Russo I, Holoborodko V, Frangogiannis NG. Characterization of a mouse model of obesity-related fibrotic cardiomyopathy that recapitulates features of human heart failure with preserved ejection fraction. *The American Journal of Physiology-Heart and Circulatory Physiology*. 2018;315:H934–49.
264. Prakoso D, de Blasio MJ, Qin C, Rosli S, Kiriazis H, Qian H, et al. Phosphoinositide 3-kinase (p110 α) gene delivery limits diabetes-induced cardiac NADPH oxidase and cardiomyopathy in a mouse model with established diastolic dysfunction. *Clinical Science*. 2017;131:1345–60.
265. Schiattarella GG, Altamirano F, Tong D, French KM, Villalobos E, Kim SY, et al. Nitrosative stress drives heart failure with preserved ejection fraction. *Nature*. 2019;568:351–6.
266. Wang B, Chandrasekera PC, Pippin JJ. Leptin-and Leptin Receptor-Deficient Rodent Models: Relevance for Human Type 2 Diabetes. *Current Diabetes Reviews*. 2014;10:131–45.
267. Kodama H, Fujita M, Yamaguchi I. Development of hyperglycaemia and insulin resistance in conscious genetically diabetic (C57BL/KsJ-db/db) mice. *Diabetologia*. 1994;37:739–44.

268. Bonora E, Calcaterra F, Lombardi S, Bonfante N, Formentini G, Bonadonna RC, et al. Plasma Glucose Levels Throughout the Day and HbA 1c Interrelationships in Type 2 Diabetes Implications for treatment and monitoring of metabolic control. *Diabetes Care*. 2001;24:2023–9.
269. Koliaki C, Liatis S, Kokkinos A. Obesity and cardiovascular disease: revisiting an old relationship. *Metabolism: Clinical and Experimental*. 2019. p. 98–107.
270. Everett BM, Cornel JH, Lainscak M, Anker SD, Abbate A, Thuren T, et al. Anti-inflammatory therapy with canakinumab for the prevention of hospitalization for heart failure. *Circulation*. 2019;139:1289–99.
271. Alexandraki KI, Piperi C, Ziakas PD, Apostolopoulos N v., Makrilakis K, Syriou V, et al. Cytokine secretion in long-standing diabetes mellitus type 1 and 2: Associations with low-grade systemic inflammation. *Journal of Clinical Immunology*. 2008;28:314–21.
272. Duncan BB, Inês Schmidt M, Pankow JS, Ballantyne CM, Couper D, Vigo A, et al. Low-Grade Systemic Inflammation and the Development of Type 2 Diabetes The Atherosclerosis Risk in Communities Study. *Diabetes*. 2003;52:1799–805.
273. Nagareddy PR, Kraakman M, Masters SL, Stirzaker RA, Gorman DJ, Grant RW, et al. Adipose tissue macrophages promote myelopoiesis and monocytosis in obesity. *Cell Metabolism*. 2014;19:821–35.
274. Marwick TH, Ritchie R, Shaw JE, Kaye D. Implications of Underlying Mechanisms for the Recognition and Management of Diabetic Cardiomyopathy. *Journal of the American College of Cardiology*. 2018;71:339–51.
275. Einarson TR, Acs A, Ludwig C, Panton UH. Prevalence of cardiovascular disease in type 2 diabetes: A systematic literature review of scientific evidence from across the world in 2007-2017. *Cardiovascular Diabetology*. 2018;17.
276. Galderisi M. Diastolic Dysfunction and Diabetic Cardiomyopathy. Evaluation by Doppler Echocardiography. *Journal of the American College of Cardiology*. 2006;48:1548–51.
277. From AM, Scott CG, Chen HH. The Development of Heart Failure in Patients With Diabetes Mellitus and Pre-Clinical Diastolic Dysfunction. A Population-Based Study. *Journal of the American College of Cardiology*. 2010;55:300–5.
278. De Blasio MJ, Huynh N, Deo M, Dubrana LE, Walsh J, Willis A, et al. Defining the Progression of Diabetic Cardiomyopathy in a Mouse Model of Type 1 Diabetes. *Frontiers in Physiology*. 2020;11.
279. Hall ME, Maready MW, Hall JE, Stec DE. Rescue of cardiac leptin receptors in db/db mice prevents myocardial triglyceride accumulation. *American Journal of Physiology - Endocrinology and Metabolism*. 2014;307.
280. Fontes-Carvalho R, Ladeiras-Lopes R, Bettencourt P, Leite-Moreira A, Azevedo A. Diastolic dysfunction in the diabetic continuum: Association with insulin resistance, metabolic syndrome and type 2 diabetes. *Cardiovascular Diabetology*. 2015;14.
281. Lavie CJ, Nunez BD, Garavaglia GE, Messerli FH. Hypertensive Concentric Left Ventricular Hypertrophy: When Is Ventricular Ectopic Activity Increased? *Southern Medical Journal*. 1988;81:696–700.

282. Norden PR, Kume T. The Role of Lymphatic Vascular Function in Metabolic Disorders. *Frontiers in Physiology*. 2020;11:404.
283. Alitalo K. The lymphatic vasculature in disease. *Nature Medicine*. 2011. 17:1371-80.
284. Scallan JP, Hill MA, Davis MJ. Lymphatic vascular integrity is disrupted in type 2 diabetes due to impaired nitric oxide signalling. *Cardiovascular Research*. 2015;107:89–97.
285. Nitti MD, Hespe GE, Kataru RP, García Nores GD, Savetsky IL, Torrisi JS, et al. Obesity-induced lymphatic dysfunction is reversible with weight loss. *Journal of Physiology*. 2016;594:7073–87.
286. Haemmerle M, Keller T, Egger G, Schachner H, Steiner CW, Stokic D, et al. Enhanced lymph vessel density, remodeling, and inflammation are reflected by gene expression signatures in dermal lymphatic endothelial cells in type 2 diabetes. *Diabetes*. 2013;62:2509–29.
287. Kovacic JC, Dimmeler S, Harvey RP, Finkel T, Aikawa E, Krenning G, et al. Endothelial to Mesenchymal Transition in Cardiovascular Disease: JACC State-of-the-Art Review. *Journal of the American College of Cardiology*. 2019;73:190–209.
288. Zhang H, Lui KO, Zhou B. Endocardial cell plasticity in cardiac development, diseases and regeneration. *Circulation Research*. 2018;122:774–89.
289. Popov D, Sima A, Stern D, Simionescu M. The pathomorphological alterations of endocardial endothelium in experimental diabetes and diabetes associated with hyperlipidemia. *Acta Diabetologia*. 1996;33:41–7.
290. Icardo JM. Endocardial Cell Arrangement: Role of Hemodynamics. *The Anatomical Record*. 1989;225:150–5.
291. Libby P, Nahrendorf M, Swirski FK. Leukocytes Link Local and Systemic Inflammation in Ischemic Cardiovascular Disease. *Journal of the American College of Cardiology*. 2016;67:1091–103.
292. Westman J, Grinstein S, Marques PE. Phagocytosis of Necrotic Debris at Sites of Injury and Inflammation. *Frontiers in Immunology*. 2020.
293. Yu XY, Chen HM, Liang JL, Lin QX, Tan HH, Fu YH, et al. Hyperglycemic myocardial damage is mediated by proinflammatory cytokine: Macrophage migration inhibitory factor. *PLoS One*. 2011;6.
294. Wang Q, Wei S, Zhou S, Qiu J, Shi C, Liu R, et al. Hyperglycemia aggravates acute liver injury by promoting liver-resident macrophage NLRP3 inflammasome activation via the inhibition of AMPK/mTOR-mediated autophagy induction. *Immunology and Cell Biology*. 2020;98:54–66.
295. van Dijk CGM, Nieuweboer FE, Pei JY, Xu YJ, Burgisser P, van Mulligen E, et al. The complex mural cell: Pericyte function in health and disease. *International Journal of Cardiology*. 2015;190:75-89.
296. Rajendran S, Seetharaman S, Dharmarajan A, Kuppan K. Microvascular cells: A special focus on heterogeneity of pericytes in diabetes associated complications. *International Journal of Biochemistry and Cell Biology*. 2021;134.
297. Warmke N, Griffin KJ, Cubbon RM. Pericytes in diabetes-associated vascular disease. *Journal of Diabetes and its Complications*. 2016;30:1643–50.

298. Cheung N, Mitchell P, Wong TY. Diabetic retinopathy. *The Lancet*. 2010;376:124–36.
299. Podestà F, Romeo G, Liu WH, Krajewski S, Reed JC, Gerhardinger C, et al. Bax is increased in the retina of diabetic subjects and is associated with pericyte apoptosis in vivo and in vitro. *American Journal of Pathology*. 2000;156:1025–32.
300. Durham JT, Dulmovits BM, Cronk SM, Sheets AR, Herman IM. Pericyte chemomechanics and the angiogenic switch: Insights into the pathogenesis of proliferative diabetic retinopathy? *Investigative Ophthalmology and Visual Science*. 2015;56:3441–59.
301. Geraldès P, Hiraoka-Yamamoto J, Matsumoto M, Clermont A, Leitges M, Marette A, et al. Activation of PKC-and SHP-1 by hyperglycemia causes vascular cell apoptosis and diabetic retinopathy. *Nature Medicine*. 2009;15:1298–306.
302. Ishii H, Jirousek MR, Koya D, Takagi C, Xia P, Clermont A, et al. Amelioration of Vascular Dysfunctions in Diabetic Rats by an Oral PKC β Inhibitor. *Science*. 1996;272:728–31.
303. Hinkel R, Howe A, Renner S, Ng J, Lee S, Klett K, et al. Diabetes Mellitus-Induced Microvascular Destabilization in the Myocardium. *Journal of the American College of Cardiology*. 2017;69:131–43.
304. Sharpe PC, Liu WH, Yue KKM, McMaster D, Catherwood MA, McGinty AM, et al. Glucose-induced oxidative stress in vascular contractile cells: Comparison of aortic smooth muscle cells and retinal pericytes. *Diabetes*. 1998;47:801–9.
305. Ruiz E, Gordillo-Moscoso A, Padilla E, Redondo S, Rodriguez E, Reguillo F, et al. Human vascular smooth muscle cells from diabetic patients are resistant to induced apoptosis due to high Bcl-2 expression. *Diabetes*. 2006;55:1243–51.
306. Hall JL, Matter CM, Wang X, Gibbons GH. Hyperglycemia inhibits vascular smooth muscle cell apoptosis through a protein kinase C-dependent pathway. *Circulation Research*. 2000;87:574–80.
307. Clarke MCH, Figg N, Maguire JJ, Davenport AP, Goddard M, Littlewood TD, et al. Apoptosis of vascular smooth muscle cells induces features of plaque vulnerability in atherosclerosis. *Nature Medicine*. 2006;12:1075–80.
308. Martínez-Hervás S, Vinué Á, Núñez L, Andrés-Blasco I, Piqueras L, TomásReal J, et al. Insulin resistance aggravates atherosclerosis by reducing vascular smooth muscle cell survival and increasing CX3CL1/CX3CR1 axis. *Cardiovascular Research*. 2014;103:324–36.
309. Wynn TA. Cellular and molecular mechanisms of fibrosis. *Journal of Pathology*. 2008;214:199–210.
310. Fang P, Li X, Shan H, Saredy JJ, Cueto R, Xia J, et al. Ly6C⁺ inflammatory monocyte differentiation partially mediates hyperhomocysteinemia-induced vascular dysfunction in type 2 diabetic db/db Mice. *Arteriosclerosis, Thrombosis, and Vascular Biology*. 2019;39:2097–119.
311. Monnerat G, Alarcón ML, Vasconcellos LR, Hochman-Mendez C, Brasil G, Bassani RA, et al. Macrophage-dependent IL-1 β production induces cardiac arrhythmias in diabetic mice. *Nature Communications*. 2016;7.

312. Moreno PR, Murcia AM, Palacios IF, Leon MN, Bernardi VH, Fuster V, et al. Coronary Composition and Macrophage Infiltration in Atherectomy Specimens From Patients With Diabetes Mellitus. 2000;102:2180-4.
313. Hulsmans M, Clauss S, Xiao L, Aguirre AD, King KR, Hanley A, et al. Macrophages Facilitate Electrical Conduction in the Heart. *Cell*. 2017;169:510-522.e20.
314. Barouch LA, Berkowitz DE, Harrison RW, O'Donnell CP, Hare JM. Disruption of leptin signaling contributes to cardiac hypertrophy independently of body weight in mice. *Circulation*. 2003;108:754-9.
315. McGaffin KR, Witham WG, Yester KA, Romano LC, Odoherty RM, McTiernan CF, et al. Cardiac-specific leptin receptor deletion exacerbates ischaemic heart failure in mice. *Cardiovascular Research*. 2011;89:60-71.
316. Aasum E, Hafstad AD, Severson DL, Larsen TS. Age-Dependent Changes in Metabolism, Contractile Function, and Ischemic Sensitivity in Hearts From db/db Mice. *Diabetes*. 2003;52:434-41.
317. Hamdani N, Hervent AS, Vandekerckhove L, Matheeußen V, Demolder M, Baerts L, et al. Left ventricular diastolic dysfunction and myocardial stiffness in diabetic mice is attenuated by inhibition of dipeptidyl peptidase 4. *Cardiovascular Research*. 2014;104:423-31.
318. Kessler EL, Rivaud MR, Vos MA, van Veen TAB. Sex-specific influence on cardiac structural remodeling and therapy in cardiovascular disease. *Biology of Sex Differences*. 2019;10.
319. Alicic RZ, Rooney MT, Tuttle KR. Diabetic kidney disease: Challenges, progress, and possibilities. *Clinical Journal of the American Society of Nephrology*. American Society of Nephrology; 2017;12:2032-45.
320. Buglioni A, Burnett JC. Pathophysiology and the cardiorenal connection in heart failure. Circulating hormones: Biomarkers or mediators. *Clinica Chimica Acta*. 2015;443:3-8.
321. Tan K, Sethi SK. Biomarkers in cardiorenal syndromes. *Translational Research*. 2014;164:122-34.
322. Fujii H, Goto S, Fukagawa M. Role of uremic toxins for kidney, cardiovascular, and bone dysfunction. *Toxins*. 2018;10:202.
323. Radovits T, Korkmaz S, Loganathan S, Barnucz E, Bömicke T, Arif R, et al. Comparative investigation of the left ventricular pressure-volume relationship in rat models of type 1 and type 2 diabetes mellitus. *American Journal of Physiology - Heart and Circulatory Physiology*. 2009;297.
324. Che Y, Wang ZP, Yuan Y, Zhang N, Jin YG, Wan CX, et al. Role of autophagy in a model of obesity: A long-term high fat diet induces cardiac dysfunction. *Molecular Medicine Reports*. Spandidos Publications; 2018;18:3251-61.
325. van den Bergh A, Flameng W, Herijgers P. Type II diabetic mice exhibit contractile dysfunction but maintain cardiac output by favourable loading conditions. *European Journal of Heart Failure*. 2006;8:777-83.
326. Pedersen TM, Boardman NT, Hafstad AD, Aasum E. Isolated perfused working hearts provide valuable additional information during phenotypic assessment of the diabetic mouse heart. *PLoS One*. 2018;13.

327. Pinto AR. Matricellular Proteins as Critical Regulators of Fibrosis. *Circulation Research*. 2021;1036–8.
328. Hamilton TG, Klinghoffer RA, Corrin PD, Soriano P. Evolutionary Divergence of Platelet-Derived Growth Factor Alpha Receptor Signaling Mechanisms. *Molecular and Cellular Biology*. American Society for Microbiology; 2003;23:4013–25.
329. Niu XZ, Zhang B, Marszalek RT, Ces O, Edel JB, Klug DR, et al. Droplet-based compartmentalization of chemically separated components in two-dimensional separations. *Chemical Communications*. 2009;6159–61.
330. Alexanian M, Przytycki PF, Micheletti R, Padmanabhan A, Ye L, Travers JG, et al. A transcriptional switch governs fibroblast activation in heart disease. *Nature*. 2021;595:438–43.
331. Litviňuková M, Talavera-López C, Maatz H, Reichart D, Worth CL, Lindberg EL, et al. Cells of the adult human heart. *Nature*. 2020;588:466–72.
332. Tucker NR, Chaffin M, Fleming SJ, Hall AW, Parsons VA, Bedi KC, et al. Transcriptional and Cellular Diversity of the Human Heart. *Circulation*. 2020;142:466–82.
333. Weinmaster G. The Ins and Outs of Notch Signaling. *Molecular and Cellular Neuroscience*. 1997;9:91–102.
334. Neufeld G, Cohen T, Gengrinovitch S, Poltorak Z. Vascular endothelial growth factor (VEGF) and its receptors. *FASEB*. 1999;13:9–22.
335. Qin CX, Finlayson SB, Al-Sharea A, Tate M, de Blasio MJ, Deo M, et al. Endogenous Annexin-A1 Regulates Haematopoietic Stem Cell Mobilisation and Inflammatory Response Post Myocardial Infarction in Mice in Vivo. *Scientific Reports*. 2017;7.
336. Perera N, Ritchie RH, Tate M. The Role of Bone Morphogenetic Proteins in Diabetic Complications. *ACS Pharmacology and Translational Science*. 2020. p. 11–20.
337. Canty EG, Kadler KE. Procollagen trafficking, processing and fibrillogenesis. *Journal of Cell Science*. 2005;118:1341–53.
338. Döring Y, Pawig L, Weber C, Noels H. The CXCL12/CXCR4 chemokine ligand/receptor axis in cardiovascular disease. *Frontiers in Physiology*. 2014;5.
339. Nishida K, Wang L, Morii E, Park SJ, Narimatsu M, Itoh S, et al. Requirement of Gab2 for mast cell development and KitL/c-Kit signaling. *Blood*. 2002;99:1866–9.
340. Zhao Q, Eichten A, Parveen A, Adler C, Huang Y, Wang W, et al. Single-cell transcriptome analyses reveal endothelial cell heterogeneity in tumors and changes following antiangiogenic treatment. *Cancer Research*. 2018;78:2370–82.
341. Hu S, Zhu L. Semaphorins and their receptors: From axonal guidance to atherosclerosis. *Frontiers in Physiology*. 2018;9.
342. Schröder B. The multifaceted roles of the invariant chain CD74 - More than just a chaperone. *Biochimica et Biophysica Acta - Molecular Cell Research*. 2016;1863:1269–81.
343. Khandelwal S, Roche PA. Distinct MHC class II molecules are associated on the dendritic cell surface in cholesterol-dependent membrane microdomains. *Journal of Biological Chemistry*. 2010;285:35303–10.

344. Knowles PP, Murray-Rust J, Kjær S, Scott RP, Hanrahan S, Santoro M, et al. Structure and chemical inhibition of the RET tyrosine kinase domain. *Journal of Biological Chemistry*. 2006;281:33577–87.
345. Koenen J, Bachelier F, Balabanian K, Schlecht-Louf G, Gallego C. Atypical chemokine receptor 3 (ACKR3): A comprehensive overview of its expression and potential roles in the immune system. *Molecular Pharmacology*. 2019;96:809–18.
346. Doyle EL, Ridger V, Ferraro F, Turmaine M, Saftig P, Cutler DF. CD63 is an essential cofactor to leukocyte recruitment by endothelial P-selectin. *Blood*. 2011;118:4265–73.
347. Ruppert PMM, Michielsen CCJR, Hazebroek EJ, Pirayesh A, Olivecrona G, Afman LA, et al. Fasting induces ANGPTL4 and reduces LPL activity in human adipose tissue. *Molecular Metabolism*. 2020;40.
348. Barrett TJ, Distel E, Murphy AJ, Hu J, Garshick MS, Ogando Y, et al. Apo AI (Apolipoprotein AI) promotes atherosclerosis regression in diabetic mice by suppressing myelopoiesis and plaque inflammation. *Circulation*. 2019;140:1170–84.
349. Nauseef WM, McCormick SJ, Clark RA. Calreticulin functions as a molecular chaperone in the biosynthesis of myeloperoxidase. *Journal of Biological Chemistry*. 1995;270:4741–7.
350. Baumhueter S, Singer MS, Henzel W, Hemmerich S, Renz M, Rosen SD, et al. Binding of L-Selectin to the Vascular Sialomucin CD34. *Science*. 1993;262:436–8.
351. Baumkötter F, Schmidt N, Vargas C, Schilling S, Weber R, Wagner K, et al. Amyloid precursor protein dimerization and synaptogenic function depend on copper binding to the growth factor-like domain. *Journal of Neuroscience*. 2014;34:11159–72.
352. Irving SG, Zipfel PF, Balke J, McBride OW, Morton CC, Burd PR, et al. Two Inflammatory mediator cytokine genes are closely linked and variably amplified on chromosome 17q. *Nucleic Acids Research*. 1990;18:3261–70.
353. Fagerberg L, Hallström BM, Oksvold P, Kampf C, Djureinovic D, Odeberg J, et al. Analysis of the human tissue-specific expression by genome-wide integration of transcriptomics and antibody-based proteomics. *Molecular and Cellular Proteomics*. 2014;13:397–406.
354. Tsou CL, Peters W, Si Y, Slaymaker S, Aslanian AM, Weisberg SP, et al. Critical roles for CCR2 and MCP-3 in monocyte mobilization from bone marrow and recruitment to inflammatory sites. *Journal of Clinical Investigation*. 2007;117:902–9.
355. Low H, Hoang A, Forbes J, Thomas M, Lyons JG, Nestel P, et al. Advanced glycation end-products (AGEs) and functionality of reverse cholesterol transport in patients with type 2 diabetes and in mouse models. *Diabetologia*. 2012;55:2513–21.
356. Makki N, Thiel KW, Miller FJ. The epidermal growth factor receptor and its ligands in cardiovascular disease. *International Journal of Molecular Sciences*. 2013;14:20597–613.
357. Belmadani S, Palen DI, Gonzalez-Villalobos RA, Boulares HA, Matrougui K. Elevated epidermal growth factor receptor phosphorylation induces resistance artery dysfunction in diabetic db/db mice. *Diabetes*. 2008;57:1629–37.

358. Liang D, Zhong P, Hu J, Lin F, Qian Y, Xu Z, et al. EGFR inhibition protects cardiac damage and remodeling through attenuating oxidative stress in STZ-induced diabetic mouse model. *Journal of Molecular and Cellular Cardiology*. 2015;82:63–74.
359. Zou C, Li W, Pan Y, Khan ZA, Li J, Wu X, et al. 11 β -HSD1 inhibition ameliorates diabetes-induced cardiomyocyte hypertrophy and cardiac fibrosis through modulation of EGFR activity. *Oncotarget*. 2017;8:96263-96275.
360. Neubauer A, Dodge RK, George SL, Davey FR, Silver RT, Schiffer CA, et al. Prognostic Importance of Mutations in the ras Proto-Oncogenes in De Novo Acute Myeloid Leukemia. *Blood*. 1994;83:1603–11.
361. Wang Y. Mitogen-activated protein kinases in heart development and diseases. *Circulation*. 2007;116:1413–1423.
362. Plotnikov A, Zehorai E, Procaccia S, Seger R. The MAPK cascades: Signaling components, nuclear roles and mechanisms of nuclear translocation. *Biochimica et Biophysica Acta - Molecular Cell Research*. 2011;1813:1619–33.
363. Westermann D, Rutschow S, van Linthout S, Linderer A, Bucker-Gärtner C, Sobirey M, et al. Inhibition of p38 mitogen-activated protein kinase attenuates left ventricular dysfunction by mediating pro-inflammatory cardiac cytokine levels in a mouse model of diabetes mellitus. *Diabetologia*. 2006;49:2507–13.
364. Tang M, Zhang W, Lin H, Jiang H, Dai H, Zhang Y. High glucose promotes the production of collagen types I and III by cardiac fibroblasts through a pathway dependent on extracellular-signal-regulated kinase 1/2. *Molecular and Cellular Biochemistry*. 2007;301:109–14.
365. Tang M, Zhong M, Shang Y, Lin H, Deng J, Jiang H, et al. Differential regulation of collagen types I and III expression in cardiac fibroblasts by AGEs through TRB3/MAPK signaling pathway. *Cellular and Molecular Life Sciences*. 2008;65:2924–32.
366. Luo B, Li B, Wang W, Liu X, Liu X, Xia Y, et al. Rosuvastatin alleviates diabetic cardiomyopathy by inhibiting NLRP3 inflammasome and MAPK pathways in a type 2 diabetes rat model. *Cardiovascular Drugs and Therapy*. 2014;28:33–43.
367. Hammoudi N, Jeong D, Singh R, Farhat A, Komajda M, Mayoux E, et al. Empagliflozin Improves Left Ventricular Diastolic Dysfunction in a Genetic Model of Type 2 Diabetes. *Cardiovascular Drugs and Therapy*. 2017;31:233–46.
368. Huang A, Yang YM, Yan C, Kaley G, Hintze TH, Sun D. Altered MAPK signaling in progressive deterioration of endothelial function in diabetic mice. *Diabetes*. 2012;61:3181–8.
369. Schiekofer S, Andrassy M, Chen J, Rudofsky G, Schneider J, Wendt T, et al. Acute Hyperglycemia Causes Intracellular Formation of CML and Activation of ras, p42/44 MAPK, and Nuclear Factor B in PBMCs. *Diabetes*. 2003;52:621–33.
370. Nick JA, Young SK, Brown KK, Avdi NJ, Arndt PG, Suratt BT, et al. Role of p38 Mitogen-Activated Protein Kinase in a Murine Model of Pulmonary Inflammation. *The Journal of Immunology*. The American Association of Immunologists; 2000;164:2151–9.
371. Wende AR, Abel ED. Lipotoxicity in the heart. *Biochimica et Biophysica Acta*. 2010. p. 311–9.

372. Janani C, Ranjitha Kumari BD. PPAR gamma gene - A review. *Diabetes and Metabolic Syndrome: Clinical Research and Reviews*. 2015;9:46–50.
373. Rangwala SM, Lazar MA. Peroxisome proliferator-activated receptor γ in diabetes and metabolism. *Trends in Pharmacological Sciences*. 2004. p. 331–6.
374. Burkart EM, Sambandam N, Han X, Gross RW, Courtois M, Gierasch CM, et al. Nuclear receptors PPAR β/δ and PPAR α direct distinct metabolic regulatory programs in the mouse heart. *Journal of Clinical Investigation*. 2007;117:3930–9.
375. Mori J, Patel VB, Alrob OA, Basu R, Altamimi T, DesAulniers J, et al. Angiotensin 1-7 ameliorates diabetic cardiomyopathy and diastolic dysfunction in db/db mice by reducing lipotoxicity and inflammation. *Circulation: Heart Failure*. 2014;7:327–39.
376. Liu L, Zhuang X, Jiang M, Guan F, Fu Q, Lin J. Angptl4 mediates the protective role of PPAR γ activators in the pathogenesis of preeclampsia. *Cell Death and Disease*. 2017;8.
377. Sadeghabadi ZA, Nourbakhsh M, Alaei M, Larijani B, Razzaghy-Azar M. Peroxisome proliferator-activated receptor gamma expression in peripheral blood mononuclear cells and angiopoietin-like protein 4 levels in obese children and adolescents. *Journal of Endocrinological Investigation*. 2018;41:241–7.
378. Mandard S, Zandbergen F, van Straten E, Wahli W, Kuipers F, Müller M, et al. The fasting-induced adipose factor/angiopoietin-like protein 4 is physically associated with lipoproteins and governs plasma lipid levels and adiposity. *Journal of Biological Chemistry*. 2006;281:934–44.
379. Cushing EM, Chi X, Sylvers KL, Shetty SK, Potthoff MJ, Davies BSJ. Angiopoietin-like 4 directs uptake of dietary fat away from adipose during fasting. *Molecular Metabolism*. 2017;6:809–18.
380. Moore KJ, Tabas I. Macrophages in the pathogenesis of atherosclerosis. *Cell*. 2011;145:341–55.
381. Purvis GSD, Solito E, Thiernemann C. Annexin-A1: Therapeutic potential in microvascular disease. *Frontiers in Immunology*. 2019;10.
382. Rentero C, Blanco-Muñoz P, Meneses-Salas E, Grewal T, Enrich C. Annexins—coordinators of cholesterol homeostasis in endocytic pathways. *International Journal of Molecular Sciences*. 2018;19:1444.
383. Shen X, Zhang S, Guo Z, Xing D, Chen W. The crosstalk of ABCA1 and ANXA1: A potential mechanism for protection against atherosclerosis. *Molecular Medicine*. 2020;26.
384. Qin C, Buxton KD, Pepe S, Cao AH, Venardos K, Love JE, et al. Reperfusion-induced myocardial dysfunction is prevented by endogenous annexin-A1 and its N-terminal-derived peptide Ac-ANX-A12-26. *British Journal of Pharmacology*. 2013;168:238–52.
385. Qin CX, May LT, Li R, Cao N, Rosli S, Deo M, et al. Small-molecule-biased formyl peptide receptor agonist compound 17b protects against myocardial ischaemia-reperfusion injury in mice. *Nature Communications*. 2017;8.
386. Kim C-W, Moon Y-A, Wook Park S, Cheng D, Joo Kwon H, Horton JD, et al. Induced polymerization of mammalian acetyl-CoA carboxylase by MIG12 provides a tertiary level of

- regulation of fatty acid synthesis. *Proceedings of the National Academy of Sciences of the United States of America*. 2010;107:9626-31.
387. Hunkeler M, Hagmann A, Stutfeld E, Chami M, Guri Y, Stahlberg H, et al. Structural basis for regulation of human acetyl-CoA carboxylase. *Nature*. 2018;558:470–4.
388. Westerbacka J, Kolak M, Kiviluoto T, Arkkila P, Sirén J, Hamsten A, et al. Genes involved in fatty acid partitioning and binding, lipolysis, monocyte/macrophage recruitment, and inflammation are overexpressed in the human fatty liver of insulin-resistant subjects. *Diabetes*. 2007;56:2759–65.
389. Rabold K, Aschenbrenner A, Thiele C, Boahen CK, Schiltmans A, Smit JWA, et al. Enhanced lipid biosynthesis in human tumor-induced macrophages contributes to their protumoral characteristics. *Journal for Immunotherapy of Cancer*. 2020;8.
390. Young SG, Fong LG. Lowering Plasma Cholesterol by Raising LDL Receptors — Revisited. *New England Journal of Medicine*. 2012;366:1154–5.
391. Zhang L, Reue K, Fong LG, Young SG, Tontonoz P. Feedback regulation of cholesterol uptake by the LXR-IDOL-LDLR axis. *Arteriosclerosis, Thrombosis, and Vascular Biology*. 2012;32:2541–6.
392. Kusters DHM, Chatrou ML, Willems BAG, de Saint-Hubert M, Bauwens M, van der Vorst E, et al. Pharmacological treatment with annexin A1 reduces atherosclerotic plaque burden in LDLR^{-/-} mice on Western Type Diet. *PLoS One*. 2015;10.
393. Rosenson RS, Bryan Brewer ; H, Davidson ; W Sean, Fayad ZA, Fuster V, Goldstein J, et al. Contemporary Reviews in Cardiovascular Medicine Cholesterol Efflux and Atheroprotection Advancing the Concept of Reverse Cholesterol Transport. *Circulation*. 2012;125:1905–19.
394. Zanotti I, Pedrelli M, Potì F, Stomeo G, Gomaraschi M, Calabresi L, et al. Macrophage, but not systemic, apolipoprotein e is necessary for macrophage reverse cholesterol transport in vivo. *Arteriosclerosis, Thrombosis, and Vascular Biology*. 2011;31:74–80.
395. Azzam KM, Fessler MB. Crosstalk between reverse cholesterol transport and innate immunity. *Trends in Endocrinology and Metabolism*. 2012;23:169–78.
396. Attie AD, Kastelein JP, Hayden MR. Pivotal role of ABCA1 in reverse cholesterol transport influencing HLD levels and susceptibility to atherosclerosis. *Journal of Lipid Research*. 2001;42:1717–26.
397. Bengtsson E, Hultman K, Edsfeldt A, Persson A, Nitulescu M, Nilsson J, et al. CD163⁺ macrophages are associated with a vulnerable plaque phenotype in human carotid plaques. *Scientific Reports*. 2020;10.
398. Haasken S, Auger JL, Taylor JJ, Hobday PM, Goudy BD, Titcombe PJ, et al. Macrophage Scavenger Receptor 1 (Msr1, SR-A) Influences B Cell Autoimmunity by Regulating Soluble Autoantigen Concentration. *The Journal of Immunology*. 2013;191:1055–62.
399. Uehara Y, Engel T, Li Z, Goepfert C, Rust S, Zhou X, et al. Polyunsaturated Fatty Acids and Acetoacetate Downregulate the Expression of the ATP-Binding Cassette Transporter A1. *Diabetes*. 2002;51:2922–8.

400. Mauldin JP, Srinivasan S, Mulya A, Gebre A, Parks JS, Daugherty A, et al. Reduction in ABCG1 in type 2 diabetic mice increases macrophage foam cell formation. *Journal of Biological Chemistry*. 2006;281:21216–24.
401. Nishimura M, Naito S. Tissue-specific mRNA Expression Profiles of Human ATP-binding Cassette and Solute Carrier Transporter Superfamilies. 2005;20:452-77.
402. Solbach TF, Kfnig J, Fromm MF, Zolk O. ATP-Binding Cassette Transporters in the Heart. 2006;16:7–15.
403. Wolf D, Ley K. Immunity and Inflammation in Atherosclerosis. *Circulation Research*. 2019;124:315–327.
404. Wang X, Collins HL, Ranalletta M, Fuki I v., Billheimer JT, Rothblat GH, et al. Macrophage ABCA1 and ABCG1, but not SR-BI, promote macrophage reverse cholesterol transport in vivo. *Journal of Clinical Investigation*. 2007;117:2216–24.
405. Yvan-Charvet L, Ranalletta M, Wang N, Han S, Terasaka N, Li R, et al. Combined deficiency of ABCA1 and ABCG1 promotes foam cell accumulation and accelerates atherosclerosis in mice. *Journal of Clinical Investigation*. 2007;117:3900–8.
406. Abacı A, Og A, Kahraman S, Kemal Eryol N, Arınç H, Ergin A. Effect of Diabetes Mellitus on Formation of Coronary Collateral Vessels. 1999;99:2239–2242.
407. Anthony Ware J, Simons M. Angiogenesis in ischemic heart disease. *Nature*. 1997;3:158–64.
408. Mouquet F, Cuilleret F, Susen S, Sautire K, Marboeuf P, Ennezat PV, et al. Metabolic syndrome and collateral vessel formation in patients with documented occluded coronary arteries: Association with hyperglycaemia, insulin-resistance, adiponectin and plasminogen activator inhibitor-1. *European Heart Journal*. 2009;30:840–9.
409. Jamaiyar A, Juguilon C, Dong F, Cumpston D, Enrick M, Chilian WM, et al. Cardioprotection during ischemia by coronary collateral growth. *American Journal of Physiology-Heart and Circulatory Physiology*. 2019;316:1–9.
410. Hou R, Shen M, Wang R, Liu H, Gao C, Xu J, et al. Thioredoxin1 Inactivation Mediates the Impairment of Ischemia-Induced Angiogenesis and Further Injury in Diabetic Myocardium. *Journal of Vascular Research*. 2020;57:76–85.
411. Hinkel R, Howe A, Renner S, Ng J, Lee S, Klett K, et al. Diabetes Mellitus-Induced Microvascular Destabilization in the Myocardium. *Journal of the American College of Cardiology*. 2017;69:131–43.
412. Hammes HP, Du X, Edelstein D, Taguchi T, Matsumura T, Ju Q, et al. Benfotiamine blocks three major pathways of hyperglycemic damage and prevents experimental diabetic retinopathy. *Nature Medicine*. 2003;9:294–9.
413. Tan X, Hu L, Shu Z, Chen L, Li X, Du M, et al. Role of CCR2 in the development of streptozotocin-treated diabetic cardiomyopathy. *Diabetes*. 2019;68:2063–73.
414. Kolattukudy PE, Niu J. Inflammation, endoplasmic reticulum stress, autophagy, and the monocyte chemoattractant protein-1/CCR2 pathway. *Circulation Research*. 2012;110:174–89.
415. Karimabad MN, Hassanshahi G. Significance of CXCL12 in Type 2 Diabetes Mellitus and Its Associated Complications. *Inflammation*. 2015;38:710–7.

416. Cavallero S, Shen H, Yi C, Lien CL, Kumar SR, Sucov HM. CXCL12 Signaling is Essential for Maturation of the Ventricular Coronary Endothelial Plexus and Establishment of Functional Coronary Circulation. *Developmental Cell*. 2015;33:469–77.
417. Rattan V, Shen Y, Sultana C, Kumar D, Kalra VK. Glucose-induced transmigration of monocytes is linked to phosphorylation of PECAM-1 in cultured endothelial cells. *American Journal of Physiology*. 1996;271:711–7.
418. Eshaq RS, Harris NR. The role of tumor necrosis factor- α and interferon- γ in the hyperglycemia-induced ubiquitination and loss of platelet endothelial cell adhesion molecule-1 in rat retinal endothelial cells. *Microcirculation*. 2021;28:e12717.
419. Eshaq RS, Harris NR. Loss of platelet endothelial cell adhesion Molecule-1 (PECAM-1) in the diabetic retina: Role of matrix metalloproteinases. *Investigative Ophthalmology and Visual Science*. 2019;60:748–60.
420. Scallan JP, Zawieja SD, Castorena-Gonzalez JA, Davis MJ. Lymphatic pumping: mechanics, mechanisms and malfunction. *Journal of Physiology*. 2016;594:5749–68.
421. Harvey NL, Srinivasan RS, Dillard ME, Johnson NC, Witte MH, Boyd K, et al. Lymphatic vascular defects promoted by Prox1 haploinsufficiency cause adult-onset obesity. *Nature Genetics*. 2005;37:1072–81.
422. Norden PR, Kume T. The Role of Lymphatic Vascular Function in Metabolic Disorders. *Frontiers in Physiology*. 2020;11:404.
423. Montani JP, Carroll JF, Dwyer TM, Antic V, Yang Z, Dulloo AG. Ectopic fat storage in heart, blood vessels and kidneys in the pathogenesis of cardiovascular diseases. *International Journal of Obesity*. 2004;28:S58–65.
424. Bundred N, Foden P, Todd C, Morris J, Watterson D, Purushotham A, et al. Increases in arm volume predict lymphoedema and quality of life deficits after axillary surgery: a prospective cohort study. *British Journal of Cancer*. Springer Nature; 2020;123:17–25.
425. Shallwani SM, Hodgson P, Towers A. Examining obesity in lymphedema: A retrospective study of 178 new patients with suspected lymphedema at a Canadian hospital-based clinic. *Physiotherapy Canada*. 2020;72:18–25.
426. Larsson L, Frisén J, Lundeberg J. Spatially resolved transcriptomics adds a new dimension to genomics. *Nature Methods*. 2021;18:15–8.
427. Majmudar MD, Keliher EJ, Heidt T, Leuschner F, Truelove J, Sena BF, et al. Monocyte-directed RNAi targeting CCR2 improves infarct healing in atherosclerosis-prone mice. *Circulation*. 2013;127:2038–46.
428. Saederup N, Cardona AE, Croft K, Mizutani M, Cotleur AC, Tsou CL, et al. Selective chemokine receptor usage by central nervous system myeloid cells in CCR2-red fluorescent protein knock-in mice. *PLoS One*. 2010;5.
429. Zhang H, Yang Z, Zhang W, Niu Y, Li X, Qin L, et al. White blood cell subtypes and risk of type 2 diabetes. *Journal of Diabetes and its Complications*. 2017;31:31–7.

430. Borné Y, Smith JG, Nilsson PM, Melander O, Hedblad B, Engström G. Total and differential leukocyte counts in relation to incidence of diabetes mellitus: A prospective population-based cohort study. *PLoS One*. 2016;11.
431. Kuo TY, Wu CZ, Lu CH, Lin JD, Liang YJ, Hsieh CH, et al. Relationships between white blood cell count and insulin resistance, glucose effectiveness, and first- and second-phase insulin secretion in young adults. *Medicine*. 2020;99:e22215.
432. Gutensohn K, Magens M, Krüger W, Kröger N, Kühnl P. Comparison of flow cytometry vs. a haematology cell analyser-based method to guide the optimal time-point for peripheral blood stem cell apheresis. *Vox Sanguinis*. 2006;90:53–8.
433. Dzik S, Moroff G, Dumont L. A multicenter study evaluating three methods for counting residual WBCs in WBC-reduced blood components: Nageotte hemocytometry, flow cytometry, and microfluorometry. *Transfusion*. 2000;40:513–20.
434. Wall VZ, Barnhart S, Kanter JE, Kramer F, Shimizu-Albergine M, Adhikari N, et al. Smooth muscle glucose metabolism promotes monocyte recruitment and atherosclerosis in a mouse model of metabolic syndrome. *JCI Insight*. 2018;3.
435. Yang J, Zhang L, Yu C, Yang XF, Wang H. Monocyte and macrophage differentiation: Circulation inflammatory monocyte as biomarker for inflammatory diseases. *Biomarker Research*. 2014;2.
436. Shi C, Pamer EG. Monocyte recruitment during infection and inflammation. *Nature Reviews Immunology*. 2011;11:762–74.
437. Kapellos TS, Bonaguro L, Gemünd I, Reusch N, Saglam A, Hinkley ER, et al. Human monocyte subsets and phenotypes in major chronic inflammatory diseases. *Frontiers in Immunology*. 2019;10:1–13.
438. Soma P, Swanepoel AC, du Plooy JN, Mqoco T, Pretorius E. Flow cytometric analysis of platelets type 2 diabetes mellitus reveals “angry” platelets. *Cardiovascular Diabetology*. 2016;15.
439. Springhorn C, Matsha TE, Erasmus RT, Essop MF. Exploring leukocyte O-GlcNAcylation as a novel diagnostic tool for the earlier detection of type 2 diabetes mellitus. *Journal of Clinical Endocrinology and Metabolism*. 2012;97:4640–9.
440. Tuchin V, Tarnok A, Zharov VP, . *In Vivo Flow Cytometry : A Horizon of Opportunities*. *Cytometry A*. 2013;79:737-745.
441. Nikolich-Zugich J. The twilight of immunity: Emerging concepts in aging of the immune system review-article. *Nature Immunology*. 2018;19:10–9.
442. Shen L, Chng MHY, Alonso MN, Yuan R, Winer DA, Engleman EG. B-1a lymphocytes attenuate insulin resistance. *Diabetes*. 2015;64:593–603.
443. Silveira PA, Grey ST. B cells in the spotlight: innocent bystanders or major players in the pathogenesis of type 1 diabetes. *Trends in Endocrinology and Metabolism*. 2006;17:128-35.
444. Singh K, Martinell M, Luo Z, Espes D, Stålhammar J, Sandler S, et al. Cellular immunological changes in patients with LADA are a mixture of those seen in patients with type 1 and type 2 diabetes. *Clinical and Experimental Immunology*. 2019;197:64–73.

445. Felton JL, Maseda D, Bonami RH, Hulbert C, Thomas JW. Anti-Insulin B Cells Are Poised for Antigen Presentation in Type 1 Diabetes. *The Journal of Immunology*. 2018;201:861–73.
446. Deng C, Xiang Y, Tan T, Ren Z, Cao C, Huang G, et al. Altered peripheral B-lymphocyte subsets in type 1 diabetes and latent autoimmune diabetes in adults. *Diabetes Care*. 2016;39:434–40.
447. Cipolletta C, Ryan KE, Hanna E v, Trimble ER. Activation of Peripheral Blood CD14 Monocytes Occurs in Diabetes. *Diabetes*. 2005;54:2779–86.
448. Komura T, Sakai Y, Honda M, Takamura T, Matsushima K, Kaneko S. CD14+ monocytes are vulnerable and functionally impaired under endoplasmic reticulum stress in patients with type 2 diabetes. *Diabetes*. 2010;59:634–43.
449. Poitou C, Dalmas E, Renovato M, Benhamo V, Hajduch F, Abdenmour M, et al. CD14-CD16+ and CD14+CD16+ monocytes in obesity and during weight loss: Relationships with fat mass and subclinical atherosclerosis. *Arteriosclerosis, Thrombosis, and Vascular Biology*. 2011;31:2322–30.
450. Rothe G, Herr AS, Stöhr J, Abletshauser C, Weidinger G, Schmitz G. A more mature phenotype of blood mononuclear phagocytes is induced by fluvastatin treatment in hypercholesterolemic patients with coronary heart disease. *Atherosclerosis*. 1999;144:251–61.
451. Yoshida N, Yamamoto H, Shinke T, Otake H, Kuroda M, Terashita D, et al. Impact of CD14++CD16+ monocytes on plaque vulnerability in diabetic and non-diabetic patients with asymptomatic coronary artery disease: A cross-sectional study. *Cardiovascular Diabetology*. 2017;16.
452. Lou M, Luo P, Tang R, Peng Y, Yu S, Huang W, et al. Relationship between neutrophil-lymphocyte ratio and insulin resistance in newly diagnosed type 2 diabetes mellitus patients. *BMC Endocrine Disorders*. 2015;15.
453. Huang J, Xiao Y, Xu A, Zhou Z. Neutrophils in type 1 diabetes. *Journal of Diabetes Investigation*. 2016;7:652–63.
454. Lin Q, Zhou W, Wang Y, Huang J, Hui X, Zhou Z, et al. Abnormal peripheral neutrophil transcriptome in newly diagnosed type 2 diabetes patients. *Journal of Diabetes Research*. 2020;9519072.
455. He Z, Ryan P, Hoxha J, Wang S, Carini S, Sim I, et al. Multivariate analysis of the population representativeness of related clinical studies. *Journal of Biomedical Informatics*. 2016;60:66–76.
456. Lord JM, Butcher S, Killampali V, Lascelles D, Salmon M. Neutrophil ageing and immunesenescence. *Mechanisms of Ageing and Development*. 2001;122:1521–35.
457. Aprahamian T, Takemura Y, Goukassian D, Walsh K. Ageing is associated with diminished apoptotic cell clearance in vivo. *Clinical and Experimental Immunology*. 2008;152:448–55.
458. Montgomery RR, Shaw AC. Paradoxical changes in innate immunity in aging: recent progress and new directions. *Journal of Leukocyte Biology*. 2015;98:937–43.
459. Serra JA, Ribera JM, Pé Rez-blas M, Regueiro JR, Ban A, Jover JA. Functional integrity of the CD28 co-stimulatory pathway in T lymphocytes from elderly subjects. *Age and Ageing*. 1999;28:221–7.

460. Aydar Y, Eter Balogh P', Tew JG, Szakal AK. Age-related depression of FDC accessory functions and CD21 ligand-mediated repair of co-stimulation. *European Journal of Immunology*. 2002;32:2817–26.
461. Qi Q, Liu Y, Cheng Y, Glanville J, Zhang D, Lee JY, et al. Diversity and clonal selection in the human T-cell repertoire. *Proceedings of the National Academy of Sciences of the United States of America*. 2014;111:13139–44.
462. Zhuge F, Ni Y, Nagashimada M, Nagata N, Xu L, Mukaida N, et al. DPP-4 inhibition by linagliptin attenuates obesity-related inflammation and insulin resistance by regulating M1/M2 macrophage polarization. *Diabetes*. 2016;65:2966–79.
463. Jing Y, Wu F, Li D, Yang L, Li Q, Li R. Metformin improves obesity-associated inflammation by altering macrophages polarization. *Molecular and Cellular Endocrinology*. 2018;461:256–64.
464. Radlinger B, Hornsteiner F, Folie S, Salvenmoser W, Haubner BJ, Schuetz T, et al. Cardioprotective effects of short-term empagliflozin treatment in db/db mice. *Scientific Reports*. 2020;10.
465. Iannantuoni F, de Mara  n AM, Diaz-Morales N, Falcon R, Ba  uls C, Abad-Jimenez Z, et al. The SGLT2 inhibitor empagliflozin ameliorates the inflammatory profile in type 2 diabetic patients and promotes an antioxidant response in leukocytes. *Journal of Clinical Medicine*. 2019;8.
466. Agarwal R, Roudebush RL. Anti-inflammatory effects of short-term pioglitazone therapy in men with advanced diabetic nephropathy. *The American Journal of Physiology - Renal Physiology*. 2006;290:600–5.
467. Thomas GD, Hamers AAJ, Nakao C, Marcovecchio P, Taylor AM, McSkimming C, et al. Human Blood Monocyte Subsets: A New Gating Strategy Defined Using Cell Surface Markers Identified by Mass Cytometry. *Arteriosclerosis, Thrombosis, and Vascular Biology*. 2017;37:1548–58.
468. Rubler S, Dlugash J, Yuceoglu YZ, Kumral T, Branwood AW, Grishman A. New type of cardiomyopathy associated with diabetic glomerulosclerosis. *The American Journal of Cardiology*. 1972;30:595–602.
469. Kannel WB, Hjortland M, Castelli WP. Role of diabetes in congestive heart failure: The Framingham study. *The American Journal of Cardiology*. 1974;34:29–34.
470. Pearson ER. Type 2 diabetes: a multifaceted disease. *Diabetologia*. 2019;62:1107–12.
471. Nagueh SF, Appleton CP, Gillebert TC, Marino PN, Oh JK, Smiseth OA, et al. Recommendations for the Evaluation of Left Ventricular Diastolic Function by Echocardiography. *Journal of the American Society of Echocardiography*. 2009;22:107–33.
472. Nagueh SF, Middleton KJ, Kopelen HA, Zoghbi WA, Qui  ones MA. Doppler tissue imaging: A noninvasive technique for evaluation of left ventricular relaxation and estimation of filling pressures. *Journal of the American College of Cardiology*. 1997;30:1527–33.
473. Zhou P, Pu WT. Recounting cardiac cellular composition. *Circulation Research*. 2016;118:368–370

474. Hilgendorf I, Gerhardt LMS, Tan TC, Winter C, Holderried TAW, Chousterman BG, et al. Ly-6C high monocytes depend on nr4a1 to balance both inflammatory and reparative phases in the infarcted myocardium. *Circulation Research*. 2014;114:1611–22.
475. Wang S, Ding L, Ji H, Xu Z, Liu Q, Zheng Y. The role of p38 MAPK in the development of diabetic cardiomyopathy. *International Journal of Molecular Sciences*. 2016;17:1037.
476. Adhikary L, Chow F, Nikolic-Paterson DJ, Stambe C, Dowling J, Atkins RC, et al. Abnormal p38 mitogen-activated protein kinase signalling in human and experimental diabetic nephropathy. *Diabetologia*. 2004;47:1210–22.
477. Lim AKH, Nikolic-Paterson DJ, Ma FY, Ozols E, Thomas MC, Flavell RA, et al. Role of MKK3-p38 MAPK signalling in the development of type 2 diabetes and renal injury in obese db/db mice. *Diabetologia*. 2009;52:347–58.
478. Jia G, Hill MA, Sowers JR. Diabetic cardiomyopathy: An update of mechanisms contributing to this clinical entity. *Circulation Research*. 2018;122:624–38.
479. Arnold AC, Robertson D. Defective Wnt signaling: A potential contributor to cardiometabolic disease? *Diabetes*. 2015;64:3342–4.
480. Akhmetshina A, Palumbo K, Dees C, Bergmann C, Venalis P, Zerr P, et al. Activation of canonical Wnt signalling is required for TGF- β -mediated fibrosis. *Nature Communications*. 2012;3.
481. Souilhol C, Harmsen MC, Evans PC, Krenning G. Endothelial-mesenchymal transition in atherosclerosis. *Cardiovascular Research*. 2018;114:565-577.
482. Cao E, Watt MJ, Nowell CJ, Quach T, Simpson JS, de Melo Ferreira V, et al. Mesenteric lymphatic dysfunction promotes insulin resistance and represents a potential treatment target in obesity. *Nature Metabolism*. 2021;3:1175–88.
483. Greene AK, Grant FD, Slavin SA. Lower-Extremity Lymphedema and Elevated Body-Mass Index. *New England Journal of Medicine*. 2016;366:2136–7.
484. Vasileiou AM, Bull R, Kitou D, Alexiadou K, Garvie NJ, Coppack SW. Oedema in obesity; Role of structural lymphatic abnormalities. *International Journal of Obesity*. 2011;35:1247–50.
485. Zawieja SD, Wang W, Wu X, Nepiyushchikh Z v., Zawieja DC, Muthuchamy M. Impairments in the intrinsic contractility of mesenteric collecting lymphatics in a rat model of metabolic syndrome. *American Journal of Physiology - Heart and Circulatory Physiology*. 2012;302.
486. Simonavicius N, Ashenden M, van Weverwijk A, Lax S, Huso DL, Buckley CD, et al. Pericytes promote selective vessel regression to regulate vascular patterning. *Blood*. 2012;120:1516–27.
487. Lin SL, Kisseleva T, Brenner DA, Duffield JS. Pericytes and perivascular fibroblasts are the primary source of collagen-producing cells in obstructive fibrosis of the kidney. *American Journal of Pathology*. 2008;173:1617–27.
488. Clarke MCH, Talib S, Figg NL, Bennett MR. Vascular smooth muscle cell apoptosis induces interleukin-1-directed inflammation: Effects of hyperlipidemia-mediated inhibition of phagocytosis. *Circulation Research*. 2010;106:363–72.
489. Kolattukudy PE, Niu J. Inflammation, endoplasmic reticulum stress, autophagy, and the monocyte chemoattractant protein-1/CCR2 pathway. *Circulation Research*. 2012;110:174–189.

490. Martinovic I, Abegunewardene N, Seul M, Vosseler M, Horstick G, Buerke M, et al. Elevated Monocyte Chemoattractant Protein-1 Serum Levels in Patients at Risk for Coronary Artery Disease. *Circulation Journal*. 2005;69:1484–9.
491. Deo R, Khera A, McGuire DK, Murphy SA, de P. Meo Neto J, Morrow DA, et al. Association among plasma levels of monocyte chemoattractant protein-1, traditional cardiovascular risk factors, and subclinical atherosclerosis. *Journal of the American College of Cardiology*. 2004;44:1812–8.
492. Tan X, Hu L, Shu Z, Chen L, Li X, Du M, et al. Role of CCR2 in the development of streptozotocin-treated diabetic cardiomyopathy. *Diabetes*. 2019;68:2063–73.
493. McLellan MA, Rosenthal NA, Pinto AR. Cre-loxP-Mediated Recombination: General Principles and Experimental Considerations. *Current Protocols in Mouse Biology* 2017;7:1–12.
494. Wagner DE, Klein AM. Lineage tracing meets single-cell omics: opportunities and challenges. *Nature Reviews Genetics*. 2020;21:410–27.
495. Yata Y, Scanga A, Gillan A, Yang L, Reif S, Breindl M, et al. DNase I-hypersensitive sites enhance $\alpha 1(I)$ collagen gene expression in hepatic stellate cells. *Hepatology*. 2003;37:267–76.
496. Kaczmarczyk SJ, Andrikopoulos S, Favaloro J, Domenighetti AA, Dunn A, Ernst M, et al. Threshold effects of glucose transporter-4 (GLUT4) deficiency on cardiac glucose uptake and development of hypertrophy. *Journal of Molecular Endocrinology*. 2003;31:449–59.
497. Domenighetti AA, Danes VR, Curl CL, Favaloro JM, Proietto J, Delbridge LMD. Targeted GLUT-4 deficiency in the heart induces cardiomyocyte hypertrophy and impaired contractility linked with Ca^{2+} and proton flux dysregulation. *Journal of Molecular and Cellular Cardiology*. 2010;48:663–72.
498. Wang J, Xu E, Elliott MH, Zhu M, Le YZ. Müller cell-derived VEGF is essential for diabetes-induced retinal inflammation and vascular leakage. *Diabetes*. 2010;59:2297–305.
499. Karlstad MD, Jason Collier J, Eder AE, Boulos MS, Batdorf HM, Noland RC, et al. db / db Mice Exhibit Features of Human Type 2 Diabetes That Are Not Present in Weight-Matched C57BL/6J Mice Fed a Western Diet . *Journal of Diabetes Research*. 2017;2017:1–17.
500. Sattar N, Lee MMY, Kristensen SL, Branch KRH, del Prato S, Khurmi NS, et al. Cardiovascular, mortality, and kidney outcomes with GLP-1 receptor agonists in patients with type 2 diabetes: a systematic review and meta-analysis of randomised trials. *The Lancet Diabetes & Endocrinology*. 2021;9.
501. McGuire DK, Shih WJ, Cosentino F, Charbonnel B, Cherney DZI, Dagogo-Jack S, et al. Association of SGLT2 inhibitors with cardiovascular and kidney outcomes in patients with type 2 diabetes: A Meta-analysis. *JAMA Cardiology*. 2021;6:148–58.

Chapter 9

Appendix

9.1 Review: New perspectives of the cardiac cellular landscape: mapping cellular mediators of cardiac fibrosis using single-cell transcriptomics

Crisdion Krstevski^{1,2*}, **Charles D. Cohen**^{1,2*}, Malathi S.I. Dona¹ and Alexander R. Pinto^{1,2}

** indicates equal authorship*

DOI: https://doi.org/10.1042/BST-2019-1255C_COR

¹Cardiac Cellular Systems, Baker Heart and Diabetes Institute, Prahran, VIC, Australia; ²Centre for Cardiovascular Biology and Disease Research, La Trobe University, Melbourne, VIC, Australia

9.1.1 Statement of contributions

Name	Nature of contribution
Crisdion Krstevski*	Collated relevant literature, prepared initial draft of the manuscript, prepared figures, edited the manuscript.
Charles D. Cohen*	Collated relevant literature, prepared initial draft of the manuscript, prepared figures, edited the manuscript.
Malathi S.I. Dona	Prepared figures, edited the manuscript.
Alexander R. Pinto	Collated relevant literature, prepared initial draft of the manuscript, prepared figures, edited the manuscript, and approved the final manuscript.

Review Article

New perspectives of the cardiac cellular landscape: mapping cellular mediators of cardiac fibrosis using single-cell transcriptomics

Crisdion Krstevski^{1,2,*}, Charles D. Cohen^{1,2,*}, Malathi S.I. Dona¹ and  Alexander R. Pinto^{1,2}

¹Cardiac Cellular Systems, Baker Heart and Diabetes Institute, Prahran, VIC, Australia; ²Centre for Cardiovascular Biology and Disease Research, La Trobe University, Melbourne, VIC, Australia

Correspondence: Alexander R. Pinto (alex.pinto@baker.edu.au)

Single-cell transcriptomics enables inference of context-dependent phenotypes of individual cells and determination of cellular diversity of complex tissues. Cardiac fibrosis is a leading factor in the development of heart failure and a major cause of morbidity and mortality worldwide with no effective treatment. Single-cell RNA-sequencing (scRNA-seq) offers a promising new platform to identify new cellular and molecular protagonists that may drive cardiac fibrosis and development of heart failure. This review will summarize the application scRNA-seq for understanding cardiac fibrosis and development of heart failure. We will also discuss some key considerations in interpreting scRNA-seq data and some of its limitations.

Introduction

The extracellular matrix (ECM) is the three-dimensional framework of macromolecules that provides structural, mechanical and signaling support to surrounding cells. Comprised of polysaccharides and proteins such as collagens, laminin and elastin, the ECM has broad effects on tissue and cellular function [1,2]. These include cell signaling through integrins — cell surface proteins that bind ECM macromolecules — and receptors for other factors that interact with the ECM [3]. Moreover, the ECM can regulate cell motility and mechanical function of a tissue [4,5]. The latter is particularly pertinent to the heart where rhythmic movement is critical for cardiac function. Therefore, the ECM is highly and dynamically regulated by an array of enzymes such as *matrix metalloproteinases* (MMPs) and *tissue inhibitory metalloproteinases* (TIMPs), extensively reviewed in [6]. Excess accumulation of ECM can have deleterious physiological effects and is referred to as fibrosis.

While fibrosis has been studied for many decades in the context of the heart, new technical advances — such as single-cell transcriptomics — is providing a new and detailed picture of the complex and orchestrated cellular events driving cardiac fibrosis. This mini-review aims to summarize some of these recent developments, and some key limitations and future applications of single-cell transcriptomics for understanding cardiac fibrosis.

Major types of fibrosis

Fibrosis is heterogeneous, and can differ in composition, tissue localization and the pathophysiology that initiates its development. In the heart, fibrosis can be classified to at least three major types: (i) interstitial fibrosis; (ii) perivascular fibrosis; and (iii) replacement fibrosis [7] (Figure 1). Interstitial fibrosis is the pathological accumulation of ECM within the interstitium — in the heart, the fluid-filled space between cardiomyocytes and supporting stromal cells. Interstitial fibrosis is particularly associated with chronic physiological stresses such as hypertension [8] and diabetes [9–11]. It can lead to impaired relaxation and filling of the heart ventricles after contraction (diastolic dysfunction) and is particularly associated with heart failure with preserved ejection fraction (HFpEF) — one of the

*These authors contributed equally to this work.

Received: 21 September 2020

Revised: 27 October 2020

Accepted: 29 October 2020

Version of Record published:
1 December 2020

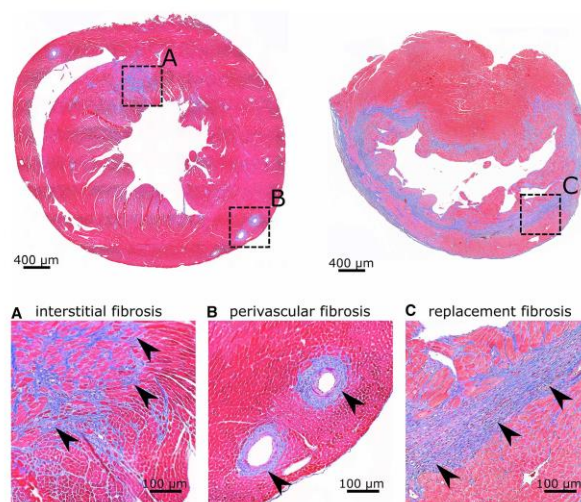


Figure 1. Key types of cardiac fibrosis in the hearts from AngII-treated and MI-day 7.

Representative bright-field micrographs of Masson's trichrome stained mouse heart sections. Blue staining indicates tissue fibrosis. Magnified views show interstitial (A) and perivascular fibrosis (B) in a heart of an Angiotensin II treated (2 weeks, 1.4 mg/kg) mouse and replacement fibrosis in mouse heart (C) seven days post-experimental myocardial infarction. Arrows indicate regions of fibrosis.

fastest-growing cardiac morbidities [12]. Perivascular fibrosis describes the pathological accumulation of ECM surrounding the adventitia of major blood vessels (Figure 1). The increase in collagen I and II deposition obstructs blood flow and ultimately leading to impaired vascular function, tissue hypoxia and cell loss [13–15]. Impaired coronary flow is a key clinical feature of patients with HF due to hypertensive heart disease [13] or hypertrophic cardiomyopathy [16]. Finally, replacement fibrosis occurs after heart injury such as myocardial infarction (MI) to replace lost cardiomyocytes and tissue mass. Unlike interstitial fibrosis, replacement fibrosis typically results in a scar that stabilizes vascular wall integrity. The establishment of the scar follows an orchestrated cellular response to heart injury which can be divided to three phases: 'inflammatory', 'proliferative' and 'maturation' [17]. The inflammatory response to damaged or dying cardiomyocytes begins with the degranulation of non-nucleated cells such as platelets [18], followed by the rapid recruitment of neutrophils that accumulate within ischemic lesion within hours [19,20]. Following this, macrophages differentiating from circulating monocytes, become the dominant cardiac cell type, participating in phagocytosis of tissue debris and efferocytosis [21]. During the subsequent 'proliferative phase', macrophages contribute to the resolution of inflammation and decline in number, with angiogenesis and development of myofibroblasts (reviewed recently [22]). In the maturation phase, differentiation of myofibroblasts recedes and the scar matures comprising specialized fibroblasts that persist in the scar [23].

It is a prevailing view that the primary cellular driver of fibrosis are myofibroblasts [24,25]. Multiple pathways have been identified that promote myofibroblasts differentiation, including TGF β [26], angiotensin II (AngII) [27] and 'Wingless-related integration site' (WNT) [28] signaling pathways. Of these, TGF β is the predominant, which with mechanical stress, is critical for myofibroblast differentiation [29,30]. Myofibroblasts provide mechanical support to stress of damaged hearts with an expression of hallmark genes such as *alpha smooth-muscle actin* (ACTA2) [30,31]. However, single-cell transcriptomics has altered our view of myofibroblasts and other fibrogenic cell types in cardiac fibrosis, and also challenged the concept that myofibroblasts are integral for all forms of fibrosis.

Single-cell transcriptomics

Single-cell 'omics' is the quantification of an analyte following isolation of individual cells either physically or spatially. Many types of single-cell omics exist with more recent single-cell omics technologies enabling analysis of DNA [32], RNA [33], chromatin states [34], methylation [35] and proteins [36]. Here we focus on single-cell RNA sequencing (scRNA-seq), which is the most frequently applied of these new single-cell technologies.

Single-cell transcriptomics aims to resolve individual cellular transcriptomes to infer cellular phenotypes and diversity. There are currently various approaches that have been developed with the most common requiring analysis of single-cell or single-nucleus suspensions [37]. Three commonly used approaches include: deposition of individual cells into micro-wells [38]; 'split-pool' sequencing where transcripts of individual cells are processed for sequencing within individual cells or nuclei [39]; and droplet-based sequencing, where individual cells are processed in reagent filled droplets suspended in oil [40–43]. All three approaches yield cDNA with DNA sequences identifying individual RNA molecules with *unique molecular identifiers* (UMIs) [44] and the cell of origin. The cDNA is then sequenced before subsequent data analysis.

Data generated in scRNA-seq studies are large and complex. Multiple software packages and pipelines are available to process the datasets with common outputs. Most analyses will, for example, display cellular diversity of scRNA-seq data presented as scatter dot plots. Two- or three-dimensional coordinates for dots corresponding to cells are determined from 'dimensionality reduction' algorithms such as *principal component analysis* (PCA), *t-distributed stochastic neighbor embedding* (t-SNE) or *uniform manifold approximation and projection* (UMAP) [45,46]. These plots typically show cellular diversity as clusters or sub-clusters corresponding to cell types and subtypes, respectively (Figure 2). Following determination of cell clusters, a wide range of analyses can be performed to compare distinct gene expression profiles between cell populations and conditions. While this is a powerful approach for studying cellular landscapes, a number of parameters influence



Figure 2. Emergence of new fibrogenic cell types in the stressed murine heart.

tSNE visualization of hearts cells from mice undergone experimental myocardial infarction (A, A' and A'') [62] or Ang-II-induced cardiac fibrosis (B, B' and B'') [56]. Each dot represents a cell. Cells were clustered based on their gene expression patterns where 'islands' of cells represent distinct cell populations. Cells in A'-A'' and B'-B'' are colored based on average transcript expression level of *Postn* (a key fibrosis-associated gene). Note, mapping of cells in two-dimensional tSNE space is divided into hexagonal bins to avoid the bias of over-lapping cells (A'-A'' and B'-B'').

how the data may be interpreted. For example, the number of clusters identified may be due to arbitrary settings applied during the course of data analysis. Alternatively, data quality filtering parameters such as a minimum number of genes/cell or mitochondrial gene proportion may bias which cell types are included in the final data output and therefore inferences of cellular diversity (Table 1). Low numbers of genes detected per cell may limit the ability to resolve true cellular subtypes (for example subtypes of T cells). This may particularly concern approaches such as single-nuclei RNA sequencing where low genes/cell are typically detected. Finally, the tissue dissociation strategy for preparation of cell suspensions may vastly affect the quantity, diversity and quality of cells analyzed and interpreted results [47,48].

The cellulome of the homeostatic heart

The mammalian heart is a complex ecosystem of diverse and interconnected cell types. Although, the vast majority of cardiac muscle volume is composed of cardiomyocytes, non-myocytes are more abundant [48]. Indeed, for many years the prevailing view was that fibroblasts are the most abundant cell type in the heart [49], however recent research has shown that these cells are less prevalent. Endothelial cells are the most abundant cardiac cell population [48]. Given the substantial metabolic activity of the heart [50], the high proportion of endothelial cells is comprehensible. Smooth muscle cells and pericytes as well as a variety of immune cells, (predominantly macrophages), also contribute to the other major non-myocyte cell types [21,51]. The heterogeneity of non-myocytes underscores the diverse array of functions required for maintaining cardiac homeostasis. However, beyond providing structural, and house-keeping support, non-myocytes are also required for basic rudimentary physiological functioning of the heart, such as rhythmic beating, with electrical coupling of cells such as endothelial cells, fibroblasts and macrophages [52–54].

Table 1. Single-cell transcriptomic studies investigating cellular and molecular drivers of cardiac fibrosis in heart failure

Context	Reference	Cells	Mean Reads/cell	Technology	Notes and key findings
Mouse myocardial infarction	[97]	426	16 874	Sort-Seq	3-days post-MI and sham control mice <i>n</i> = 3/group <i>Ckap4</i> proposed as a novel driver of myofibroblast differentiation.
Mouse myocardial infarction	[60]	13 331	~35 000	10X Chromium	3- and 7-days post-MI and sham control <i>n</i> = 1/time point/group Identified heterogeneous fibroblast and myofibroblast subsets involved in fibrosis.
Mouse hypertension (Angiotensin II infusion)	[59]	29 615	~80 000	10X Chromium	2 weeks AngII-induced experimental hypertension and control mice <i>n</i> = 4/sex/group Novel fibroblasts <i>Fibro-Clp</i> and <i>Fibro-Thbs4</i> implicated in AngII-induced fibrosis Almost all cardiac cell types contribute to ECM remodeling after AngII treatment Extensive cell and sex-specific gene expression patterns in the non-stressed and stressed hearts.
Mouse myocardial infarction	[65]	36 874	~46 000	10X Chromium	1, 3, 5, 7, 14- and 28-days post-MI and sham control <i>n</i> = ~3/group. Identified heterogeneous fibroblast and myofibroblast subsets involved in fibrosis Early differentiation of myofibroblasts are associated with cardiac rupture.
Healthy and heart failure human patients	[96]	21 422	~300 000 (Median reads/cell)	iCell8	Healthy organ donors and patients with HF <i>n</i> = 14 healthy controls, 8 HF patients Endothelial cells and fibroblasts are key players in cellular crosstalk in progression of HF

Expanding our understanding of the heart, scRNA-seq has provided substantial new detail regarding the phenotypes and interconnectedness of disparate cardiac cell types [55–59]. For instance, we have gained novel insights into the cell types that support macrophages, which are highly dependent on *colony stimulating factor 1 receptor* (CSF1R) signaling for cell viability and chemotaxis [55,60,61]. scRNA-seq has shown that fibroblasts are the key trophic cell type for supporting cardiac macrophage viability [55], with epicardial cells — cells that form the single-cell outer layer of the heart — the most highly enriched cell type for *Csf1* transcripts [56]. Moreover, pericytes were also identified as highly expressing *interleukin-34* (Il34), an alternative ligand for CSF1R, suggesting that they too have capacity to support macrophages [55,56]. Moreover, cardiomyocytes were determined as the primary support cell type for endothelial cells, with high enrichment of transcripts corresponding to *Vegfa* — the dominant endothelial growth factor [56]. Finally, pericytes and smooth muscle cells were highly enriched for *nerve growth factor* and *neurotrophin 3* transcripts suggesting important neurotrophic activity of these cells [55,56]. These observations highlight the interconnectedness of the cardiac cellome.

scRNA-seq identifies new players in cardiac ECM maintenance in homeostasis

Confirming well-established paradigms of the roles of fibroblasts in the heart, scRNA-seq shows that fibroblasts are the primary ECM-producing cell type in the homeostatic heart. However, scRNA-seq has revealed new cellular complexity within cardiac fibroblasts, most notably identifying a new and distinct fibroblast population characterized by the distinct expression of *Wnt inhibitory factor 1* ('*Wif1*') [55,62]. These fibroblasts ('Fibroblast-*Wif1*') are dispersed throughout the myocardium and highly express the fibrosis-associated marker periostin (*Postn*; Figure 2) [56,62]. They are also enriched for transcripts corresponding to genes associated with fibrillogenesis and inhibition of TGF β and WNT pathways and fibrillogenesis [63,64], such as *Wif1*, *Fmod* and *Cilp* [23,33,55,62,65]. However, little is known of these cells and their relative importance for cardiac homeostasis.

An array of fibroblast and myofibroblast subtypes emerge after acute cardiac injury

Given the relatively recent availability of scRNA-seq approaches for profiling cellular diversity, there are very few studies that have examined the impact of acute and chronic physiological stresses on the development of cardiac pathology and fibrosis (Table 1). Nevertheless, these recent studies have broadened our understanding of the cellular responses driving the fibrotic process of the heart in context of interstitial and replacement fibrosis.

In the context of ischemic injury, two recent studies using mouse myocardial infarction models [62,66] have provided important new insights towards cardiac pathological remodeling. Both studies are characterized by large increases in macrophage proportions in the inflammatory phase post-MI and characterize the development of myofibroblasts. Myofibroblast express high levels of TGF β — which further supports myofibroblast differentiation — and other ECM components [67,68]. A key finding of the scRNA-seq analyses is that myofibroblasts are not homogeneous and comprise cells within a phenotypic continuum, including those that are proliferative [66] and those varying in expression levels of *Tgfb1*, *Cilp*, *Thbs4* and *Postn* (Figure 2 *A'* and *A''*) [62]. Genes defining myofibroblast phenotypes also included *Scx* and *Wisp1*, which are modulators of WNT signaling suggesting nuanced regulation of the type of fibrogenic activity of myofibroblast subtypes.

Beyond myofibroblasts, both studies also identified several activated fibroblast subsets that contribute to fibrosis. Emerging during the inflammatory phase of MI, activated fibroblasts (termed 'F-Act' or 'LR' fibroblasts in [62] and [66], respectively) increase in number and are characterized by expression of numerous fibrillogenesis genes including *Cthrc1* and *Postn* [63,69,70] (Figure 2) and others that are negative regulators of TGF β such as '*Cilp*' and '*Adamts2*' [70,71]. The presence of 'matrifibrocytes' [23] — quiescent cells in the mature scar after MI that develop within 7 and 14 days post-MI [66] — are also confirmed. These cells distinctly express genes such as '*Comp*', '*Sfrp2*' and '*Wisp2*' in addition to the aforementioned genes *Cilp* and *Thbs4* found in other activated fibroblasts [66]. Together, scRNA-seq analyses of the MI model has shown that diverse fibrogenic cell populations exist in the heart with distinct gene expression patterns mediated by TGF β and WNT-associated and independent pathways.

Myofibroblasts are not major players in chronic stress-induced fibrosis

In attempting to better understand the mechanisms driving fibrosis during chronic physiological stress, we recently examined the effect of continuous AngII infusion on pathological remodeling of the heart [56]. By examining 8 control and 8 AngII treated mouse hearts (four female, four male) we were able to interrogate gene expression shifts in a vast array of cell types including cardiomyocytes, and develop an atlas of the heart in response to chronic AngII exposure (Figure 2B, B' and B''; Table 1). Extensive fibrosis and hypertrophy were evident after AngII treatment, further characterized by up-regulation of heart failure biomarkers including *Sparc*, *Bgn*, *Nppa* and *Nppb* [72–75], although the latter two were (unsurprisingly) up-regulated only in cardiomyocytes [72,73]. We found that every cell type alters its gene expression in response to AngII, and almost every cell type in the heart contributes to ECM remodeling; including up-regulation of key fibrogenic genes collagen I, III and VIII. Indeed, genetic programs corresponding to ECM organization were amongst the most frequently up-regulated.

Similar to the MI studies, we also noted the emergence of new fibroblast cell populations. We termed these cell populations Fibroblast-*Cilp* and Fibroblast-*Thbs4*, based on the top genes that were distinct to these cells compared with all other cells analyzed in the dataset (Figure 2B). We found that Fibroblast-*Cilp* is the most fibrogenic cell type in AngII-treated hearts. Fibroblast-*Cilp* and *Thbs4* were also found to occupy different spatial loci, with *Thbs4*⁺ cells almost completely absent from regions of perivascular fibrosis. Notably, Fibroblast-*Cilp* and Fibroblast-*Thbs4* do not correspond to ACTA2⁺ myofibroblasts, determined transcriptomically or by immunostaining. This finding is particularly important given that the current dogma suggests that myofibroblasts are the main protagonists driving pathological fibrosis [24]. Indeed, similar fibrosis absent of myofibroblasts induction is reported in the context of diabetic cardiomyopathy [76]. Our study underscores that the accumulation of extensive fibrosis in the heart is not dependent on ACTA2⁺ myofibroblasts.

Another crucial paradigm challenged by this work is the necessity of local inflammation for excess fibrosis in the heart. We observed increased leukocyte subpopulations in a sex-dependent manner from AngII infusion. Surprisingly, cardiac cells consistently down-regulated genes involved in leukocyte trafficking [56]. Therefore, while hypertension and other chronic physiological stresses may increase systemic inflammation [77,78], the early response of the cardiac cellome to hypertension may be compensatory, by attempting to dampen leukocyte infiltration into the cardiac interstitium.

Finally, this study revealed the extent of sexual dimorphisms in the heart during homeostasis and hypertensive stress. Hearts of AngII-infused mice revealed sex-disparities in cardiac function and extent of fibrosis, including the distribution of fibrotic lesions within the heart [55,56]. Importantly, female hearts exhibited a more HFpEF-like phenotype compared with males, which is recapitulated in clinical HF [12,79]. Examination of cell-specific gene expression patterns also showed extensive sex-dependent differences in the healthy and stressed heart with Fibroblast-*Cilp* exhibiting the greatest level of sex-specific genes of all cell types in the AngII-infused hearts.

Future directions

Application of single-cell omics to understand cardiac fibrosis is still at its nascent stages and has already yielded novel insights. Undoubtedly, more studies by independent research groups and in varying context of heart stress will reveal common and distinct mechanism that drive fibrosis in the heart. Moreover, comparison of cellular processes uncovered by scRNA-seq analysis of fibrosis in other tissues such as lung [80–82], kidney [83], liver [84] and breast tissue [85] — where scRNA-seq is also revealing novel cellular fibrosis mechanisms — will provide a holistic insight to systemic stressors such as hypertension and diabetes where fibrosis effects multiple organ systems.

One of the greatest requirements needed to follow scRNA-seq studies discussed here is empirical determination of the importance of cell types and genes associated with fibrosis. For example, our analysis of top genes up-regulated in AngII-treated mouse hearts identified genes such as *Anks3*, *Fastkd1*, *Oxsm* and *Zmat1*, that are exclusively up-regulated in epicardial cells [56]. Given the importance of the epicardium in cardiac stress responses, particularly in context of paracrine regulation of the cardiac cellular milieu [86], the importance of these genes warrants further examination. Informed by scRNA-seq data, we envisage precise mouse genetic tools such as Cre/LoxP systems [56] for cell-specific ablation of such genes.

Validation of genes and pathways will also be aided by better understanding gene-regulatory networks driving cell-specific phenotypes. Identifying regulators will support the development of therapeutics approaches to address fibrosis. Indeed, software packages such as SCENIC [87] attempt to achieve this by considering both the co-expression of genes and transcription factors, and the enrichment of cis-regulatory elements of genes putatively

regulated by transcription factors using scRNA-seq data [88]. Moreover, application of technologies such as single-cell ATAC sequencing, which identifies open chromatin states, enabling identification of transcriptional regulators, and multi-omic approaches such as paired-seq and CITE-seq [34,89–91] will further accelerate this aim.

These efforts will also support determination of cellular ontology and differentiation of cell types discovered by scRNA-seq. To gain insight towards the development of fibrogenic cell populations ‘pseudo-temporal’ algorithms have been utilized [56,62,66]. These include algorithms that aim to place cells on a continuum of phenotypes based on transcription patterns (such as Monocle [92], Slingshot [93] and others [62]) or those that consider gradients of mature and immature transcripts to determine development vectors between cellular populations (for example scVelo, velocity in [56]). These approaches in combination with emerging spatial transcriptomic approaches such as StarMap [94], FISSEQ [95] or spot-sequencing [96] — which aim to resolve cell or region-specific gene expression patterns within a tissue — will provide important spatial context-dependent data of cell type development.

Finally, further examination of variance between strains of experimental models, sexes and species to identify fundamental mechanisms of disease development and the clinical relevance is required. For example, comparison of MI responses of C57BL/6 and 129S1/SvImJ strains of mice identified important differences in cardiac remodeling and scarring [97]. Moreover, as aforementioned we have identified a number of sex-dependent differences in cellular responses to AngII [56] including base-line differences in cardiac cellularity that is controlled by gonadal hormones [48,56,98]. These underscore the potential sex- and population-dependent heterogeneity in cardiac stress responses that may be expected in human cohorts. Indeed, concordance of new fibrogenic processes uncovered by scRNA-seq using experimental models, with mechanisms underlying human disease remains to be validated. While examination of bulk RNA-seq data of human hearts supports the existence of fibrogenic cell types such as Fibroblast-*Cilp* and Fibroblast-*Thbs4* [56], human single-cell data confirming the presence of these distinct cell types is lacking. Single-nuclei RNA-seq datasets of human samples are now emerging [99], including in context of failed hearts [100] which are likely to be useful here.

Concluding remarks

While single-cell transcriptomics has only recently been accessible to researchers, it has shed new light on the complex cellular processes, and changes to the cardiac cell network, that take place during the development of cardiac fibrosis. In addition to complicating our knowledge of well-known cellular protagonists of fibrosis, such as the myofibroblasts, it has identified new drivers of fibrosis that appear in context of chronic physiological stress. Application of this and other single-cell ‘omic’ technologies, coupled with more conventional genetic and biochemical approaches, promises fertile grounds for future research. Consideration of biological sex, environment, and behavior in experimental models and in clinical contexts will paint a detailed picture of the changes that take place in the cardiac cellular landscape and key molecular mechanisms that underpin fibrosis of the heart following tissue stress.

Perspectives

- *Importance of the field:* Cardiac fibrosis has no effective treatment, and is a critical antecedent to cardiac dysfunction resulting from myocardial infarction (heart attack) or from chronic diseases such as hypertension and diabetes. Single-cell transcriptomics promises to provide new insight towards the cellular and molecular drivers of fibrosis at unprecedented detail.
- *Current thinking:* While application of single-cell transcriptomics in resolving the cellular and molecular events underpinning cardiac dysfunction is still at the nascent stages, it has already revealed new cellular protagonists of fibrosis and expanded our knowledge of well-known participants in cardiac fibrosis — such as the myofibroblast.
- *Future Directions:* Much work is required to apply single-cell transcriptomics in a wider variety of cardiac stress-inducing contexts and to validate key genes and cellular networks already identified by this technology. Achieving this, will advance the development of new therapeutic strategies to address cardiac fibrosis.

Data Availability

The following previously published datasets were used. Mclellan MA, Skelly DA, Dona MSI, Squiers GT, Farrugia GE, Gaynor TL, Cohen CD, Pandey R, Diep H, Vinh A, Rosenthal NA, Pinto AR. 2020. High-resolution transcriptomic profiling of the heart during chronic stress reveals cellular drivers of cardiac fibrosis and hypertrophy. ArrayExpress database: E-MTAB-8810. Farbehi, N, Patrick R, Dorison A, Xaymardan, M, Wystub-Lis K, Janbandhu, V, Ho JWK, Nordon RE, Harvey RP. 2019. Single-cell RNA-seq of mouse cardiac interstitial cells 3 and 7 days after sham or myocardial infarction injury. ArrayExpress database: E-MTAB-7376.

Abbreviations

ACTA, alpha smooth-muscle actin; AngII, angiotensin-II; CSF1R, colony stimulating growth factor-1 receptor; ECM, extracellular matrix; Fibroblast-*Cilp*, fibroblasts with high expression of *Cilp*; Fibroblast-*Thbs4*, fibroblasts with high expression of *Thbs4*; Fibroblast-*Wif1*, fibroblasts with high expression of *Wif1*; HF, heart failure; HFpEF, heart failure with preserved ejection fraction; MI, myocardial infarction; MMPs, matrix metalloproteinases; PCA, principal component analysis; scRNA-seq, single-cell RNA sequencing; TGF β , transforming growth factor- β ; TIMPs, tissue inhibitory metalloproteinases; t-SNE, t-distributed stochastic neighbor embedding; UMAP, uniform manifold approximation and projection; UMI, unique molecular identifiers; WNT, wingless-related integration site.

Competing Interests

The authors declare that there are no competing interests associated with the manuscript.

Funding

C.K. and C.D.C. are supported by the La Trobe University Postgraduate Research Scholarship (LTUPRS), Research Training Program Fees Off-set (RTP-Fo) Scholarship. CDC is supported by a Baker Institute 'Bright Sparks' Scholarship. A.R.P. is supported by a National Health and Medical Research Council (Australia) Ideas Grant (GNT1188503) and a Diabetes Australia General Grant (Y20G- Pina).

Author Contributions

C.K. and C.D.C. collated relevant literature, C.K., C.D.C. and A.R.P. prepared initial draft of the manuscript. C.K., C.D.C., M.S.I.D. and A.R.P. prepared figures and edited the manuscript. A.R.P. approved the final draft of the manuscript.

Acknowledgements

The authors thank Dr. Daniel G. Donner of the Preclinical Cardiology, Microsurgery and Imaging Laboratory at the Baker Heart and Diabetes Institute, for providing images of the infarcted mouse heart (Figure 1).

References

- Lockhart, M., Wirrig, E., Phelps, A. and Wessels, A. (2011) Extracellular matrix and heart development. *Birth Defects Res. Part A Clin. Mol. Teratol.* **91**, 535–550 <https://doi.org/10.1002/bdra.20810>
- Bonnans, C., Chou, J. and Werb, Z. (2014) Remodelling the extracellular matrix in development and disease. *Nat. Rev. Mol. Cell Biol.* **15**, 786–801 <https://doi.org/10.1038/nrm3904>
- Kechagia, J.Z., Ivaska, J. and Roca-Cusachs, P. (2019) Integrins as biomechanical sensors of the microenvironment. *Nat. Rev. Mol. Cell Biol.* **20**, 457–473 <https://doi.org/10.1038/s41580-019-0134-2>
- Conroy, K.P., Kitto, L.J. and Henderson, N.C. (2016) Av integrins: key regulators of tissue fibrosis. *Cell Tissue Res.* **365**, 511–519 <https://doi.org/10.1007/s00441-016-2407-9>
- Bon, H., Hales, P., Lumb, S., Holdsworth, G., Johnson, T., Qureshi, O. et al. (2019) Spontaneous extracellular matrix accumulation in a human in vitro model of renal fibrosis is mediated by α v integrins. *Nephron* **142**, 329–350 <https://doi.org/10.1159/000499506>
- Krebber, M.M., van Dijk, C.G.M., Vernooij, R.W.M., Brandt, M.M., Emter, C.A., Rau, C.D. et al. (2020) Matrix metalloproteinases and tissue inhibitors of metalloproteinases in extracellular matrix remodeling during left ventricular diastolic dysfunction and heart failure with preserved ejection fraction: a systematic review and meta-analysis. *Int. J. Mol. Sci.* **21**, 1–22 <https://doi.org/10.3390/ijms21186742>
- Hinderer, S. and Schenke-Layland, K. (2019) Cardiac fibrosis: a short review of causes and therapeutic strategies. *Adv. Drug Deliv. Rev.* **146**, 77–82 <https://doi.org/10.1016/j.addr.2019.05.011>
- Morisot, C. and Dubos, J.P. (1988) Arterial hypertension in the neonate. *Pediatrics* **43**, 725–733 <https://doi.org/10.1093/cvr/26.7.671>
- Liu, T., Song, D., Dong, J., Zhu, P., Liu, J., Liu, W. et al. (2017) Current understanding of the pathophysiology of myocardial fibrosis and its quantitative assessment in heart failure. *Front. Physiol.* **8**, 238 <https://doi.org/10.3389/fphys.2017.00238>
- Mizushige, K., Yao, L., Noma, T., Kiyomoto, H., Yu, Y., Hosomi, N. et al. (2000) Alteration in left ventricular diastolic filling and accumulation of myocardial collagen at insulin-resistant prediabetic stage of a type II diabetic rat model. *Circulation* **101**, 899–907 <https://doi.org/10.1161/01.CIR.101.8.899>

- 21 Singh, V.P., Le, B., Khode, R., Baker, K.M. and Kumar, R. (2008) Intracellular angiotensin II production in diabetic rats is correlated with cardiomyocyte apoptosis, oxidative stress, and cardiac fibrosis. *Diabetes* **57**, 3297–3306 <https://doi.org/10.2337/db08-0805>
- 22 Beale, A., Nanayakkara, S., Segal, L., Vizi, D., Evans, S., Mariani, J. et al. (2019) Sex differences in heart failure With preserved ejection fraction: an invasive hemodynamic analysis. *J. Am. Coll. Cardiol.* **73**, 921 [https://doi.org/10.1016/S0735-1097\(19\)31528-1](https://doi.org/10.1016/S0735-1097(19)31528-1)
- 23 Dai, Z., Aoki, T., Fukumoto, Y. and Shimokawa, H. (2012) Coronary perivascular fibrosis is associated with impairment of coronary blood flow in patients with non-ischemic heart failure. *J. Cardiol.* **60**, 416–421 <https://doi.org/10.1016/j.jicc.2012.06.009>
- 24 Pries, A.R., Badimon, L., Bugiardini, R., Camici, P.G., Dorobantu, M., Duncker, D.J. et al. (2015) Coronary vascular regulation, remodelling, and collateralization: mechanisms and clinical implications on behalf of the working group on coronary pathophysiology and microcirculation. *Eur. Heart J.* **36**, 3134–3146 <https://doi.org/10.1093/eurheartj/ehv100>
- 25 Ytrehus, K., Hulot, J.S., Perrino, C., Schiattarella, G.G. and Madonna, R. (2018) Perivascular fibrosis and the microvasculature of the heart. Still hidden secrets of pathophysiology? *Vascul. Pharmacol.* **107**, 78–83 <https://doi.org/10.1016/j.vph.2018.04.007>
- 26 Ismail, T.F., Hsu, L.Y., Greve, A.M., Gonçalves, C., Jabbour, A., Gulati, A. et al. (2014) Coronary microvascular ischemia in hypertrophic cardiomyopathy: a pixel-wise quantitative cardiovascular magnetic resonance perfusion study. *J. Cardiovasc. Magn. Reson.* **16**, 1–10 <https://doi.org/10.1186/s12968-014-0049-1>
- 27 Shinde, A.V. and Frangogiannis, N.G. (2014) Fibroblasts in myocardial infarction: a role in inflammation and repair. *J. Mol. Cell. Cardiol.* **70**, 74–82 <https://doi.org/10.1016/j.jmcc.2013.11.015>
- 28 Mauler, M., Herr, N., Schoenichen, C., Witsch, T., Marchini, T., Härdtner, C. et al. (2019) Platelet serotonin aggravates myocardial ischemia/Reperfusion injury via neutrophil degranulation. *Circulation* **139**, 918–931 <https://doi.org/10.1161/CIRCULATIONAHA.118.033942>
- 29 Hilgendorf, I., Gerhardt, L.M.S., Tan, T.C., Winter, C., Holderried, T.A.W., Chousterman, B.G. et al. (2014) Ly-6 chigh monocytes depend on nr4a1 to balance both inflammatory and reparative phases in the infarcted myocardium. *Circ. Res.* **114**, 1611–1622 <https://doi.org/10.1161/CIRCRESAHA.114.303204>
- 30 Frangogiannis, N.G., Lindsey, M.L., Michael, L.H., Youker, K.A., Bressler, R.B., Mendoza, L.H. et al. (1998) Resident cardiac mast cells degranulate and release preformed TNF- α , initiating the cytokine cascade in experimental canine myocardial ischemia/reperfusion. *Circulation* **98**, 699–710 <https://doi.org/10.1161/01.CIR.98.7.699>
- 31 Epelman, S., Lavine, K.J., Beaudin, A.E., Sojka, D.K., Carrero, J.A., Calderon, B. et al. (2014) Embryonic and adult-derived resident cardiac macrophages are maintained through distinct mechanisms at steady state and during inflammation. *Immunity* **40**, 91–104 <https://doi.org/10.1016/j.immuni.2013.11.019>
- 32 Lavine, K.J., Pinto, A.R., Epelman, S., Kopecky, B.J., Clemente-Casares, X., Godwin, J. et al. (2018) The macrophage in cardiac homeostasis and disease: JACC macrophage in CVD series (Part 4). *J. Am. Coll. Cardiol.* **72**, 2213–2230 <https://doi.org/10.1016/j.jacc.2018.08.2149>
- 33 Fu, X., Blaxall, B.C. and Molkentin, J.D. (2018) Specialized fibroblast differentiated states underlie scar formation in the infarcted mouse heart. *J. Clin. Invest.* **128**, 2127–2143 <https://doi.org/10.1172/JCI98215>
- 34 Gourdie, R.G., Dimmeler, S. and Kohl, P. (2016) Novel therapeutic strategies targeting fibroblasts and fibrosis in heart disease. *Nat. Rev. Drug Discov.* **15**, 620–638 <https://doi.org/10.1038/nrd.2016.89>
- 35 Gurtner, G.C., Werner, S., Barrandon, Y. and Longaker, M.T. (2008) Wound repair and regeneration. *Nature* **453**, 314–321 <https://doi.org/10.1038/nature07039>
- 36 Fu, K., Corbley, M.J., Sun, L., Friedman, J.E., Shan, F., Papadatos, J.L. et al. (2008) SM16, an orally active TGF- β type I receptor inhibitor prevents myofibroblast induction and vascular fibrosis in the rat carotid injury model. *Arterioscler. Thromb. Vasc. Biol.* **28**, 665–671 <https://doi.org/10.1161/ATVBAHA.107.158030>
- 37 Molkentin, J.D., Bugg, D., Ghearing, N., Dorn, L.E., Kim, P., Sargent, M.A. et al. (2017) Fibroblast-specific genetic manipulation of p38 mitogen-activated protein kinase in vivo reveals its central regulatory role in fibrosis. *Circulation* **136**, 549–561 <https://doi.org/10.1161/CIRCULATIONAHA.116.026238>
- 38 Blyszczuk, P., Müller-Edenborn, B., Valenta, T., Osto, E., Stellato, M., Behnke, S. et al. (2017) Transforming growth factor- β -dependent Wnt secretion controls myofibroblast formation and myocardial fibrosis progression in experimental autoimmune myocarditis. *Eur. Heart J.* **38**, 1413–1425 <https://doi.org/10.1093/eurheartj/ehw116>
- 39 Hinz, B., Mastrangelo, D., Iselin, C.E., Chaponnier, C. and Gabbiani, G. (2001) Mechanical tension controls granulation tissue contractile activity and myofibroblast differentiation. *Am. J. Pathol.* **159**, 1009–1020 [https://doi.org/10.1016/S0002-9440\(10\)61776-2](https://doi.org/10.1016/S0002-9440(10)61776-2)
- 40 Tomasek, J.J., Gabbiani, G., Hinz, B., Chaponnier, C. and Brown, R.A. (2002) Myofibroblasts and mechano: regulation of connective tissue remodeling. *Nat. Rev. Mol. Cell Biol.* **3**, 349–363 <https://doi.org/10.1038/nrm809>
- 41 Hinz, B., Celetta, G., Tomasek, J.J., Gabbiani, G. and Chaponnier, C. (2001) Alpha-smooth muscle actin expression upregulates fibroblast contractile activity. *Mol. Biol. Cell* **12**, 2730–2741 <https://doi.org/10.1091/mbc.12.9.2730>
- 42 Xu, X., Hou, Y., Yin, X., Bao, L., Tang, A., Song, L. et al. (2012) Single-cell exome sequencing reveals single-nucleotide mutation characteristics of a kidney tumor. *Cell* **148**, 886–895 <https://doi.org/10.1016/j.cell.2012.02.025>
- 43 Zheng, G.X.Y., Terry, J.M., Belgrader, P., Rykin, P., Bent, Z.W., Wilson, R. et al. (2017) Massively parallel digital transcriptional profiling of single cells. *Nat. Commun.* **8**, 14049 <https://doi.org/10.1038/ncomms14049>
- 44 Buenostro, J.D., Giresi, P.G., Zaba, L.C., Chang, H.Y. and Greenleaf, W.J. (2013) Transposition of native chromatin for fast and sensitive epigenomic profiling of open chromatin, DNA-binding proteins and nucleosome position. *Nat. Methods* **10**, 1213–1218 <https://doi.org/10.1038/nmeth.2688>
- 45 Cokus, S.J., Feng, S., Zhang, X., Chen, Z., Merriman, B., Haudenschild, C.D. et al. (2008) Shotgun bisulphite sequencing of the arabidopsis genome reveals DNA methylation patterning. *Nature* **452**, 215–219 <https://doi.org/10.1038/nature06745>
- 46 O'Huallachain, M., Bava, F.A., Shen, M., Dallett, C., Paladugu, S., Samusik, N. et al. (2020) Ultra-high throughput single-cell analysis of proteins and RNAs by split-pool synthesis. *Commun. Biol.* **3**, 213 <https://doi.org/10.1038/s42003-020-0896-2>
- 47 Ding, J., Adiconis, X., Simmons, S.K., Kowalczyk, M.S., Hession, C.C., Marjanovic, N.D. et al. (2020) Systematic comparison of single-cell and single-nucleus RNA-sequencing methods. *Nat. Biotechnol.* **38**, 737–746 <https://doi.org/10.1038/s41587-020-0465-8>
- 48 Muraro, M.J., Dharmadhikari, G., Grün, D., Groen, N., Dielen, T., Jansen, E. et al. (2016) A single-Cell transcriptome atlas of the human pancreas. *Cell Syst.* **3**, 385–394.e3 <https://doi.org/10.1016/j.cels.2016.09.002>

- 39 Rosenberg, A.B., Roco, C.M., Muscat, R.A., Kuchina, A., Sample, P., Yao, Z. et al. (2018) Single-cell profiling of the developing mouse brain and spinal cord with split-pool barcoding. *Science* **360**, 176–182 <https://doi.org/10.1126/science.aam8999>
- 40 Klein, A.M., Mazutis, L., Akartuna, I., Tallapragada, N., Veres, A., Li, V. et al. (2015) Droplet barcoding for single-cell transcriptomics applied to embryonic stem cells. *Cell* **161**, 1187–1201 <https://doi.org/10.1016/j.cell.2015.04.044>
- 41 Macosko, E.Z., Basu, A., Satija, R., Nemesh, J., Shekhar, K., Goldman, M. et al. (2015) Highly parallel genome-wide expression profiling of individual cells using nanoliter droplets. *Cell* **161**, 1202–1214 <https://doi.org/10.1016/j.cell.2015.05.002>
- 42 Mazutis, L., Gilbert, J., Ung, W.L., Weitz, D.A., Griffiths, A.D. and Heyman, J.A. (2013) Single-cell analysis and sorting using droplet-based microfluidics. *Nat. Protoc.* **8**, 870–891 <https://doi.org/10.1038/nprot.2013.046>
- 43 Niu, X.Z., Zhang, B., Marszalek, R.T., Ces, O., Edel, J.B., Klug, D.R. et al. (2009) Droplet-based compartmentalization of chemically separated components in two-dimensional separations. *Chem. Commun.* **41**, 6159–6161 <https://doi.org/10.1039/b918100h>
- 44 Casbon, J.A., Osborne, R.J., Brenner, S. and Lichtenstein, C.P. (2011) A method for counting PCR template molecules with application to next-generation sequencing. *Nucleic Acids Res.* **39**, e81 <https://doi.org/10.1093/nar/gkr217>
- 45 Becht, E., McInnes, L., Healy, J., Dutertre, C.A., Kwok, I.W.H., Ng, L.G. et al. (2018) Dimensionality reduction for visualizing single-cell data using UMAP. *Nat. Biotechnol.* **37**, 38–47 <https://doi.org/10.1038/nbt.4314>
- 46 van der Maaten, L. and Hinton, G. (2008) Visualizing data using t-SNE. *Mach. Learn. Res.* **219**, 187–202
- 47 Van Den Brink, S.C., Sage, F., Vértessy, A., Spanjaard, B., Peterson-Maduro, J., Baron, C.S. et al. (2017) Single-cell sequencing reveals dissociation-induced gene expression in tissue subpopulations. *Nat. Methods* **14**, 935–936 <https://doi.org/10.1038/nmeth.4437>
- 48 Pinto, A.R., Illykh, A., Ivey, M.J., Kuwabara, J.T., D'antoni, M.L., Debuque, R. et al. (2016) Revisiting cardiac cellular composition. *Circ. Res.* **118**, 400–409 <https://doi.org/10.1161/CIRCRESAHA.115.307778>
- 49 Banerjee, I., Fuseler, J.W., Price, R.L., Borg, T.K. and Baudino, T.A. (2007) Determination of cell types and numbers during cardiac development in the neonatal and adult rat and mouse. *Am. J. Physiol. Heart Circ. Physiol.* **293**, 1883–1891 <https://doi.org/10.1152/ajpheart.00514.2007>
- 50 Pauly, T.J., Zarnstorff, W.C. and Bittar, N. (1973) Myocardial metabolic activity as a determinant of reactive hyperaemia responses in the dog heart. *Cardiovasc. Res.* **7**, 90–94 <https://doi.org/10.1093/cvr/7.1.90>
- 51 Pinto, A.R., Paolicelli, R., Salimova, E., Gospocic, J., Slonimsky, E., Bilbao-Cortes, D. et al. (2012) An abundant tissue macrophage population in the adult murine heart with a distinct alternatively-activated macrophage profile. *PLoS ONE* **7**, e36814 <https://doi.org/10.1371/journal.pone.0036814>
- 52 Hulsmans, M., Clauss, S., Xiao, L., Aguirre, A.D., King, K.R., Hanley, A. et al. (2017) Macrophages facilitate electrical conduction in the heart. *Cell* **169**, 510–522.e20 <https://doi.org/10.1016/j.cell.2017.03.050>
- 53 Camelliti, P., Green, C.R., LeGrice, I. and Kohl, P. (2004) Fibroblast network in rabbit sinoatrial node: structural and functional identification of homogeneous and heterogeneous cell coupling. *Circ. Res.* **94**, 828–835 <https://doi.org/10.1161/01.RES.0000122382.19400.14>
- 54 Liao, Y., Day, K.H., Damon, D.N. and Duling, B.R. (2001) Endothelial cell-specific knockout of connexin 43 causes hypotension and bradycardia in mice. *Proc. Natl Acad. Sci. U.S.A.* **98**, 9989–9994 <https://doi.org/10.1073/pnas.171305298>
- 55 Skelly, D.A., Squiers, G.T., McLellan, M.A., Bolisetti, M.T., Robson, P., Rosenthal, N.A. et al. (2018) Single-cell transcriptional profiling reveals cellular diversity and intercommunication in the mouse heart. *Cell Rep.* **22**, 600–610 <https://doi.org/10.1016/j.celrep.2017.12.072>
- 56 McLellan, M., Skelly, D., Dona, M., Squiers, G., Farrugia, G., Gaynor, T. et al. (2020) High-resolution transcriptomic profiling of the heart during chronic stress reveals cellular drivers of cardiac fibrosis and hypertrophy. *Circulation* **142**, 1448–1463 <https://doi.org/10.1161/CIRCULATIONAHA.119.045115>
- 57 Broughton, K.M., Khieu, T., Nguyen, N., Rosa, M., Mohsin, S., Quijada, P. et al. (2019) Cardiac interstitial tetraploid cells can escape replicative senescence in rodents but not large mammals. *Commun. Biol.* **2**, 1–14 <https://doi.org/10.1038/s42003-019-0453-z>
- 58 Schaum, N., Karkanias, J., Neff, N.F., May, A.P., Quake, S.R., Wyss-Coray, T. et al. (2018) Single-cell transcriptomics of 20 mouse organs creates a *tabula muris*. *Nature* **562**, 367–372 <https://doi.org/10.1038/s41586-018-0590-4>
- 59 Hu, P., Liu, J., Zhao, J., Wilkins, B.J., Lupino, K., Wu, H. et al. (2018) Single-nucleus transcriptomic survey of cell diversity and functional maturation in postnatal mammalian hearts. *Genes Dev.* **32**, 1344–1357 <https://doi.org/10.1101/gad.316802.118>
- 60 Sudo, T., Nishikawa, S., Ogawa, M., Kataoka, H., Ohno, N., Izawa, A. et al. (1995) Functional hierarchy of c-kit and c-fms in intramarrow production of CFU-M. *Oncogene* **11**, 2468–2476 PMID:8545103
- 61 Conway, J.G., McDonald, B., Parham, J., Keith, B., Rusnak, D.W., Shaw, E. et al. (2005) Inhibition of colony-stimulating-factor-1 signaling in vivo with the orally bioavailable cFMS kinase inhibitor GW2580. *Proc. Natl Acad. Sci. U.S.A.* **102**, 16078 <https://doi.org/10.1073/pnas.0502000102>
- 62 Farbehi, N., Patrick, R., Dorison, A., Xaymardan, M., Janbandhu, V., Wystub-Lis, K. et al. (2019) Single-cell expression profiling reveals dynamic flux of cardiac stromal, vascular and immune cells in health and injury. *eLife* **8**, e43882 <https://doi.org/10.7554/eLife.43882>
- 63 Van Nieuwenhoven, F.A., Munts, C., Op'T Veld, R.C., González, A., Díez, J., Heymans, S. et al. (2017) Cartilage intermediate layer protein 1 (CILP1): a novel mediator of cardiac extracellular matrix remodelling. *Sci. Rep.* **7**, 1–9 <https://doi.org/10.1038/s41598-017-16201-y>
- 64 He, X., Guo, X., Zhang, H., Kong, X., Yang, F. and Zheng, C. (2017) Mechanism of action and efficacy of LY2109761—a TGF- β receptor inhibitor, targeting tumor microenvironment in liver cancer after TACE. *Oncotarget* **9**, 1130–1142 <https://doi.org/10.18632/oncotarget.23193>
- 65 Meyer, I.S., Jungmann, A., Dieterich, C., Zhang, M., Lasitschka, F., Werkmeister, S. et al. (2017) The cardiac microenvironment uses non-canonical WNT signaling to activate monocytes after myocardial infarction. *EMBO Mol. Med.* **9**, 1279–1293 <https://doi.org/10.15252/emmm.201707565>
- 66 Forte, E., Skelly, D.A., Chen, M., Daigle, S., Morelli, K.A., Hon, O. et al. (2020) Dynamic interstitial cell response during myocardial infarction predicts resilience to rupture in genetically diverse mice. *Cell Rep.* **30**, 3149–3163.e6 <https://doi.org/10.1016/j.celrep.2020.02.008>
- 67 Dobaczewski, M., Chen, W. and Frangogiannis, N.G. (2011) Transforming growth factor (TGF)- β signaling in cardiac remodeling. *J. Mol. Cell Cardiol.* **51**, 600–606 <https://doi.org/10.1016/j.jmcc.2010.10.033>
- 68 Frangogiannis, N.G. and Kovacic, J.C. (2020) Extracellular matrix in ischemic heart disease, part 4/4: JACC focus seminar. *J Am Coll Cardiol.* **75**, 2219–2235 <https://doi.org/10.1016/j.jacc.2020.03.020>
- 69 Koo, B.H., Le, G.C., Jungeers, K.A., Vasanji, A., O'Flaherty, J., Weyman, C.M. et al. (2007) ADAMTS-like 2 (ADAMTSL2) is a secreted glycoprotein that is widely expressed during mouse embryogenesis and is regulated during skeletal myogenesis. *Matrix Biol.* **26**, 431–441 <https://doi.org/10.1016/j.matbio.2007.03.003>
- 70 Zhang, C.L., Zhao, Q., Liang, H., Qiao, X., Wang, J.Y., Wu, D. et al. (2018) Cartilage intermediate layer protein-1 alleviates pressure overload-induced cardiac fibrosis via interfering TGF- β 1 signaling. *J. Mol. Cell Cardiol.* **116**, 135–144 <https://doi.org/10.1016/j.jmcc.2018.02.006>

- 71 Le Goff, C., Morice-Picard, F., Dagoneau, N., Wang, L.W., Perrot, C., Crow, Y.J. et al. (2008) ADAMTS2 mutations in geleophysic dysplasia demonstrate a role for ADAMTS-like proteins in TGF- β bioavailability regulation. *Nat. Genet.* **40**, 1119–1123 <https://doi.org/10.1038/ng.199>
- 72 Moe, G.W. (2006) B-type natriuretic peptide in heart failure. *Curr. Opin. Cardiol.* **21**, 208–214
- 73 Sergeeva, I.A. and Christoffels, V.M. (2013) Regulation of expression of atrial and brain natriuretic peptide, biomarkers for heart development and disease. *Biochim. Biophys. Acta Mol. Basis Dis.* **1832**, 2403–2413 <https://doi.org/10.1016/j.bbdis.2013.07.003>
- 74 Bradshaw, A.D., Baicu, C.F., Rentz, T.J., van der Laarse, A., Boggs, J., Lacy, J.M. et al. (2008) Pressure-overload induced alterations in fibrillar collagen content and myocardial diastolic function: role of SPARC in post-synthetic procollagen processing. *Circulation* **119**, 269–280 <https://doi.org/10.1161/CIRCULATIONAHA.108.773424>
- 75 Beetz, N., Rommel, C., Schnick, T., Neumann, E., Lothar, A., Monroy-Ordóñez, E.B. et al. (2016) Ablation of biglycan attenuates cardiac hypertrophy and fibrosis after left ventricular pressure overload. *J. Mol. Cell Cardiol.* **101**, 145–155 <https://doi.org/10.1016/j.yjmcc.2016.10.011>
- 76 Alex, L., Russo, I., Holoborodko, V. and Frangogiannis, N.G. (2018) Characterization of a mouse model of obesity-related fibrotic cardiomyopathy that recapitulates features of human heart failure with preserved ejection fraction. *Am. J. Physiol. Heart Circ. Physiol.* **315**, H934–H949 <https://doi.org/10.1152/ajpheart.00238.2018>
- 77 Rodríguez-Iturbe, B., Pons, H. and Johnson, R.J. (2017) Role of the immune system in hypertension. *Physiol. Rev.* **97**, 1127–1164 <https://doi.org/10.1152/physrev.00031.2016>
- 78 Lowe, G., Woodward, M., Hillis, G., Rumley, A., Li, Q., Harrap, S. et al. (2014) Circulating inflammatory markers and the risk of vascular complications and mortality in people with type 2 diabetes and cardiovascular disease or risk factors: the advance study. *Diabetes* **63**, 1115–1123 <https://doi.org/10.2337/db12-1625>
- 79 Beale, A.L., Nanayakkara, S. and Kaye, D.M. (2019) Impact of sex on ventricular-vascular stiffness and long-term outcomes in heart failure with preserved ejection fraction: topcat trial substudy. *J. Am. Heart Assoc.* **8**, 1–8 <https://doi.org/10.1161/JAHA.119.012190>
- 80 Aran, D., Looney, A.P., Liu, L., Wu, E., Fong, V., Hsu, A. et al. (2019) Reference-based analysis of lung single-cell sequencing reveals a transitional profibrotic macrophage. *Nat. Immunol.* **20**, 163–172 <https://doi.org/10.1038/s41590-018-0276-y>
- 81 Reyman, P.A., Walter, J.M., Joshi, N., Anekalla, K.R., McQuattie-Pimentel, A.C., Chiu, S. et al. (2019) Single-cell transcriptomic analysis of human lung provides insights into the pathobiology of pulmonary fibrosis. *Am. J. Respir. Crit. Care Med.* **199**, 1517–1536 <https://doi.org/10.1164/rccm.201712-24100C>
- 82 Xie, T., Wang, Y., Deng, N., Huang, G., Taghavifar, F., Geng, Y. et al. (2018) Single-cell deconvolution of fibroblast heterogeneity in mouse pulmonary fibrosis. *Cell Rep.* **22**, 3625–3640 <https://doi.org/10.1016/j.celrep.2018.03.010>
- 83 Kramann, R., Machado, F., Wu, H., Kusaba, T., Hoeff, K., Schneider, R.K. et al. (2018) Parabiosis and single-cell RNA sequencing reveal a limited contribution of monocytes to myofibroblasts in kidney fibrosis. *JCI Insight* **3**, 1–14 <https://doi.org/10.1172/jci.insight.99561>
- 84 Ramachandran, P., Dobie, R., Wilson-Kanemori, J.R., Dora, E.F., Henderson, B.E.P., Luu, N.T. et al. (2019) Resolving the fibrotic niche of human liver cirrhosis at single-cell level. *Nature* **575**, 512–518 <https://doi.org/10.1038/s41586-019-1631-3>
- 85 Bartoschek, M., Oskolkov, N., Bocci, M., Lövdot, J., Larsson, C., Sommarin, M. et al. (2018) Spatially and functionally distinct subclasses of breast cancer-associated fibroblasts revealed by single cell RNA sequencing. *Nat. Commun.* **9**, 5150 <https://doi.org/10.1038/s41467-018-07582-3>
- 86 Zhou, B., Honor, L.B., He, H., Ma, Q., Oh, J., Butterfield, C. et al. (2011) Adult mouse epicardium modulates myocardial injury by secreting paracrine factors. *J. Clin. Invest.* **121**, 1894 <https://doi.org/10.1172/JCI45529>
- 87 Saelens, W., Cannoodt, R., Todorov, H. and Saeys, Y. (2019) A comparison of single-cell trajectory inference methods. *Nat. Biotechnol.* **37**, 547–554 <https://doi.org/10.1038/s41587-019-0071-9>
- 88 Albar, S., González-bias, C.B., Moerman, T., Huynh-thu, V.A., Imrichova, H., Huiselmans, G. et al. (2018) Europe PMC funders group Europe PMC funders author manuscripts SCENIC: single-cell regulatory network inference and clustering. *Nat. Methods* **14**, 1083–1086 <https://doi.org/10.1038/nmeth.4463>
- 89 Shalek, A.K., Satija, R., Adiconis, X., Gertner, R.S., Gaublomme, J.T., Raychowdhury, R. et al. (2013) Single-cell transcriptomics reveals bimodality in expression and splicing in immune cells. *Nature* **498**, 236–240 <https://doi.org/10.1038/nature12172>
- 90 Zhu, C., Yu, M., Huang, H., Juric, I., Abnoui, A., Hu, R. et al. (2019) An ultra high-throughput method for single-cell joint analysis of open chromatin and transcriptome. *Nat. Struct. Mol. Biol.* **26**, 1063–1070 <https://doi.org/10.1038/s41594-019-0323-x>
- 91 Stoeckli, M., Hafemeister, C., Stephenson, W., Houck-Loomis, B., Chattopadhyay, P., Swerdlow, H. et al. (2017) Large-scale simultaneous measurement of epitopes and transcriptomes in single cells. *Nat. Methods* **14**, 865–868 <https://doi.org/10.1038/nmeth.4380>
- 92 Trapnell, C., Cacchiarelli, D., Grimsby, J., Pokharel, P., Li, S., Morse, M. et al. (2014) The dynamics and regulators of cell fate decisions are revealed by pseudotemporal ordering of single cells. *Nat. Biotechnol.* **32**, 381–386 <https://doi.org/10.1038/nbt.2859>
- 93 Street, K., Rizzo, D., Fletcher, R.B., Das, D., Ngai, J., Yosef, N. et al. (2018) Slingshot: cell lineage and pseudotime inference for single-cell transcriptomics. *BMC Genomics* **19**, 1–16 <https://doi.org/10.1186/s12864-018-4772-0>
- 94 Wang, X., Nolan, G.P., Wright, M.A., Liu, J., Sylvestrak, E.L., Evans, K. et al. (2018) Three-dimensional intact-tissue sequencing of single-cell transcriptional states. *Science* **361**, eaat5691 <https://doi.org/10.1126/science.aat5691>
- 95 Lee, J.H., Daugherty, E.R., Scheiman, J., Kalhor, R., Ferrante, T.C., Terry, R. et al. (2015) Fluorescent in situ sequencing (FISSEQ) of RNA for gene expression profiling in intact cells and tissues. *Nat. Protoc.* **10**, 442–458 <https://doi.org/10.1038/nprot.2014.191>
- 96 Asp, M., Giacomello, S., Larsson, L., Wu, C., Fürth, D., Qian, X. et al. (2019) A spatiotemporal organ-wide gene expression and cell atlas of the developing human heart. *Cell* **179**, 1647–1660.e19 <https://doi.org/10.1016/j.cell.2019.11.025>
- 97 Forte, E., Furtado, M.B. and Rosenthal, N. (2018) The interstitium in cardiac repair: role of the immune–stromal cell interplay. *Nat. Rev. Cardiol.* **15**, 601–616 <https://doi.org/10.1038/s41569-018-0077-x>
- 98 Squiers, G.T., Mclellan, M.A., Illykh, A., Branca, J., Rosenthal, N.A., Pinto, A.R. et al. (2020) Cardiac cellularity is dependent upon biological sex and is regulated by gonadal hormones. *Cardiovasc. Res.* (preprint) <https://doi.org/10.1093/cvr/cvaa265>
- 99 Tucker, N.R., Chaffin, M., Fleming, S.J., Hall, A.W., Parsons, V.A., Bedi, K.C. et al. (2020) Transcriptional and cellular diversity of the human heart. *Circulation* **142**, 466–482 <https://doi.org/10.1161/CIRCULATIONAHA.119.045401>
- 100 Wang, L., Yu, P., Zhou, B., Song, J., Li, Z., Zhang, M. et al. (2020) Single-cell reconstruction of the adult human heart during heart failure and recovery reveals the cellular landscape underlying cardiac function. *Nat. Cell Biol.* **22**, 108–119 <https://doi.org/10.1038/s41556-019-0446-7>